NANYANG TECHNOLOGICAL UNIVERSITY

Doctor of Philosophy

MODELING AND OPTIMIZATION OF PHOTOVOLTAIC SYSTEMS UNDER PARTIALLY SHADED AND RAPIDLY CHANGING CONDITIONS

JIANG LIANLIAN

JIANG LIANLIAN

SCHOOL OF COMPUTER ENGINEERING

2014

JIANG LIANLIAN

2014

MODELING AND OPTIMIZATION OF PHOTOVOLTAIC SYSTEMS UNDER PARTIALLY SHADED AND RAPIDLY CHANGING CONDITIONS

JIANG LIANLIAN

SCHOOL OF COMPUTER ENGINEERING

A thesis submitted to the Nanyang Technological University in partial fulfillment of the requirement for the degree of Doctor of Philosophy

2014

ACKNOWLEDGEMENTS

Time flies. Four years of my PhD life will come to an end soon. In these four years, I put a lot of effort in this research. However, it would not have been possible without the encouragement and guidance of many individuals and organizations. Therefore, I would like to express my sincere thanks to them here.

First of all, I would like to give my gratitude to my mentor and supervisor, Associate Professor Douglas Maskell. His supervision and support truly helped me in the research work. From the topic selection to the paper writing and discussion, he was always ready to give useful suggestions, and helped me to find other collaborations to improve my work. Apart from this, the most touching thing is that he always shows patience and gives a lot of valuable advice to me whenever I need his help. Second, my grateful thanks also go to my co-supervisor, Assistant Professor Jagdish Chandra Patra. During the research period, he not only gave me constructive suggestions on the topic we were working on but also taught me many precious skills on how to write a good research paper, and how to do the research. I believe these precious suggestions and attitude will become valuable wealth in my research career. Third, I also would like to show my gratitude to another co-supervisor, Associate Professor Don Mahinda Vilathgamuwa. He has a nice attitude to research and helped me a lot to review my papers. He always shows his great support for our research group, which inspired me so much.

Then, I would like to give my thanks to my colleagues, Jayaraman Ramkumar, who I had a lot of discussions with and helped me in collecting the experiment data, and Dulika Nayanasiri, who gave me a lot of valuable suggestions and guidelines when I was building the experimental setup. Without their help, it is not possible to finish the project. Many thanks also go to Ms. Merilyn Yap and Mr. Chua Ngee Tat, the laboratory executives at the Centre for High Performance Embedded Systems (CHiPES). Mr. Chua is one of the most devoted technicians I have ever met in the laboratory. Besides, I also want to give my sincere thanks to my friends and colleagues at CHiPES for their support and encouragement. They are Dr. Liu Yongchao, Dr. Cui Jin, Dr. Chen Yupeng, Dr. Qian Hanhua, Dr. Lin Mengda, Mr. Cui Yingnan, Mr. Zhang Li, Mr. Liang Hao, Mr. Mao Fubing, Mr. Zhang Longqi, Mr. Luo Tao, Mr. Gu Xiaozhe, Mr. Yang Liwei, Mr. Ye Deheng, Dr. Xue Bai, Dr. Zhou Bing, Mr. Zhu Fengjun, Ms. Wu Meiqing, Mr. Dang Khoa Pham, Mr. Thinh Pham, Ms. Cheah Hui Yan, Mr.

Mathias Faust, Mr. Shreejith Shanker, Mr. Rakesh Varier, Dr. Sharad Sinha, Mr. Abhishek Ambede, Dr. Sumit Darak, Ms. Supriya Sath, Mr. Narendar Madhavan, Mr. Prashob Nair, Ms. Neethu Robinson, Mr. Sumedh Somanath Dhabu, Mr. Abhishek Kumar Jain, Mr. Ronak Bajaj, Dr. Smitha Sreekumar and many other friends, who are not listed. Here, I'd like to give my special thanks to my friend, Vipin Kizheppatt, who helped me in preparing papers, shared many precious life experiences and gave many helpful suggestions for my work.

Due to the cooperation, I have a great opportunity to meet many awesome friends at power electronics research lab (PERL) in School of Electrical and Electronics Engineering (EEE). I feel so lucky to join this group. We had a lot of discussions and interesting activities that can enhance our research abilities and friendships. So I also want to take this opportunity to thank them. They are Dr. Arie nawawi, Mr. Ong Chuan En Andrew, Dr. Tong Chin Foong, Dr. Zhang Xinan, Mr. Yap Heng Goh, Mr. Gou Jianguang, Dr. Wei Deyuan, Mr. Rudy Tjandra, Mr. Kevin Grandhika, Mr. Xuan Bac, Mr. Karthik Kandasamy, Mr. Deepu Mohan, Mr. Robin Tanzania, Ms. Lan Lan, Mr. Hu Xiaolei, Mr. Yin Shan, Mr. Wei Feng, Dr. Liu Yitao, Ms. Wang Tao, Mr. Zhang Mengqi, Mr. Jayathurathnage Sampath, Ms. Acel, Dr. Tan Yen Kheng, Mr. Aaron Cai, Mr. Aaron Pereira and many other friends who are not listed here.

Furthermore, I would like to thank my very good friend, Ms. Dan Yufang and Ms. Shang Zhiqin, for their consistent support in my study and life. My thanks also go to my cute roommate Ms. Ma Lin and another good friend Ms. Li Fenfang from School of Physical and Mathematical Science (SPMS). We had a lot of fun together in these four years and I will never forget the happiness when we were together. There are also many other friends from SPMS that I want to thank. They are Dr. Xia Xinhui, Dr. Luo Jingshan, Dr. Pan Guoxiang, Dr. Li Dan, Dr. Heiner Diesinger, Ms. Daniela Korthower, Mr. Christoph Hartlmuller, Dr. Maithu Khuc, and Ms. Shrividhya Gurumurthi. Besides, I also want to thank another good friend Mr. Kjell Bault. His enthusiasm about creativity really cheered me. The friendships we built among friends during these years gave me a lot to memorize for the rest of my life. I also would like to take this opportunity to give special thanks to Dr. Gagik G. Gurzadyan, my roommate's supervisor from SPMS. We really enjoyed the moment when we were talking together with other friends in his office. His attitude towards research and life really helped me a lot.

Finally, I'd like to give my deepest thank to my lovely parents, brother, sister in-law and my cute nephew. They always motivate me and give me continuous support in my education and work.

TABLE OF CONTENTS

ABSTRACT

This thesis focuses on maximum power point tracking (MPPT) techniques for PV systems under partial shading and rapidly changing irradiance conditions. However, during the initial investigation of this topic, we realized that parameter extraction and modeling of the photovoltaic (PV) cell/module/array were fundamental to our analysis and simulation of MPPT systems. Limitations to existing parameter extraction and modeling techniques for PV systems resulted in the scope of this thesis being extended to also cover these topics.

In Chapter 1, the PV system is introduced and the motivations for the research on this topic are presented. In Chapter 2, various methods for modeling the PV cell/module/array and the MPPT techniques in the literature are reviewed. The performance of each method is evaluated and compared with each other in a table. Since the existing methods show either low accuracy in derived parameters of the PV array or too much complexity in their calculation, in Chapter 3, we proposed a Chebyshev functional link neural network (CFLNN) to model the PV module. Due to the absence of hidden layers in the network configuration, the complexity of the network based model is reduced and a better modeling accuracy is obtained using the proposed method. The results of current prediction using two other modeling methods – the two diode model and multilayer perceptron (MLP), are compared with that by the proposed method. The experimental results show that, compared to the analytical model, the CFLNN modeling method provides better prediction of the output current, and compared to the conventional MLP model, it has a reduced computational complexity. The determination of the parameters of the PV cell is of great importance to solar energy related research such as for investigating the performance of the MPPT system under various irradiance conditions, analyzing the performance of more complex grid-connected PV systems, and studying the insight to the known physical processes so that it can be used in quality control during the development of the devices and for fabrication process optimization etc. In the second part of Chapter 3, an improved adaptive differential evolutionary (IADE) algorithm is proposed to extract the parameters of the electrical circuit for PV modules. The principle is to apply the feedback of fitness value in the evolutionary process. Comparisons of parameter estimation results with existing methods for solar cell and module under various environmental conditions are conducted using both synthetic and experimental data. The proposed method eliminates the requirement for users to manually tune the control parameters of the differential evolutionary algorithms and offers better accuracy of the extracted parameters.

After analyzing the disadvantages of the existing MPPT techniques, we proposed an ant colony optimization (ACO) based MPPT for the PV system to work under partial shading environments. The ACO based MPPT, which is introduced in Chapter 4, is then verified using simulations and an experimental setup. This is the first time that ACO has been directly used for MPPT in a PV system. As other related evolutionary algorithms can also be applied to the MPPT in a similar way, a uniform implementation scheme for other evolutionary algorithms under several different PV array topologies is proposed. Furthermore, a strategy to accelerate the convergence speed is also investigated. It provides an essential and useful guideline to implement the related evolutionary algorithms into the MPPTs.

In Chapter 5, another type of MPPT technique, a hybrid MPPT which combines an artificial neural network (ANN)-based MPPT and a conventional MPPT, is proposed for PV systems operating under conditions with rapid irradiance change. The ANN is utilized to initially categorize the MPP region based on the irradiance pattern when irradiance sensors are available or based on spot current measurements along the I-V curve when irradiance sensors are not available. This classification is then used to force a conventional MPPT such as the perturb and observe (P&O) or extremum seeking control (ESC) to search near the identified MPP, resulting in the system tracking the global MPP. The direct prediction of the global MPP region in one step guarantees a fast system response. The implementation without irradiance sensors can accurately track the global MPP and features a relatively low cost. The effectiveness of the proposed hybrid MPPT is verified using both simulation and an experimental setup. The results show that it can effectively track the global MPP resulting in a significant power increase and as such, can be applied in locations with rapid irradiance change, such as in the tropics.

Finally, in Chapter 6, the conclusions of this thesis are made and the possible areas that we can continue to work on in the future are discussed.

PUBLICATIONS

This thesis is based on the following publications.

Journal papers:

L.L. Jiang, D.L. Maskell and J.C. Patra, "Hardware implementation of ant colony optimization based MPPT for PV systems under partial shading conditions and its comparison with particle swarm optimization and differential evolution." In preparation.

L. L. Jiang, D. R. Nayanasiri, D. L. Maskell, and D. M. Vilathgamuwa, "A hybrid maximum power point tracking for partially shaded photovoltaic systems in the tropics," *Renewable Energy*, vol. 76, pp. 53-65, 2015.

L.L. Jiang, D.L. Maskell, and J.C. Patra, "Parameter estimation of solar cells and modules using an improved adaptive differential evolution algorithm," Applied Energy, vol. 112, pp. 185-193, 2013.

L.L. Jiang, D.L. Maskell, and J.C. Patra, "A novel ant colony optimization-based maximum power point tracking for photovoltaic systems under partially shaded conditions," Energy and Buildings, vol. 58, pp. 227-236, 2013.

Conference papers:

L.L. Jiang and D.L. Maskell, "A uniform implementation scheme for evolutionary optimization algorithms and the experimental implementation of an ACO based MPPT for PV systems under partial shading," IEEE Symposium Series on Computational intelligence, Orlando, Florida, USA, Accepted.

L.L. Jiang, and D.L. Maskell, "A simple hybrid MPPT technique for photovoltaic systems under rapidly changing partial shading conditions," in The 40th IEEE Photovoltaic Specialists Conference, Denver, Colorado, USA, June, 2014.

L.L. Jiang, D.R. Nayanasiri, D.L. Maskell et al., "A simple and efficient hybrid maximum power point tracking method for PV systems under partially shaded condition," in The 39th Annual Conference of the IEEE Industrial Electronics Society, Vienna, Austria, 2013, pp. 1513-1518.

L.L. Jiang, D.L. Maskell, and J.C. Patra, "Chebyshev functional link neural network-based modeling and experimental verification for photovoltaic arrays," in IEEE International Joint Conference on Neural Network (IJCNN), Australia, 2012, pp. 1-8.

L.L. Jiang, D.L. Maskell, and J. C. Patra, "A FLANN-based controller for maximum power point tracking in PV systems under rapidly changing conditions," in IEEE International Conference on Acoustics, Speech, and Signal Processing (ICASSP), Kyoto, Japan, 2012, pp. 2141-2144.

J. C. Patra, L.L. Jiang, and D.L. Maskell, "Estimation of external quantum efficiency for multi-junction solar cells under influence of charged particles using artificial neural networks," in IEEE International Conference on Systems, Man, and Cybernetics, Anchorage, Alaska, USA, 2011, pp. 465-470.

Chapter 1 Introduction

1.1 Overview

Due to the limited supply of fossil fuel based energy and the constantly growing environmental concerns, the renewable energy has experienced consistent growth. Nowadays, these non-conventional energy sources are attracting more and more global attention. Solar energy systems as a renewable energy source are of particular interest due to their almost zero post-production pollution, the abundance of the energy source, low maintenance and the advancements in semiconductor and power electronic devices. It is an effective approach that alleviates the contradiction between society's development and the resource crisis.

Photovoltaic (PV) systems represent the fastest growing renewable energy segment, with operating capacity increasing at approximately 58% annually [1]. PV systems have a relatively low carbon footprint and energy payback time (EPBT) [2] with many large solar PV power stations in operation all over the world. Even in the midst of the economic uncertainty, the solar PV market continued to grow in 2013, with new grid-connected PV capacity rising by 35% to a total of 136.7 GW [3]. The global PV capacity grew from 40.7 GW at the end of 2010 to 136.7 GW by the end of 2013, which implies 0.85% of the worldwide electricity demand [4] is generated by PV. Moreover, there are many large PV plants under construction, and plans for future PV systems in many different countries.

Even though PV installed capacity and the governmental support for PV are increasing dramatically, the efficiency of the electricity transformation, not only from the perspective of the cell technology but also from the systems perspective, needs to be improved to further reduce the cost of energy production. This motivates us towards research involving more efficient power converters and other affiliated electrical parts (referred to as balance of system (BOS)) to extract the maximum available power from the PV arrays while reducing BOS costs.

1.2 Photovoltaic systems

There are two major ways to utilize solar energy in power plants, depending upon the energy conversion technique. The first one uses the photovoltaic effect to directly convert light energy into electricity. The second is concentrating solar thermal (CST) power, which uses the light energy to produce heat which is used to run a heat engine for generating electricity. Different working fluids can be heated by the concentrated sunlight,

including water, oil, salts, air, nitrogen etc. [5]. There are four main types of concentrating technologies, namely dish Stirling, parabolic trough, linear Fresnel reflector, and solar tower [6]. The efficiency of each technology varies depending on the method for tracking the sun and focusing the light. In our research, we only investigate PV systems, which directly convert solar energy into the electricity [7]. In PV systems, the smallest unit is the solar cell. Usually, multiple cells are connected in series and/or parallel to form a module in order to achieve higher voltage or current output. Large numbers of solar modules are then connected together in series and/or parallel to produce a solar array. A large solar power station usually consists of a large number of solar arrays.

Depending on the different load connections, PV systems can be classified into three types: grid-connected, stand-alone, and hybrid PV systems. In the grid-connected PV systems, the generated surplus electricity is sent to the power grid and the grid provides power when there is not enough sunshine. The stand-alone PV system, with battery backup, can provide users with electricity when there is no sunshine, such as at night or during cloudy weather. It is especially cost effective to set up and is suitable for remote areas. A hybrid energy system generally consists of two or more renewable energy sources such as wind power generators and biomass power generation system. They are used together to provide increased system efficiency as well as greater balance in energy supply. In a typical hybrid system, the generated power is harvested using battery banks first and then connected to the AC load through the inverters. The hybrid system would create more output from the wind turbine during the winter, whereas during the summer, the solar panels would produce their peak output. Since the peak operating times for wind and solar systems happen at different times of the day and year, hybrid systems can complement each other in order to produce a more continuous power supply.

A typical grid connected PV system is shown in Fig. 1.1. In this system, the power generated by the PV array, which is usually made up of multiple PV modules in series and parallel, can be either used by the household appliances or transmitted back to the electricity grid. The inverter between the system load and the PV array has a maximum power point tracking (MPPT) controller, which tracks the maximum power point (MPP) so that the PV arrays always output maximum power. MPPT can be connected in either centralized mode (multiple modules are controlled by a single MPPT) or distributed mode (each single module is equipped with an MPPT) between the PV array and system load. For a standalone PV system, the difference is that there are additional battery banks inserted between the MPPT controller and the inverter used to store the surplus energy. When there is not enough sunlight, the inverter will discharge the battery bank to supply the load.

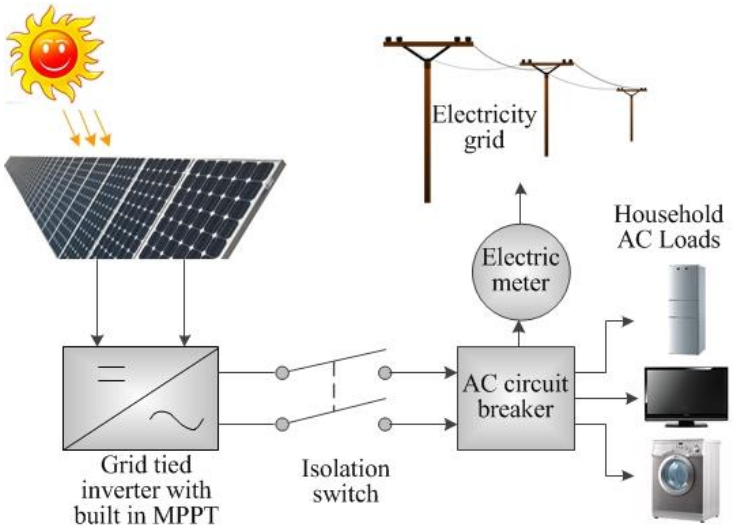

Fig. 1.1 Grid connected PV system with built in MPPT in the inverter.

1.2.1 Modeling the solar array

Building an accurate model of the solar array is a very important research issue in PV systems especially when studying the PV array characteristics, forecasting the power output, and developing systems to extract maximum power, such as MPPT. The critical problem with building a model for PV modules is the nonlinear relation that exists between the current and voltage output, especially for the cases when the solar arrays are exposed under rapidly changing and partially shaded conditions.

When several PV cells or modules in the PV panel are shaded by passing clouds or by surrounding trees and buildings, the voltage (or current) of the entire PV array cannot be determined just by multiplying the voltage (or current) of each module by the number of solar modules connected in series (or in parallel). Usually, the partial shading condition makes the shaded modules reverse biased causing them to act as a load rather than a generator, with the power dissipated in the form of heat. This phenomenon not only limits the current output of the entire PV module branch, but may also cause areas of increased temperature (also called hot spots) [8]. Even worse, when the heat caused by the hot spots exceeds the maximum power tolerance of the PV modules, the PV system could be damaged permanently.

In order to solve this problem, many manufactures have externally coupled bypass diodes to the PV module. Generally, for crystalline silicon modules, the number of the solar cells across one bypass diode is 18 [9]. With the bypass diode across the solar cell, the excess current produced by the unshaded PV module can flow through the external diode. As a result, hot spots can be prevented. Simultaneously, a blocking diode is also introduced to prevent the inverse current flowing back into the PV arrays from the battery, which may

also result in damage to the PV array. However, modeling the PV arrays with bypass and blocking diodes becomes more complex. In addition, the conventional analytical modeling techniques are not suitable for modeling systems under real weather conditions. This will be explained further in the literature review in Chapter 2.

1.2.2 MPPT under partially shaded conditions

MPPT is a technique that the inverters, solar battery chargers and similar devices use to get the maximum possible power from the photovoltaic devices. Because of the nonlinear relationship between the current and voltage in a PV module, there exists a unique MPP for a particular irradiance condition when the irradiance distribution on the PV system is uniform [1-14]. The MPP tracker is designed to guarantee that the PV system is operated at the MPP, so as to extract as much power from the PV array as possible. Weather conditions influence the efficiency of the MPPTs, particularly the degree of uniformity of the irradiance distribution on the PV modules and the speed of irradiance variation.

When the PV arrays are working under uniform and slowly varying irradiance, MPPTs using conventional MPPT algorithms such as perturb and observe (P&O) and incremental conductance (IncCond), which will be introduced in Chapter 2, work very well and can produce almost as much power as the PV array can output. However, when the PV systems are working under partially shaded conditions, the power versus voltage (P-V) curve exhibits multiple local maxima, which can result in the conventional MPPT becoming trapped at a local maxima resulting in a significant energy loss (up to almost 70%) [10-12]. This shading problem can be caused by clouds passing over the solar arrays, long-lasting dust, nearby trees or buildings, snowfall, frost, bird droppings, and so on.

In order to illustrate the power loss mechanism due to the partial shading conditions, we investigate two PV modules connected in series as shown in Fig. 1.2. The corresponding current versus voltage (I-V) curve for each module is shown in Fig. 1.3 (a) and (b). The currents of these two modules are equal due to the series connection. Therefore, the I-V curve of this series connected assembly can be obtained by adding the voltage of these two PV modules while keeping the current value of each PV module constant as shown in Fig. 1.3 (c). From the I-V curve of these two modules, we can see two local maxima (G_1 and G_2) in the resultant P-V curve, as shown in Fig. 1.4. When the same two modules are exposed under uniform irradiance conditions, there is only one MPP (G_3), as shown in Fig. 1.4. In order to maximize the power output from the PV array, the system should be operated at the global MPP (G_3 or G_1, depending on the irradiance level). Many existing MPPT algorithms, which will be introduced in Chapter 2, can only successfully follow the global MPP G_3 under uniform irradiance. In contrast, they tend to become trapped at the local maximum point G_2 under partially shaded conditions, and hence fail to extract

maximum power. The corresponding power loss mechanism under such circumstances will be examined in more detail in Chapter 4.

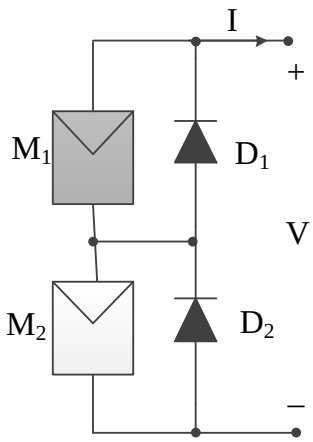

Fig. 1.2 A PV system with two PV modules connected in series, one (M_1) of modules is shaded and the other one (M_2) is receiving normal irradiance (1000W/m^2).

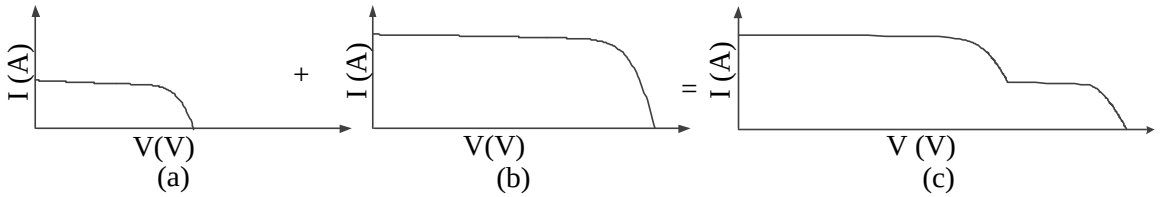

Fig. 1.3 (a) I-V curve of the shaded module (b) I-V curve of the unshaded module (c) I-V curve of the modules connected in series.

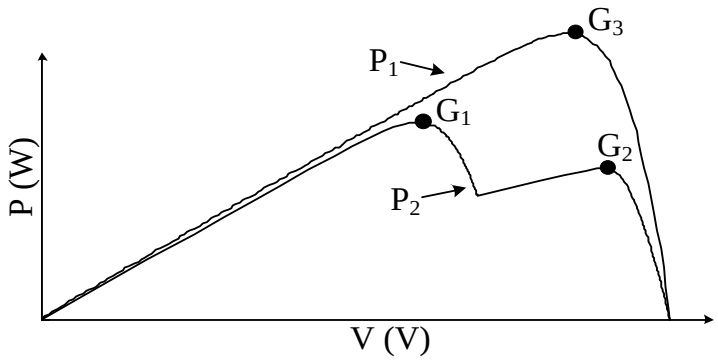

Fig. 1.4 The P-V curve for two series connected modules. (Top) under uniform irradiance and (bottom) the irradiance pattern of Fig. 1.2 and Fig. 1.3.

Besides the power loss caused by partial shading, rapid irradiance change is also a significant problem effecting existing PV systems. In tropical areas, rapidly changing irradiance conditions commonly occur when clouds pass above the PV arrays. For example, in Fig. 1.5, it shows a large number of rapid irradiance changes which are measured on a normal day (6th Jan. 2012) in Singapore. In order to quantify the large

irradiance changes, the criteria of classify the categories of irradiance change provided in [13] has been used. Table 1.1 shows the number of events that were measured during the month of Aug. 2010 according to the corresponding category in [13]. Assuming an 8 hour solar day, there are 14880 minutes (18600 if a 10hr day is used) in the month of August/2010. Thus, from Table 1.1, we can see that we are getting an event every minute in all categories. When a conventional MPPT technique, which will be introduced in the literature review in the following Chapter 2, is applied to the PV system, it cannot quickly track the global MPP under these varying conditions. This will significantly reduce the energy extraction, particularly in conjunction with the partial shading of PV arrays caused by the passing clouds.

Therefore, it is meaningful to investigate a general algorithm, which is able to track the global MPP with a speed faster than that of the irradiance change under various shading conditions. In the Singapore context, we expect the tracking algorithm to track the new global MPP within 1 second. After reviewing the literature, we found that existing MPPT techniques do not meet the requirement for global tracking with the fast tracking speed under various irradiance and temperature conditions. Thus, in our work, we focus on finding an MPPT for PV systems not only suitable for the partial shading conditions but also for rapid irradiance change.

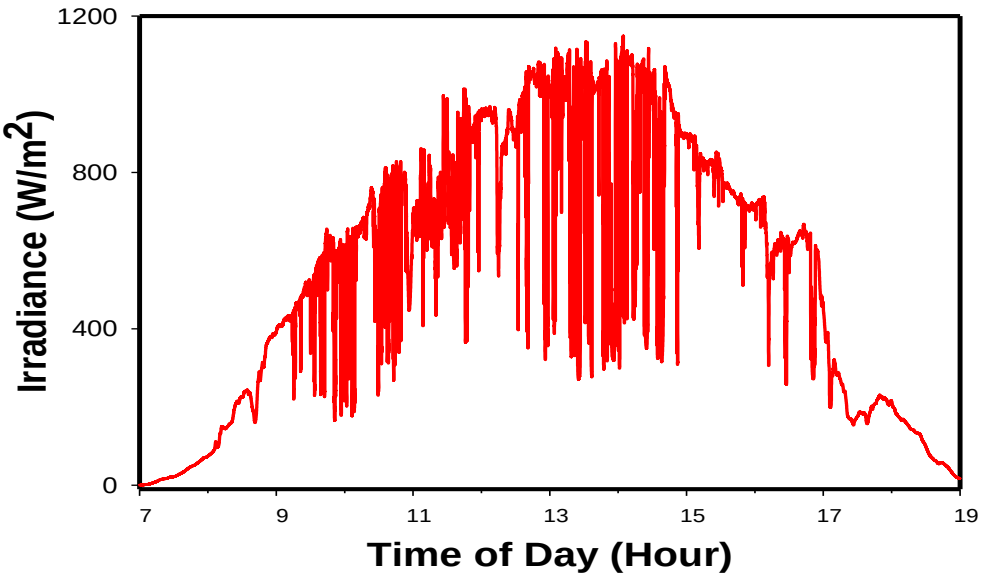

Fig. 1.5. Global horizontal irradiance on 6 Jan 2012.

Table 1.1 Measured number of irradiance transition event according to the categories in [13].

Categories from [13]		Singapore measured events	
Time scale	Largest realistic variation (W/m^2)	No. of events measured	Largest measured event (W/m^2)
Very fast (within 1s)	27	17041	292

Fast (within 5s)	103	20581	738
Slow (within 30s)	441	15602	842

1.3 Main contributions

The main contributions from this work include:

(1) A review of PV modeling, parameter extraction and MPPT algorithms.

(2) A Chebyshev functional link neural network (CFLNN) based modeling approach for PV arrays is developed. This model provides better accuracy compared to the analytical method (two diode model), and requires less computational complexity than the popularly used multilayer perceptron.

(3) An improved adaptive differential evolution (IADE) based parameter extraction for PV cells and modules is proposed. The proposed IADE algorithm makes use of the fitness value as a feedback mechanism in the evolutionary process. It provides better accuracy for estimation of parameters for solar cells and modules than other popular optimization methods, such as particle swarm optimization (PSO), simulated annealing (SA), genetic algorithm (GA), conventional DE, and the recently proposed analytical method.

(4) A novel ant colony optimization (ACO)-based MPPT technique for PV systems working under partial shading conditions is proposed. This heuristic algorithm based method not only has the ability to track the global MPP, but also reduces the system cost and provides a simpler control scheme. A comparison with other widely used evolutionary algorithms is conducted and a hardware implementation is demonstrated. Along with the ACO based MPPT, a uniform scheme for applying other related evolutionary algorithms to PV systems with various structures along with a strategy to accelerate the tracking speed of these algorithms is proposed.

(5) A hybrid MPPT for PV systems under partially shaded conditions with rapid irradiance change is proposed. This hybrid MPPT combines conventional MPPT and artificial neural network (ANN)-based MPPT. It results in an MPPT with a relatively low cost, fast response, and simple structure.

1.4 Organization of this thesis

The remainder of this thesis is organized as follows:

1. Chapter 2 gives a literature review, which presents the state-of-the-art in PV systems modeling and MPPT techniques. The pros and cons of the existing techniques are provided.

2. Chapter 3 introduces the proposed CFLNN-based modeling method for the PV array. The experimental verification of this approach and comparison with other methods are conducted. In the second section of this Chapter, the proposed IADE based parameter estimation for the PV array is introduced.

3. Chapter 4 introduces a novel ant colony optimization algorithm based MPPT. A new PV array structure for the application of ACO based MPPT is proposed. In addition, a uniform framework for applying related evolutionary algorithms to MPPT for PV systems is introduced. A strategy to accelerate the MPPT algorithm is also introduced and the effectiveness of the proposed MPPT method is verified by simulation and experiment. Comparisons with other widely used computational algorithms are provided.

4. Chapter 5 presents a hybrid MPPT technique for PV systems working under partially shaded conditions with rapid irradiance change. This technique uses a combination of a computational algorithm and a conventional MPPT. Comparisons are made with other popular MPPTs.

5. Finally, Chapter 6 concludes the thesis and discusses the possible future research directions.

Chapter 2 Literature review

2.1 PV array models

Many types of models for solar arrays have been proposed during the last two decades. Generally, modeling solar arrays can be categorized into three types: analytical methods, experimental methods, and artificial intelligence methods.

2.1.1 The analytical method

The solar cell is described by the equivalent electrical circuit with several unknown parameters. These parameters can be determined by calculating mathematical equations with environmental input variables such as irradiance and temperature values. The analytical methods, which are mainly used among researchers, are described below:

2.1.1.1 The single diode model (or four-parameter model)

The single diode model consists of a current source, a diode which represents the diffusion current component, and a series resistance which is responsible for the losses caused by the internal series resistance, contacts, and other line interconnections between each solar cell and module [14, 15]. A typical model of a solar cell is shown in Fig. 2.1.

From the equivalent circuit in Fig. 2.1, we can get the current output from the solar cell as:

$$I = I_{pv} - I_d \tag{2.1}$$

where I is the current output of the solar cell, I_{pv} is the light generated current from the solar cell, and I_d is the current passing through the diode.

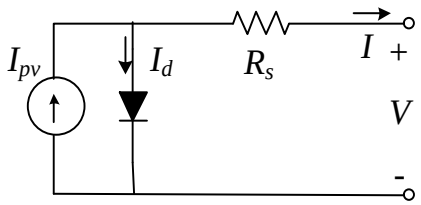

Fig. 2.1 The equivalent circuit of the solar cell using single diode model.

The light generated current is described by:

$$I_{pv} = (I_{pv\_STC} + K_{sc}(T - T_{STC}))\frac{G}{G_{STC}} \tag{2.2}$$

where I_{pv_STC} is the light generated current under the standard test conditions (STC) with temperature T_{STC} = 25°C and irradiance G_{STC} = 1000 w/m^2 , and K_i is the short circuit current coefficient that shows the change rate of the short circuit current with the temperature increase.

By applying Shockley's equation, the diode current can be written as [16]:

$$I_d = I_0[\exp(\frac{V + IR_s}{aV_t} - 1)] \tag{2.3}$$

where V is the solar cell output voltage (V), V_t the thermal voltage of the diodes ($V_t = k\,T\,/\,q$), k the Boltzman constant (k = 1.3806505 ×10-23J / K), T the present temperature (K), q the charge of an electron (1.60217646 × 10-19 C), a the diode ideality factor and R_s the series resistance (Ω).

The reverse saturation current of the diode is given by:

$$I_0 = I_d(\frac{T}{T_{STC}})^3 \exp[\frac{qE_g}{ak}(\frac{1}{T_{STC}} - \frac{1}{T})] \tag{2.4}$$

where E_g is the bandgap energy in eV [17, 18], given as:

$$E_g = 1.16 - 7.02 \times 10^{-4} \frac{T^2}{T + 1108}. \tag{2.5}$$

Even though some researchers assume that the value of bandgap is constant, actually it depends on the value of the instantaneous temperature. By substituting Eqs. (2.2) - (2.5) into Eq. (2.1) , Eq. (2.1) is rewritten as:

$$I = I_{pv} - I_0[\exp(\frac{V + IR_s}{aV_t}) - 1]. \tag{2.6}$$

Actually, Eq. (2.6) can be represented as $I = f\,(I, V)$ with four unknown parameters, namely I_{pv}, I_0, R_s, and a. Because of these four parameters, which can be calculated using different methods, Eq. (2.6) is also called the four-parameter model. For a given voltage, the standard Newton-Raphson method can be used to solve this nonlinear equation. Therefore, for a given voltage, the solar cell current can be calculated with Eq. (2.1) - (2.5) and the Newton-Raphson method.

When calculating the current from a solar module or solar array, as shown in Fig. 2.2 where the envelop shape is a common symbol to represent the PV module used in the PV system, the corresponding parameters need to be changed. Consider a solar array with N_{ss} PV modules in series in each string and N_{pp} PV strings in parallel, where each module comprises N_s solar cells, the current output of a PV array is given by [15]:

$$I = I_{pv}N_{pp} - I_0 N_{pp}[\exp(\frac{V + \lambda IR_s}{aN_s V_t N_{ss}}) - 1] \quad (2.7)$$

where λ is the factor of proportionality between N_{ss} and N_{pp} ($\lambda = N_{ss} / N_{pp}$).

The advantage of this model is that no complicated computation is required during modeling because some of the physical process is neglected and simplified. However, the internal recombination of the current in the space charge region is not considered, making the model inaccurate.

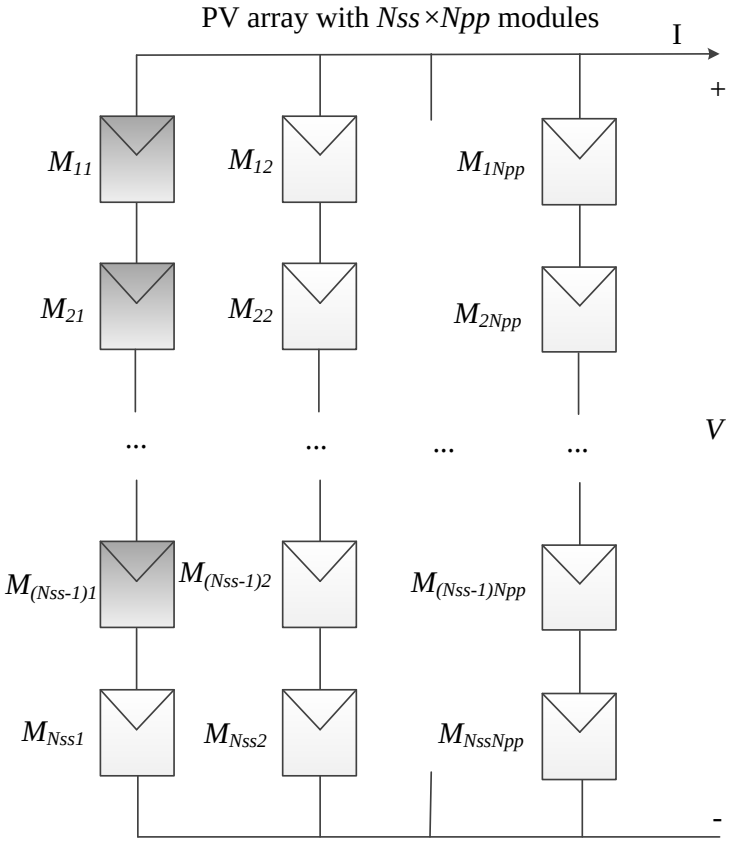

Fig. 2.2 A PV array with $N_{ss} \times N_{pp}$ modules.

2.1.1.2 The single diode model with shunt resistance (or the five-parameter model)

This model takes the p-n junction leakage current into consideration. From the equivalent circuit of the solar cell, as shown in Fig. 2.3, we can see that a shunt resistance (R_p) is added to represent the effect of leakage current, crystal imperfections and impurities [14, 19].

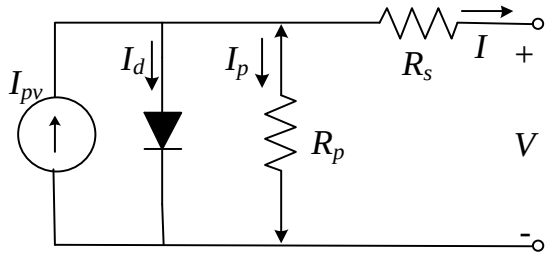

Fig. 2.3 The equivalent circuit of the single diode model with shunt resistance.

Therefore, the current Eq. (2.6) is changed as:

$$I = I_{pv} - I_0[\exp(\frac{V + IR_s}{aV_t}) - 1] - \frac{V + IR_s}{R_p} \tag{2.8}$$

where R_p is the shunt resistance for a solar cell.

Similarly, when considering multiple solar modules connected in series and parallel, Eq. (2.8) needs to be rewritten as:

$$I = I_{pv}N_{pp} - I_0N_{pp}[\exp(\frac{V + \lambda IR_s}{aN_sV_tN_{ss}}) - 1] - \frac{V + \lambda IR_s}{\lambda R_p} \tag{2.9}$$

Compared to the single diode model, this model is more accurate due to its consideration of the series resistance losses and other current leakage.

2.1.1.3 The two diode model with shunt resistance

This method adds another diode to the model, which is connected in parallel with the previous five-parameter model to imitate the losses caused by the carrier recombination in the space charge region of the junction and surface recombination. Its equivalent circuit is shown in Fig. 2.4 [20].

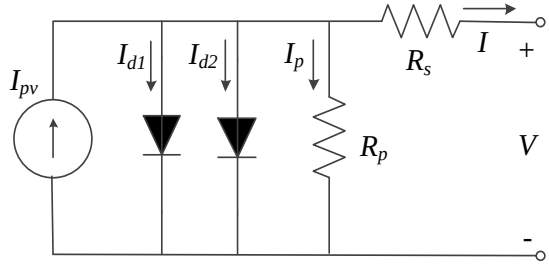

Fig. 2.4 The equivalent circuit of the two diode model with shunt resistance.

From the equivalent circuit, the current equation is derived as [20, 21]:

$$I = I_{pv} - I_{01}[\exp(\frac{V + IR_s}{a_1V_t}) - 1] - I_{02}[\exp(\frac{V + IR_s}{a_2V_t}) - 1] - \frac{V + IR_s}{R_p} \tag{2.10}$$

where I_{01} and I_{02} are the reverse saturation current of these two diodes, and a_1 and a_2 are the ideality factors of each diode.

For a PV array as shown in Fig. 2.2, the equation is formed with additional coefficients as [21]:

$$I = N_{pp}I_{pv} - N_{pp}I_{01}[\exp(\frac{V+\lambda IR_s}{a_1V_tN_{ss}N_s})-1] - N_{pp}I_{02}[\exp(\frac{V+\lambda IR_s}{a_2V_tN_{ss}N_s})-1] - \frac{V+\lambda IR_s}{\lambda R_p} \quad (2.11)$$

Compared to the previous models, this model provides the most accurate current output [21]. However, the corresponding computational complexity increases with the additional diode.

There are also other models which can be derived from these three basic models, such as the three diode model [22], which is rarely used because the additional computational complexity is too high, and the two diode model without the simplified reverse saturation current equation [19-21], and so on.

Mathematical equations make it easier to model the solar array. Most researchers using the analytical method to model solar arrays consider a constant value for the series resistance, R_s, the parallel resistance, R_p, and ideality of the diode, a [19, 20, 23, 24]. In reality, all of these parameters vary with changes in the temperature and irradiance [25]. For example, on cloudy days, the value of the parallel resistance (R_p) is very low which causes performance degradation due to the power reductions. Thus, it is unrealistic to assume the constant value of these parameters under such circumstances. The change in series resistance and parallel resistance values can be seen in the experimental results of the parameter estimation section. Since many factors can affect the power harvest of the PV systems, such as the mismatch losses in solar cells/modules, ohmic losses, angular and spectral losses, failure of the MPPT algorithms under shading effects and bad environmental conditions, it is still difficult to accurately model the characteristics of solar modules just using the analytical method [26]. In addition, these analytical models are computationally expensive and are sensitive to the initial values of the parameters.

2.1.1.4 Simulation tools

Simulation tools also use analytical modeling techniques. The main principle of this type of modeling is to simulate the equivalent circuit of the solar cell/module with commercial simulation software, such as PSpice [27, 28], PSIM [29], Saber [30] and so on. These software packages are specially designed for the simulation of analog and digital circuits and can be integrated with other complex systems. A PV module can be constructed by connecting several solar cells. There are several advantages of using the simulation method: the process required to build a circuit model in the simulation environment is

simpler than using mathematical equations; Large PV systems can be easily expanded or modified by editing the topology of the basic solar cell unit; The transient response from the system can be observed by the output tools integrated in the simulation platform; A large number of complex non-linear or iteration procedures are avoided. However, it is not very flexible when simulating a system with dynamic parameters. When one of the parameters changes, the simulation should be run from the beginning [15]. In other words, the attribute of each component in the simulated circuit is not allowed to change online, which makes it difficult to simulate the cases with varying parameters under changing weather conditions.

2.1.2 The experimental method

The basic principle of the experimental method is to build the model of a solar cell or solar array using several key points in the I-V curve measured by experiment. These key points usually include the short circuit point (point A as shown in Fig. 2.5), the maximum power point (B), and the open circuit point (C). For the four-parameter model, only four equations are required to calculate the four parameters (I_0, I_{pv}, a, R_s). Therefore, for a four-parameter model, by substituting the points A, B, C and the zero value of the derivative of the power with respect to the voltage, that is the MPP D, into Eq. (2.6) separately, these four parameters can be obtained. When the five-parameter model is considered, another point, E, which is the voltage midway between the open circuit voltage and the MPP voltage point, needs to be taken into account. The voltage value of this point can be given by:

$$V_m = \frac{1}{2}(V_{mp} + V_{oc}) . \tag{2.12}$$

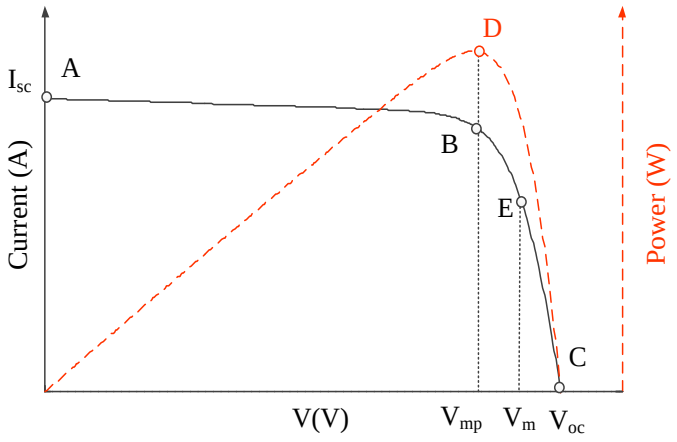

Fig. 2.5 The current and power under the condition of constant temperature and irradiance.

The solar cell/module model can be easily calculated online by using this method. However, the parameters calculated are significantly influenced by the single point chosen to calculate the model. Even the system noise can largely affect the results.

2.1.3 The artificial intelligence methods

Compared to the analytical methods, artificial intelligence methods, such as the artificial neural network (ANN) [25, 26, 31, 32], exhibit better performance without the requirement for prior knowledge of the internal system, and provide a compact solution to multivariable problems. The basic idea of the ANN [33, 34] is to approximate a linear or non-linear function representing the relationship between the inputs and outputs. A widely used fundamental structure for the ANN is the multilayer perceptron (MLP) with a single hidden layer as shown in Fig. 2.6. Multiple layers can also be used in different applications. There are many types of ANN, including the feedforward neural network [35, 36], Kohonen network [37], back propagation (BP) network [38], Hopfield network [36], and radial basis function (RBF) network [39] etc. In theory, it is demonstrated that the feedforward ANN with a single hidden layer can approximate a nonlinear continuous function with arbitrary accuracy [34, 40, 41]. Before using this network to predict the output value corresponding to the input value, the network is trained using training samples by varying the parameters in the training algorithm, the connection weights, or the specification of the architecture such as the number of neurons or their connectivity [42]. After training, the weights between each layer are determined.

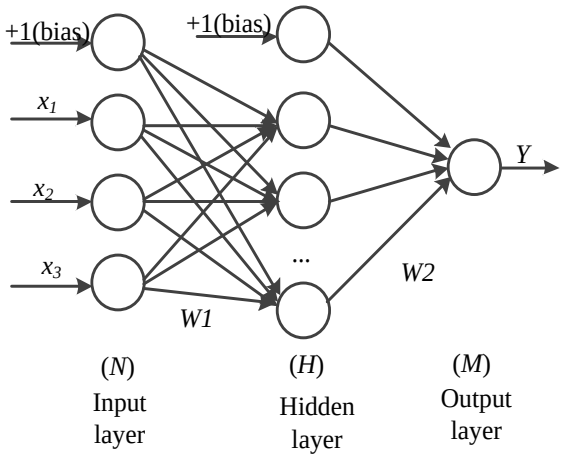

Fig. 2.6 A basic structure of ANN with a single hidden layer.

There are two ways of using an ANN to model a PV array. The first one is to predict these classical five or seven circuit parameters primarily and then use the predicted results to calculate the conventional five or seven-parameter models. For instance, Karatepe et al. [25] use an ANN to estimate the electrical circuit parameters first and then apply the estimated parameters to the one diode model for PV modules. The other method is to

predict the current or voltage directly from the irradiance and temperature inputs. For instance, Celik et al. [23, 43] utilize the generalized regression neural network to estimate the current output from the mono-crystalline PV modules according to the measured voltage, and irradiance and temperature levels. The main disadvantage of this method is that training datasets are needed to train the neural network before using it as the model. For the comprehensive review of ANN techniques in PV systems please refer to the review in [44-47].

In conclusion, the comparison of above modeling techniques according to its accuracy and computational complexity are given in Table 2.1. The factors affecting the performance of each method are described in the last column.

Table 2.1. Comparison of different modeling methods.

Modeling method	Accuracy	Computational complexity	Affected factors and Limitations
The single diode model	Low	Low	Without considering the internal recombination of the current in the space charge region.
The single diode model with shunt resistance	Medium	Medium	Taking series resistance losses and leakage current into consideration.
Two diode model with shunt resistance	High	Medium	Better accuracy than the above two models but higher computational complexity.
Model with more diodes	Very high	High	High computational complexity.
Experimental method	Low	Low	Not flexible when simulating a system with dynamic parameters.
Simulation tools	Medium	Medium	Low flexibility, difficult to simulate dynamic environmental conditions
Artificial intelligence method	Very high	Medium	Training datasets are required.

2.2 MPPT techniques

MPPT methods in PV systems can be categorized by different criteria such as the direct seeking method, intelligent seeking method, and compensation method. In recent years many MPPT techniques have been proposed [9, 46, 48-52]. The direct seeking methods measure the actual current, voltage, and power directly from the PV array terminals, and calculate the reference voltage or current signal based on different MPPT algorithms. The direct seeking methods are simple to implement, but sometimes, the system fall into at a local maximum point. The intelligent seeking methods use artificial intelligence based methods to seek the MPP, such as ANN [53], particle swarm optimization (PSO) [54, 55], genetic algorithm (GA) [56, 57], fuzzy logic [58], or hybrid techniques of these methods

[59, 60]. In our work, we review MPPT techniques by their ability to track the global MPP. Finally, the advantage and disadvantage of each method will be given in a table.

2.2.1 Perturb-and-observe (P&O) or hill climbing

The basic idea of P&O is to periodically perturb (increase or decrease) the terminal voltage of the PV arrays and compare the instantaneous power $P(k)$ with the previous power $P(k\text{-}1)$, to determine the perturbation direction in the next step. When a perturbation causes an increase in the PV array power, the direction of the current perturbation is maintained for the next perturbation; otherwise, the perturbation direction is reversed [10]. For example, supposing that the perturbation starts from point A_1 in
Fig. 2.7. After a positive voltage perturbation, a power increase at A_2 is observed. Therefore, the direction of the next voltage perturbation will be the same as the previous step, which is to increase the voltage reference. By repeating this procedure periodically, the operating point will be located at the MPP (G), but with oscillations. For other cases, it will also arrive at the operating point G. For the PV system with a two stage inverter which consists of a DC-DC converter in the first stage and a DC-AC inverter in the second stage [61, 62], the voltage is adjusted by tuning the duty ratio of the DC-DC converter. The duty ratio is the ratio between the time duration that power switch is active and the operating period of the DC-DC converter. The corresponding flowchart of the basic P&O algorithm is shown in Fig. 2.8.

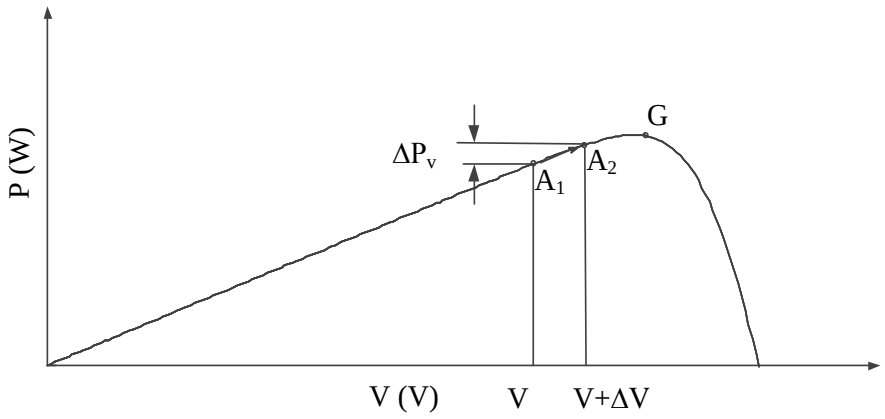

Fig. 2.7 The P-V curve to illustrate the direction of voltage perturbation.

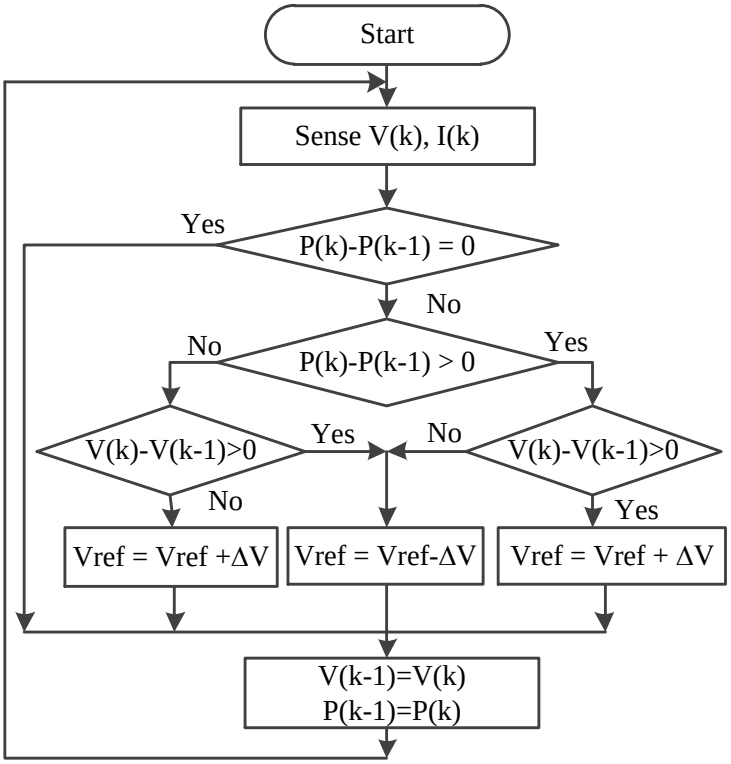

Fig. 2.8 The flowchart of the P&O algorithm for MPPT in PV system [14].

The oscillation around the MPP can be reduced by decreasing the voltage perturbation step size. A small voltage step size improves the accuracy but slows down the tracking speed, while a large step size leads to a fast tracking speed but with large oscillations around the MPP. Therefore, when applying this method for MPPT in PV systems, a tradeoff between the oscillation size and accuracy should be made.

The advantage of this algorithm is the simplicity. However, when the system is under rapidly changing irradiance conditions, the algorithm may direct the operating point away from the MPP. Moreover, it tends to become trapped at a local power maxima when partially shading conditions occur.

2.2.2 Incremental conductance (IncCond)

The main principle of the IncCond method is that the derivative of the output power, *P*, in terms of voltage, *V*, at the peak power point is equal to zero (*dP/dV* = 0) [11]. Therefore, from the equation *P=IV*, the following equation is obtained [10]:

$$\frac{dP}{dV} = V\frac{dI}{dV} + I = 0 \text{ (at the MPP).} \tag{2.13}$$

Therefore, within one sampling period, Eq.(2.13) can be rewritten as:

$$\frac{\Delta I}{\Delta V} = -\frac{I}{V}. \tag{2.14}$$

Eq. (2.13) means that, at the MPP, the opposite of the instantaneous conductance of PV array on the left side of the equation equals the incremental conductance on the right hand side. Thus, the derivative of the points should be greater than zero on the left of the MPP (point G as shown in Fig. 2.7), while, less than zero on the right side. It is illustrated as follows [10, 11]:

$$\text{If } \frac{dP}{dV} = 0 \ \left(\frac{dI}{dV} = -\frac{I}{V}\right), \text{ then MPP is reached.} \tag{2.15}$$

$$\text{If } \frac{dP}{dV} > 0 \ \left(\frac{dI}{dV} > -\frac{I}{V}\right), \text{ then increase } V_{ref}. \tag{2.16}$$

$$\text{If } \frac{dP}{dV} < 0 \ \left(\frac{dI}{dV} < -\frac{I}{V}\right), \text{ then decrease } V_{ref}. \tag{2.17}$$

By comparing the incremental conductance ($\Delta I/\Delta V$) with the instantaneous conductance (I/V), the MPP can be tracked. The basic flowchart of IncCond is shown in Fig. 2.9. The algorithm starts with the sensed voltage and current values and calculates the voltage and current changes compared to the previous step. The direction of the voltage movement in the next step depends on the comparison between the result of incremental conductance ($\Delta I/\Delta V$) and the instantaneous conductance (I/V). If the voltage and current changes are both measured to be zero, then keep the present voltage and current values for the calculation in the next step. If the voltage change value is measured to be zero and the current change is non-zero, then the voltage change direction in the next step is to increase the voltage when ΔI is larger than zero or reduce the voltage when ΔI is less than zero. Otherwise, the voltage direction is changed according to Eqs. (2.16) and (2.17).

Some studies have compared the efficiency of the IncCond and P&O algorithms, [11, 63] and shown that IncCond has a better efficiency than that of P&O. However, Houssamo, et al. [64] and D. P. Hohm et al. [65] showed that when the perturbation step size and the sampling period are properly optimized, the IncCond and P&O algorithms exhibit the same MPPT efficiency. Even though the efficiency of these two methods are similar, the main disadvantage of both methods is the power loss due to oscillations around the MPP, the slow tracking speed when choosing a small perturbation step, and the failure to track the global MPP on the P-V characteristic curve under partially shaded conditions. Although these two MPPT methods are not so efficient under partially shaded and rapidly changing irradiance conditions, they act as good basic algorithms for comparison purposes when investigating global MPP tracking.

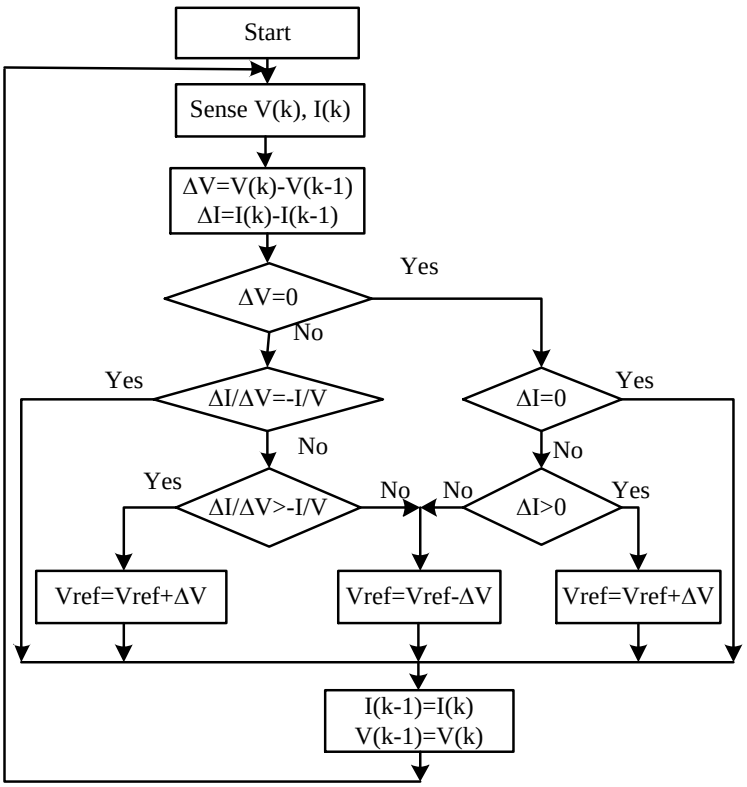

Fig. 2.9 The flowchart of the IncCond algorithm for MPPT in PV system.

2.2.3 Fractional open circuit voltage/ short circuit current

The fractional open circuit voltage based MPPT technique uses the approximate linear relationship between the optimal voltage at the MPP (V_{mpp}) and the open circuit voltage (V_{oc}) under different irradiance levels to calculate the optimal working point. The equation is given by:

$$V_{MPP} = k_1 V_{oc} \tag{2.18}$$

where k_1 is the proportional constant which is reported to be between 0.71 and 0.78 [66]. The open circuit voltage is periodically measured under different irradiance and temperature conditions. By replacing the open circuit voltage with the short circuit current, the optimal current at the MPP can be obtained using a similar equation:

$$I_{MPP} = k_2 I_{sc} \tag{2.19}$$

This method is simple to implement and does not require high performance microcontrollers or digital processors, and thus can reduce the system cost. However, the MPP is not always located at the region with the same percentage of the open circuit voltage under different environmental conditions. Thus setting a constant proportion value

for all environmental conditions will cause power losses. In addition, this method fails to track the global MPP when the PV system is working under partial shading conditions.

2.2.4 Bisection search theorem (BST)

The bisection search theorem uses a bracketing method to shorten the search range by half at each step so that the midpoint of the successive range gets close to the root of the equation, $y = f(x) = 0$. This method is based on the intermediate value theorem that if a continuous function has values of opposite sign within an interval, then it has a root in that interval. For example, we assume that the function $y = f(x)$ is valid within an interval $[a, b]$ which contains a root x^* of $f(x)$. The value of the midpoint c in the range of $[a, b]$ is $f(c)$. The criteria for the direction of movement in the next halving step is as follows (as shown in Fig. 2.10): (1) If the function value $f(c)$ of the midpoint c and $f(a)$ have the opposite sign ($f(a) \times f(c) < 0$), then the root lines in $[a, c]$ which becomes the range for the next halving. (2) If $f(a) \times f(c) > 0$), then the root must line in $[c, b]$. (3) If $f(a) \times f(c) = 0$, then c is the root. This process continues until the range is shortened to be small enough to approximate the final solution. The convergence speed to the final solution is obtained as $(b\text{-}a)/2^n$, where n is the number of halving steps.

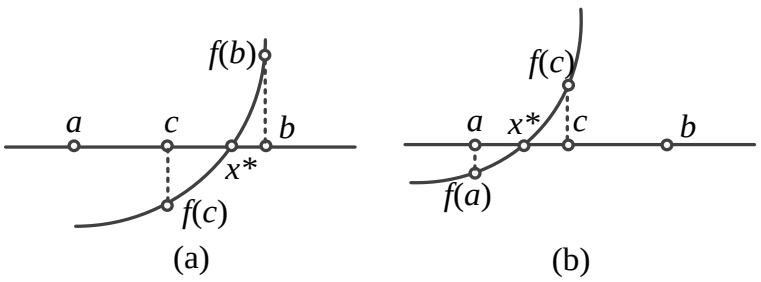

Fig. 2.10 The decision process for bisection search. (a) When $f(c)$ and $f(b)$ have negative sign, then the root of $f(x) = 0$ lies in $[c, b]$. (b) When $f(a)$ and $f(c)$ have negative sign, the root of $f(x) = 0$ lies in $[a, c]$.

In the case of MPPT for the PV system, the power change $\Delta P_{pv} = f(V_{pv})$ can be considered as the function and the root V_{mpp} lies in the range $[0, V_{oc}]$ at the beginning of search. Note that the duty ratio of the converter (D) which is the ratio between the time interval when the power switch is active (explained in detail in Chapter 4) and the sampling period and the current of the PV array (I_{pv}) can also be considered as the control variable x. This search method can track the MPP relatively fast, within a few steps [67]. However, it is limited to unimodal functions and when applied to MPPT for PV systems, it is not suitable for the case with multiple peaks on P-V characteristic curve, such as occur during partial shading.

2.2.5 Three point MPPT method

In this algorithm, three continuously measured points on the P-V curve are compared at each step [52]. These three points include the power value at the current operating point $P(k)$, and the two previous steps $P(k\text{-}1)$ and $P(k\text{-}2)$. For a PV system with a three point MPPT, the voltage of the next step is set by the rules given in Table 2.2. These three points are compared with each other after each perturbation. With these rules, the operating point can move close to the MPP. The advantage of this technique is that it is simple to implement. However, system noise has a significant influence on the accuracy of this technique and the tracking speed is similar to that of the conventional P&O method with a fixed step. In addition, this method is only appropriate for uniform irradiance conditions.

Table 2.2. The rule of comparison in the three point MPPT [52].

Rule number	Comparison of three points	Voltage for next step
1	P(k) > P(k-1) and P(k-1) >P(k-2)	Increase
2	P(k) < P(k-1) and P(k-1) < P(k-2)	Decrease
3	P(k) < P(k-1) and P(k-1) > P(k-2)	MPP
4	P(k) = P(k-1) and P(k-1) < P(k-2)	MPP
5	P(k) = P(k-1) and P(k-1) > P(k-2)	MPP
6	P(k) = P(k-1) and P(k-1) = P(k-2)	MPP
7	P(k) > P(k-1) and P(k-1) = P(k-2)	MPP
8	P(k) < P(k-1) and P(k-1) = P(k-2)	Decrease

2.2.6 Variable step size incremental resistance (INR)

As described in the standard P&O and IncCond methods, a large step size result in a fast tracking speed but also large oscillations around the MPP. A small step size will reduce the oscillations around the MPP but will result in a slow tracking speed. It is difficult to make a tradeoff between the oscillation size and the tracking speed. This problem can be solved by adding a variable step to P&O and IncCond. The basic idea of these modified algorithms is that when the working point is far away from the MPP, a large iterative step can be applied to accelerate the tracking speed according to the power gradient or the slop of the P-V curve. When the operating point is moving to the proximity of MPP, small steps can be implemented to reduce the oscillation. The step size can be varied in following ways [68]:

$$D(k) = D(k-1) \pm N\frac{\Delta P}{\Delta I} \tag{2.20}$$

$$D(k) = D(k-1) \pm N\frac{\Delta P}{\Delta V} \tag{2.21}$$

$$D(k) = D(k-1) \pm N \frac{\Delta P}{\Delta D} \tag{2.22}$$

$$D(k) = D(k-1) \pm \alpha \Delta P \tag{2.23}$$

where N is a scaling factor that determines the performance of the MPPT system and is set during the tuning process. Here, ΔP, ΔI, ΔV and ΔD are the change of power, current, voltage and duty ratio in the previous sampling period, respectively. In Eq. (2.23), α is a constant value to control the movement toward the MPP and the convergence accuracy [69]. The technique for tuning the parameter N is discussed in depth in [70].

With this variable step size perturbation strategy, the tracking speed can be greatly improved. However, for partial shading conditions, it is unable to accurately track the global MPP and for rapidly changing irradiance conditions, it has difficulty tracking the varying MPP.

2.2.7 Extremum seeking control (ESC) and ripple correlation control (RCC)

Extremum seeking control (ESC) uses the fact that the switching actions in the power converter can cause voltage and current ripples on the PV array [71]. Thus, the induced ripple in the power can be controlled to perform the MPPT. A simplified block diagram of applying ESC to MPPT with external current perturbation is shown in Fig. 2.11, where the current of the PV array is the control variable. The voltage of the PV array can also be used as the control variable. The external current perturbation effect propagates to the power output $p(t)$. The input $\varepsilon(t)$ is provided by multiplying the perturbation signal and the time derivative of the power output. The resulting portion ρ is extracted by a high pass filter which attenuates the nonzero average or offset of the power output $p(t)$. The sign of $p'(t)$ is positive on the left side of MPP and negative on the right side of MPP. The integration of $\varepsilon(t)$ can further eliminate the higher order harmonics.

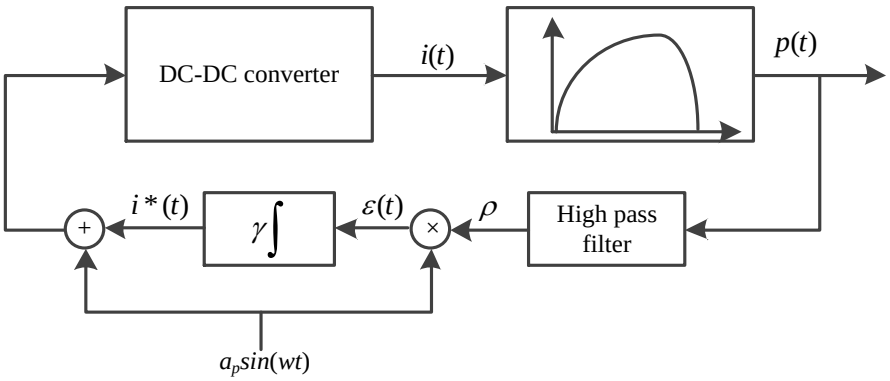

Fig. 2.11 ESC applied in MPPT with external perturbation source.

In RCC, the time derivative of the time-varying array power (p') is correlated with the time derivative of the time-varying PV array voltage (v') or current (i') to drive the system to MPP. In fact, the variation in dp/dv is used to change the duty ratio of the power converter. Since dp/dv cannot be obtained directly from the measurement of the circuit. The following law has the same effect as dp/dv:

$$d(t) = k\int \dot{p}\dot{v}dt \tag{2.24}$$

where k is the constant gain which is negative when using voltage control and a boost converter. Generally, the derivatives in (2.24) are not available but they can be realized by a high pass filter with a cutoff frequency higher than the ripple frequency. Fig. 2.12 shows the practical implementation process of RCC for MPPT. Since direct usage of differentiation amplifies circuit noise in the measurement of the power value, the sign of the integrand is sufficient for a unimodal function. Thus, it can be simplified as:

$$d(t) = k\int sign(\dot{p}) \cdot sign(\dot{v})dt\ . \tag{2.25}$$

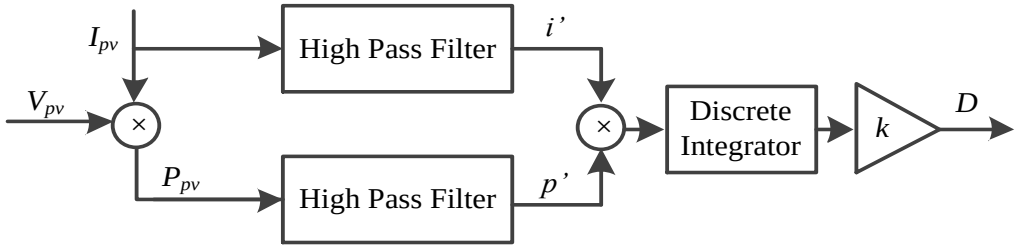

Fig. 2.12 Block diagram of the implemented RCC in MPPT.

Both RCC and ESC utilize perturbations to evaluate the objective function gradient and thus lead to the optimum operating point. The advantage of these techniques is that the tracking speed is as high as the order of the switching frequency of the power converter. The difference of these two similar techniques is that RCC uses high frequency inherent ripple, whereas ESC uses injected or inherent relatively low frequency perturbations. The disadvantages are that the performance of the system can be easily influenced by the electromagnetic interference and signal measurement noise. The perturbation frequency, the parameters for the high pass filter and the constant gain are not so easy to set. Moreover, the reactive parasitic elements such as output shunt capacitance and series inductance can influence the overall algorithm efficiency. In [72], the equilibrium point reached by the RCC considering both pure sinusoidal excitation and realistic distorted AC signals, and the effects of the shunt parasitic capacitance and series parasitic inductance in terms of equilibrium point and dynamic response are investigated. The results show that when the frequency of the converter is set too high, the effects of these reactive parasitic components can lead to large errors in the PV system using RCC based MPPT. In [73], the

multivariable control with Newton based ESC, which treats the entire module cascade as the control objective, is proposed for the distributed PV systems where each PV module is equipped with an MPPT. This method reduces the effect of Hessian which is subject to the variability of weather conditions such as irradiance and temperature and influences the convergence rate of gradient based designs. However, the design process is onerous and the computational complexity is very high.

2.2.8 DC link capacitor droop control

DC link capacitor droop control is only applicable to two stage PV systems containing both a DC-DC converter and a DC-AC inverter. The bus voltage (V_{link}) between the DC-DC converter and DC-AC inverter is kept constant. Increasing the current drawn from the DC-DC converter causes an increase in the power output from the PV array. When the power demand by the inverter exceeds the maximum power available from the PV array, the bus voltage V_{link} will droop [74]. That means that at the moment when the bus voltage (V_{link}) starts to droop, the PV array is operating at MPP. Thus, by observing the bus voltage (V_{link}) droop between the DC-DC converter and DC-AC inverter, the maximum point of PV array can be obtained. The advantage of this method is that it does not require the computation of the PV array power and it can be easily implemented using an analog circuit. However, the response of the system deteriorates compared to methods with direct power measurement due to the performance dependence on the response of the DC voltage control loop in the inverter [10].

2.2.9 Temperature based MPPT

This method uses the fact that the output voltage of a PV array is proportional to the temperature on the PV array surface [75, 76]. The relationship between the optimal voltage and the measured temperature is given by:

$$V_{mpp}(T) = V_{mpp}(T_{ref}) + K_{oc}(T - T_{ref}) \tag{2.26}$$

where T and T_{ref} are the measured and reference temperature respectively. $V_{mpp}(T)$ and $V_{mpp}(T_{ref})$ are the optimal voltage value at the MPP with temperature T and T_{ref} respectively. K_{oc} is the temperature coefficient of voltage which can be obtained from the datasheet. Thus using Eq. (2.26), the optimal voltage at MPP can be easily calculated online. In this method, only a single temperature sensor is required and the implementation is simple. However, this method suffers from nonuniform distribution of the temperature on the PV module. In addition, since the temperature usually responds slowly to irradiance changes, it is unable to track rapid irradiance changes, resulting in a power loss.

2.2.10 Variable inductor MPPT

This method uses the maximum power transfer theorem, that is, the PV array outputs maximum power only when the resistance of the PV panel is equal to the resistance of the load. The DC-DC converter, which can be a buck or boost type, is connected between the PV array and the load, working in continuous mode so that the relationship between the input (R_{in}) and output resistance (R_{out}) of the converter (taking buck converter as an example) satisfies the following equation:

$$R_{in} = \frac{1}{D^2} R_{out} \tag{2.27}$$

where D is the duty ratio of the buck converter which is adjusted to shift the operating point of the PV system to the MPP. In order to keep the converter working as a continuous current mode, the conductance value of the inductor should be greater than the minimum inductance value. As shown in Fig. 2.13 [77] only an inductor with an inductance value larger than the dashed line can work in continuous mode. When the inductance value is set to a constant value, for instance L_1 as shown in Fig. 2.13, continuous current mode can only work when the load is larger than I_{o1}. We can also see that the minimum inductance requirement for the load current at I_{o2} is only L_2 which is much smaller than the constant inductance L_1. In this case, an inductor with a small size would be sufficient for the converter to work as a continuous mode [77].

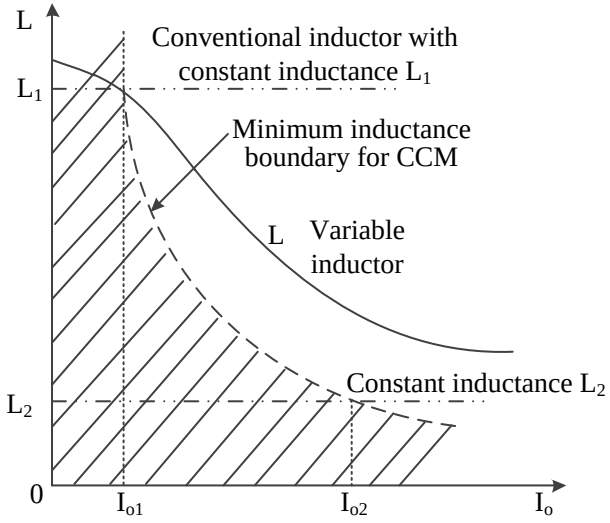

Fig. 2.13 The characteristic of the variable inductor and the minimum inductance boundary for CCM.

Since the inductance of the variable inductor dynamically changes with the change of the current as shown in Fig. 2.13, a variable inductor can be used in the converter. For the variable inductor, a current increase can induce a decrease in the inductance of the inductor which is just as the requirement of the inductance for the converter to work as a continuous current mode. This variable inductance can be achieved using a sloped air-gap

(SAG). With this technique, the size of the inductor can be largely reduced and the load range can be increased. However, this method requires prior knowledge of the PV array characteristics to get the settings for the variable inductor and it does not work for partial shading conditions.

2.2.11 Parasitic capacitance MPPT

Parasitic capacitance MPPT can be regarded as an extended version of the IncCond method. In this method, the parasitic junction capacitance C_{pv}, which models charge storage in the p-n junction of the solar cells, is taken into consideration. The parasitic capacitance is modeled as a capacitor connected in parallel with the solar cell. It increases the effective capacitance of the entire PV array. By adding parasitic junction capacitance into the modeling process, the current in the solar cell model is written as[78]:

$$I_{pv} = I_L - I_o[\exp(\frac{V_{pv} + R_s I_{pv}}{V_t}) - 1] - \frac{V_{pv} + R_s I_{pv}}{R_p} - C_{pv}\frac{dV_{pv}}{dt} = F(V_{pv}) - C_{pv}\frac{dV_{pv}}{dt} \quad (2.28)$$

.

The first term on the right hand of the equation is a function of the voltage and the second term represents the current of the parasitic capacitance. By rearranging (2.28), it can be rewritten as [78]:

$$F(V_{pv}) = I_{pv} + C_{pv}\frac{dV_{pv}}{dt} \quad (2.29)$$

$$\frac{dF(V_{pv})}{dV_{pv}} + \frac{F(V_{pv})}{V_{pv}} = \frac{dI_{pv}}{dV_{pv}} + \frac{I_{pv}}{V_{pv}} I_{pv} + C_{pv}(\frac{\dot{V}_{pv}}{V_{pv}} + \frac{\ddot{V}_{pv}}{\dot{V}_{pv}}) = 0. \quad (2.30)$$

When the parasitic capacitance is neglected, the third component of (2.30) is zero. Then this equation simplifies to the IncCond algorithm described previously. In this method, the first and second derivative of the PV array voltage is used for maximum point tracking. By taking parasitic parameters into consideration, the tracking accuracy of the MPP is better than the original IncCond algorithm. However, as in IncCond, this method does not work for PV systems with multiple peaks on the P-V curve.

2.2.12 dP - P&O method

The dP-P&O algorithm is proposed to improve the tracking ability of the conventional P&O algorithm, which is unable to accurately track the MPP under rapidly changing irradiance condition. In this technique, an additional measurement of the power value between two sampling points without any perturbation is performed, as described in
Fig. 2.14. The change in power between P_m and P_k only reflects an irradiance change as P_m is measured at the same impedance operating point at this time instant, while the power difference between P_m and P_{k-1} includes both the power changes caused by an irradiance

change and the perturbation of the operating point. Therefore, when we assume a constant rate of change in the irradiance during one MPPT sampling period, the power change induced by MPPT perturbation is computed as:

$$dP = dP_1 - dP_2 = (P_m - P_{k-1}) - (P_k - P_m) = 2P_m - P_k - P_{k-1} \tag{2.31}$$

where P_1 is the power change between the two points (P_m and P_{k-1}) as shown in Fig. 2.14, and dP_2 is the power change between the current operating point (P_k) and the middle measured point (P_m).

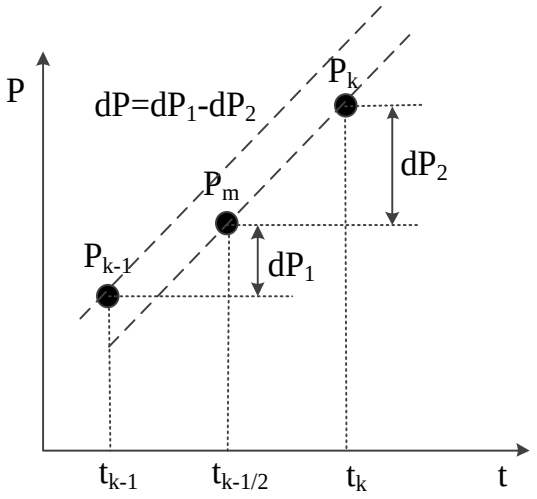

Fig. 2.14 Additional measurement of power point between two perturbation points.

This method has a simple implementation structure and does not need additional hardware devices, just a modification of the original P&O algorithm in software. This technique is improved for rapidly changing irradiance conditions, but for PV systems with multiple peaks on P-V curve, it still cannot track the global MPP.

2.2.13 Load line MPPT

The load line MPPT moves the operating point to the vicinity of the global maximum first and then applies a conventional MPPT method such as P&O or IncCond to search for the global MPP within the local area. The vicinity of the global MPP is calculated by the intersection of the load line under uniform irradiance conditions and the I-V curve under nonuniform irradiance conditions. There are two types of load line MPPTs in the literature. Type I is based on the intersection between the load line of the MPP P_1 as shown in Fig. 2.15 and the I-V curve under partial shading conditions [79]. In this method, when the shading occurs, the working point moves to the intersection point C and then shifts to the optimal point P_2 using a conventional MPPT method. The direction of movement of the operating point for this method is P_1-C-P_2. Type II [12] is slightly different from the type I. In this method, the load line is formed by P_0 as shown in Fig. 2.15, which is given by:

$$R_{load} = \frac{N_{ss} V_{oc}}{N_{pp} I_{sc}} \tag{2.32}$$

where N_{ss} is the number of PV modules connected in series in the PV string and N_{pp} is the number of PV strings connected in parallel in the PV array. When the irradiance condition changes from uniform to nonuniform, the direction of movement of the operating point is P_1-A-B-P_2.

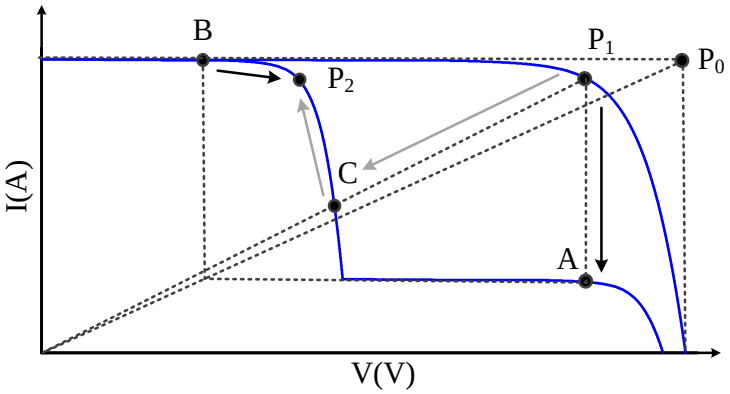

Fig. 2.15 The shift in operating point under partial shading conditions using load line based MPPT, where the locus P_1-C-P_2 is for type I and P_1-A-B-P_2 is type II.

These two methods all can be easily implemented in hardware. However, the technique is unable to ensure that the intersections for both methods are located in the vicinity of the global MPP for all shading patterns. When applied in a large-scale PV system, which may lead to complex local peaks on the P-V curves, the load line technique may result in a large power loss.

2.2.14 Dividing rectangles (DIRECT)

This method is the extension of the Lipschitz optimization based method [80]. It samples at the midpoint of the search space. It requires no knowledge of the Lipschitz constant or the objective function to be Lipschitz continuous [80]. Instead, it uses all possible values to determine whether an interval should be broken into three subintervals during the current iteration. For the uniformly bounded fitness function $P(v)$, with voltage as the control variable, the following is obtained [81]:

$$P(v) \le \max(P(v)) \le P(v_1) + M \frac{b-a}{2} \tag{2.33}$$

where v_1 is the center of the range [a, b], M is the maximum value of the gradient value $\partial P / \partial V$ within the range of [a, b]. At each step, the search range found by the previous iteration, which is called potentially optimal hyper-rectangles, is divided into three equal subintervals. The potentially optimal hyper-rectangles are chosen based on the criteria that if there exists a constant $k > 0$ such that [81]:

$$P(v_i) + k\frac{b_i - a_i}{2} \geq P(v_j) + k\frac{b_j - a_j}{2}, \forall j \tag{2.34}$$

$$P(v_i) + k\frac{b_i - a_i}{2} \geq P_{\max} + \varepsilon|P_{\max}| \tag{2.35}$$

where v_i is the center of the hyper-rectangle i, and the parameter ε is used so that $f(c_j)$ exceeds the current best solution by a non-trivial amount. In the iteration process, there may be more than one potentially optimal hyper-rectangle identified. Once these potential intervals are found, they are divided into three subrectangles along the maximal length dimension. This process is repeated until the maximum number of function evaluations or iterations reached. In [81], this method can increase the power output and the tracking efficiency is measured to be above 95%.

DIRECT has the ability to track the global MPP under partial shading conditions efficiently and can easily be implemented with an inexpensive microcontroller. Voltage and current sensors are required to measure the voltage and current values of the PV array. However, the performance of the algorithm is significantly influenced by the initial point and the control parameters in the algorithm. When inappropriate control parameters are chosen for the algorithm, it may direct the system to work at a local MPP.

2.2.15 Fibonacci search MPPT

Fibonacci search MPPT is one of the efficient bracketing search methods. It uses the Fibonacci number sequence to iteratively narrow down the search range so that the final search range is short enough to get close to the optimal point. The original Fibonacci line search is an optimization technique which is generally used for single-dimensional and unimodal functions. The golden ratio search method is a specific condition of the Fibonacci search method. The Fibonacci numbers are defined as the following sequence [82]:

$$F_0 = 0;\ F_1 = 1;\ F_2 = 1;\ F_n = F_{n-1} + F_{n-2},\ n = 2,\ 3,\ 4,\ \ldots \tag{2.36}$$

Thus the Fibonacci numbers are sequences of 0, 1, 1, 2, 3, 5, 8, 13, 21, 34, 55, … . For a minimum problem min$f(x)$, the final optimal point of the function can be approximated by gradually shortening the search range of the problem. The shift direction during the search process is decided by the evaluation of the function at two check points in the range. Assuming the function is unimodal in the interval [a, b], as shown in Fig. 2.16. The new interval is updated with the following rules:

$$\text{If } f(x_1) <= f(x_2), \text{ then } b = x_2;\ x_2 = x_1;\ x_1 = b + \frac{fib(n-1)}{fib(n)}(a-b) \tag{2.37}$$

$$\text{If } f(x_1) > f(x_2), \text{ then } a = x_1;\ x_1 = x_2;\ x_2 = a + \frac{fib(n-1)}{fib(n)}(b-a) \tag{2.38}$$

where *fib*(*n*) is the Fibonacci number of *n*th order. Thus, by repeating this process, the search range will finally be short enough so that the middle point of the final range is close to the minimum point.

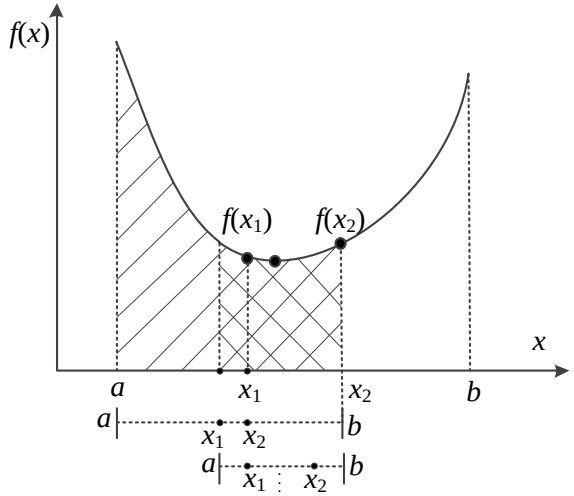

If $f(x_1)<=f(x_2)$, then the new search range $[a, b] = [a,x_2]$.
If $f(x_1)>f(x_2)$, then the new search range $[a, b] = [x_1,b]$.

Fig. 2.16 The shift direction of the Fibonacci search algorithm.

When this technique is applied to the MPPT problem, the variable *x* can be considered as the voltage/current output of the PV array or the duty ratio of the power converter. The power output calculated by multiplying the measured current with voltage is considered as the fitness/evaluation value for the Fibonacci search algorithm. This method has a fast convergence speed and does not require temperature and irradiance measurements or prior knowledge of the PV array configuration. However, it does not always converge to the global MPP under all shading patterns as using the original Fibonacci algorithm may result in the MPP moving outside of the search range due to a sudden irradiance change. An improved Fibonacci search method in [83] was proposed to widen the search range if the shift is in the same direction for a certain number of iterations. This method improves the search algorithm under sudden irradiance change. However, it still cannot guarantee tracking the global MPP under all the partial shading patterns.

2.2.16 State space based MPPT

In this method, the switching-averaged model [84] is used to model the PV system as a nonlinear time-varying system. By applying MPP conditions in the controller design, the MPPT problem is reduced to an ordinary problem of dynamic system stability in state space. In [84], the time varying dynamic feedback controller is applied to make sure the closed-loop system is asymptotically stable. This method is robust to parameter changes of

the PV system and the disturbance from the load. However, this method is system specific. Moreover, it has a complex design procedure and requires more sensors.

2.2.17 Voltage window search (VWS)

In this method, the power operating triangle (POT) method [85] is used to narrow down the search range in order to find the global MPP. A POT is defined on the P−V curve by the voltage axis and two straight lines, namely a constant voltage ($0.9V_{oc}$) and a constant current as shown by the dashed lines in Fig. 2.17. In [85], $V_{max} = 0.9V_{oc}$ is considered as the constant voltage line, which is also the upper limit of the search range. A variable P_{store} is used to store the maximum power measured in the search process. At the beginning, an arbitrary starting operating point with a power value of P_Q is chosen to be the starting point (see Fig. 2.17) and is assigned to P_{store}. The first voltage window (POT_{STC}) is defined by the POT under the standard test condition. The lower search limit of the new voltage window is defined as $V_{minSTC} = P_{store}/I_{sc}$. Thus, the search range of the new voltage window is $[V_{minSTC}, V_{max}]$. Consequently, the power at point 1 (P_1), which is computed by $V_{min1} = P_{store}/I_1$, is checked. If P_1 is smaller than the stored maximum power P_{store}, $P_1 < P_{store}$, then calculate the voltage points $V = V_1 + k\,\Delta V_{step}$; $k = 1, 2, \ldots$, and choose the minimum voltage falling inside the new voltage window (V_{min} lines in $[V_{min1}, V_{max}]$). The new voltage window changes to $[V_{min1}, V_{max}]$. Point 2 is then calculated to be the point with the minimum voltage within $[V_{min1}, V_{max}]$. Then, the power at point 2 (P_2) is checked. From Fig. 2.17, P_2 is still smaller than the stored maximum power value P_{store}, so the new voltage window is then updated to $[V_{min2}, V_{max}]$. Again, the voltage points from P_2 is continuously computed $V = V_2 + k\,\Delta V_{step}$, where $k = 1, 2, \ldots$ and P_3 is calculated to be the minimum voltage inside the new voltage window (POT_2). Since the power value of P_3 is larger than the stored maximum point P_{store}, the value of P_{store} is then replaced by the power value of point P_3 ($P_{store} = P_3$). Thus, the algorithm continues to check the next voltage values $V_j = V_{j-1} + \Delta V_{step}$, ($j = 4, 5$). The stored maximum power value is updated whenever there is a measured higher power value. In Fig. 2.17, point 4 is measured as the maximum power value. Since $P_5 < P_4$, a new POT_5 is generated. Thus, the new voltage window is defined within $[V_{min5}, V_{max}]$. Again, the voltage points from P_5, $V = V_5 + k\,\Delta V_{step}$ where $k = 1, 2, \ldots$, are computed. Whereas, V_6 is calculated to be outside of the search range. Therefore, all the points on the right side of the V_{max} are skipped. Finally, the global search process ends and a

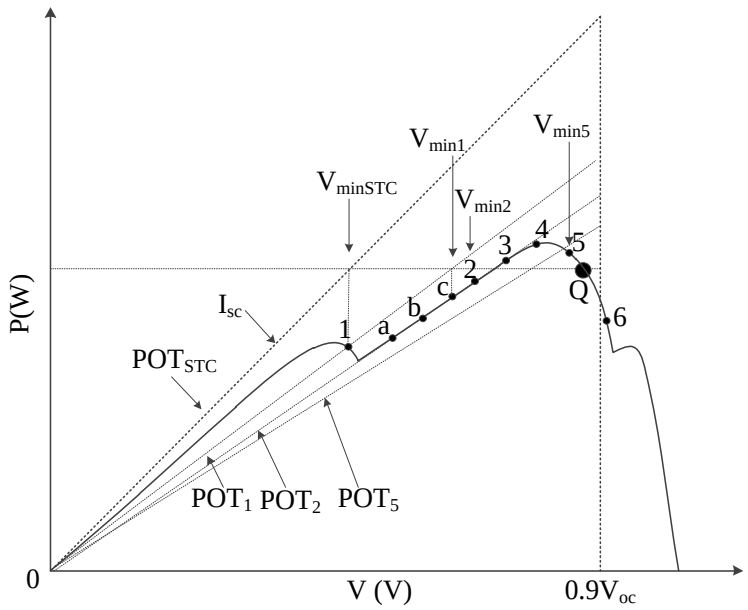

Fig. 2.17 The operation process of the VWS algorithm with narrowing POT iteratively on the P-V curve.

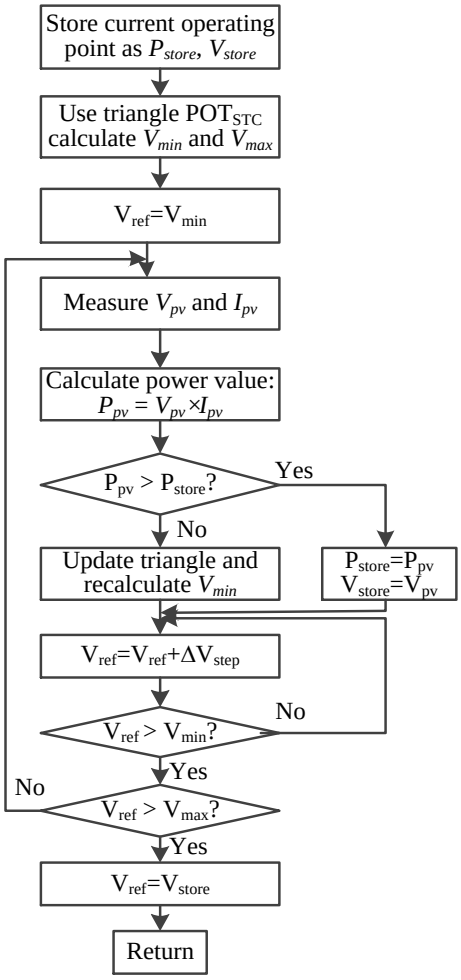

Fig. 2.18 Flowchart of the voltage window search algorithm.

conventional MPPT such as P&O or IncCond is then used to track the global MPP around the area of the stored optimal point P_4. The flowchart of the VWS algorithm is shown in Fig. 2.18. It is a subroutine of the entire global search process and is usually combined with the P&O algorithm.

The author indicated that the tracking ability of the proposed method does not depend on the choice of the initial operating point. However, it may fail to track the global MPP under rapidly changing irradiance conditions. In addition, its tracking speed largely depends on the choice of the initial point because when the power of the initial point is too low the search scheme will be similar to the P&O with a fixed step size and it may converge to the local MPP.

2.2.18 Evolutionary algorithm based MPPT

2.2.18.1 Particle swarm optimization (PSO)

The particle swarm optimization (PSO) algorithm was invented by Russell Eberhart and James Kennedy in 1995 [86]. It is a biologically inspired population based algorithm motivated by the flocking patterns of birds and fish. Originally it was used to simulate birds flocking around food sources and later was found to be an efficient technique to solve multivariable nonlinear optimization problems. The population consists of a set of potential solutions, which are also called particles. The particles in the population evolve from generation to generation so that the optimum solution to the nonlinear problem is obtained. Each particle has two variables for the movement: velocity v_i^k and position s_i^{g+1}. The movement of the particles is affected by the global best position among all the particles and its personal best position. Each particle shares information in the search process. The velocity and position of each particle is updated according to the following equations [54]:

$$v_i^{g+1} = wv_i^g + c_1 r_1 p_{best}^i + c_2 r_2 g_{best}^g \tag{2.39}$$

$$s_i^{g+1} = s_i^g + v_i^{g+1} \tag{2.40}$$

where v_i^g and s_i^g are the velocity and the position of the i^{th} particle at gth generation, respectively; c_1 and c_2 are two positive constants; w is the inertia weight where a large value favors a global search, while a small value favors a local search; r_1 and r_2 are randomly generated numbers within the (0, 1) interval; p_{best}^i is the personal best position of the i^{th} particle; g_{best}^g is the global best position of all the particles at the current g^{th} generation. A constraint v_{max} is usually imposed on v_i^g to ensure convergence of the algorithm. The value is set to $[-v_i^{max}, v_i^{max}]$, where v_i^{max} is the maximum value of the particle position. This stochastic mechanism adds the diversity to the population, due to its random selection of parameters such as r1 and r2. The stochastic convergence analysis is

provided in [87, 88]. The theoretical and empirical method of selecting these parameters can be found in [87, 89-92].

In [54], PSO based MPPT is proposed for a modular PV system which is controlled by a centralized MPPT. Each PV module is equipped with a DC-DC converter. The voltage across the individual modules (V_1, V_2, …, V_N) is considered as a N-dimensional control variable. The position of the particle at the k^{th} time instant (s^k) is:

$$s^k = [V_1^k, V_2^k, ..., V_i^k, ..., V_N^k] \tag{2.41}$$

where N is the number of PV modules in the system, V_i^k is the voltage of the i^{th} PV module at the k^{th} instant time. The velocity (v) is considered as the voltage difference between two continuous time instants and is written as:

$$v^k = [V_1^k - V_1^{k-1}, V_2^k - V_2^{k-1}, ..., V_i^k - V_i^{k-1}, ..., V_N^k - V_N^{k-1}]. \tag{2.42}$$

The objective function is the summation of the power generated by all PV modules. All the particles in the population are applied in a successive manner. When the maximum generation is reached or the power changes become small enough, the tracking process is considered complete. In [54], the PSO MPPT is tested with a 300W/50V PV system. For the MPPT update period of 0.05s, the time required to track the global MPP is about 2s which means 40 steps (N_{step}=2s/0.05s) for the predefined shading patterns. The results also show the advantage of PSO over the other three MPPTs tested, namely fixed voltage, hill climbing, and Fibonacci search methods. The power output of the PV system using the PSO algorithm under four similar clear days is 8.8%, 3.4% and 10.9% higher than these three methods respectively.

2.2.18.2 Differential evolution (DE)

Differential evolution (DE) is a stochastic evolution strategy based on a direct optimization method. It is capable of solving complex nonlinear and multimodal objective functions without calculating differentiation of the functions. The stochastic analysis of the DE has been investigated in [93]. Similar to PSO, potential solutions in a population with a D-dimensional search space are evolved from generation to generation to find the final optimum solution. The DE scheme consists of three main processes: mutation, crossover and selection. In the evolutionary strategy, DE generates new solutions by the combination of solutions randomly chosen from the current population. This framework incorporates information of neighboring individuals to guide the search towards the global optimum in a more efficient manner. The stochastic selection mechanism is reflected by randomly choosing a solution from the population to generate the new solution. The crucial idea behind this algorithm is the scheme for generating new trial solutions for the population. Basically, a new solution is generated by adding the weighted difference

between two vectors chosen randomly from the current population to a third vector, represented by:

$$V_i^g = X_{best}^g + F(X_{r_1}^g - X_{r_2}^g) \tag{2.43}$$

where $r_1 \neq r_2 = \{1, 2, \ldots, N_p\}$ are randomly generated integers respectively, X^g_{best} is the vector with the best fitness value among the individuals, X^g_{r1} and X^g_{r2} are two vectors selected randomly among the population, $F \in (0, 2]$ is the scaling factor which determines the amplification of the differential variation and V_i^g is the velocity vector which is represented by $[v^g_{i,1}, v^g_{i,2}, \ldots, v^g_{i,D}]$. For the mutation scheme, the strategies described in [94] can also be used in DE. The crossover process is introduced to increase the diversity of the population and is realized by accepting the mutated vector according to a stochastic probability. When the variable, randomly generated with uniform probability distribution, is not greater than CR ($0 < CR < 1$), the j^{th} component of the mutant vector is accepted. Otherwise, this mutated vector is rejected and the original component remains. Consequently, after the crossover operation the trial vector is generated and it is given by:

$$u_{i,j}^g = \begin{cases} v_{i,j}^g, & \text{if } (rm_{i,j}^g \le CR) \text{ or } j = rm_{i,j}^g \\ x_{i,j}^g, & \text{if } (rm_{i,j}^g > CR) \text{ and } j \neq rm_{i,j}^g \end{cases}, \quad (i = 1, 2, \cdots, N_p, \quad j = 1, 2, \cdots, D) \tag{2.44}$$

where $u^g_{i,j}$ is a component of $U_i^g = [u^g_{i,1}, u^g_{i,2}, \ldots, u^g_{i,D}]$. After the crossover operation, whether the generated trial vector is accepted to be a member of the offspring in the next generation (the $(g+1)^{th}$ generation) is based on the following selection criteria:

$$X_i^{g+1} = \begin{cases} U_i^g, & \text{if } \mathit{fitness}(U_i^g) < \mathit{fitness}(X_i^g) \\ X_i^g, & \text{otherwise} \end{cases}. \tag{2.45}$$

For a minimization problem, the generated trial vector will be accepted as one of the particles in the next generation only when the fitness value of the trial vector, $\mathit{fitness}(U_i^g)$, is smaller than that of the original vector, $\mathit{fitness}(X_i^g)$. Otherwise, it is rejected and the original vector is retained. The above update processes are repeated until all the particles are updated or the stop criteria is satisfied. The stop criteria can be when the fitness function value reaches a predefined minimum limit (ε_p) or when the maximum number of generations (G_{max}) is achieved. Finally the best solution with the minimum fitness value is obtained in the last iteration step.

When applying this optimization algorithm into MPPT, the control vector (X) can be considered to be the voltage, current or duty ratio of the converter connected to the PV arrays in the two stage inverter. With the above process, the global MPP can be obtained [95, 96] for various shading patterns. However, the performance of the algorithm significantly depends on the control parameters set by the user, such as the crossover rate (CR) and scaling factor (F).

2.2.18.3 Genetic algorithms (GA)

Genetic algorithms (GA) are inspired by Darwin's theory of evolution. The solution is represented to the problem as a chromosome. Like population based evolution algorithms such as PSO and DE, the solutions are updated from generation to generation so that better solutions can be included in the population. In this update procedure, there are four main operators: selection, crossover, mutation and acceptance. The basic implement of GA is as follows.

Step 1: *Initialization*. Generate a random population of *n* chromosomes.
Step 2: *Evaluation*. Evaluate the fitness value for the generated population.
Step 3: *Generation of a new solution.* The new solutions in the population are generated by following steps.
  Step 3.1: *Selection*, Choose two parent chromosomes from the current population according to the fitness value.
  Step 3.2: *Crossover*. The parents are crossed over to generate the new offspring according to a crossover probability. The uncrossed parents are passed to the new generation directly.
  Step 3.3: *Mutation*. The new offspring is mutated with a mutation probability to increase the diversity of the population.
  Step 3.4: *Acceptance.* The newly generated offspring are put together to form the new population.
Step 4: If the termination condition is satisfied, terminate the search process.
Step 5: Otherwise, return to Step 2 and repeat the above processes in Step 3.

GA can be applied to MPPT in a number of different ways, such as using GA to optimize a fuzzy logic controller for the MPPT or in the direct search for the MPP using GA. For example, in [97], GA is directly applied to MPPT. However, due to the slow search process of GA, the tracking speed is limited. Therefore, GA is usually used by combining with other computational intelligence based methods. In [98], a model, which is represented by a radial basis function neural network trained by genetic algorithm, is used to predict the MPP for a grid connected PV system. The measured irradiance and temperature levels are considered as inputs to the neural network. The current and voltage values at the MPP are directly predicted using a radial basis function neural network which is trained by GA. The combined method usually provides good accuracy and tracking speed. However, it has the same disadvantages as the original neural network method before combination.

2.2.19 Fuzzy logic (FL)

The FL MPPT controller consists of three stages: fuzzification, inference with rule base, and defuzzification as shown in Fig. 2.19 [99]. As fuzzy logic is able to process incomplete data and provides an approximate solution to the problem that other methods find difficult to solve, it can be used in MPPT.

The control inputs with crisp values, as shown in Fig. 2.19, are transformed into fuzzy sets in the fuzzification block, according to the membership function in Fig. 2.20. The membership function and the rule base contain the modeling information about the system is the basis for the inference process. After going through the reasoning process with the rule base as shown in Table 2.3 [10] and the inference mechanism, the control output is generated by the defuzzification block, which converts an output fuzzy set back to a crisp value using defuzzification methods, such as center of singleton method (COS), center of gravity method (COG), maximum methods [99] and so on.

Usually, the input variables to the Fuzzy controller for MPPT are the error E and the variation of the error ΔE. The definitions of E and ΔE depend upon the user. For example, Khaehintung et al. consider the derivative of power in terms of the voltage (dP/dV) as the error E, and the change of this variable is ΔE [58].

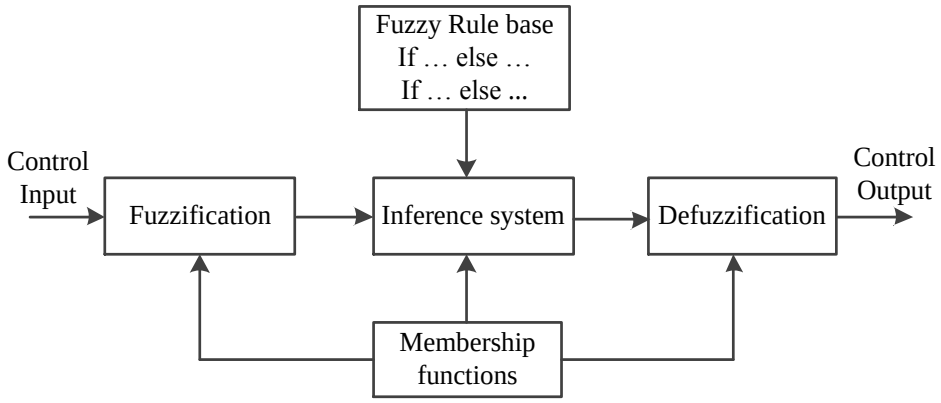

Fig. 2.19 A typical structure of the fuzzy system.

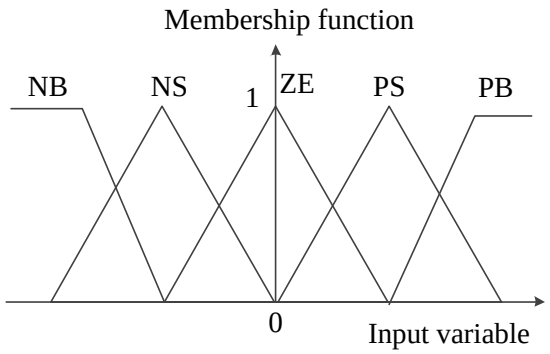

Fig. 2.20 Membership function [10].

Table 2.3. Fuzzy rule base table [10]

ΔE / E	NB	NS	ZE	PS	PB
NB	ZE	ZE	NB	NB	NB
NS	ZE	ZE	NS	NS	NS
ZE	NS	ZE	ZE	ZE	PS
PS	PS	PS	PS	ZE	ZE
PB	PB	PB	PB	ZE	ZE

The advantage of the fuzzy logic controller based MPPT is that it performs well under varying weather conditions. Some other modified fuzzy logic control methods [100-102], which adaptively change the membership functions or the fuzzy rule base, are also proposed to make the MPPT algorithm more adaptive to the changing conditions. However, the fuzzy rule, which depends on the algorithm developer's experience, largely influences the MPPT performance. In addition, most of the existing fuzzy rules are based on the error in the derivative of the power in terms of the voltage, and have similar disadvantages to the IncCond algorithm.

2.2.20 Look up table

The look up table based method stores prior knowledge of the PV array characteristics determined off line under various environmental conditions, including temperature, irradiance and different materials used in the PV modules. This method can directly determine the optimal point of the PV system by checking the table values (filled with voltage and current data points generated under various atmospheric conditions [103]). It has a simple structure and a fast tracking speed. However, the system requires a large memory capacity due to the large amount of I-V data required before running the MPPT system. This prior data can be difficult to acquire, especially for varying atmospheric conditions. In addition, when the characteristics of the PV module changes due to the aging process, this method does not provide good tracking accuracy.

2.2.21 Curve fitting

The curve fitting method [104, 105] finds the MPP by continuously sampling and fitting the characteristic P-V curve for the PV module every several millisecond. It requires the model of the PV array, which could be the single/two diode model. However, due to the complex process of solving nonlinear equations, $V = I(V)$, representing the characteristic of the PV generator, the polynomial equation is usually used for calculating the MPP. For example, the P-V characteristic of the PV generator is given by [105]:

$$P_{pv} = aV_{pv}^3 + bV_{pv}^2 + cV_{pv} + d \tag{2.46}$$

where *a*, *b*, *c* and *d* are the coefficients of the polynomial model which can be obtained by sampling several operating points of the PV array. Then the optimal point of the PV array voltage is calculated by:

$$V_{mpp} = -b\sqrt{b^2 - 3ac}\,/\,3a\,. \tag{2.47}$$

To adapt to environmental changes, this process is conducted every few milliseconds to find the MPP for different environmental conditions. The advantage of this method is that it has a simple tracking process and can produce a relatively accurate value of the optimum point. However, due to the continuous calculation of the parameters for the model during the tracking process, a large memory is required. Moreover, prior knowledge of the adaptive model of the PV array is also needed.

2.2.22 Artificial neural network (ANN)

Since the ANN can be utilized for approximation of non-linear functions, it provides a good solution for the complex problem of MPPT in PV systems, especially under partially shaded and rapidly changing conditions [53, 102]. Many ANN based MPPTs have been studied [53, 106-109]. The basic idea of the ANN used in MPPT for PV systems is to predict the optimal output current (or voltage) based on the measured meteorological irradiance and temperature conditions. A typical structure of the MPPT controller based on an ANN is shown in Fig. 2.21. The ANN predicts the optimal voltage (V_{mpp}^{*}), the optimal current (I_{mpp}^{*}) and the maximum power (P_{mpp}*) for PV arrays from the sensed input variables, such as irradiance and temperature. Before using an ANN to predict the optimal values of voltage, current or power for PV arrays, the network needs to be trained with previously measured training data.

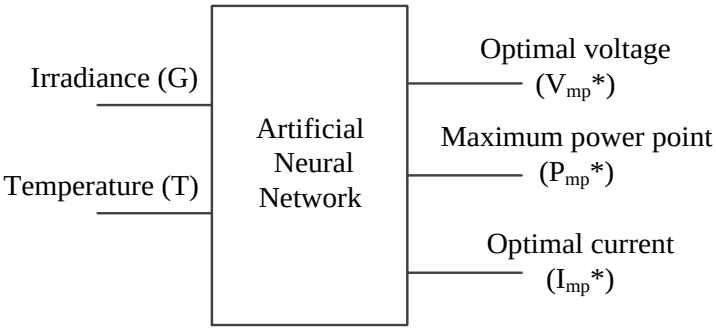

Fig. 2.21 The basic structure of an ANN based method for predicting the MPP.

In this conventional way of applying ANN in MPPT, the ANN is used to predict the optimal points according to the irradiance and temperature input values. However, it is not suitable for small-scale, low-cost PV systems because the irradiance and the temperature are required to be measured during the prediction process. In addition, aging of the PV

array may cause inaccuracy of the ANN model. A comprehensive review of the artificial intelligence techniques used in photovoltaic applications is given in [42]. Therefore, a different technique for applying ANN in MPPT in combination with a conventional MPPT, which are efficient for nonuniform irradiance conditions, will be introduced in Chapter 5. Moreover, the case without irradiance and temperature sensors is also discussed.

2.2.23 Sweeping methods

The sweeping methods can be classified into three types: power, voltage and current sweeping method. The common principle of these methods is to perturb the working point successively by increasing the power, current or voltage (based on the type of sweep) of the PV arrays. These three types of sweeping methods are introduced as follows.

2.2.23.1 Power sweep

The power sweep method uses an adjustable power converter to find the optimal point by successively increasing the power flowing to the DC-DC converter. The operating point starts from the open circuit condition and then progressively moves forward to the global MPP. When a drop in the PV array voltage is detected, the power increase process is stopped and then the previous operating point is considered as the best operating point-so-far. Thus, the operating point of the PV array is set to the best operating point which is in the vicinity of the global MPP. Finally, the conventional P&O or IncCond algorithm is used to track the global MPP. For a system using a buck converter, the input power of the DC-DC converter can be adjusted to the desired value by tuning the parameter V_c' in the following equation:

$$P_{pv} = V_c' V_o - \frac{V_o^2 T_s}{2L} \tag{2.48}$$

where V_c' is a control signal to adjust the input power of the buck converter; L the inductance of the inductor in the buck converter; V_o the constant voltage output of the converter which can be the bus voltage between the DC-AC inverter and the DC-DC converter in a grid connected system or the constant voltage of the battery bank in a standalone system, and T_s is the switching period of the PWM in the power converter.

This method has the advantage of not requiring any prior knowledge about the PV array characteristics or configurations and can track the global MPP for any environmental conditions. For the case study in [110], the tracking speed of the power sweep method is about three times that of the PSO algorithm. However, generally the power sweep method is much slower, particularly for large scale PV arrays, where more steps are required to reach the global MPP. In addition, when many local peaks exist on the P-V curve, the incremental step for the power sweep method must be chosen very carefully. Too large a

step size may miss tracking the global MPP, while too small a step size results in a slow search speed.

2.2.23.2 Voltage sweep

This method finds the global MPP by sweeping the voltage of the PV array in a range. In [111], the global MPP is obtained by searching two sides of the P-V curve in conjunction with a DC-DC converter. The general process can be explained as follows. A flag signal (*flag*) is used to indicate the two sides of the initial stable point, such as point *C* in Fig. 2.22. The flag at the left side of the point *C* is marked as 1 and the right as -1. The sign after multiplying the slope of the P-V curve with the flag signal ($flag \times dP/dV$) is used to indicate the existence of the new local MPP. For instance, assume a sudden variation in power (ΔP), caused by an irradiance change (larger than a certain critical power variation (ΔP_{crit})), is detected. Initially, the method starts to search the left side of point *C*. The search is realized by perturbing the voltage with a step size of ΔV_{large}, which is designed to be smaller than the minimum possible displacement between two successive peaks. When searching the left side of the point *C*, if the indicator ($flag \times dP/dV$) is calculated to be positive, then the perturbation is continued in the same direction until the minimum voltage value is reached. Otherwise, if the indicator is calculated to be negative, it means that a new peak in the search direction (point *B*) exists in the vicinity. Then, a conventional MPPT algorithm, such as P&O or IncCond, is applied to track this new peak (point *B*). After obtaining the new MPP, the power value at the new MPP is compared with the previously stored MPP value. If it is larger than the previous stored local MPP (point *C*), then the stored MPP value is changed to the new MPP value. Otherwise, the previous MPP value is maintained. This process is repeated until the minimum possible voltage value on the left side is reached. Subsequently, a similar search process is applied to the right side of point *C*. Thus, by searching both sides of the point *C*, the global MPP (point *B*) can eventually be found.

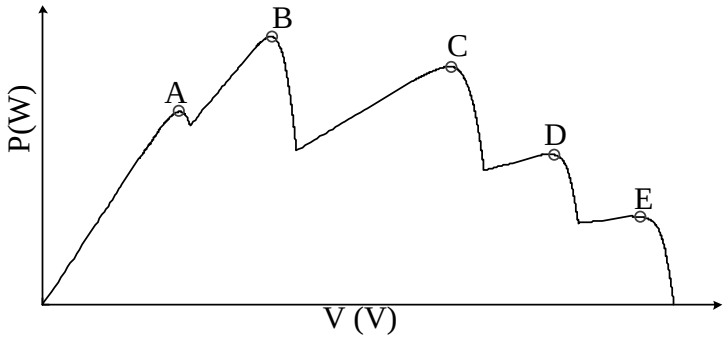

Fig. 2.22 A P-V curve with multiple peaks.

This method has a simple implementation procedure. However, it is based on the sweeping technique, which is usually considered to be slow when applied to a large scale PV system. In addition, the perturbation step size needs to be carefully chosen since too large a step size risks missing the global peak, while too small a step size results in a slow tracking speed.

2.2.23.3 Current sweep

The principle behind the current sweep method is to sweep the I-V curve of the PV module with a predefined sweep waveform of the PV module current periodically so that the optimal operating point can be obtained [112]. The sweep current is defined as an exponentially decreasing function and is similar to a capacitor discharging through a resistor. The sweep waveform equation is given by:

$$i(t) = I_0 e^{-t/\tau} \tag{2.49}$$

where I_0 is the maximum sweep current and τ is the time constant of the circuit. With this current sweep waveform, the optimal operating voltage can be determined by checking the sign of the following equation:

$$\psi = \tau \frac{dV_{pv}(t)}{dt} + V_{pv}(t). \tag{2.50}$$

If $\psi > 0$, then the operating point is on the left side of P-I curve; if $\psi < 0$, then the operating point is on the right side of P-I curve; if $\psi = 0$, then it is the optimal operating point. With this method, there is no need to calculate the power value, which means that multiplications are avoided, making it easy to implement using analog circuits. However, the sweeping process results in a slow tracking speed and it does not work for partial shading conditions.

2.2.24 Beta method

The beta method uses an intermediate variable β to find the MPP. This intermediate variable is defined as:

$$\beta = \ln(\frac{I_{pv}}{V_{pv}}) - cV_{pv} \tag{2.51}$$

where V_{pv} and I_{pv} are the online measured voltage and current of the PV array respectively, c is the diode constant equal to $q/kTaN_s$ .When the environmental conditions change, β remains almost constant at the optimum operating point. Thus by continuously measuring one variable (current or voltage) from the PV array, the value of the other variable can be calculated based on Eq. (2.51).

This method has the advantage of a very simple implantation. However, it only applies to PV systems operating under uniform irradiance conditions and the performance of the MPPT can be influenced by the aging of the PV array.

2.2.25 Slide mode control

Slide mode control is usually used for solving nonlinear problems. It is robust under the presence of parameter uncertainties and environmental variations [113, 114]. In [113], instead of directly measuring the current output of the PV array, the slide mode observer is used to predict the solar array current. The MPP reference voltage is generated by the controller which is fed with the predicted current information. The configuration of a single stage grid connected PV system is shown in Fig. 2.23.

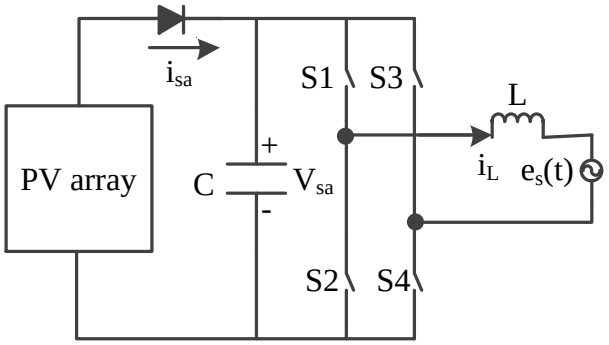

Fig. 2.23 The configuration of a single stage grid connected PV system.

Since the finite sampling time causes a chattering phenomenon in the estimated value, the measured solar array voltage and estimated current are averaged over a half cycle of the AC utility grid frequency. The overall controller configuration for slide mode control in MPPT is shown in Fig. 2.24. It consists of a slide mode observer, P&O based MPPT, PI controller for voltage control, and current controller for the inductor current control. The current is estimated according to the following equations:

$$\dot{\hat{v}}_{sa} = \frac{1}{C}(-i_L \cdot u + \hat{i}_{sa}) + L_1 \operatorname{sgn}(e_y) \tag{2.52}$$

$$\dot{\hat{i}}_{sa} = L_2(L_1 \operatorname{sgn}(e_y)) \tag{2.53}$$

$$e_y = y - \hat{y} = v_{sa} - \hat{v}_{sa} \tag{2.54}$$

$$\operatorname{sgn}(e_y) = \begin{cases} +1, & e_y > 0 \\ -1, & e_y < 0 \end{cases} \tag{2.55}$$

where C is the capacitance; $\dot{\hat{v}}_{sa}$ and $\dot{\hat{i}}_{sa}$ are the estimated values for $\dot{v}_{sa}$ and $\dot{i}_{sa}$ respectively; L_1 and L_2 are the positive gains of the observer. These gain values can be arbitrarily assigned to attain robustness against disturbances but should ensure a stable observer.

Since the chatter magnitude is highly dependent on the observer gain, a tradeoff should be made to ensure robustness and stability [115]. After obtaining the power change by multiplying the average voltage and average estimated current of PV arrays, the reference voltage of the MPP is updated according to the following equation:

$$V_{ref}(k+1) = V_{ref}(k) + flag \times \Delta V \tag{2.56}$$

where ΔV is the step size of the perturbation, and *flag* is the sign of the derivative of the operating point on the P-V curve. The output of the voltage controller is the inductor *DC* current reference (I_{ref}) which is obtained as:

$$I_i^* = K_p(V_{sa} - V_{ref}^*) + K_i \int (V_{sa} - V_{ref}^*)dt \tag{2.57}$$

$$I_{ref}^* = \sqrt{2} I_i^* \sin(\omega_s t) \tag{2.58}$$

where K_p and K_i are the proportional and integral gain values of the PI controller, respectively. The predictive current controller outputs the inverter voltage control signal as:

$$V_{INV}^*(i+1) = e_s(i) + \frac{L}{T_s}(I_{ref}^*(i) - i_L(i)) . \tag{2.59}$$

Finally, the voltage control signal of the inverter is compared with the PWM ramp voltage to generate signals S1,S2,S3, and S4 to control the power switches.

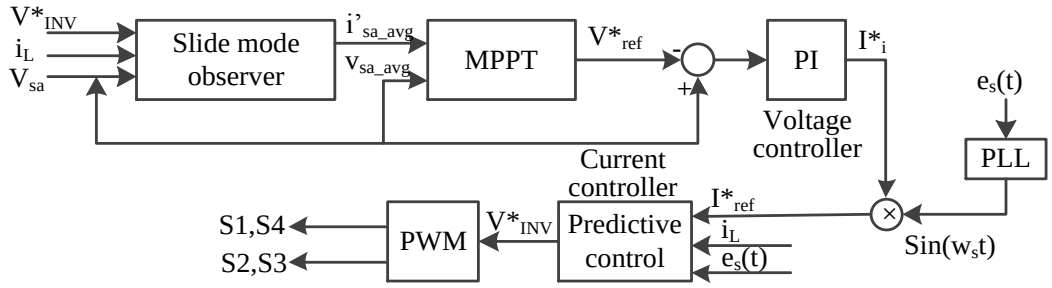

Fig. 2.24 The configuration of the slide mode based MPPT control.

The tracking speed of this method is fast and the efficiency is comparable to other conventional methods. However, the price of keeping the system robust to external noise and system uncertainties is inducing fluctuations to the power output and voltage output. In addition, the performance of this method depends on the choice of L_1, L_2, K_i, and K_p, which makes the design process more complex.

2.2.26 Hybrid MPPT

Many MPPTs (including some already described above) are combinations of simpler MPPT algorithms which together form a hybrid MPPT merging the advantages of both methods. Some of the hybrid methods include:

2.2.26.1 Model + Heuristic technique

A hybrid MPPT based on the model and heuristic technique is proposed in [116]. In the model based MPPT, the MPP locus is calculated using a PV array model and the optimal point at the MPP in the next iteration step is located from the locus for a pair of measured voltage and current values. In this hybrid MPPT, the IncCond algorithm is considered as the heuristic technique. The optimal reference voltage values generated by these two methods are added together and applied to the system simultaneously. The control structure is shown in Fig. 2.25. The model based MPPT is calculation-intensive and requires irradiance and temperature sensors, but it usually provides good tracking accuracy and fast tracking speed. The heuristic method has a relatively slow tracking speed due to its iterative tracking process, but it does not require information from the PV array and has a low computational complexity. Thus, the combination of these two methods brings out the positive aspects of both and produces a robust system. However, this method does not consider bypass diode in the PV modules and cannot track the global MPP for partial shading conditions.

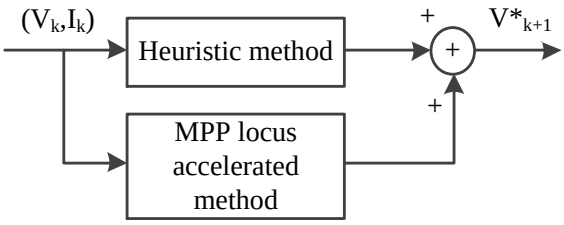

Fig. 2.25 Diagram of combining the MPP locus accelerated method and heuristic MPPT.

2.2.26.2 RCC + Model reference adaptive control

In [117], a two-level MPPT control algorithm is proposed by combining ripple correlation control (RCC) in the first stage and model reference adaptive control in the second stage. The control structure is as shown in Fig. 2.26. In the first stage, the voltage and power values measured from the PV array are considered as the inputs for the RCC unit. The duty ratio of the converter $d(t)$ is then calculated so that the optimal point can be applied. In the second stage, the error between the voltage output of the reference model and the plant is used to tune the parameters in the feedforward and feedback controllers. With this structure, the potential transient oscillations in the voltage output of the PV system can be eliminated. However, calculating the controller parameters is complex.

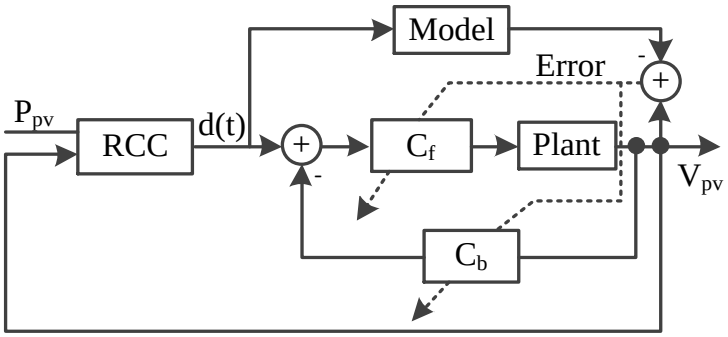

Fig. 2.26 The principle of MPPT using model reference adaptive control.

2.2.26.3 ANN + Fuzzy

In [53], ANN and fuzzy logic with polar information controller are combined to perform MPPT for a PV system under partial shading conditions. The ANN is used to predict the optimal voltage at the global MPP. The configuration of the proposed system, as shown in Fig. 2.27, consists of the ANN predictor, the fuzzy logic controller and the DC-DC converter. The optimal reference voltage (V^*_{dc}) is predicted by the ANN using the input irradiance (*Irr*) and temperature (*Temp*). The fuzzy logic controller outputs the control signal for the converter. The inputs to the fuzzy logic controller include the scaling factor of the error (A_s) in the polar phase plane, the radius member (D_r) and the error (e) between the reference voltage (V^*_{dc}) and the measured voltage from the PV array (V_{dc}). The effectiveness of the neruro-fuzzy based MPPT is verified using an experimental real-time simulator for different configurations such as bridge-link (BL), series-parallel (SP), and total cross tied (TCT). In addition, in [118, 119], the genetic algorithm is also used to optimize the fuzzy logic control rules and the system is shown to be robust under varying environmental conditions. However, since the fuzzy rules are significantly dependent on the experience, in these fuzzy based hybrid MPPTs, an inappropriate choice of fuzzy rules may influence the performance of the system.

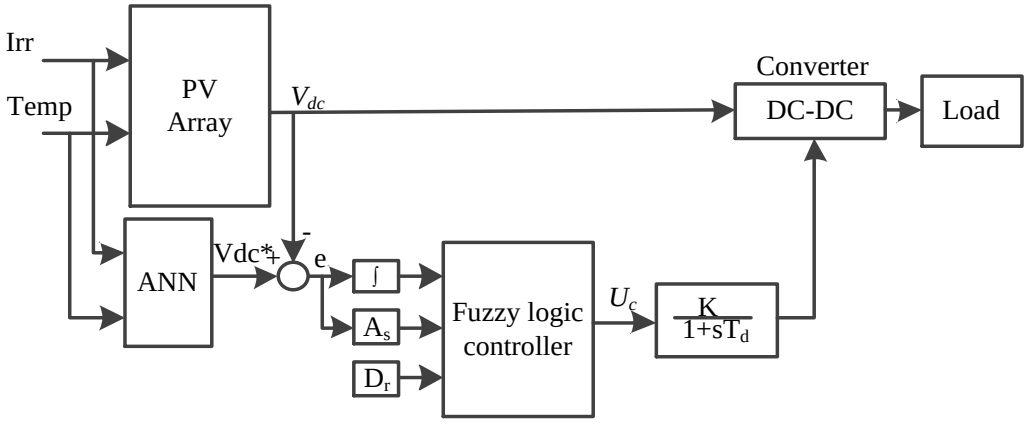

Fig. 2.27 Configuration of neruro-fuzzy based MPPT.

2.2.27 Other MPPTs

There are other types of MPPT methods which are designed to maximize the power capture from the PV array, namely power/voltage compensation methods, distributed MPPT, and the reconfigurable PV array etc.

The power compensation method [120, 121] involves a control strategy that adopts energy storage devices, such as a battery or supercapacitor, to compensate for the power loss when partially shaded conditions occur. Compared to the methods that use a bypass diode to balance the operational current between the shaded and non-shaded PV modules, this compensation methods can provide more power output [120, 121]. However, since many factors need to be considered and additional devices are required, this power compensation adds considerable complexity to the system design.

Karatepe et al. [122] proposed a voltage-based power compensation method for the MPPT problem under partial shading conditions. The basic idea of this compensator is to deactivate the shaded PV modules by forward biasing the parallel bypass diode according to a decision unit, which is based on the shading level of the PV module. This method is suitable for systems with multiple modules in series and parallel. However, additional devices need to be installed, such as DC-DC converters and decision units. In addition, since the shaded modules are fully deactivated, the potential power from those shaded modules is wasted.

Distributed MPPT (DMPPT) [123-125] is another promising technique to extract the maximum power from the PV system under partially shaded conditions. Compared to the centralized MPPT, it provides a significant increase in energy harvest during partial shading condition. This increase can be up to 39% for a large plant with parallel high voltage thin-film module strings, and up to 58% for smaller systems using a lower voltage with 8 series thin-film modules per string [126]. In addition, a power increase of more than 30% has been reported for mono-crystalline Si PV modules [123]. However, the advantages of DMPPT are dependent on the particular installation and the cost of the additional electronics, and are usually not cost effective for small to medium sized stand-alone PV systems.

All of the above mentioned MPPT methods have their own advantages and disadvantages. The ability to track the global MPP for PV systems under partial shading and a fast tracking speed are the two important factors for MPPT. An ideal MPPT method should 1) be able to reach the global MPP with a fast speed, 2) be robust to the rapidly changing environment, 3) have low implementation complexity, 4) be system independent and 5) be cost-effective and energy efficient. Table 2.4 shows different aspect of each reviewed MPPT technique. The factors which are most likely to affect the performance of each

technique are illustrated in the last column. These factors can also be considered as the main disadvantages of each method.

2.3 Summary

In this chapter, a number of different methods for modeling the solar array and tracking the MPP are reviewed. The methods used to model the solar array include analytical, experimental, simulation, and artificial intelligence methods. From the literature survey, it is clear that the existing methods for modeling the PV array need better accuracy and efficiency under real weather conditions. The parameters in the mathematical model show a dramatic difference with changes in insolation and temperature. Unfortunately, most of existing models assume these parameters to be constant, which introduce errors to the PV model. Most of the intelligent modeling methods can model the PV arrays precisely, but result in additional complexity in the computational process. Therefore, an efficient and accurate modeling method with less computational complexity needs to be investigated for the PV array under the real weather conditions.

For the MPPT methods, they need to be able to track the global MPP with fast speed, low implementation complexity, non-system-dependency and low system cost. As in Table 2.4, each method has its pros and cons. Some of the existing methods are able to track the global MPP under partial shading conditions but they have disadvantage of either more complexity or a slow tracking speed. Other MPPTs are only effective for the uniform irradiance. Since in tropical areas, the irradiance profile is characterized by a large number of rapid transitions. The partial shading on the PV module caused by the surroundings and clouds, especially in Singapore, where the space is limited, is very common. Therefore, an MPPT which is able to operate under partial shading and rapid changing irradiance needs to be proposed. These topics will be discussed in the following chapters.

Table 2.4. Comparison of different MPPT techniques.

No.	MPPT techniques	Global MPP	PV system dependency	Tracking accuracy	Transient tracking speed	Complexity	Required sensors	Analog or digital	Online or offline	Factors affecting performance
1	Perturb and observe /hill climbing	No	No	Medium	Medium	Simple	V, I	Both	Online	Step size; rapid changing environmental conditions; partial shading.
2	Incremental conductance (IncCond)	No	No	Medium	Medium	Medium	V, I	Both	Online	Step size; rapid changing environment; partial shading.
3	Fractional V_{oc} or I_{sc}	No	Yes	Low	Fast	Simple	V or I	Both	Online	PV panel aging; irradiance variation; partial shading.
4	Bisection search theorem (BST)	No	No	High	Medium	Medium	V, I	Digital	Indirect	Partial shading.
5	Three point MPPT method	No	No	High	Fast	Simple	V, I	Digital	Online	Partial shading.
6	Variable step size incremental resistance (INR)	No	No	Very high	Very fast	Complex	V, I	Digital	Online	Partial shading; rapid changing environment.

7	Ripple correlation control (RCC) and extremum seeking control (ESC)		No	No	High	Very fast	Complex	V, I	Both	Online	Partial shading; inductor frequency.
8	DC link capacitor droop control		No	No	High	Fast	Complex	V, I	Both	Indirect	System noise; partial shading.
9	Temperature based MPPT		No	Yes	Low	Medium	Simple	T, V	Both	Online	Rapid changing irradiance; partial shading; Nonuniform temperature distribution.
10	Variable inductor MPPT		No	Yes	Medium	Medium	Medium	V, I	Analog	Online	Reduced inductor size; partial shading.
11	Parasitic capacitance MPPT		No	No	Very high	Fast	Complex	V, I	Both	Online	Partial shading; rapid changing irradiance.
12	dP - P&O method		No	No	High	Medium	Simple	V, I	Both	Online	Sampling period; partial shading.
13	Load line MPPT		Partially	No	Medium	Medium	Medium	V, I	Both	Online	PV panel aging; rapid changing; partial shading.
14	Dividing rectangles		Partially	No	Medium	Medium	Complex	V, I	Digital	Online	Rapid changing; choice of control parameters.
15	Fibonacci search MPPT		Partially	No	Very high	Fast	Medium	V, I	Digital	Online	Partial shading; rapid changing irradiance; uncertain convergence.
16	State space based MPPT		Yes	Yes	High	Fast	Very Complex	V, I	Digital	Online	Partial shading; rapid changing irradiance; complex design procedure.
17	Voltage window search (VWS)		Yes	No	Medium	Medium	Complex	V, I	Digital	Online	Initial working point; rapid changing irradiance.
18	Evolutionary algorithm based MPPT	Particle swarm optimization (PSO)	Yes	No	Very high	Fast	Medium	V, I	Digital	Online	Limited speed.
		Differential evolution (DE)	Yes	No	Very high	Fast	Medium	V, I	Digital	Online	Limited speed.
		Genetic algorithms (GA)	Yes	No	Very high	Slow	Medium	V, I	Digital	Online	Slow tracking speed.
19	Fuzzy logic		Yes	Yes	Very high	Fast	Complex	V, I	Digital	Indirect	Requirement of experience based fuzzy rule
20	Look up table		Yes	Yes	Low	Fast	Medium	G, V or I	Digital	Offline	PV panel aging; system dependence.
21	Curve fitting		Yes	No	Low	Slow	Medium	V or I	Digital	Offline	Rapid changing irradiance; limited speed; high complexity.
22	Artificial neural network (ANN)		Yes	Yes	Very high	Very fast	Medium	G, T	Digital	Offline	Requirement of training dataset.
23	Sweeping methods	Power sweep	Yes	No	Very high	Slow	Complex	V, I	Digital	Online	Step size of power increase; limited speed.
		Voltage sweep	Yes	No	Very high	Slow	Simple	V, I	Digital	Online	Step size of voltage perturbation; limited speed.
		Current sweep	Yes	Yes	Very high	Slow	Medium	V, I	Digital	Online	Step size of voltage perturbation; limited speed.
24	Beta method		Yes	No	High	Fast	Simple	V, I	Digital	Indirect	Partial shading.
25	Slide mode control		Yes	No	Medium	Fast	Very Complex	V, I	Digital	Online	Complex process of controller design.
26	Hybrid MPPT	Model+Heuristic technique	No	Yes	Very high	Medium	Complex	V, I	Digital	Indirect	Requirement of system model; PV array aging.
		RCC+Model reference adaptive control	No	Yes	Very high	Fast	Complex	V, I	Both	Indirect	Requirement of system model; PV array aging.
		ANN + Fuzzy	Yes	Yes	Very high	Very fast	Complex	G, T, V	Digital	Indirect	Requirement of training data and fuzzy rules.

Chapter 3 Modeling and parameter estimation of PV cells and array

In this Chapter, we introduce modeling techniques for the PV array. In the first, we use the Chebyshev functional link neural network (CFLNN) as it can provide estimated current values with lower complexity compared to the conventional artificial neural network based model and better prediction accuracy than that of the prevailing analytical modeling method. Even though the analytical methods such as single diode (or two diode) model have a lower accuracy than the CFLNN method as presented in the first section, they are still an efficient and widely used method to simulate PV systems, especially in MATLAB/SIMULINK, due to their simplicity. Thus, in the second section, an efficient improved adaptive differential evolution (IADE) algorithm is presented to estimate the parameters for these analytical models.

3.1 Chebyshev functional link neural network (CFLNN)-based modeling for PV array

3.1.1 Introduction

As discussed in the literature review in Chapter 2, three modeling methods, namely: analytical method, experimental method, and artificial intelligence method, are usually used to model the PV cells/modules. The disadvantage of the analytical methods is that they assume that the values of the series and parallel resistances remain constant. However, these parameters change with environmental conditions, e.g. irradiance and temperature levels [25]. Furthermore, as described in Section 2.1.1, many factors, such as PV cell/module mismatch losses in the same PV string, the failure of the MPPT algorithm caused by partial shading effects, ohmic losses due to connections, angular and spectral losses, and the cloudy environment etc., can influence the power output of the PV systems, and so using analytical methods will reduce the model accuracy. Moreover, the sensitivity to the initial values of these parameters and the high computational complexity are also disadvantages.

The artificial intelligence methods, such as the ANN [25, 31, 32], present better performance without knowledge of the internal system, and provide a compact solution to multivariable problems compared to analytical methods. Generally, there are two ways to apply the ANN technique in modeling PV arrays. The first one is to estimate the five or seven circuit parameters in the first stage and then apply the estimated parameter values to the analytical models. The second method is to predict the current or voltage output of the PV array directly from the measured irradiance and temperature values. In our study, the latter method is used to estimate the current output from the PV array. Compared to the analytical and classical modeling methods, the ANN based method takes second order effects into account and provides better prediction performance. The multilayer perceptron (MLP) with back propagation (BP) algorithm is usually applied in modeling the PV array. However, the high computational complexity and long training time make it unappealing for this application, as will be demonstrated later. Compared to the conventional MLP, the functional link ANN (FLANN) has a faster convergence speed, better accuracy of model prediction and low computational complexity. These advantages make it suitable for modeling nonlinear systems [129, 130]. Among the FLANN, the Chebyshev functional link neural network (CFLNN) is chosen and is applied in our work. It is a class of FLANN, which is computationally more efficient than conventional MLP networks [129, 130]. FLANN has been successfully applied in various research areas such as modeling electrical characteristics of solar cells with dual junctions, estimating the external quantum efficiency, and MPPT [131]. Thus, in our work, the CFLNN is chosen and utilized to predict the current output of the PV array based on the measured irradiance, temperature and voltage values under the real environmental condition.

3.1.2 Conventional two diode model for PV modules

In order to evaluate the performance of the proposed CFLNN based model, the results of the predicted current from the given inputs are compared with their counterparts obtained from the two diode model. This two diode model has been introduced concisely in Chapter 2. In order to illustrate it clearly, we rewrite the equations in detail here.

We consider a PV array that consists of N_{pp} PV strings connected in parallel and N_{ss} PV modules connected in series in each PV string. In each module, there are N_s series connected solar cells. The equivalent electrical circuit for the two diode model of a solar cell is given in [20]. From the equivalent circuit, the output current of the PV array is given by:

$$I = I_{pv} - I_{d1} - I_{d2} - I_p \tag{3.1}$$

where I is the current output of PV array, I_{d1} and I_{d2} are the currents through the two diodes, respectively, I_{pv} is the light generated current and I_p is the leakage current through the

parallel resistance R_p. By substituting each element of Eq. (3.1) with electrical equations, Eq. (3.1) can be rewritten as:

$$I = I_{pv}N_{pp} - I_{01}N_{pp}[\exp(\frac{V+\lambda IR_s}{a_1V_tN_{ss}})-1] - I_{02}N_{pp}[\exp(\frac{V+\lambda IR_s}{a_2V_tN_{ss}})-1] - \frac{V+\lambda IR_s}{\lambda R_p} \quad (3.2)$$

where V is the output voltage of the PV array, $\lambda = N_{ss} / N_{pp}$, V_t is the thermal voltage of the two diodes ($V_t = N_s k\ T / q$), k is the Boltzman constant, q is the electron charge, R_s and R_p are the series and parallel resistances, respectively, and n_1, n_2 are the ideal constants of the two diodes. The light generated current is given by:

$$I_{pv} = (I_{pv\_STC} + K_{sc}(T - T_{STC}))\frac{G}{G_{STC}} \quad (3.3)$$

where I_{pv_STC} denotes the light generated current under STC with temperature $T_{STC} = 25^oC$ and irradiance G_{STC} = 1000 (W/m^2), and K_{sc} is the short circuit current coefficient. The reverse saturation current of the diode is given by:

$$I_{01} = I_{02} = \frac{I_{sc\_STC} + K_{sc}\Delta T}{\exp((V_{oc\_STC} + K_{oc}\Delta T)/V_t) - 1} \quad (3.4)$$

where I_{sc_STC} is the short circuit current under STC, K_{oc} is the open circuit voltage coefficient and V_{oc_STC} is the open circuit voltage under STC. In fact, Eq. (3.1) can be treated as an implicit nonlinear function, $I = f\ (I, V)$ with seven unknown parameters (n_1, n_2, I_{pv}, I_{01}, I_{02}, R_s, and R_p). Thus, for a given voltage this implicit nonlinear function can be solved using the standard Newton-Raphson method.

The process of using the two diode model to generate a current value for a given voltage of the PV array includes following steps: (1) calculate the resistances, R_s and R_p, based on the parameters of PV array from the datasheet using the method with a fast convergence speed given in [19, 20], (2) calculate the values of I_{pv}, I_{01}, I_{02} based on Eqs. (3.3) and (3.4), where the value of diode ideal constants n_1 and n_2 we use for the two diode model are chosen to be 1 and 1.2 [20], respectively, and the values of R_s and R_p are calculated to be 1.12 Ω and 1100.43 Ω, respectively, and then (3) based on the given voltage value, calculate the current output using the Newton-Raphson method with seven known parameters, n_1, n_2, I_{pv}, I_{01}, I_{02}, R_s, and R_p.

3.1.3 Chebyshev neural network based modeling for PV modules

Functional link neural networks are higher-order neural networks without hidden units, introduced by Klassen and Pao [132] in 1988. As shown in Fig. 3.1, the FLANN [43] is made up of a functional expansion block (FEB) and a single-layer perceptron. The input variables are expanded from a lower dimension to a higher dimension. This expansion function can be implemented by many methods, such as Chebyshev polynomials,

trigonometric polynomials and other orthogonal polynomials [129, 130]. Because Chebyshev polynomials have the advantages of high efficiency and flexibility, low computational complexity, and good prediction capability in different applications, they were selected as the expansion function. After being transferred into a higher dimension by the FEB, the inputs are directly linked to the output layer. The output layer is then activated by the hyperbolic tangent transfer function. Thus, the computational complexity is greatly reduced compared to an MLP network as there is no hidden layer in the network. Before using CFLNN, it needs to be trained with a training dataset. There are many training functions for ANNs, such as Quasi-Newton, Resilient Back-propagation, scaled conjugate gradient, etc. [133]. It is very difficult to know which training algorithm will be the best for a given problem, because the performance depends on many factors, including the complexity of the problem, the error goal, the number of weights and biases in the network, the number of data points in the training set and whether the network is being used for pattern recognition (discriminant analysis) or function approximation (regression). Since there is no such a strict rule for choosing the size of training datasets, we choose the datasets based on different trials [134, 135]. However, according to these literature reviews, there is a general principle detailing how to choose the training dataset. It is very important that the training dataset should contain enough information relating to the tested system. Finally, we decided to choose the dataset, measured on a day with the most number of large transitions, to be the training dataset. The detailed investigation on how the training dataset influences the results in this system could be a topic for our future work. In the training process, the weights between the output and the expanded input layer are adjusted until the cost function reaches a particular limit. Levenberg - Marquardt (LM) [136] is a fast training function for approximation functions with medium sized weights and bias (Less than thousands of weights) [133]. It performs better on nonlinear regression problems than on pattern recognition problems [133]. For training large networks and pattern recognition networks, the resilient backpropagation and the scaled conjugate gradient are good choices due to their small memory requirement [133]. In our work, we chose the LM algorithm to train the network. In order to explain the structure of CFLNN and the training process, the input vector, X, is represented by:

$$X = [x_1, x_2, x_3]' \tag{3.5}$$

where x_1, x_2, x_3 indicate three attributes of the input samples, and [.]' denotes the transposition operation. After going through the FEB, the inputs are expanded by the following Chebyshev polynomials [129]:

$$
\begin{aligned}
&L_0(x_p) = 1, \\
&L_1(x_p) = x_p, \\
&L_2(x_p) = 2x_p^2 - 1, \\
&L_3(x_p) = 4x_p^3\text{-}3x_p, \\
&L_4(x_p) = 8x_p^4 - 8x_p^2 + 1
\end{aligned}
\tag{3.6}
$$

where x_p denotes one of the network inputs to the FEB, $-1 < x_p < 1$, $p = \{1, 2, 3\}$. The remaining Chebyshev polynomials with higher dimensions are created using the following recursive formula:

$$L_n(x_p) = 2x_p L_{n-1}(x_p) - L_{n-2}(x_p) \tag{3.7}$$

where n is the dimension of the expanded space for each input. If the input vector has p attributes, then the dimension of the expanded space, N, is $n \times p + 1$. A bias with a constant value of '1' is added into the expanded space.

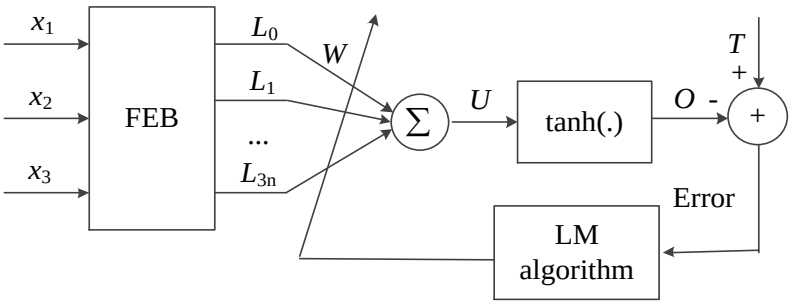

Fig. 3.1 Basic configuration of the FLANN.

The structure of a conventional MLP network is shown in Fig. 3.2. The outputs of the j^{th} neuron from the hidden layer are calculated as:

$$\phi_j(x) = G_j \sum_{i=1}^{N} W_{ji} \times x_i \tag{3.8}$$

where G_j is the activation function for the j^{th} node in the hidden layer, W_{ji} is the weight connecting the j^{th} hidden node with the i^{th} input x_i. The k^{th} network output in the output layer is calculated as:

$$Y_k = G_k\left(\sum_{j=1}^{H} W_{kj} \times \phi_j(x)\right) \tag{3.9}$$

where G_k is the activation function for the k^{th} node in the output layer, W_{kj} is the weight connecting k^{th} output node with the j^{th} node in hidden layer. Therefore, with the space transformation, the input space $\{x_1, x_2, x_3, .., x_N\}$ is transferred into another space, $\{\phi_1(x), \phi_2(x), \phi_3(x), ..., \phi_H(x)\}$, with a higher dimension. Thus, in this space with higher dimension, the linear discrimination becomes easier than the original input space with low dimensions. Instead of using the MLP to find the learnable arbitrary functions in the hidden layer, Chebyshev polynomials are applied to expand the original inputs.

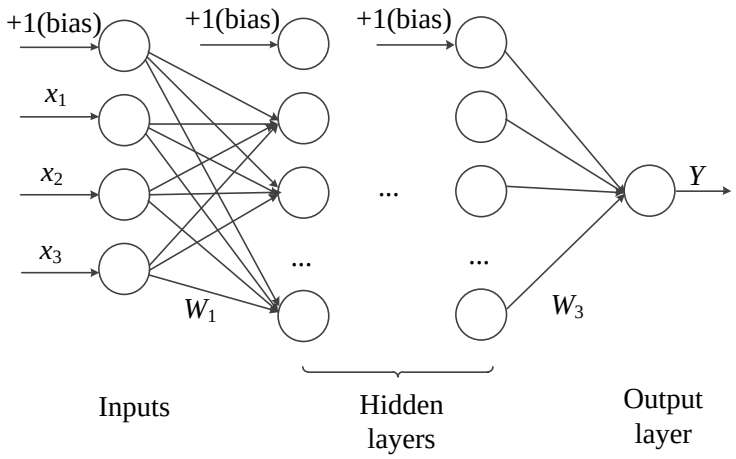

Fig. 3.2 The structure of the MLP.

After trying different functional expansions of the Chebyshev polynomials, we found that adding cross products of expanded inputs into the expanded space improves the performance of the prediction. Additionally, [132, 137, 138] also recommend that these cross products be added to the expanded inputs. For example, we added products of each component, x_1x_2, x_1x_3, x_2x_3, $x_1x_2x_3$. The detailed two-stage functional expansion block is shown in Fig. 3.3. Thus, the total number of the expanded dimension was computed to be 29 (29 = 7×4+1), resulting in the expanded input $L = [L_0, L_1, L_2, ..., L_{28}]'$. By using the LM training algorithm, the weights (W), and the biases between inputs and outputs are updated until the cost function is minimized within a predefined limit. The cost function for the t^{th} sample data is given by:

$$E_t = \frac{1}{2}(T_t - O_t)^2 \tag{3.10}$$

where T_t is the target and O_t is the network output:

$$O_t = f(U_t) = \tanh(U_t) \tag{3.11}$$

where the input of the hyperbolic tangent transfer function is given by:

$$U_t = W_t' L_t \tag{3.12}$$

where $W_t=[w_{t,0}, w_{t,1}, w_{t,2}, ..., w_{t,28}]'$ is the weight vector for the t^{th} sample.

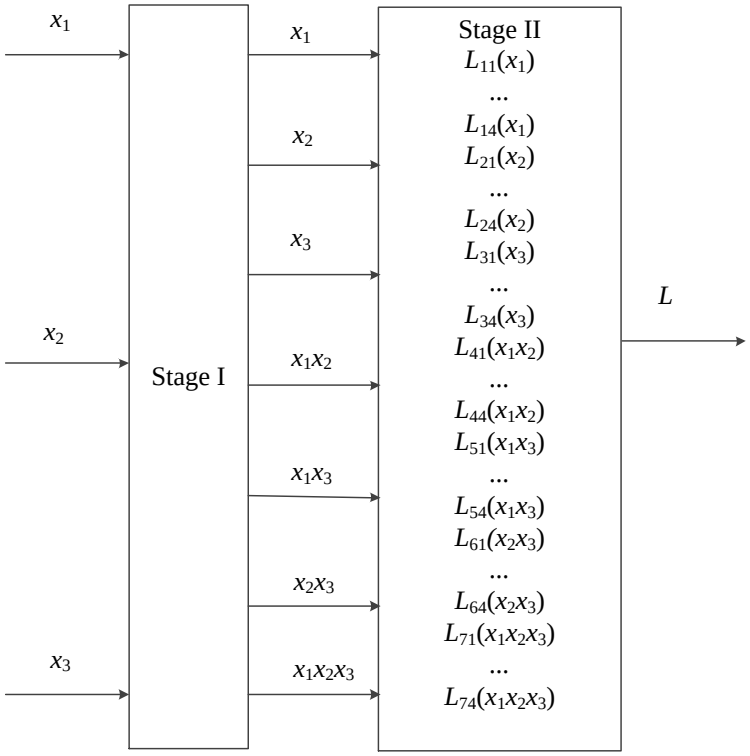

Fig. 3.3 The structure of two-stage expansion block in CFLNN.

3.1.4 Experimental setup and data acquisition

In this section, the experimental architecture of the data acquisition for the PV system and the network training process for the two types of ANNs (i.e., MLP and CFLNN) used in this study are presented.

The proposed CFLNN model for the solar array is shown in Fig. 3.4. The inputs are the irradiance, module temperature, and voltage measured from the terminal of the PV array. The output is the estimated current from the PV array. Before using CFLNN to predict the current output, the network is trained and tested with previously measured data. In order to get realistic dataset samples to train the network and verify the performance of the CFLNN modeling approach, an outdoor experimental setup was built on the rooftop of one of the buildings in Singapore (1.34^{o}N, 103.68^{o}E).

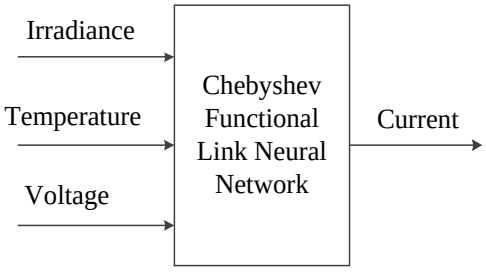

Fig. 3.4 CFLNN model for the solar array.

3.1.4.1 Experimental setup

The experimental PV system for data acquisition, as shown in Fig. 3.5, consists of PV modules, storage batteries, the system load, and the MPPT device connected between the PV modules and the load. The data logger is used to record the measured current, voltage, irradiance, and temperature values. The PV array consists of two 80W mono-crystalline PV modules in parallel and in each PV module there are 36 solar cells connected in series. The PV modules are from the Sinopuren Energy Group. The parameters of mono-crystalline PV modules used in the experiment are given in Table 3.1. Two 65Ah/12V sealed type lead-acid batteries are connected in series and are used to store the excess energy generated by the PV modules during daytime. The batteries provide the load power when solar energy is insufficient from the PV modules. The commercial MPPT controller (SS-MPPT-15L) (from Morningstar Corporation) which is used in this system to maximize the power output from the PV array can limit the current to the batteries to avoid overcharging them. Two 120W/24V light bulbs were used as the system load. Fig. 3.6 shows the PV modules situated on rooftop of the building and titled at an angle of 20° facing south. The PV output voltage and current are recorded by a data logger at an interval of one second for further processing. The temperature sensors are mounted at the back of the PV modules to sense the temperature. This makes temperature measurement more accurate than the values measured from the environment. The PV modules provide the electricity for the load and batteries during daytime. The load, the light bulb, consumes power from the battery at night. Therefore, this PV testing system does not need to discharge the batteries manually and has good temporal accuracy of the recorded data, with a one second sampling period compared to some other works [43, 54].

Table 3.1. Specification of the PV module.

Panel name	SL80CE-36M	Short circuit current (I_{sc})	2.44A
Maximum power (P_{max})	80W	Number of series cells in module	36
Optimum voltage (V_{mp})	35.1V	Temp. coefficient of I_{sc} (A/^{o}C)	0.976×10^{-3}
Optimum current (I_{mp})	2.28A	Temp. coefficient of V_{oc} (V/^{o}C)	-0.16416
Open circuit voltage (V_{oc})	43.2V	Module efficiency	15%

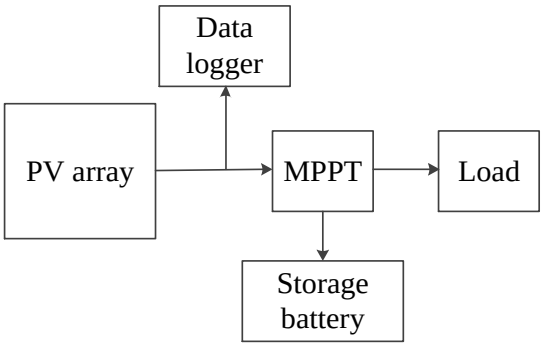

Fig. 3.5 Configuration of the PV system for data acquisition.

Fig. 3.6 PV modules installed on the building rooftop.

3.1.4.2 Data acquisition

A large number of datasets which include the global horizontal irradiance, the temperature of PV modules, and the current and terminal voltage of the PV array were acquired. It is important to note that the datasets selected to train the network has a significant influence on the performance of the neural network. Moreover, the accurate prediction of the current and voltage of the PV module is very critical for estimating the energy produced from the PV system. Therefore, four datasets are selected to train and verify the proposed CFLNN model for PV module. Their characteristics are shown in Table 3.2 where each dataset is sampled on a different day, denoted by number - 1, 2, 3, and 4, respectively. The minimum irradiance for each day is zero. Before using these datasets, the average values of measured datasets in every one minute from 8:20 AM to 5:20 PM are calculated to filter the signal noise. Finally, 540 groups of data are generated for each dataset. In this experiment, since the dataset on July 19, 2011 contains enough information for network training, it is chosen

to train the network. The other three datasets are applied to test and verify the model. It is important to point out that a large number of datasets is required to train the network when using the network to predict the current output for a long-term operation. Otherwise, the network needs to be trained frequently after a period of operation.

Table 3.2 The important statistics of datasets measured from experimental setup.

Dataset (#)	Date	Irradiance (W/m^2)		Temperature (℃)		Voltage (V)		Current (A)	
		Max.	*Avg.*	*Max.*	*Avg.*	*Max.*	*Avg.*	*Max.*	*Avg.*
1	May 8, 2011	983.59	743.87	52.94	46.94	32.16	30.71	4.22	3.14
2	May 11, 2011	1093.10	621.26	57.26	47.94	34.46	29.98	5.18	2.82
3	July 19, 2011	1064.00	548.62	51.71	42.49	35.51	30.68	4.99	2.48
4	July 24, 2011	986.89	496.92	50.59	42.14	33.48	31.11	4.35	2.19

3.1.5 Results and discussion

In order to verify that CFLNN has (i) lower computational complexity than that of the conventional MLP, and (ii) accuracy similar to MLP but better than the analytical two diode model, two experiments are conducted using MATLAB. In addition, two aspects of the proposed CFLNN model are compared with the MLP model and two diode analytical model, namely the computational complexity and the performance of the current prediction.

3.1.5.1 Experiment 1

The computational complexity of CFLNN and MLP during the training process is compared in this experiment. The execution time for each epoch during the training period is used to evaluate the computational complexity of the neural network. For each dataset, twenty runs were conducted for each network- MLP and CFLNN. The common training parameters for these two algorithms are set to be the same. For example, the training goal of the MSE between the normalized current predicted by the network and the normalized target current output is set to 0.001, the maximum training iterations is 200, the learning rate is 0.2, with the other parameters set to the default values. Since theoretically any nonlinear function can be approximated by an MLP with a hidden layer by adding enough hidden neurons, the number of hidden nodes in MLP was set to 10. The number of hidden layers was decided by trial and error to trade-off the computational complexity and the accuracy of the predictor. A larger number of hidden nodes produces better accuracy but adds to the computational complexity to the predictor and too few hidden nodes reduce the accuracy of the result. The training style is set to batch training, in which the weights and biases are only adjusted after the complete set of training samples are applied to the

network. Because the initial values of weights between each layer are generated randomly at the beginning of the training process, the results of weights and biases are different after each training. In order to evaluate the general performance, we run each algorithm for 20 times for each dataset.

Thus, after training each neural network with dataset of July 19, 2011, the maximum, minimum and average number of iterations for finishing the training process within 20 runs is determined as shown in Table 3.3. We observe that the average number of iterations by CFLNN is about half that by MLP, and that the average execution time of one epoch by CFLNN is about 3.8 times lower than that of MLP. The execution time of the functional expansion in CFLNN, 7.27×10^{-2} ms, can be ignored. Therefore, the execution time of each epoch by CFLNN is far less than that by MLP. Even though the offline training time is not so important, it still shows the training time advantage of FLANN. When the algorithm is implemented in the physical hardware (in this case, a processor which can be a digital signal processor (DSP), microcontroller, or a computation core implemented using a field programmable gate array (FPGA)), CFLNN is more computationally efficient than MLP. In addition, the number of adders and multipliers in one iteration can also be calculated to compare the complexity of MLP and CFLNN using the equations provided in [129].

Table 3.3 The comparison of execution time for training MLP and CFLNN after 20 times each.

Network	Min. iterations	Max. iterations	Avg. iterations	Avg. execution time / epoch (ms)	Network structure
MLP	7	105	40	435.40	3-10-1
CFLNN	6	34	19	113.45	29-1

3.1.5.2 Experiment 2

The accuracy of the PV output current determined by three methods – the two diode model, MLP and CFLNN is compared in this experiment. The performance of each method is evaluated using the mean absolute percentage error (MAPE) and the mean squared error (MSE). MAPE is defined by [43]:

$$MAPE = \left\{ \frac{1}{D} \sum_{i=1}^{D} \left| \frac{I_{meas} - I_{pred}}{I_{meas}} \right| \right\} \times 100 \tag{3.13}$$

where I_{pred} is the predicted current by CFLNN, MLP or two diode model, I_{meas} the measured current output (target output), and D the number of data points in one dataset. The MSE is defined by:

$$MSE = \frac{1}{D} \sum_{i=1}^{D} (I_{meas} - I_{pred})^2 . \tag{3.14}$$

The training datasets are randomly divided into three parts, of which 80% is used for training, 10% for validation, and 10% for testing. After training the networks - MLP and CFLNN, the regression plots showing the targets (measured current) relative to the outputs predicted from the networks are shown in Fig. 3.7 and Fig. 3.8. The parameter *R* represents the correlation between the target output and the predicted output by the two networks. The ideal value of *R* equals one. We can see from Fig. 3.7 and Fig. 3.8 that the points are almost located on the line of the best regression, which means both networks can accurately predict the current for training dataset.

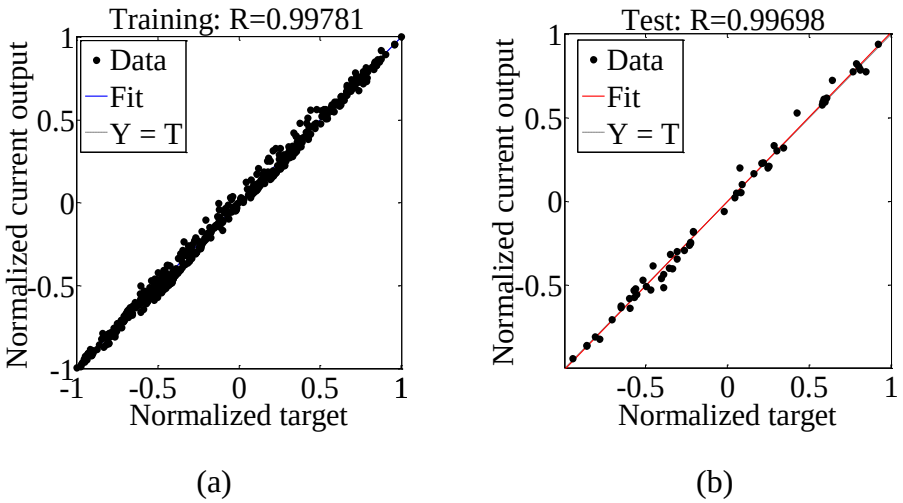

Fig. 3.7 Normalized target and estimated daily current for (a) validation (80% of the training dataset) and (b) testing (10% of the training dataset) on July 19, 2011, (MLP method).

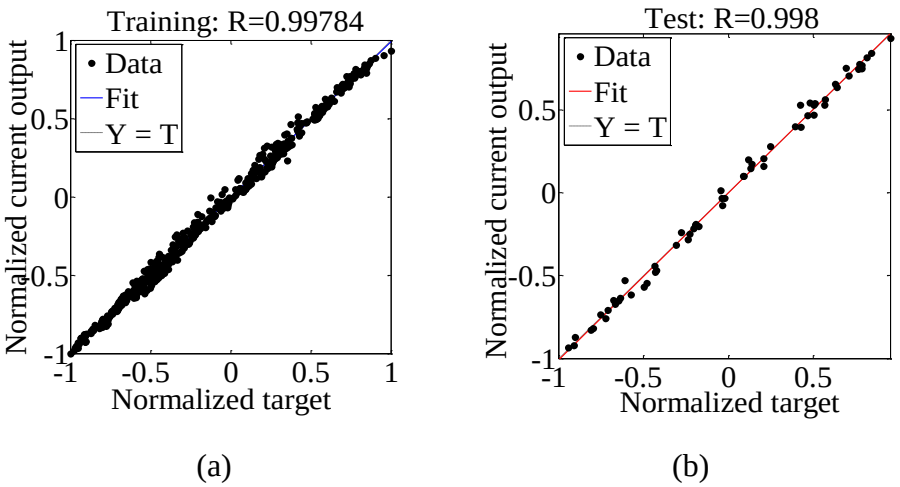

Fig. 3.8 Normalized target and estimated daily current for (a) validation (80% of the training dataset) and (b) testing (10% of the training dataset) on July 19, 2011, (CFLNN method).

After applying the single day dataset to each model, the values of MAPE and MSE for the current output predicted by the three different modeling methods - CFLNN, MLP and the two diode model, are computed, as shown in Table 3.4.

Table 3.4 MAPE and MSE of predicted current by the two diode, MLP, and CFLNN model after 20 runs.

Parameter	Dataset 1			Dataset 2			Dataset 3			Dataset 4		
	Two diode model	*MLP*	*CFLNN*	*Two diode model*	*MLP*	*CFLNN*	*Two diode model*	*MLP*	*CFLNN*	*Two diode model*	*MLP*	*CFLNN*
Minimum MAPE (%)	---	1.00	1.26	---	3.37	3.75	---	3.87	4.19	---	3.55	3.69
Mean MAPE (%)	9.47	1.78	1.40	6.24	4.58	3.91	9.23	4.34	4.43	5.73	3.95	3.86
Minimum MSE	---	0.011	0.012	---	0.0057	0.008	---	0.0063	0.0074	---	0.0085	0.0088
Mean MSE	0.095	0.032	0.013	0.0079	0.014	0.009	0.014	0.0085	0.0075	0.015	0.011	0.011

From the table, the following observations can be made:

(1) For dataset 1, the values of the minimum MAPE and MSE by CFLNN and MLP are about nine times lower than that by the two diode model. Whereas, the average MAPEs by MLP and CFLNN are almost five times smaller than those by the two diode model.

(2) For dataset 2, even though the average value of MSE produced by MLP and CFLNN is slightly higher than that by the two diode model, we still find that the minimum MSE by these two ANN methods are smaller than that by the two diode model.

(3) For dataset 3, we can see that the values of the minimum and average MAPE by the ANN methods are half of that of the two diode model. At the same time, the minimum and mean of the MSE produced by CFLNN and MLP are also much smaller than of the two diode model.

(4) For dataset 4, all the values of MSE and MAPE by MLP and CFLNN are smaller than that by the two diode model. For example, the MAPE produced by the two diode model is 5.73%, which is about 1.6 times that by MLP and about 1.5 times that of CFLNN. Similarly, the values of MSE by these two ANN models are smaller than by the two diode model.

To better illustrate the differences, the daily current output by these three methods from 8:20 AM to 5:20 PM is presented in Fig. 3.9 and a zoomed section from 9:00 AM to 11:15 AM is shown in Fig. 3.10 to emphasize the detailed transition points. Here, we only show the performance of one dataset, of July 24, 2011. From the curves in Fig. 3.10, it is clear that the two diode model overestimates the current. However, MLP and CFLNN give better prediction of the current. For the analytical method, the inaccuracy in the prediction of the PV array model can be caused by many uncertainties such as panel aging, module/cell mismatch, inaccuracies in the datasheet provided by manufactures, and so on.

The above results indicate that the models using ANN methods give better current prediction with a smaller error compared to the two diode modeling method. Compared to MLP model, CFLNN offers lower computational complexity at similar prediction accuracy.

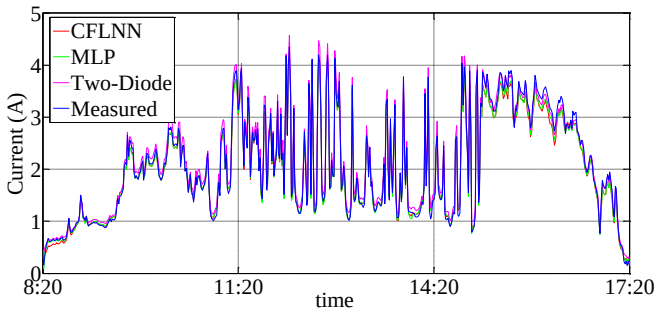

Fig. 3.9 Measured and predicted current by three methods - FLANN, MLP, and two diode model with environment data for July 24, 2011.

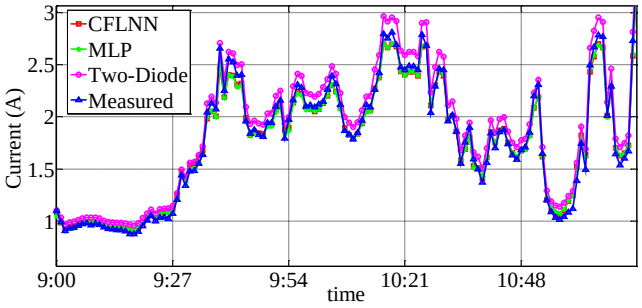

Fig. 3.10 An enlarged section of Fig. 3.9 from 9:00 to 11:15 on July 24, 2011.

3.2 Parameter estimation of PV cells and array

In the above section, the modeling of a PV array has been investigated. The proposed modeling method can be used to model the PV array with better accuracy than the conventional analytical modeling techniques and has a simpler computational complexity than the widely used MLP model. Even though the analytical method, such as the single/two diode model, is not as accurate as the proposed FLANN modeling method, these models are widely used and thus are still very useful in many areas. Various strategies have been proposed to improve the efficiency of the solar energy systems, such as: creating effective solar cell structures [139], using different composite materials [140], designing more efficient maximum power point tracking (MPPT) algorithms and electrical power converters for energy harvesting [10, 111, 139, 141, 142], and new architectures for photovoltaic (PV) arrays [141, 143]. The determination of the parameters of the electrical model of the PV cell (referred to as parameter extraction) is of great importance to solar energy related research as the parameters extracted from the current-voltage (I-V) curves of the PV cell can be used in various applications, such as for investigating the

performance of the MPPT system under different irradiance conditions and analyzing the performance of more complex grid-connected PV systems. In addition, the insight provided by the parameters, which are closely associated with the known physical processes, can be used in quality control during the development of the devices and for fabrication process optimization [144]. The electrical parameters are very important for our proposed hybrid MPPT method which will be introduced in a later Chapter.

3.2.1 Introduction

Various strategies have been proposed to improve the efficiency of the solar energy systems, such as: creating effective solar cell structures [139], using different composite materials [140], designing more efficient maximum power point tracking (MPPT) algorithms and electrical power converters for energy harvesting [10, 111, 139, 141, 142], and new architectures for photovoltaic (PV) arrays [141, 143]. The determination of the parameters of the PV cell (referred to as parameter extraction) is of great importance to solar energy related research as the parameters extracted from the current-voltage (I-V) curves of the PV cell can be used in various applications, such as for investigating the performance of the MPPT system under different irradiance conditions and analyzing the performance of more complex grid-connected PV systems. In addition, the insight provided by the parameters, which are closely associated with the known physical processes, can be used in quality control during the development of the devices and for fabrication process optimization [144].

Parameter extraction refers to the process of extracting the electrical parameters of the solar cells/modules from the measured I-V curves. These I-V curves can be under dark [145] or illuminated [144] conditions. In our work, two widely used nonlinear lumped-parameter equivalent circuit models: the single diode model [146] and the two diode model [146] as introduced in Chapter 2, are considered for parameter extraction of solar cells. For the single diode model, the extracted parameters include the saturation current (I_{s1}), the photocurrent (I_{ph}), the ideality factor (n) and the parasitic series and shunt resistance (R_s and R_p). For the two diode solar cell model, two additional parameters: the ideality factor (n_2) and the saturation current (I_{s2}) of the second diode need to be added.

In the previous literature review, many methods for parameter estimation of solar cells have been introduced. Generally, the parameter estimation methods can be categorized into analytical methods [146] and numerical methods [147-156]. In the analytical method, several key points from the characteristic of the I-V curve, such as the optimal power point, the short circuit current, the open circuit voltage, and the slopes at the axis intersections [146] are used to calculate the parameters. This method is relatively simple. However, the accuracy of the extracted parameters depends significantly on the locations of these key

points. Unfortunately, the measured data usually contains noise due to the device inaccuracy and other electrical disturbances. Moreover, since the I-V characteristics in the datasheet are measured under standard test conditions (STC) which are usually different from real weather conditions, significant errors can be caused when using the values from the datasheet provided by the manufacturer. Therefore, it is unrealistic to use the key data points from the datasheet to calculate the model parameters.

To reduce the uncertainties in the analytical method, many researchers have explored numerical methods, such as the Newton-Raphson method [147], particle swarm optimization (PSO) [149], the genetic algorithm (GA) [148], harmony search (HS) [151], simulated annealing (SA) [150], pattern search (PS) [152], differential evolution (DE) [153], artificial neural network (ANN) [154, 155, 157], etc. For the conventional NR method, the final results are heavily dependent upon the initial values of the parameters in the iteration. Additionally, it is computationally intensive due to the need to calculate the Jacobian matrix in each iteration. Even worse, when the Jacobian matrix is very close to singular, the NR method may fail to converge. Compared to the conventional NR method, the GA method provides better results with no initial condition dependency. However, GA requires many more iterations to determine the parameters [153]. In [149], the PSO is proposed to extract the solar cell parameters from the illuminated I-V characteristics. The results show that PSO gives better parameter precision and higher computational efficiency than GA. However, the randomly generated initial values significantly influence the accuracy of the extracted parameter values. In order to solve this problem, Sandrolini *et al.* [156] used cluster analysis to determine whether the parameter mean values adequately represented the PV module. Among the different clusters obtained from analysis, the one with the highest density is chosen from which the parameters are extracted. However, this procedure requires a large amount of memory, and when applied to a real-time system, the tracking speed will be limited. For SA, the initial temperature and the cooling scheme have a significant effect on the results. Similarly, HS and PS have several shortcomings, including the lack of accuracy and a slow search speed. ANN based technique is suitable when sufficient data for network training can be provided. In addition to the shortcomings identified above, the specific characteristics of the process for parameter estimation should also be considered. For example, the parameter estimation method should be accurate, reliable and fast, for a range of different types of cells. Among the parameter estimation techniques mentioned above, the conventional DE seems to be a good choice for estimation since it exhibits high accuracy and fast convergence speed [153]. However, the results depend on the control parameters of the DE algorithm and an inappropriate choice of these parameters may result in DE failing to converge or in a very slow convergence to the global optimal point.

In this section, an improved adaptive DE (IADE) based parameter estimation method is proposed. IADE has a simple structure and automatically adjusts the two control parameters for the DE algorithm. Compared to the standard DE optimization algorithm, our proposed IADE algorithm reduces the number of control parameters to be tuned manually. It not only ensures the accuracy of the extracted parameters but also simplifies and accelerates the optimization process. The feasibility of the proposed method is verified with both synthetic data and experimental I-V data. It can also be applied to estimate the parameters of the auxiliary function [158-160] which is defined to transform the original variable space into another space so that the relationship between I or V and the auxiliary function can be represented as simple polynomial equations. This method makes the process of parameter estimation for solar cells/modules easier because the parameters can then be extracted using the relationship between the original parameters and newly formed parameters in the auxiliary function.

3.2.2 Parameter estimation process

The single diode model with shunt resistance, as shown in Section 2.1.1, is used to describe the electrical characteristics of a solar cell/module. The lumped parameter equivalent electrical circuit of this model is described as Eq. (2.9) [19]. The equivalent circuit expression can also be used for solar modules. However, for the PV module, it should be noted that even though the extracted parameters show good association with the experimental data, they cannot be exactly related to the physical phenomena due to the differences between the solar cells connected to form the modules [147].

For the single diode model the values of the five unknown parameters, the photocurrent generated by the solar cell (I_{ph}), saturation current (I_o), series resistance (R_s), parallel resistance (R_p), and ideality factor (n) are to be estimated. The model of the PV cell/module can be implemented on many platforms such as MATLAB, Mathematic, Labview, etc. To model the PV module, the current relationship in the single diode model is represented by Eq.(2.8), which is a nonlinear transcendental function. The Newton-Raphson method is used to solve this nonlinear function. By moving the terms of the current equation (the single-diode model Eq. (2.8)) on the right side to the left, the error can be calculated as the value of the term on the left side with measured current and voltage values. The fitness function [149, 153] is defined as the root mean square error (RMSE) between the calculated current value using the current equation of the single-diode model Eq. (2.8) indicated in Section 2.1.1.2 and the measured current value in the experiment. Thus, for a given voltage value, the current value is solved by Newton-Raphson method. For N measured data points (the combination of current and voltage values), the fitness (or objective) function in the optimization process is defined as:

$$fitness\ (\theta) = \sqrt{\frac{1}{N}\sum_{i=1}^{N}\varepsilon(V_i, I_i, \theta)^2} \tag{3.15}$$

where

$$\varepsilon(V_i, I_i, \theta) = I_i - I_{pv} + I_0[\exp(\frac{V_i + I_i R_s}{nV_t}) - 1] + \frac{V_i + I_i R_s}{R_p} \tag{3.16}$$

where V_i and I_i are the experimental voltage and current points, and θ (θ = [I_{ph}, I_o, R_s, R_p, n]) is the vector of parameters to be extracted. The purpose of the optimization process is to determine the optimal parameters by minimizing the fitness function. A small value for the fitness function indicates a small error between the computed current and the measured current. The procedure to minimize the fitness function using the proposed IADE algorithm is described in detail in the following sections.

3.2.3 Background of differential evolution (DE) algorithm

DE is a population based stochastic function optimization algorithm which optimizes a problem by iteratively improving the solution according to predefined performance criteria. This continuous function optimizer was initially developed by Storn and Price [161] to solve the Chebychev polynomial fitting problem. The critical idea behind the DE algorithm is the mechanism for generating trial parameter vectors. DE adds the weighted difference between two population vectors to a third mutated vector. No separate probability distribution or gradient of the problem needs to be used, making the scheme fully self-organizing. This technique has been introduced in literature review, section 2.2.17.2, but for clarity, the basic steps of the standard DE algorithm are listed again as follows [161].

Step 1: *Initialization.* Set the initial conditions of the DE algorithm, such as the generation label (g = 1), the population size (N_p), maximum generations (G_{max}), the crossover rate (CR), and the scaling factor (F). Randomly generate an initial (first generation) population size of N_p D-dimensional vectors with a uniform probability distribution, within the predetermined limits (X_{Lower}, X_{Upper}) of the parameter space. The initial population can be given by:

$$X^1 = [X_1^1, X_2^1, \cdots, X_i^1, \cdots, X_{NP}^1],\ (i=1,2,\ldots,N_p) \tag{3.17}$$

$$X_i^1 = X_{Lower} + (X_{Upper} - X_{Lower})\, RM_i^1, \quad X_i^1 = [x_{i,1}^1, x_{i,2}^1, \cdots, x_{i,D}^1] \tag{3.18}$$

where each variable (x_i^1) is a D-dimensional vector, and RM_i^1 = [$rm^1_{i,1}$, $rm^1_{i,2}$, …, $rm^1_{i,D}$], is a randomly generated vector within the range of (0,1) with uniform distribution.

Step 2: *Mutation.* For each individual in the g^{th} generation, DE generates a new solution candidate (mutant vector) by adding the weighted difference between randomly selected individuals to another vector (target vector). These randomly selected individuals are

different from the target vector. In this work, we use the mutation strategy of "DE/best/1/bin" (a nomenclature scheme to reference different DE variants), where "DE" denotes differential evolution, "best" indicates that the target vector selected to compute the mutation vectors is chosen to be the individual with the best fitness value from the current population in the g^{th} generation, "1" represents the number of difference vectors adopted, and "bin" means binomial recombination. This mutation strategy was chosen due to its simple implementation and good accuracy. The mutation strategy is described by:

$$V_i^g = X_{best}^g + F(X_{r_1}^g - X_{r_2}^g) \tag{3.19}$$

where $r_1 \neq r_2 = \{1, 2, \ldots, N_p\}$ are randomly generated integers respectively, X^g_{r1}, X^g_{r2} are the randomly selected vectors among the population, X^g_{best} is the vector with the best fitness value among the individuals, $F \in (0, 2]$ is a scaling factor which controls the amplification of the differential variation and $V_i^g = [v^g_{i,1}, v^g_{i,2}, \ldots, v^g_{i,D}]$.

Other mutation strategies are possible, such as:

"DE/rand/1"

$$V_i^g = X_{r_1}^g + F(X_{r_2}^g - X_{r_3}^g) \tag{3.20}$$

"DE/best/1"

$$V_i^g = X_{best}^g + F(X_{r_1}^g - X_{r_2}^g) \tag{3.21}$$

"DE/rand/2"

$$V_i^g = X_{r_1}^g + F(X_{r_2}^g - X_{r_3}^g) + F(X_{r_4}^g - X_{r_5}^g) \tag{3.22}$$

"DE/best/2"

$$V_i^g = X_{best}^g + F(X_{r_1}^g - X_{r_2}^g) + F(X_{r_3}^g - X_{r_4}^g) \tag{3.23}$$

"DE/current-to-best/1"

$$V_i^g = X_i^g + F(X_{best}^g - X_i^g) + F(X_{r_1}^g - X_{r_2}^g) \tag{3.24}$$

where X^g_{r1}, X^g_{r2}, X^g_{r3}, X^g_{r4}, X^g_{r5} are the randomly selected vectors from the population. Details of these mutation strategies can be found in [94, 162].

Step 3: *Crossover*. In order to increase the diversity of the population, a crossover process is introduced. Crossover is realized by accepting a component of the mutant vector according to a stochastic probability. If a newly generated random value, with uniform probability distribution, is not greater than CR ($0 \leq CR \leq 1$), the j^{th} component of the

mutant vector is accepted. Otherwise, it is rejected. As a result, after the crossover operation it forms a vector called the trial vector, which is given by:

$$u_{i,j}^{g} = \begin{cases} v_{i,j}^{g}, & \text{if } (rm_{i,j}^{g} \le CR) \text{ or } j = rm_{i,j}^{g} \\ x_{i,j}^{g}, & \text{if } (rm_{i,j}^{g} > CR) \text{ and } j \ne rm_{i,j}^{g} \end{cases}, \quad (i = 1, 2, \cdots, N_p, \quad j = 1, 2, \cdots, D) \tag{3.25}$$

where $u^{g}_{i,j}$ is a component of $U_i^g = [u^{g}_{i,1}, u^{g}_{i,2}, \ldots, u^{g}_{i,D}]$.

Here, boundary constrains are used to avoid the violation of specified limits. Any particle which violates the predetermined boundary of variable space is constrained by the following equations:

$$U_i^g = \begin{cases} U_i^g + (X_H - X_L) \times rm_i, & \text{if } U_i^g \le X_L \\ U_i^g - (X_H - X_L) \times rm_i, & \text{if } U_i^g \ge X_H \end{cases}. \tag{3.26}$$

Step 4: *Selection.* After the crossover process, the generated trial vector may be chosen to be a member of the next generation (the $(g+1)^{th}$ generation) based on the selection criteria, which is given by:

$$X_i^{g+1} = \begin{cases} U_i^g, & \text{if } fitness(U_i^g) < fitness(X_i^g) \\ X_i^g, & \text{otherwise} \end{cases}. \tag{3.27}$$

For the minimization problem, if the fitness function value, $fitness(U_i^g)$, of the trial vector is smaller than that of the original vector, $fitness(X_i^g)$, the newly generated trial vector will be considered as the successful individual in the next generation. Otherwise, it is rejected and the original vector is retained.

Step 5: *Iterate.* Increase the generation step, $g = g + 1$, and repeat step 2 to step 4 until it satisfies the stop criteria which can be the maximum number of generations (G_{max}) or the fitness function values reaches a predefined minimum limit (ε_p).

Step 6: *Output.* Extract the best individual with minimum fitness function in the last generation when the predefined minimum limit or maximum number of generations is reached. Output the minimum fitness value and optimal solution (X_{opt}).

3.2.4 Proposed improved adaptive DE (IADE) algorithm

In the conventional DE, two parameters, namely the scaling factor (F) and the crossover rate (CR) are usually defined with fixed values. However, it is not an easy task to properly determine the control parameters of the DE algorithm for a particular multidimensional problem. When the control parameters are initialized with inappropriate values, the DE algorithm may take a long time or even fail to converge to the optimal value. In order to get appropriate values of these parameters, most of the previously proposed DE techniques

use a trial-and-error. However, this is neither satisfactory nor optimal and usually results in the need for many tedious optimization trials.

Various adaptive or self-adaptive DEs have been proposed to dynamically adjust the control parameters throughout the evolutionary search process. In the past few years, many adaptive DEs have been successfully proposed and applied [162, 163]. Popular adaptive DEs include self-adaptive differential evolution (SaDE) [164], a fuzzy adaptive DE (FADE) [165], jDE [166], JADE [167], differential evolution with an ensemble of parameters and strategies (EPSDE) [168], and CoDE [169], etc. In [164], Qin *et al* proposed SaDE, in which a trial vector is generated from four candidate pools based on the success rate of each mutation strategy within a certain number of generations. The values of scaling factor *F* and crossover *CR* are generated randomly on a normal distribution within a predefined range, respectively. In [165], Liu *et al* presented a FADE, it uses a fuzzy knowledge-based system to dynamically adjust the control parameters *F* and *CR*. In [166], Brest *et al* proposed jDE, in which the parameters *F* and *CR* are encoded into the individuals $X^g_i=[x^g_{i,1}, x^g_{i,2}, \ldots, x^g_{i,Np}, F^g_i, CR^g_i]$. The values of these two parameters are updated with other components in the population vector. From the experimental results, it was found that jDE provides a better result than the classic DE algorithm and FADE. In [167], Zhang *et al* proposed JADE, in which a novel mutation strategy and an external archive are applied into the evolutionary process. In the new mutation strategy, a number of explored inferior solutions stored in an archive are also considered as candidates for generating the mutation vector. Instead of using the best vector of the whole population, any of the top p' percent of individuals ($p'=100p$, where $0 < p < 1$) in the current population can be randomly selected as a component to contribute to the generation of the mutation vector ($X^p_{best,g}$). Based on the idea of SaDE, Mallipeddi *et al* proposed the EPSDE [168], in which trial vectors along with a pool of discrete *F* and *CR* compete among three mutation strategies to produce potential solutions, which are stored when the target vector survives. In a similar way, Wang *et al* [169] presented a composite DE which has a systematic framework for mutation strategies, each of which has fixed combination values of *F* and *CR*.

The experimental results of each method applied to different benchmark functions show that they provide accurate enough global optimal results. However, the common disadvantages of these algorithms include the complex implementation procedures and the large memory requirement to store the previous states for predicting the progress direction. These adaptive DEs are usually appropriate for problems with high dimension and an off-line calculation process. However, when they are utilized for online optimization, they cannot satisfy the fast response requirements. In our study, the parameters extracted from the PV cells/modules are to be used in real-time modeling of the complete PV system. A

smaller memory footprint, simpler structure, and control parameters which can be automatically tuned will better contribute to the parameter estimation process.

Therefore, an adaptive DE algorithm with a simple structure, called IADE, which can automatically adjust the control parameters according to the fitness values during the optimization process, is proposed. A better defined search range can accelerate the search process. The value ranges of *F* and *CR* vary with different optimization problems and there is no strict rule for choosing *F* and *CR*. In order to make sure the algorithm can choose *F* and *CR* wisely, the fitness values of the subsequent steps (*i*) and the previous step (*i*-1) are important factors affecting the strategy of choosing parameters *F* and *CR*. The ranges of *CR* and *F* in [153, 170] are recommended to be between 0.4 and 1. However, after trying different fixed values of *F* and *CR* manually, we found the algorithm leads to smaller error in the extracted parameters when the range of these two parameters is restricted to be between 0.5 and 1. We use an exponential function to map *F* and *CR* in the range from [0, 1] to [0.5, 1], rather than a linear function, as an exponential mapping has a smooth characteristic with arbitrary order derivatives. Since the variation range of *F* and *CR* is the same, the expressions for choosing *F* and *CR* are similar. The formulas of the scaling factor (*F*) and crossover rate (*CR*) are given by:

$$A = \frac{fitness\_best(i)}{fitness\_best(i-1)} \tag{3.28}$$

$$F = b \cdot \exp(a \cdot A \cdot rm) \tag{3.29}$$

$$CR = b \cdot \exp(a \cdot A \cdot rm) \tag{3.30}$$

where *fitness_best* (*i*) and *fitness_best* (*i*-1) are the fitness value for the i^{th} and $(i\text{-}1)^{th}$ iteration, respectively; *A* is the factor used to affiliate the current fitness value with the strategy of choosing parameters, *F* and *CR*. In order to generate the values of *F* and *CR* randomly, the random number *rm*, with a uniform distribution ($rm \in [0,1]$) is used in (3.29) and (3.30). a, and *b* are constant parameters calculated based on the predefined search ranges of *F* and *CR*. In order to map the range from [0, 1] to [0.5, 1], the value of *F* (or *CR*) should be 0.5 (or 1) corresponding to the value of *rm* at 0 (or 1). As a result, the values of these constant parameters are computed as: $a = \ln 2$ and $b = 0.5$. After substituting the values of *a* and *b* into and (3.30), we can see that when there is no improvement in fitness value between two adjacent generations, the value of *A* is equal to 1. Thus, the *F* and *CR* parameters are random values in the range [0.5, 1]. For the case when there is an improved fitness value, the value of *A* is between 0 and 1. As a result, *F* and *CR* take random values from $[0.5, 0.5 \cdot \exp \cdot (\ln 2 \cdot A)]$, which has a relatively smaller search range than [0.5, 1]. This choice of ranges for *F* and *CR*, in the event of no improvement in fitness value, provides a diverse range from which a new value can be

obtained. Thus, it adds more diversity to the population in the search process, which leads to more promising progress directions and hence avoids premature convergence. Consequently, a higher quality final solution will be provided. The pseudo code of the proposed IADE method is presented in Table 3.5.

3.2.5 Results and discussion

In order to verify the effectiveness of the proposed improved adaptive DE, both synthetic PV data and experimental PV cell (and module) data under different irradiance conditions are tested. Comparisons with other optimization algorithms for parameter estimation are also presented for the synthetic data, which is generated using the single diode solar cell/module model. Since we cannot practically guarantee optimal parameters of the experimental solar cell/module, we consider the results with the minimum root MSE (RMSE), to be the optimal solution. All the algorithms are implemented in MATLAB on a standard PC with a 3.17GHz duo core Intel CPU and 8G RAM operating under the Windows 7 operating system.

Table 3.5 Pseudo code of the IADE algorithm

Begin
Set parameters ranges [X_{Lower}, X_{Upper}], population size (N_p), max. generation (G_{max}), datasets (V_i, I_i);
Create a random initial population ;
Get the vector with best fitness value in the first generation;
Set g = 1;
*fitness_best_last*1 = min(*fitness*(X_i^1));
*fitness_best_last*2 = *fitness_best_last*1;
While ($g \le G_{max}$) and ($tol > \varepsilon_p$)
  For i = 1 to N_p
    Randomly choose X_{r1} and X_{r2} ($X_{r1} \neq X_{r2}$) from current population;
    Generate scaling factor and crossover rate;
      A = *fitness_best_last*1/*fitness_best_last*2;
      $F = b \cdot \exp(a \cdot A \cdot rm)$, CR = $b \cdot \exp(a \cdot A \cdot rm)$;
    Generate trial vector: $V_i^g = X_{best}^g + F(X_{r_1}^g - X_{r_2}^g)$;
    If $V_i^g \le X_L$ or $V_i^g \ge X_H$
      $V_i^g = X_L + (X_H - X_L) \times rm_i^g$;
    End if
    For j = 1 to D
      If $rm^g_{i,j} \le CR$ or $j = rm^g_{i,j}$
        $u_{i,j}^g = v_{i,j}^g$;
      Else if $rm^g_{i,j} >$ CR or $j \neq rm^g_{i,j}$
        $u_{i,j}^g = x_{i,j}^g$;

End if

End for

If fitness(U_i^g) < fitness(X_i^g)

$X_i^g = U_i^g$

Else $X_i^g = X_i^g$

End if

End for

Get vector with best fitness value $X_{best}^g = X(\min(fitness\ (X_i^g)))$;

*fitness_best_last*2 = *fitness_best_last*1;

*fitness_best_last*1 = min (*fitness*(X_i^g));

$g = g + 1$;

End while

3.2.5.1 Estimation results for synthetic data

The synthetic data is generated from the single diode solar cell model with following parameter values: I_{ph} = 0.7608 A, I_s = 3.223 × 10^{-7} A, R_s = 0.0364 Ω, R_p = 53.76 Ω , n = 1.4837 under the condition of G = 1000W/m^2 and T = 33^{o}C. These parameter values were chosen as they are widely used in literature [147, 149]. Before testing the proposed adaptive DE algorithm, the difficulty in selecting the proper control parameters for the DE algorithm is examined. The fitness value of the extracted parameters for different combinations of *F* and *CR*, are shown in Fig. 3.11. The values of *F* and *CR* change from 0.1 to 2 and 0.1 to 1, respectively, with a step of 0.1. Thus, there are 200 combinations of *F* and *CR*. In order to better show the error distribution, 10 points with fitness value larger than 0.025 are not shown in Fig. 3.11. From Fig. 3.11, we can see that there are a number of *F* and *CR* pairs which display a large fitness value, that is, they provide a poor estimate. If we consider that the extracted parameters with a fitness value less than 1 ×10^{-4} constitute a successful result, the success rate (defined as a ratio of the number of successful results and the total number of combinations (200 in this example)) is only 13.5%. The minimum, maximum and average fitness values for the 200 combinations of *F* and *CR* are 5.2979 ×10^{-11}, 0.2091and 0.0071, respectively. This means that even though the minimum fitness value is small, the average and the maximum fitness values are relatively large.

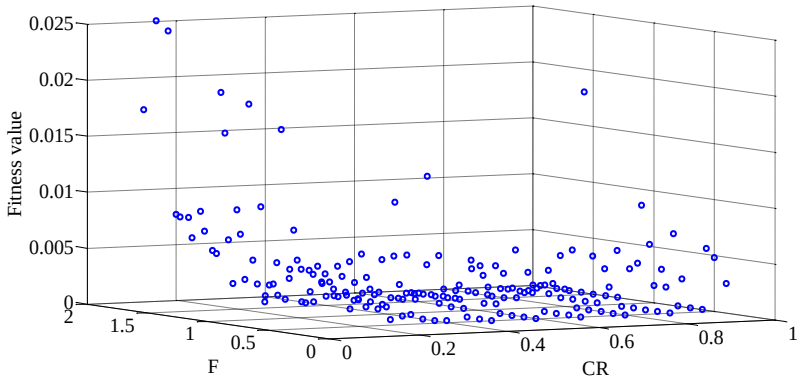

Fig. 3.11 Influence of control parameters on fitness value for different combinations of F and CR.

Next, we examine the estimation results using different optimization methods for synthetic PV data. Since the range of each parameter influences the accuracy of both the results and the search speed, we choose the search range to be ± 100% of the parameter values, similar to [149]. The maximum number of generations, (G_{max}), was set to 8000. The extracted parameters are computed from the synthetic data, using a number of different optimization methods. 30 runs of each optimization method were executed and the best results from the 30 runs are presented in Table 3.6. From Table 3.6, we can see that PSO, GA, SA, and the analytical method based on polynomial fitting and Lambert W function which is presented in [171] all show higher RMSE than our proposed IADE method. Even though the conventional P-DE algorithm gives good accuracy, it requires careful initialization of the control parameter values. If unsuitable control parameters are set, like (F = 0.7, CR=1) in Table 3.6, the algorithm shows poor accuracy. However, our proposed method is able to effectively adapt the control parameters and thus can always estimate the parameters with good accuracy.

Table 3.6 Comparison of different methods with synthetic data (G = 1000 W/m^2 and T = 33°C).

Parameters	Synthetic values	PSO	GA	SA	P-DE (F=0.7, CR=1)	P-DE (F=0.8, CR=1)	Analytical method [171]	Proposed method (IADE)
I_{ph}	0.7608	0.7609	0.7583	0.7286	0.7602	0.7608	0.7608	0.7608
I_s ($\times 10^{-7}$)	3.2230	3.0800	9.5342	8.9263	3.8686	3.2272	3.2228	3.2272
R_s	0.0364	0.0366	0.0321	0.0297	0.0357	0.0364	0.0364	0.0364
R_{sh}	53.7600	52.4725	348.8490	290.0109	64.0848	53.7965	53.76275	53.7965
n	1.4837	1.4792	1.6017	3.1979	1.5023	1.4838	1.4837	1.4838
RMSE	---	5.402×10^{-5}	1.900×10^{-3}	1.185×10^{-1}	3.229×10^{-4}	3.583×10^{-11}	5.808×10^{-5}	4.382×10^{-11}

In much of the previous work described in literature, the extracted parameters from the proposed methods are usually the best solution after trying different combinations of control parameters. However, the distribution of the fitness values within a certain number of runs is also an important indicator for evaluating the optimization algorithm. In order to

evaluate the consistency of each optimization algorithm for parameter estimation, we calculate the minimum ($fitness_{min}$), maximum ($fitness_{max}$) and average ($fitness_{avg}$) of the fitness function after 30 runs for each algorithm. These results are shown in Table 3.7. From Table 3.7, we can see that even though PSO gives better accuracy (i.e. a better minimum fitness value ($fitness_{min}$)) compared to the other non-DE optimization algorithms, PSO has a large distribution of results. This means that PSO algorithm cannot guarantee consistency in the results generated. The traditional DE with control parameter (F=0.8, CR=1) and our IADE method both give very good accuracy and consistency of results. However, the traditional DE method requires a number of trial runs, for the particular dataset, to determine the best control parameters. On the contrary, our proposed IADE method does not require exact values for the control parameters to the DE algorithm, but instead only requires a predefined range and gives better result consistency than other methods. It can automatically tune the values of F and CR, based on the fitness values in each generation step. As a result, it simplifies the time-consuming process of choosing proper control parameters for DE.

Table 3.7 Performance of different optimization algorithms for parameter estimation with synthetic data within 30 runs, $G = 1000 W/m^2$ and $T = 33^oC$.

Fitness value	PSO	GA	SA	P-DE (F = 0.7, CR = 1)	P-DE (F = 0.8, CR = 1)	Proposed method (IADE)
$fitness_{min}$	5.402×10^{-5}	1.900×10^{-3}	2.620×10^{-2}	3.229×10^{-4}	3.583×10^{-11}	4.437×10^{-11}
$fitness_{max}$	4.736×10^{-1}	1.132×10^{-1}	1.133×10^{-1}	4.600×10^{-3}	9.942×10^{-11}	9.975×10^{-11}
$fitness_{avg}$	1.050×10^{-1}	2.120×10^{-2}	5.700×10^{-2}	2.300×10^{-3}	7.449×10^{-11}	8.397×10^{-11}

3.2.5.2 Estimation results for experimental data

The experimental I-V data for a solar cell/module under different irradiance and temperature condition is used to illustrate the effectiveness of our proposed method. For the solar cell, four different irradiance conditions (G = 1003.76, 884.21, 712.03, 601.50 W/m^2) with constant temperature (T = 31 ^oC) are tested. For the solar module, two irradiance conditions (G = (1000, 400) W/m^2) and two different temperature conditions (T = (24.6, 45) ^oC) are tested.

Parameter estimation for solar cell

For the solar cell case, four I-V datasets are measured from a multi-crystalline cell using a solar simulator and a current and voltage recorder. Each dataset contains 100 points, representing pairs of current and voltage values. The irradiance values related to these four datasets are 1003.76 W/m^2, 884.21 W/m^2, 712.03W/m^2, and 601.50 W/m^2 respectively. A thermocouple was adhered to the backside of the cell to measure the temperature. The

temperature was maintained at approximately 31^{o}C using air-based cooling. The search range of each parameter to be extracted from the I-V curves are defined as follows:

$$I_{pv} \in (0, 5),\ I_s \in (1\times10^{-12}, 1\times10^{-5}),\ R_s \in (0, 2),\ R_{sh} \in (50, 5000),\ n \in (0.5, 10)\ . \quad (3.31)$$

After applying our proposed IADE method to each I-V dataset, the extracted parameter values and the RMSE are tabulated in Table 3.8. In addition, I-V curves generated using the parameters extracted by our proposed method (IADE) are plotted against the experimentally measured data for the multi-crystalline solar cell under the four different irradiance conditions. They are shown in Fig. 3.12. For the sake of clarity, we have only marked selected experimental data points, uniformly distributed within the I-V range, for each curve in Fig. 3.12. From Fig. 3.12, we can see that the calculated current values fit very well with the measured data, which means that the parameters extracted by our proposed method can represent the intrinsic parameters of the cell efficiently.

As the MPPT techniques that we will introduce in later chapters are concerned with the power at the MPP, we also consider the absolute error (ε) of the power at the optimal power point (P_{mpp}) in percent (shown in Table 3.8), calculated using the following equation:

$$\varepsilon = \frac{P_{mpp\_m} - P_{mpp\_e}}{P_{mpp\_e}} \times 100\% \quad (3.32)$$

where P_{mpp_m} is the maximum power value calculated from the PV module model using the estimated parameters and P_{mpp_e} is the maximum power value obtained from the experimental dataset for the tested PV cell/module. From Table 3.8, we can see that the absolute error of the maximum power is less than 0.9%. The negative value indicates that the power generated by the model is less than the experimental power value.

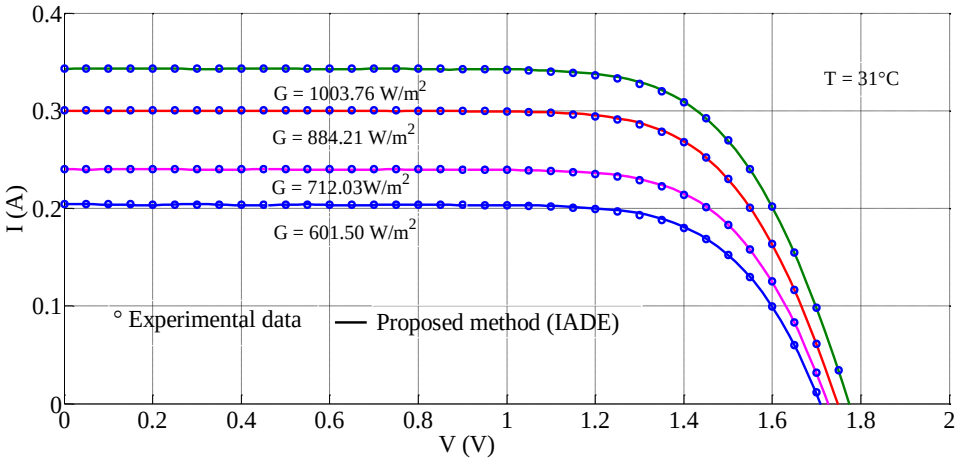

Fig. 3.12 A comparison of the I-V curves generated using the extracted parameters from our proposed IADE method (solid line) and the measured data for a multi-crystalline solar cell (dots) under four different irradiance conditions, G = 1003.76 W/m^2, 884.21 W/m^2, 712.03 W/m^2, and 601.50 W/m^2, respectively.

Table 3.8 The cell parameters extracted for the experimental solar cell using the proposed method (IADE), with different irradiance conditions and a constant temperature T = 31 °C.

Parameters	1003.76 W/m^2	884.21 W/m^2	712.03W/m^2	601.50 W/m^2
I_{ph}	0.343	0.300	0.240	0.204
I_s	2.153×10^{-8}	1.921×10^{-8}	1.859×10^{-8}	3.322×10^{-8}
R_s	0.408	0.408	0.403	0.374
R_{sh}	4968.266	4733.853	4898.204	4976.464
n	1.362	1.343	1.342	1.391
RMSE	3.940×10^{-4}	3.900×10^{-4}	2.920×10^{-4}	3.698×10^{-4}
ε (%)	-0.87%	-0.60%	-0.49%	-0.39%

Parameter estimation for solar module

In this section, we use a commercial mono-crystalline solar module (SL80CE-36M) from the Sinopuren Energy Group to verify the effectiveness of our proposed method for parameter estimation. There are 72 solar cells connected in series in the solar module. The commercial parameters of the module from the manufacture's datasheet are, maximum power: 80 W, optimum power voltage (V_{mp}): 35.1 V, optimum power current (I_{mp}): 2.28 A, open circuit voltage (V_{oc}): 43.2 V, short circuit current (I_{sc}): 2.44 A, short circuit current coefficient (K_i): 0.976 mA/ °C, and open circuit voltage coefficient (K_v): -164.16 mV/ °C. Similar to the previous solar cell experiment, four datasets corresponding to the I-V curves under different irradiance and temperature conditions ((G, T) = (24.6 °C, 999.0 W/m^2), (24.6 °C, 400.7 W/m^2), (45 °C, 400.6 W/m^2), (45 °C, 999.9 W/m^2),) are obtained. There are 800 points for each dataset. The search ranges of each parameter are defined as:

$$I_{pv} \in (0,10),\ I_s \in (1\times10^{-12}, 1\times10^{-5}),\ R_s \in (0,5),\ R_{sh} \in (50,5000),\ n \in (0.5,100)\ . \quad (3.33)$$

The extracted parameters and the RMSE after applying our proposed IADE method to these four I-V curves are given in Table 3.9. Fig. 3.13 shows the calculated I-V curves using the extracted parameters along with the experimentally measured I-V curves. Again, as in Fig. 3.13, for clarity purposes we have only marked selected experimental data points, uniformly distributed within the I-V range. From Fig. 3.13, we can see that the I-V values of the curves obtained using the extracted parameters fit reasonably well over the whole range of the experimental data, except for some points near the maximum power point which have a relatively larger error. The corresponding absolute error of the maximum power (expressed as a percentage) is calculated using Eq.(3.32).

Table 3.9 Extracted parameters for the SL80CE-36M solar module under different irradiance and temperature conditions.

Parameters	T (^{o}C)	G (W/m^2)	T (^{o}C)	G (W/m^2)	T (^{o}C)	G (W/m^2)	T (^{o}C)	G (W/m^2)
	24.6	999.0	24.6	400.7	45	400.6	45	999.9
I_{ph}	2.352		0.945		0.955		2.373	
I_s	6.548×10^{-11}		1.386×10^{-9}		2.5594×10^{-8}		1.9551×10^{-9}	
R_s	0.922		0.972		1.0973		0.9665	
R_{sh}	370.468		883.518		1180.500		442.140	
n	11.561		13.186		7.7395		6.8035	
RMSE	0.0115		0.0060		0.0071		0.0154	
ε (%)	-1.71%		-1.49%		-1.33%		-1.51%	

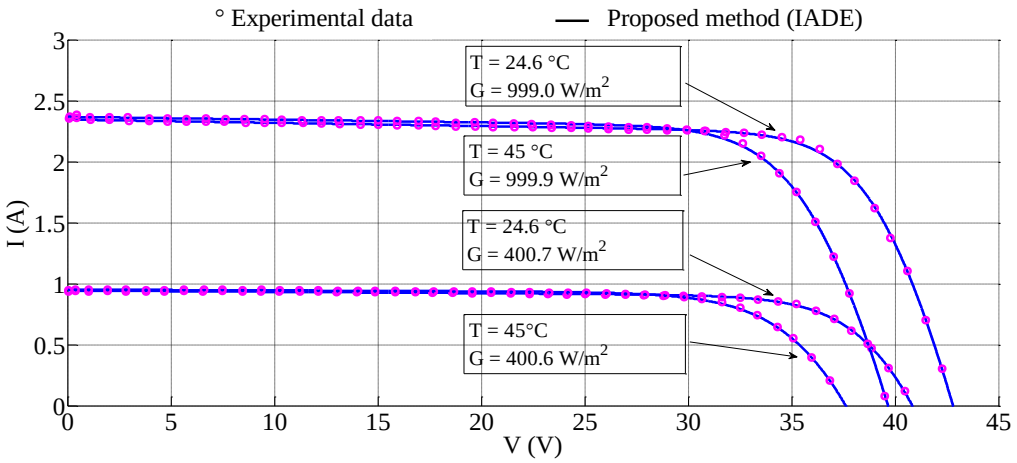

Fig. 3.13 A comparison of I-V curves generated using the extracted parameters from our proposed IADE method (solid line) and the measured data for a mono-crystalline solar module (dots) under different irradiance and temperature conditions.

In addition, we have also tested our proposed IADE method using the same experimental I-V data for the multi-crystalline cell/module as in [172] and [147]. The search range for each parameter in solar cell experiment is set as:

$$I_{pv} \in (0, 2),\ I_s \in (1\times10^{-12}, 1\times10^{-5}),\ R_s \in (0, 2),\ R_{sh} \in (10, 500),\ n \in (0.5, 4). \quad (3.34)$$

For the solar module experiment, the search range for each parameter is set as:

$$I_{pv} \in (0, 2),\ I_s \in (1\times10^{-12}, 1\times10^{-5}),\ R_s \in (0, 2),\ R_{sh} \in (50, 5000),\ n \in (0.5, 100). \quad (3.35)$$

The resultant parameter values and the evaluation values for the solar cell with the experimental dataset from [172] are shown in Table 3.10. From the Table 3.10, we can see that the RMSE computed by the proposed IADE method is much lower than the method used in [172]. Similarly, we also tested our proposed method with the experimental datasets of solar cell and module provided by [147]. Table 3.11 summarizes the estimated parameters computed using the proposed IADE method and by the method in [147]. As can be seen, for both the solar cell and the module, the RMSE values are much lower than that from [147]. In fact, the RMSE of the solar module parameters derived from our method is about 233 times smaller than that from [147].

Table 3.10 A comparison of the extracted parameters obtained from our proposed IADE method and those from [172] using the experimental data for the solar cell from [172].

Parameters	Proposed IADE method	From [172]
I_{ph} (A)	0.5810	0.5754
I_s (A)	9.1248×10^{-8}	9.4586×10^{-8}
R_s (Ω)	0.1647	0.1576
R_p (Ω)	32.2752	65.1712
n	1.4872	1.5675
RMSE	6.0057×10^{-4}	3.7000×10^{-3}

Table 3.11 A comparison of the extracted parameters obtained from our proposed method and those from [147] using the experimental data for the solar cell/module from [147].

	Solar cell		Solar module	
Parameters	Proposed method (IADE)	From [147]	Proposed method (IADE)	From [147]
I_{ph} (A)	0.7607	0.7608	1.0320	1.0318
I_s (A)	3.3613×10^{-7}	3.223×10^{-7}	3.886×10^{-6}	3.2876×10^{-6}
R_s (Ω)	0.03621	0.0364	1.189	1.2057
R_p (Ω)	54.7643	53.7634	921.850	549.450
n	1.4852	1.4837	49.068	48.450
RMSE	9.8900×10^{-4}	9.7000×10^{-3}	2.4000×10^{-3}	5.6010×10^{-1}

The smaller RMSE values in the above comparisons means that our proposed IADE method provides better accuracy. Moreover, the analytical method proposed in [172] is

highly dependent on the initial values of the extracted parameters. The advantage is that our proposed DE algorithm requires only a coarse search-range for parameter determination of solar cells/modules, thus simplifying the optimization procedure [147], unlike algorithms which require very close estimates or guesses to produce a reasonable solution. Moreover, our proposed adaptive DE algorithm has a simple structure and requires no manual tuning; instead it can automatically tune the control parameters using intelligent strategies, which contributes to making it more feasible and effective, when applied to parameter estimation for solar cells/modules.

3.2.6 Summary

This chapter investigates modeling and parameter estimation for PV cells/modules.

In the first section, the proposed Chebyshev functional link neural network (CFLNN) for modeling the PV array is introduced. The accuracy and computational complexity of the proposed model is demonstrated by comparing the test results with other two modeling methods, namely MLP and the two diode analytical model. The analytical modeling method is relatively simple to implement. However, it ignores the influence of solar irradiance and cell temperature on the parallel and series resistance and other uncertainty factors, such as panel aging, module/cell mismatch, manufacturer datasheet inaccuracy and the random choice of initial conditions etc., Therefore, large errors can be associated with analytical modeling. Despite the fact that MLP can efficiently model the solar modules as anticipated, it has a higher computational complexity when implementing it in hardware and it requires a longer training time.

The proposed CFLNN-based model considers system variations due to environmental conditions, system uncertainties, and aging effects. The output current is predicted by inputting the irradiance, temperature, and voltage values measured from the experimental setup. It gives better accuracy than the analytical method and has less computational complexity than the MLP network. Finally, the experimental test with several datasets verified the effectiveness of this modeling method.

In the second section of this Chapter, an improved DE based method for parameter estimation of the PV cells and modules is addressed. Among the many existing heuristic optimization algorithms, DE provides a fast convergence speed and better accuracy in finding the global optimal point. However, the control parameters in the traditional DE algorithm significantly influence the estimation results. Choosing suitable control parameters is a time-consuming and complex process. Additionally, the existing adaptive DE methods are usually efficient for solving problems with high dimension but require large memories and have complex procedures. In order to overcome these shortcomings,

an improved adaptive DE algorithm with a simple structure is proposed in this work. It can automatically adjust the control parameters along the search process. Our proposed IADE method has a good accuracy for extracting the electrical parameters of solar cells and modules. Comparisons with other optimization methods are also made. These comparisons show that our proposed IADE method provides better accuracy without the need to manually choose the control parameters. The results of using both synthetic and experimental data from our test setup and reference datasets from the related literature show the effectiveness of the proposed method.

Chapter 4 Ant colony optimization (ACO)-based MPPT under partially shaded condition

4.1 Introduction

As described in Chapter 1, due to the nonlinearity between the PV output voltage and current, there is a unique maximum power point (MPP) in the power-voltage (P-V) characteristics under uniform weather conditions. When the PV arrays are directly connected with the load, the potential power that could be extracted from the PV arrays is wasted because the power output of the PV arrays mainly depends on the characteristic of the load. In order to maximize the power from the PV system, an MPP tracker is usually inserted between the PV array and the load as shown in Fig. 1.1 to make sure that the system operates at the MPP. However, when PV systems are operated under partially shaded conditions, which are usually caused by the passing clouds, nearby trees, buildings, long-lasting dust, etc., the characteristic of the P-V curve shows multiple peaks. This results in many conventional maximum power point tracking (MPPT) algorithms, such as perturb and observe (P&O) and incremental inductance (IncCond), becoming trapped at a local maximum, causing a significant energy loss of up to 70% [10].

Over the years, many researchers have studied alternative MPPT algorithms (as reviewed in Chapter 2). However, as described in Table 2.4 which provides the performance of each MPPT method, they are either unable to track the global MPP, require a long search time or have a complex structure, etc. Compared to conventional MPPTs, computational intelligence based methods, such as fuzzy logic (FL) [173], artificial neural network (ANN) [106, 127, 174], evolutionary algorithms [54] and so forth, offer significant benefits. The advantages include: no requirement for knowledge of the internal system parameters, reduced computational effort and a compact solution for multivariable problems. However, for fuzzy logic based methods, the fuzzy rule based, which is dependent on the experience of algorithm developers, significantly influences the performance of MPPT. ANN based methods are only suitable for systems where there is sufficient training data. Evolutionary algorithms based methods, such as PSO and DE, are efficient for non-uniform weather conditions, however the convergence speed is limited and the convergence depends on the initial position of the agents [54].

Since ant colony optimization (ACO) has been widely used in scheduling [175], image processing [176], power electronic circuit design [177], and many other fields, we propose

using an ACO-based MPPT to track the MPP for a large-scale PV system under partially shaded conditions. We also design a PV array configuration structure along with this new MPPT algorithm. With this MPPT control scheme, only one pair of current and voltage sensors are required which simplifies the PV system and reduces the system cost. It also guarantees to find the global MPP under various partially shaded conditions and features a fast convergence speed, convergence independent of the initial conditions, and no requirement for knowledge about the characteristic of PV array.

4.2 Problem definition for partially shaded conditions

PV cells are extremely sensitive to the partial shading. If a cell or a small portion of a module in a series string is shaded, then instead of contributing to the power output, the shaded cell(s) will absorb the power from the other cells in the string. This absorbed power is converted into heat, contributing to hot spots that can damage the cell(s). Most commercial modules use bypass diodes across a series of cells to overcome this effect. Thus, the shaded cells are bypassed and as a result, only the power from the shaded series (of cells) is lost. A typical PV module consists of a series connection of cells with a bypass diode across each 18 to 20 cells. This group of cells is called a series with a bypass diode. A typical module will have 2 or 3 diodes.

When only a single cell (or a small number of cells) in a series is partially shaded the series behaves the same as if all cells in the series are shaded. To simplify the analysis, and to avoid confusion in our partial shading analysis, we have considered a module to have just a single series with bypass diode. Then a more realistic commercial module could be considered as a series connection of two or more of these simple modules, as shown in Fig. 1.2. Using such a simple model of the PV module means that there is no difference in power output, irrespective of whether a single cell or the complete module is shaded, so long as the irradiance is uniform.

In order to illustrate the characteristics of the PV modules under partial shading and full shading conditions, the I-V and P-V curves of the PV module with and without bypass diodes, for the small PV system shown in Fig. 1.2, are given in Fig. 4.1 and Fig. 4.2 respectively. Fig. 4.1 shows the I-V curves for each PV module and for the combined PV string without bypass diodes and with bypass diodes. Each PV module receives a different irradiance value (G_{M1}=300W/m^2, G_{M2}=1000W/m^2). Fig. 4.2 gives the P-V curves, and shows that there is only one peak in the P-V curve for the module string without bypass diodes. Thus without bypass diodes, the number of peaks is the same as when the irradiance on these two modules is uniform (at 300W/m^2). However, when the bypass diodes are added, each module contributes to the total power, and as such two peaks are observed in the P-V curve of the module string. Here, the number of peaks in the power

curve is related to the uniformity of the irradiance on each PV module and the number of modules (bypass diodes). For example, for a PV system with N_{ss} modules, connected in series with each module receiving a different irradiance, the number of peaks in the P-V curve will equal N_{ss}. Some researchers [9, 178] have suggested using a bypass diode for each solar cell to reduce the power loss caused by partial shading within a PV module, but this would add to the cost and complexity of the module. These different bypass diode configurations and how they could be optimized to maximize power is not within the scope of this study.

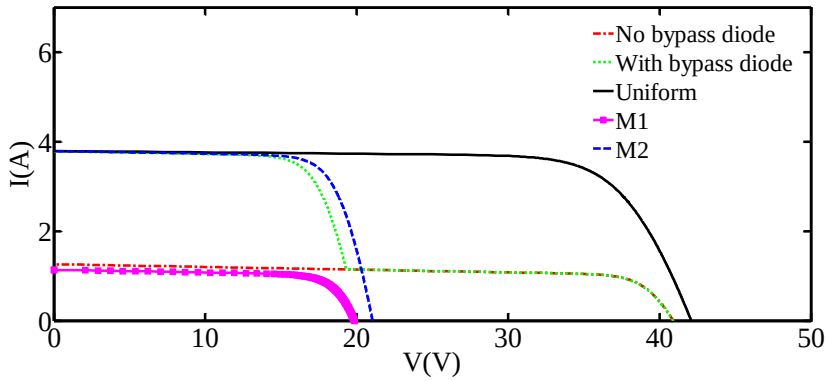

Fig. 4.1 The I-V curves for modules $M1$ and $M2$, and the two series connected module PV string, with and without bypass diodes; For the partial shading condition, the irradiance on each PV module is: G_{M1}=300w/m^2 and G_{M2}=1000w/m^2; For the uniform irradiance condition: G_{M1}=G_{M2}=1000w/m^2.

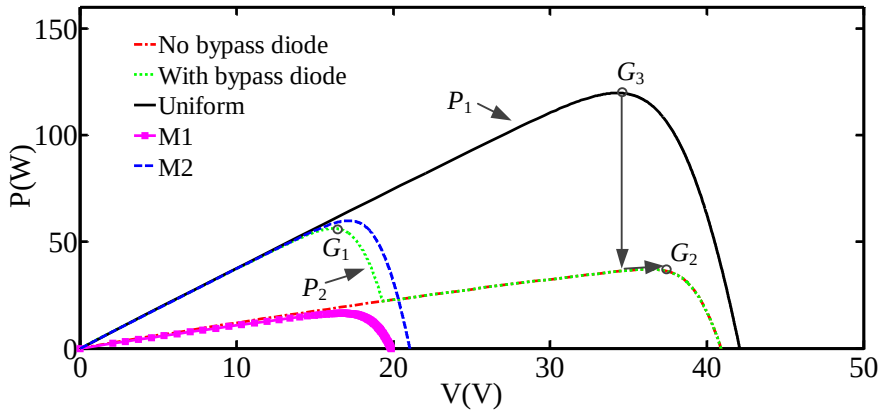

Fig. 4.2 The P-V curves of the modules with the same series assembly and same irradiance as in Fig. 4.1. P_1 and P_2 represent the PV string power for uniform and non-uniform irradiance conditions, respectively.

In the process of verifying the effectiveness of the proposed MPPT, the PV array is modeled using the two diode model [20], as shown in Section 3.1.2, using Eqs. (3.2) - (3.4). For the bypass diode, the relationship between the current and voltage of the bypass diode is described as:

$$V_b = -a_3 V_t \ln(1 + \frac{I_b}{I_{ob}}) \quad (4.1)$$

where I_b, I_{ob}, V_b, and a_3 are the current passing through the bypass diode, the saturation current, the voltage across the bypass diode, and the ideal constant of the bypass diode, respectively. The PV modules used in this work are BP MSX 60 from BP solar company, with specifications given in Table 4.1.

Table 4.1 The specifications of the PV module.

Maximum power (P_{max})	60W	Short circuit current (I_{sc})	3.8A
Optimum voltage (V_{mp})	17.1V	Number of cells (N_s in series)	36
Optimum current (I_{mp})	3.5A	Temp. coefficient of I_{sc} A / ℃℃	0.003
Open circuit voltage (V_{oc})	21.1V	Temp. coefficient of V_{oc} V / ℃ ℃	-0.08

4.3 MPPT under partially shaded conditions

As indicated above, in order to protect the PV panel from hotspots due to the module acting as a load and consuming power, bypass diodes (D_1 and D_2) are added to the PV system by connecting them in parallel with the PV modules, as shown in Fig. 1.2. In addition, the blocking diode (D_b) is usually connected in the PV string in series to prevent a reverse current from the load or unbalanced current flow from other paralleled PV strings.

Since the current through these two modules with different irradiance is equal due to their series connection, the I-V curve of this assembly (green dotted line) can be obtained by adding the voltages across them while keeping the current constant, as shown in Fig. 4.1. From the I-V curve, it is evident that two knee-points are formed, generating two peaks, or local maxima, (G_1 and G_2) in the resultant P-V curve, as shown in Fig. 4.2. When these two modules are exposed to uniform irradiance, there is only one peak, the MPP, (G_3) in the P-V curve. In order to extract the maximum power from the PV array, the system should be operated at the MPP, the global maxima (G_3 or G_1, depending on the distribution of the irradiance). However, when the irradiance changes from a uniform to a non-uniform distribution, the power curve changes from P_1 to P_2. Therefore, the operating point of the PV system with a conventional MPPT algorithm, such as P&O and IncCond, will move to the local maxima (G_2). Thus, the potential power (P_{G1}-P_{G2}) from the PV arrays is wasted. Therefore, in order to maximize the power output from PV systems, an efficient MPP tracking method is needed.

4.4 Proposed PV array configuration structure

PV modules can be connected in series, parallel or a hybrid of the two, among which, hybrid connections are popular. Generally, PV modules are not connected totally in parallel or series as they may not meet the load current and voltage requirements. In addition, it reduces the system stability. For instance, when one of the PV modules connected in series is broken, the operation of the whole string will be affected by the single faulty module. In order to illustrate the system performance clearly, we consider a PV system with two PV strings, each with three PV modules. Usually, there are two modes of MPPT control: centralized [12, 111, 179, 180] and distributed [54, 123, 124, 181-184]. Centralized control means that the entire PV array is controlled by a single MPPT controller. The control variable of each PV string has an equal value (voltage or current). Fully distributed control requires that each PV panel is equipped with an MPPT which are controlled individually. The advantage of the former mode is that it has a simple structure. However, it is easy to lose energy and may not be able to maximize the energy harvest in certain circumstances. For example, when each of the PV strings is assigned the same control value, it cannot guarantee that each PV string is working at the best operating point. The latter method can maximize the energy output, but has a complex structure and additional cost, as each PV module requires its own MPPT controller.

In our work, we examine centralized control by applying computational intelligence optimization algorithms. The difference to the conventional centralized control is that the control value of each PV string converter is different, and as a result a PV array structure based on individual strings is needed. The proposed centralized control method with a control variable per string is shown in Fig. 4.3. In this structure, each PV string is installed with a DC-DC converter instead of each PV module. Moreover, only one pair of current and voltage sensors are required, which has a lower system cost compared to the conventional control scheme which requires a pair of current and voltage sensors in each PV string. Either the current or the voltage of these PV strings can be regarded as the control variable to maximize the power output.

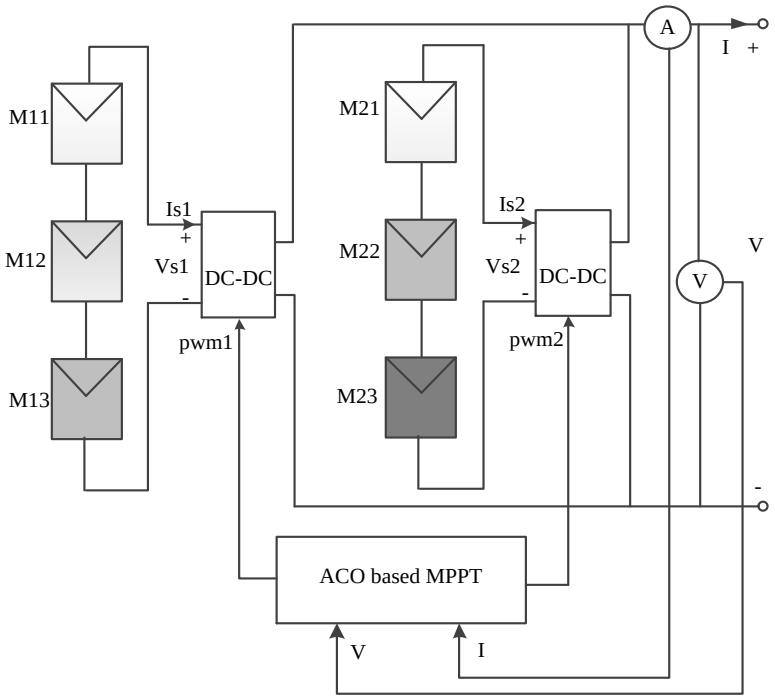

Fig. 4.3 The proposed ACO based MPPT control structure.

4.5 ACO applied to MPPT in a PV system

4.5.1 Ant colony optimization

Ant colony optimization (ACO) is a probabilistic algorithm which is used to find the global optimal solution for a nonlinear problem. ACO mimics the foraging behavior of the ants to achieve optimization of the path in a graph. The collective behaviors of a large number of ants form a positive feedback phenomenon [185, 186]: ants initially search the path randomly and lay down pheromone for other ants to follow. The more ants that travel through a path, the higher the density of pheromone on the path, and as a result, the greater likelihood that subsequent ant will choose the path. Finally, most of the ants follow the trail until the ant individuals find the shortest path through the exchange of pheromone information. Initially, the ACO algorithm was used to tackle combinational problems. Nowadays, more and more researchers have extended this technology into the continuous domain [187-189], among which Socha et al. [187] showed that the ACO_R gives better performance than other related ACO algorithms. For the continuous problem, the solution construction is a little different from the combinational problem. A pheromone archive is defined in the process of solution generation as shown in Fig. 4.4. The vectors s_i (i = 1, 2, …, j, …, K) and $f(s_i)$ are the K possible solutions and their corresponding fitness functions in the archive, respectively. In PV systems, the fitness function is the power output from the PV string. It is assumed that, for an N - dimensional problem, the number

of ants (the population size) is *NP*. The optimal solution is obtained by updating the possible solutions in the archive continuously until the termination condition is satisfied. The detailed procedures for the solution construction of an ACO based MPPT can be described as follows [187].

Step 1: *Initialization*: Set the initial values for the parameters, such as the population size (*NP*), size of the archive (*K*), balance coefficient (*Q*), maximum number of generations (e.g. iterations) (*maxIter*) and the convergence speed constant (*EP*). Generate *K* random solutions and store them in the solution archive with size *K* (*K* ≥ *NP*), and then rank these *K* solutions according to the fitness value ($f(s_i)$) (from best to worst, in the minimization problem, $f(s_1) \le f(s_2) \le \cdots \le f(s_l) \le \cdots \le f(s_K)$).

Step 2: *Generation of new solutions*: Generate a new solution by sampling the Gaussian kernel probability density function for each dimension in two steps. The first step is to choose the Gaussian probability density subfunction and the second step is to sample the chosen Gaussian probability density subfunction according to the parameterized normal distribution. In the first step, when the l^{th} Gaussian probability density subfunction is chosen, the subcomponent of the solution s_l in each dimension will be used to calculate the parameters for the chosen Gaussian subfunction in the following steps.

The probability density function of each dimension, which is a Gaussian function and consists of multiple (*K*) Gaussian subfunctions, is given by:

$$\boldsymbol{G}^i(x) = \sum_{l=1}^{K} \omega_l g_l^i(x) = \sum_{l=1}^{K} \omega_l \frac{1}{\sigma_l^i \sqrt{2\pi}} \exp\left(-\frac{(x-\mu_l^i)^2}{2\sigma_l^{i^2}}\right) \tag{4.2}$$

where $G^i(x)$ is the Gaussian kernel for the i^{th} dimension of the solution, $g_l{}^i(x)$ is the l^{th} sub-Gaussian function for the i^{th} dimension of the solution, $\mu_l{}^i$ and $\sigma_l{}^i$ are the i^{th} dimensional mean value and the standard deviation for the l^{th} solution, respectively. Three parameters of the Gaussian kernel for each dimension in Eq. (4.2) (mean, μ^i; standard deviation, σ^i; weight, ω_l), are calculated based on the solutions in the archive. They are given by:

$$\boldsymbol{\mu}^i = \{\mu_1^i, \cdots, \mu_l^i, \cdots \mu_K^i\} = \{s_1^i, \cdots, s_l^i, \cdots s_K^i\} \tag{4.3}$$

$$\sigma_l^i = \xi \sum_{j=1}^{K} \frac{\left|s_j^i - s_l^i\right|}{K-1} \tag{4.4}$$

$$\omega_l = \frac{1}{QK\sqrt{2\pi}} \exp\left(-\frac{(l-1)^2}{2Q^2K^2}\right) \text{ , } (\omega_K \le \cdots \le \omega_l \le \cdots \le \omega_2 \le \omega_1) \tag{4.5}$$

where $s^i{}_l$, the i^{th} dimensional value for the l^{th} solution, is considered as the mean value for each sub-Gaussian function, the standard deviation for the i^{th} dimension of the l^{th} solution ($\sigma_l{}^i$) is calculated by multiplying the average distance from the chosen solution s_l to other solutions in the archive with the parameter ξ, which represents the speed of convergence (the higher the value of ξ, the lower the convergence speed) [187, 190]. Here, ω_l is the

weight of solution s_l. It is considered as a value of the Gaussian function with a variable l, mean value of '1' and standard deviation of 'QK', where l is the rank of solution s_l, and Q is the algorithm parameter which represents the importance of the best ranked solutions and is also designed to control the diversification of the search process. When Q is small, the possibility of choosing the best ranking solution is larger. When it is large, the chance of choosing all the solutions is equal. Additional discussion about the parameters of Q and ξ can be found in [187].

The Gaussian subfunction is randomly chosen based on the following probability:

$$p_l = \frac{\omega_l}{\sum_{r=1}^{r=K} \omega_r}. \tag{4.6}$$

Step 3: *Ranking and archive updating*: By repeating the above process, *NP* new solutions are generated. Add the newly generated solutions to the original solutions in the archive, rank the *NP* + *K* solutions and keep only the *K* best solutions in the archive.

Step 4: Stop when the maximum generation is reached or the termination condition ($|V_{ref}(k) - V_{ref}(k\text{-}1)| < \varepsilon$) is satisfied. Otherwise, go to step 2.

Thus, with above solution construction scheme, all the ants will be effectively guided to the optimized point in the search process. The ACO combines a positive feedback mechanism, distributed computing, and a greedy search algorithm. It has a strong ability to search the optimal solution. The positive feedback mechanism ensures that the ant colony algorithm is capable of early detection of the optimal solution. Distributed computing helps the ACO to avoid premature convergence. The greedy search helps to quickly find an acceptable solution, thereby enhancing the efficiency of the system.

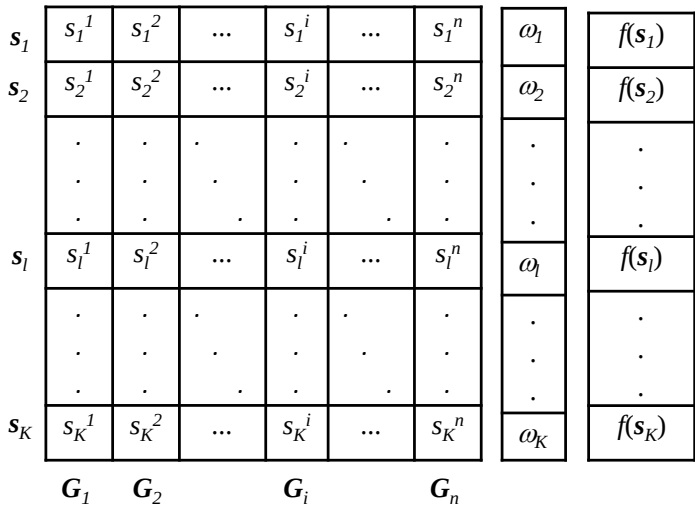

Fig. 4.4 The archive of solution generation process in ACO_R.

4.5.2 Application of ACO to the MPPT problem

The ACO-based optimization is now modified to solve the MPPT problem in PV systems. The system structure that we considered is shown in the Fig. 4.3. The control variable is the current of each PV string. The 3-D plot for the relationship between power and the PV array current (I_1, I_2) is shown in Fig. 4.5. From the figure, we can see that there are multiple local peaks when the PV arrays are illuminated under non-uniform irradiance. Actually, the MPPT for PV systems under partially shaded conditions with the proposed PV array structure can be consideredconsidered as a global optimization in a multidimensional space. For the PV array with only a single PV string, the MPPT becomes a single variable optimization problem.

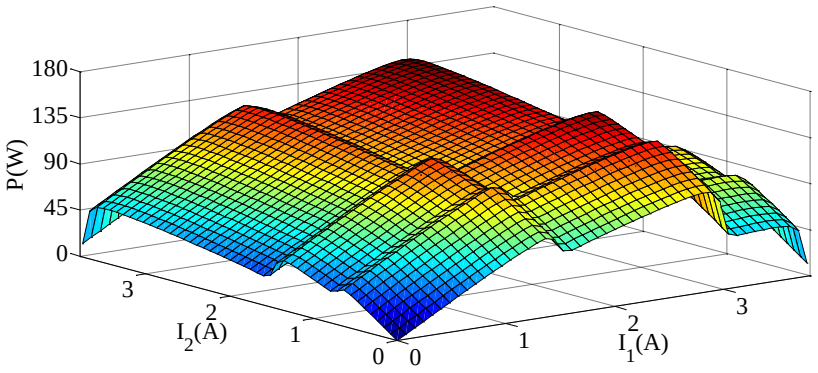

Fig. 4.5 3-D image of the power versus the current in each PV substring under the shading pattern: [M11,M12,M13;M21,M22, M23] = [1000,800,400;1000,400,200]W/m^2.

In order to illustrate the control process, we define the control vector for the PV system with multiple PV strings as:

$$\boldsymbol{s}^t = [I_1^t, I_2^t, \cdots, I_N^t] \tag{4.7}$$

where $\boldsymbol{s}^t$ is the current vector at the t^{th} step, $I_N{}^t$ is the current control value for N^{th} PV string at the t^{th} step. The objective function of this optimization problem $f(\boldsymbol{s}^t)$ is the summation of the power output from each PV substring after applying the current variable to each PV string. It can be described by:

$$f(\boldsymbol{s}^t) = \sum_{j=1}^{N_{PP}} (I_j^t \times V_j^t) \tag{4.8}$$

where I_j^t and V_j^t are the current control variable value and the voltage value for j^{th} PV string at the t^{th} step respectively. Assuming that there are M new solutions generated in each iteration and the maximum number of iterations is T, the values of current for each substring (s^t) change in the following order:

$$\begin{aligned}&(\boldsymbol{s}_1^1 \to \boldsymbol{s}_2^1 \to \cdots \to \boldsymbol{s}_M^1) \to \cdots \to (\boldsymbol{s}_1^t \to \boldsymbol{s}_2^t \to \cdots \to \boldsymbol{s}_M^t)\\ &\to (\boldsymbol{s}_1^{t+1} \to \boldsymbol{s}_2^{t+1} \cdots \to \boldsymbol{s}_M^{t+1}) \to \cdots \to (\boldsymbol{s}_1^T \to \boldsymbol{s}_2^T \to \cdots \to \boldsymbol{s}_M^T).\end{aligned} \tag{4.9}$$

The fitness value of each variable (the current vector), $f(\boldsymbol{s}^t)$, is calculated and evaluated at each stage simultaneously. During the search process, the solution archive is updated iteratively with the newly generated solutions. These processes are repeated until the global MPP is obtained. Thus, for a particular shading pattern, the global MPP can be found using this ACO-based search scheme.

Usually, the real working environment of the PV system changes continuously due to the varying weather and/or the load conditions, and as a result, the global MPP is not always one fixed point. This requires that the MPPT algorithm has the ability to search for the global MPP for the new weather conditions. In order to realize this, the search process is restarted within a specified period. The reinitialization interval can be between 15min and one hour, and is specified by the user depending on the location of the PV system. If there is a high probability of partial shading, then it is recommended to set a small value. Otherwise, it would be cost effective to set a longer interval. The reinitialization is executed depending on the detected weather conditions. Here, we use the following strategy to detect the change of shading patterns, which is given by:

$$\frac{\left|I(s_{i+1}) - I(s_i)\right|}{I(s_i)} > \Delta I \ . \tag{4.10}$$

When Eq. (4.10) is satisfied or the period set by the timer is reached, the search process will be updated and executed again. Thus, it ensures that the MPPT can always find the global MPP under various working environmental conditions. The flow chart of the proposed ACO-based MPPT algorithm for PV systems is shown in Fig. 4.6. It can be described as follows:

First, initialize the solutions in the archive range and set the algorithm parameters (block A), which include the maximum number of iterations (*MaxIter*), the size of the archive (*K*), the number of newly generated solutions in each generation (*M*), the balance coefficient (*Q*), and the convergence speed constant (*EP*). Then, sense the voltage and current from the entire PV array and calculate the power (block B). After that, mark the corresponding ant by using a sign variable (Flag_ant) and generate a new solution based on the sampling process by using Eqs. (4.2)-(4.6) (block C). By repeating process blocks, B and C, *M* new solutions are created. Thereafter, these *M* new solutions and the original solutions in the archive are put together and ranked. As a result, keep the *K* best solutions in the solution archive. The iteration number (Flag_Iter) is also marked in each step (block E). The processing of blocks (B, C, D, E, F) as shown in Fig. 4.6 is repeated until the maximum iteration number (*MaxIter*) is reached or the power value remains unchanged (or with a very small change) within a specified number of successive iterations. With the above procedures, the global MPP can be found. Finally, keep this working point (block G) until a timer interrupt occurs or a sudden irradiance change is sensed by (13) (block H).

Whenever either of these two incidents occurs, the whole algorithm will be reinitialized (block I and A) so that it can find the global MPP for the new environment conditions.

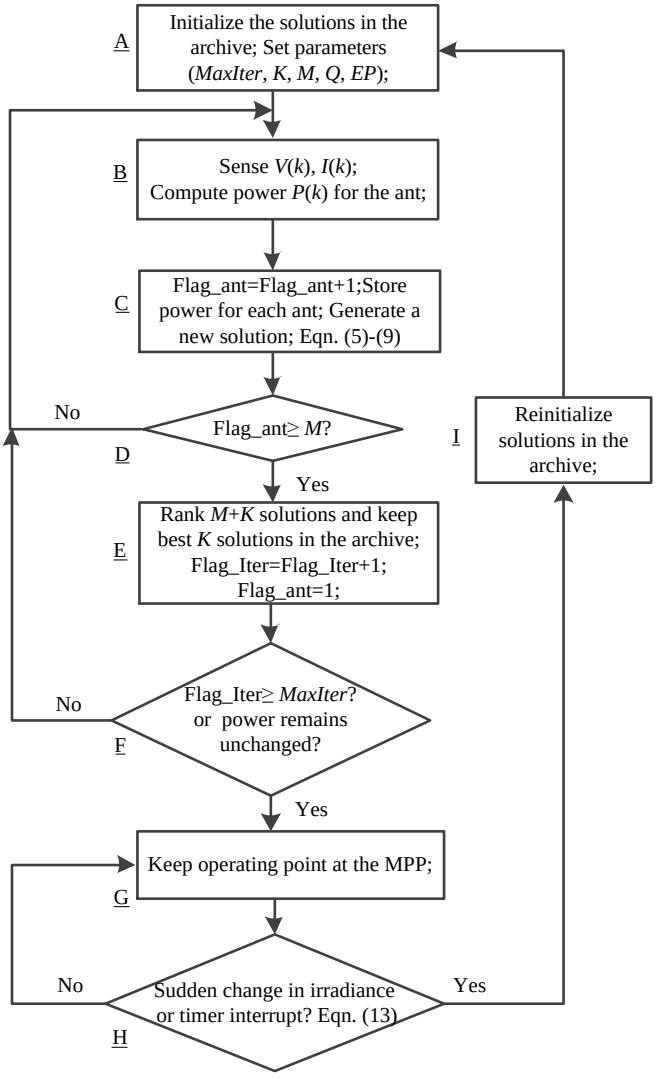

Fig. 4.6 Flow chart of ACO-based MPPT algorithm for PV system with multiple PV strings.

In the proposed MPPT algorithm, the parameters that need to be set by the user include the number of newly generated solutions in each generation (M), the size of the solution archive (K), convergence speed constant (ξ), and the locality of the search process (Q). The number of ants influences the convergence speed and the accuracy of the optimization process. More ants means it is easier to find the global MPP under different irradiance conditions, but it requires more time to transfer all the ants into the MPP. Fewer ants gives a better convergence speed, however, they can easily become trapped at one of the local power peaks. The size K of the solution archive should not be smaller than the dimension of the problem [187]. The relationship between the size of the archive and the percentage of the extracted power for all the cases investigated in the simulation is shown in Fig. 4.7. Therefore, the tradeoff between fast convergence speed and tracking accuracy should be

made when choosing the size of archive. Since our objective for the MPPT algorithm is to get fast convergence with a minimum number of ants, we choose an archive size of 7. The convergence speed constant (ξ) acts like the rate of pheromone evaporation while solving combination problems. The higher the value of ξ, the lower the convergence speed because, in this case, the search is less biased towards the space that has been searched [187]. The locality of the search process (Q) determines the balance between the diversification and intensification. Diversification in the search avoids being stuck at the local peaks, and the intensification ensures a fast search process. When Q is small, the best-ranked solutions in the archive are more likely to be chosen, while when it is large, the probability of choosing solutions is uniform [187]. In order to illustrate this phenomenon, we tested the relationship between the number of iterations for the ACO-based MPPT algorithm to converge and the value of Q. The box-plot of the number of iterations to converge for different Q values is illustrated in Fig. 4.8. It shows that a larger value of Q requires more iterations to converge. Therefore, when choosing the values of Q, the tradeoff between these two contradictory factors should also be made.

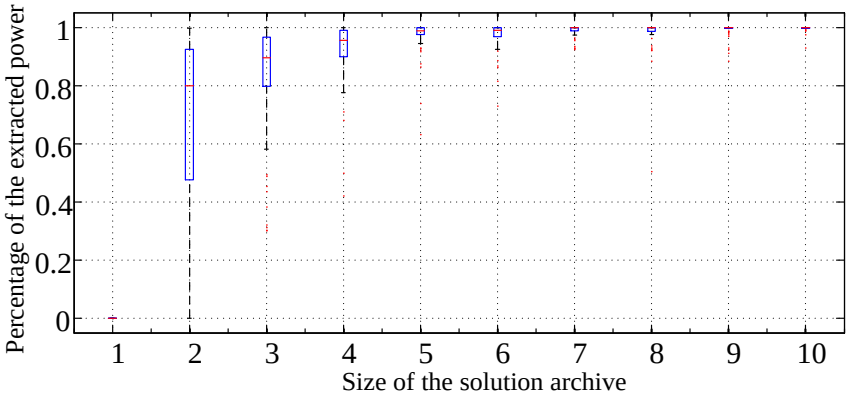

Fig. 4.7 Extracted power versus the archive size.

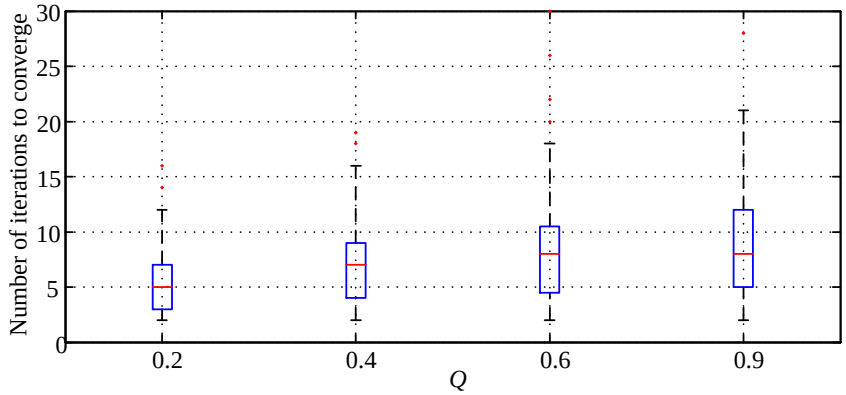

Fig. 4.8 Box-plot of the relationship between the average number of iterations to converge and the value of Q for the irradiance case B in 200 runs; the edges of the box are the 25th and 75th percentiles and the line in the middle of box indicates the average number of iterations to converge.

4.6 Results and discussion

4.6.1 Simulation results

In this section, we verify the feasibility of the proposed ACO-based MPPT using MATLAB SIMULINK. This simulation demonstrates the ability of the proposed ACO-based MPPT to track the global MPP under steady and transient shading patterns. The PV module model is based on the two-diode model, using Eqs. (3.2) – (3.4) described in Section 4.2. The electrical parameters we use in the simulation are given in Table 4.1. The MPPT algorithm is implemented with embedded blocks in SIMULINK. A boost converter is used to step up the voltage from the PV array to 120V. The structure of the PV system for this test has two PV strings and is shown in the Fig. 4.3. For this small PV system, MPPT is a two dimensional optimization problem (N = 2). Since it is very difficult to test all the non-uniform irradiance conditions, we select some circumstances to illustrate the tracking ability of the proposed MPPT method. The four shading patterns (SPs) we tested are listed in Table 4.2. For SP1, the irradiance on all the PV panels is uniform, as a result, only one peak exists in the P-I characteristic curve of the PV array. For the other three SPs, there are multiple peaks. The temperature is assumed to be $40^{o}C$. The parameters of the proposed MPPT method in the simulation are set as shown in Table 4.3. The global MPP is the unique point where the maximum power on the P-V curve occurs. For comparison purposes, we calculate the global MPP by finding the point with the maximum power from the generated P-V curve.

Table 4.2 The shading patterns for the experiment conditions.

Pattern No.	Shading pattern [M_{11}, M_{12}, M_{13}; M_{21}, M_{22}, M_{23}] (W/m^2)
SP1	[1000, 1000, 1000; 1000, 1000, 1000]
SP2	[1000, 800, 400; 1000, 400, 200]
SP3	[500, 200, 400; 800, 400, 200]
SP4	[600, 1000, 1000; 800, 400, 200]

Table 4.3 Algorithm parameters used in the experiment.

Parameter	Symbol	Value
Solution archive size	K	7
Number of newly generated solutions in one generation	M	4
Dimension of the problem	N	2
Convergence speed constant	ξ	0.82
Locality of the search process	Q	0.45

By applying the ACO-based MPPT algorithm for these four cases, the current in each PV string (I_1 and I_2), the ideal power (P_{ideal}) and the average power measured by running the proposed method (P) 200 times are shown in Table 4.4. It shows that the proposed ACO-based MPPT can track the global MPP so that the power output is almost the same as the ideal power under all four shading patterns. Note that this power output is under the assumption that there is no power leakage in the PV system due to the conversion efficiency of the DC-DC converter, power losses from the wire connection or other factors. When implementing this MPPT in a real system, the power harvest will be less than this ideal case. The box-plot distribution of the power extracted from the PV arrays over 200 runs for these four shading patterns is given in Fig. 4.9. From the figure, we can see that after 200 runs for each shading pattern, the distribution of the final power extracted from the PV system using our proposed MPP tracking method is located around the corresponding global MPP. It also indicates that the efficiency of the proposed method is not heavily dependent on the initial conditions of the search process.

Table 4.4 The individual current value in each PV string and the power capture using proposed ACO-based MPPT under various shading patterns with temperature 40°C.

	ACO-based MPPT			
Pattern No.	I_1(A)	I_2(A)	P_{ideal} (W)	P(W)
SP1	3.52	3.52	335.63	335.20
SP2	2.87	3.48	140.46	140.46
SP3	1.40	1.41	89.53	89.22
SP4	2.17	1.41	156.96	154.1

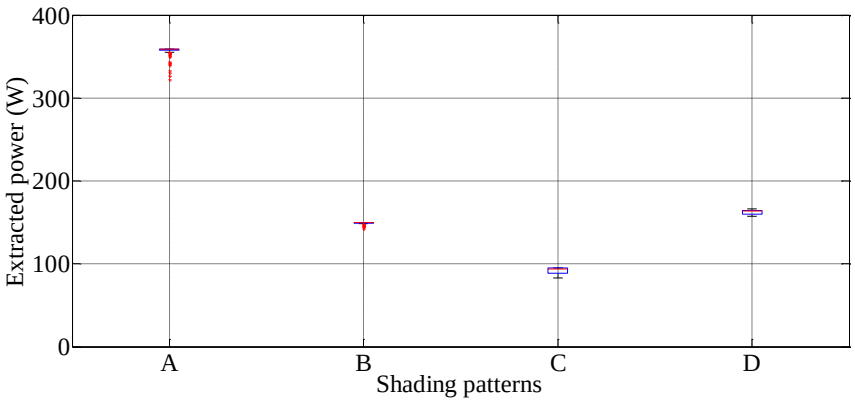

Fig. 4.9 Power extracted by the ACO-based MPPT under the four different shading patterns.

The ability to find the global MPP for new weather conditions is very important especially for places with frequent weather changes, such as in the tropics [191]. In order to illustrate the tracking ability of the proposed ACO-based MPPT algorithm under transient irradiance conditions, three cases are considered - Case 1: SP changes from SP1 to SP2;

Case 2: SP changes from SP1 to SP3, and Case 3: SP changes from SP1 to SP4. The sampling period of the MPPT algorithm is set to 0.01s. The power transient characteristics, the corresponding duty ratio which is the percentage of one period in which a signal is active, and the current variable of each PV string for Case 1. Case 2, and Case 3, are shown in Fig. 4.10, Fig. 4.11 and Fig. 4.12, respectively, where D1 and D2 refer to the duty ratio of the DC-DC converter in each string. From these three performance figures for different transition cases, it can be seen that when the shading pattern changes from a uniform condition to a partially shaded condition at 15 second (the middle of the x-axis), the proposed MPPT algorithm can find the global MPP for the new shading pattern. For example, when the changes are SP1 to SP2, SP1 to SP3 and SP1 to SP4, the power changes from 335W to 140W, 335W to 89W and 335W to 154W, respectively. By simulating all the cases, it is found that the average iterations required to converge is less than 15. Since the sampling period of the MPPT algorithm influences the tracking speed, it should be determined appropriately, according to the PV system location. When setting the sampling period of the MPPT algorithm as 0.12s, we measure that the average execution time of the ACO-based MPPT algorithm is 7.3 ms by running the algorithm 30 times, and the average runtime for the proposed MPPT algorithm to find the global MPP is less than 4 s which means 33 steps (4s/0.12s = 33) to reach the global MPP. This will be explained in detail in the following section. Thus, with this algorithm the global MPP can be found in a very short response time. This capability of fast response is very important for the systems located where there are rapidly changing irradiance conditions, such as in the tropics [191].

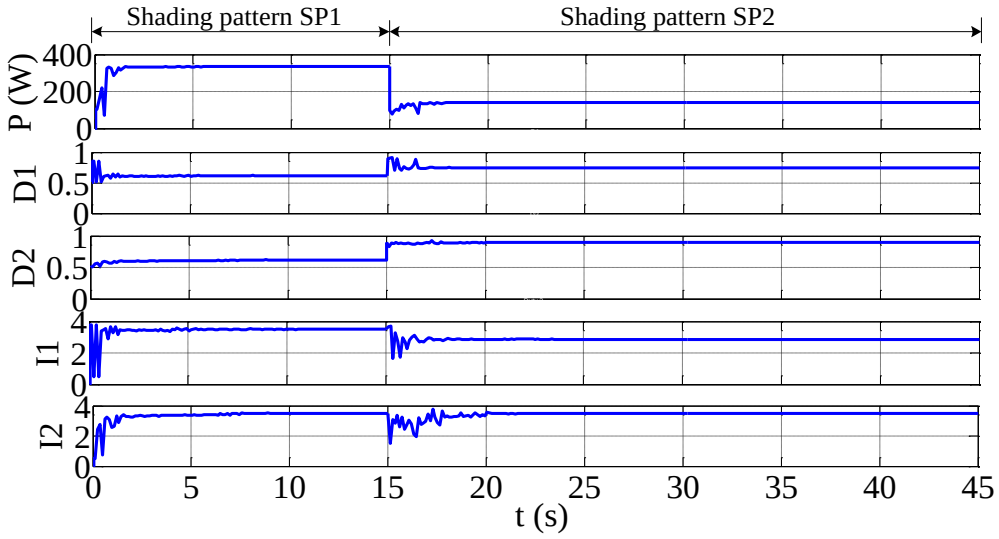

Fig. 4.10 Transient response of the proposed MPPT method for Case 1: SP change from SP1 to SP2, K=7, M=4, ξ=0.82, Q=0.45.

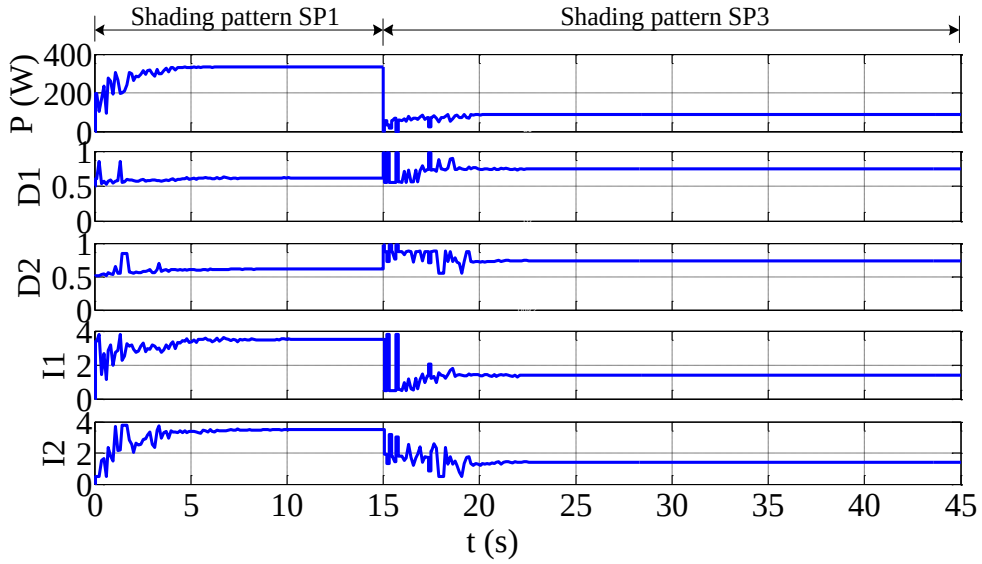

Fig. 4.11 Transient response of the proposed MPPT method for Case 2: SP change from SP1 to SP3, K=7, M=4, ξ=0.82, Q=0.45.

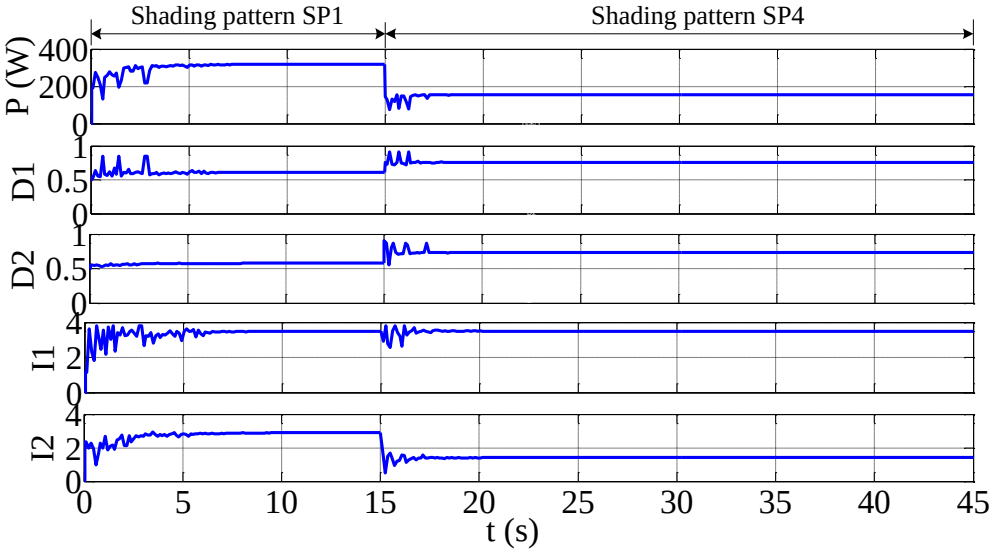

Fig. 4.12 Transient response of the proposed MPPT method for Case 3: SP change from SP1 to SP4, K=7, M=4, ξ=0.82, Q=0.45.

4.6.2 Experimental results and comparisons

Three different evolutionary algorithms, including DE [96], PSO [54] and the proposed ACO based MPPT [141], are implemented to determine their performance for MPPT in PV systems. The flowcharts of DE and PSO based MPPT are shown in Fig. 4.13 and Fig. 4.14, respectively.

The MPPT algorithms are implemented by using a simple experimental prototype as shown in Fig. 4.15. Since only one PV array simulator is available in the laboratory, a PV

array with only a single PV string as shown in Fig. 4.16 is tested. In this case, the control variable is one dimensional (N = 1). A Chroma 62150H-600S programmable PV array simulator is used to simulate the output of PV array. The PV string consists of four series connected PV modules, each of which has a bypass diode connected in parallel, as shown in Fig. 4.16. In partial shading conditions, bypass diodes are necessary to allow current to bypass shaded cells thus enabling the array to generate power and to avoid module/cell hotspots due to cell reverse bias during shading [12, 192]. Because of power limitations in the converter used in the prototype and in the range of the voltage and current sensors used to determine the MPPT operating point a very small PV module, with specifications given in Table 4.5 has been used. The two-diode model [24] is used to generate I-V curves for a number of module shading patterns. These current and voltage values on the I-V curve are then uploaded into the PV array simulator to emulate a real PV array. The PV array simulator is able to store a maximum of 100 I-V curves (with current and voltage points) of a PV array, thus simulating an array under various operating conditions. A buck converter is used to step down the voltage from the PV array to a Chroma 63802 programmable DC electronic load working as a 12 volt lead-acid battery. The switching frequency of the buck converter is set to 50 kHz. The component values used in the buck converter are given in Table 4.6. A Texas Instruments TMS-F28335 DSP is used to implement the proposed evolutionary algorithm MPPT. Two ADC channels are used to input the current and voltage values measured at the output of the PV simulator. A photograph of the prototype system is shown in Fig. 4.17.

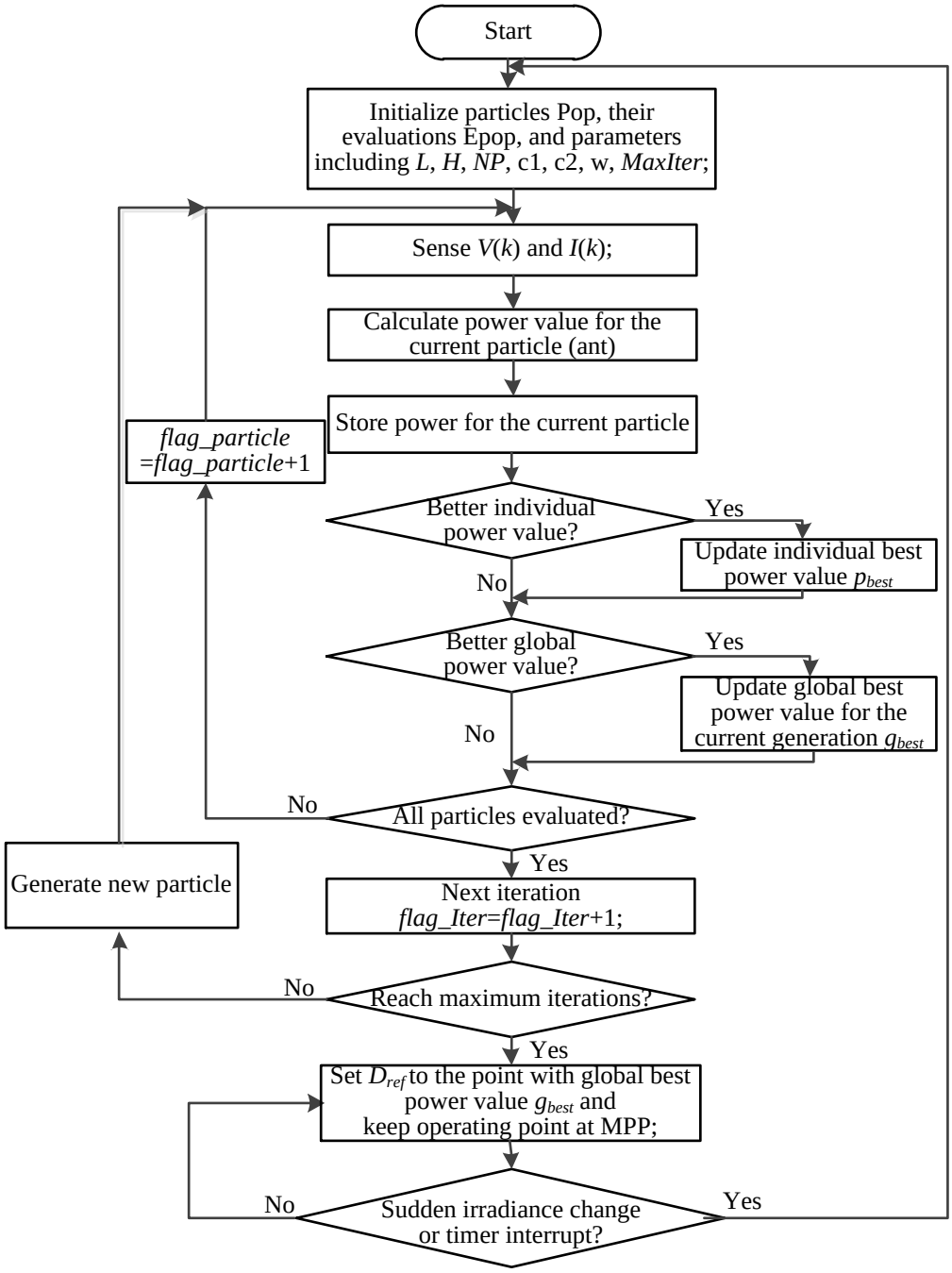

Fig. 4.13 Flowchart of the PSO based MPPT.

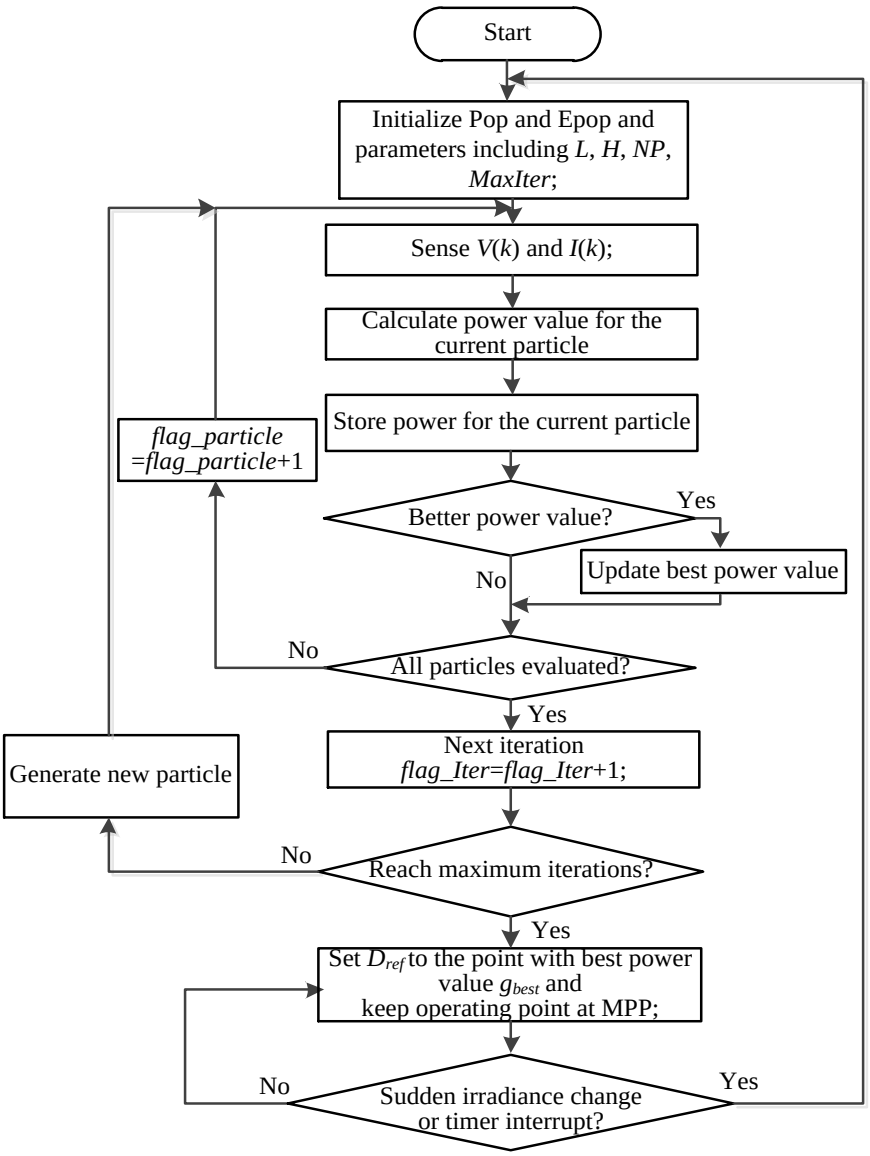

Fig. 4.14 Flowchart of the DE based MPPT.

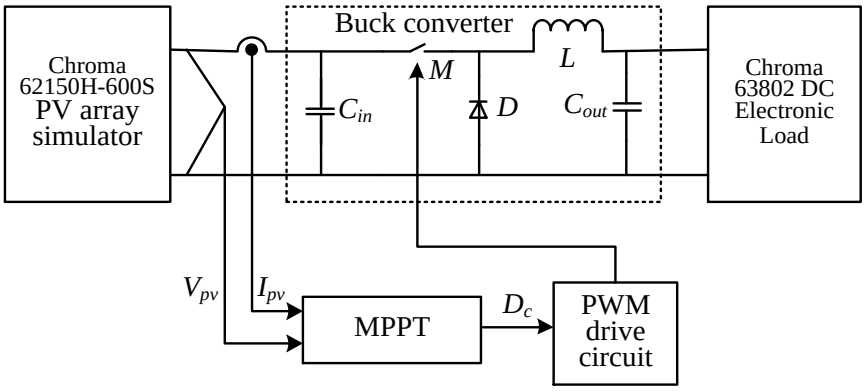

Fig. 4.15 The schematic diagram of the tested PV system with the MPPT device.

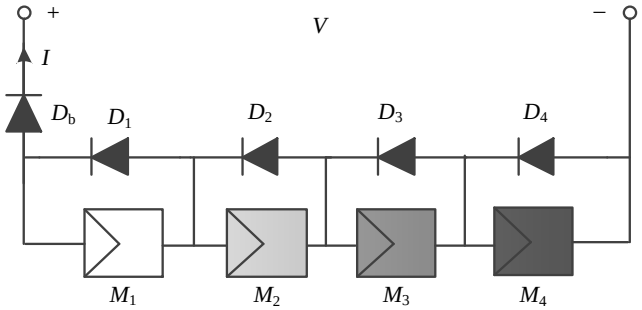

Fig. 4.16 The configuration of the tested PV array.

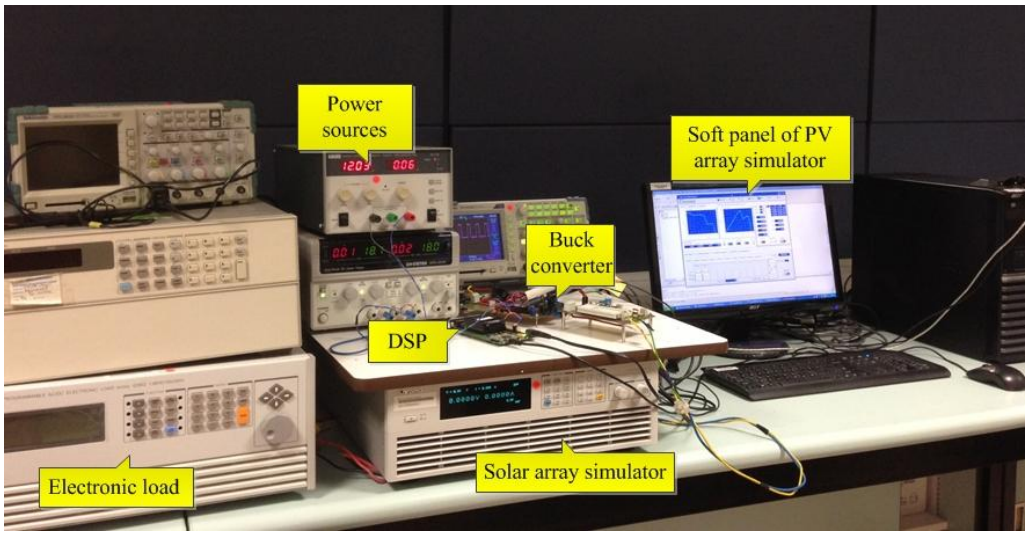

Fig. 4.17 The photo of prototype system.

Table 4.5 Parameters of the tested PV module.

Maximum power (P_{max})	15W	Short circuitcurrent (I_{sc})	1.90A
Optimum voltage (V_{mp})	8.55V	Number of cells in each module	18
Optimum current (I_{mp})	1.75A	Temp. coefficient of I_{sc} A /^oC	1.50×10^{-3}
Open circuit voltage (V_{oc})	10.55V	Temp. coefficient of V_{oc} V /^oC	-0.04

Table 4.6 Parameters of the buck convertor.

Components	Symbol	Value
Inductance	L	453μH
Diode	D	600V/8A
Input capacitor	C_{in}	2200μF
Output capacitor	C_{out}	22 μF
Mosfet switch	M	500V/13A
Switching frequency	f_{hz}	50KHz
MPPT update rate	f_{MPPT}	0.12sec

The experimental prototype is used to determine the performance of the ACO based MPPT compared with two other evolutionary algorithms, namely DE and PSO. The PSO parameters are set the same as those in [54]. For the DE algorithm, the parameters with the best performance are decided by trial and error. Additional guidelines on methods to choose the parameters for PSO, DE and ACO can be found in [193], [166] and [194], respectively. The MPPT update period (T_{mppt}) is set to 0.12 s. This requirement ensures that the system reaches steady state before the next perturbation, based on the response time of the Chroma PV array simulator to a change in the array operating point. The maximum iteration (*maxIter*) is set to 200, which is much larger than the number of iterations actually needed for convergence. The population size (*NP*) is 5. The initial operating voltage of the particles are set to [0.4 0.6 0.7 0.8 0.9] nV_{oc}, where nV_{oc} is the open circuit voltage of the whole PV string. The lower and upper limit of the search range is set to V_o/nV_{oc} and 0.99, respectively, where V_o is the output voltage of the buck converter. To ensure a valid comparison between the three algorithms, common parameters, such as the update period (T_{mppt}), maximum iterations (*maxIter*), initial operating points, lower and upper limits (*L* and *H*), are set the same. The parameters relating to the individual algorithms are listed in Table 4.7.

Table 4.7 Algorithm parameters for the experimental implementation

PSO	DE	ACO
Cognitive constant (c_1): 1.2 Social constant (c_2): 1.6 Inertia weight (w): 0.4	Scaling factor (F): 0.8 Crossover rate (CR): 0.9	Archive size (K): 8 Convergence speed constant (ξ): 0.25 Balance coefficient (Q): 0.8

In the experiment, two types of irradiance conditions, namely uniform (SP1) and nonuniform (SP2 and SP3) shading patterns, are tested, as in Table 4.8. SP1 has a unique MPP on the P-V curve. For the other two nonuniform shading patterns, there are multiple peaks, equal to the number of different irradiance values in the shading pattern. The P-V curve for each shading pattern, along with the global MPP (the dot on the P-V curve), is given in Fig. 4.18.

Table 4.8 The shading patterns tested in the simulation and experiment.

Shading pattern number	Shading patterns [M1, M2, M3, M4]
SP1	[600.0, 600.0, 600.0, 600.0]
SP2	[900.0, 400.0, 800.0, 800.0]
SP3	[400.0, 400.0, 100.0, 100.0]

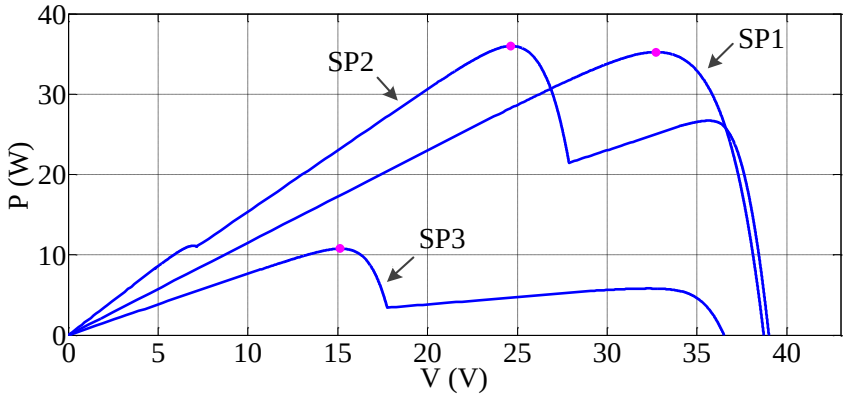

Fig. 4.18 P-V curves under shading patterns, SP1, SP2, and SP3.

Rather than using search time (i.e. convergence time) to evaluate the performance of each MPPT algorithm, it is much clearer to use the number of algorithm steps till convergence. This is because the search time depends not only on the tracking speed of the algorithm but also on the MPPT update period. It should be noted that the number of 'steps' required till convergence for the different MPPT algorithms is not simply the number of iterations or generations. This is because each particle is operated on successively, and thus the number of steps is the result of multiplying 'iterations/generations' with the population size ($N_{step} = Iter \times NP$). The convergence time could then be calculated as $t = N_{step} \times T_{mppt}$. Therefore, after applying each algorithm to the experimental PV system, the number of steps required for convergence to the global MPP under different shading patterns are listed in Table 4.9. From Table 4.9, it can be concluded that when the shading pattern changes, the number of steps required to reach the new global MPP for both ACO and DE is much less than for PSO. This is consistent with [195] which states that ACO provides better accuracy and tracking speed than PSO and with [196] which indicates that DE provides better tracking speed than PSO.

Table 4.9 Number of steps required to converge to the new global MPP after a shading pattern change.

Shading patterns	PSO	DE	ACO
SP1 to SP2	83	33	41
SP1 to SP3	50	33	33

The corresponding experimental power curves produced by each algorithm when the shading pattern changes from SP1 to SP2 and SP1 to SP3 are shown in Fig. 4.19 and Fig. 4.20. The power readings are recorded by the Chroma PV array simulator every 1 second. In each case, the shading pattern changes at the 15 second interval. Before the shading pattern changes, the system is stable and operating with uniform irradiance (SP1). From

Fig. 4.19, it can be seen that the ACO and DE based MPPTs provide similar tracking speed in achieving the new global MPP (35.9W for SP2) and both are significantly faster than that of PSO. Similar performance can be seen in Fig. 4.20, where the SP3 output power is reduced to just 10.7W. We also found that the performance of PSO is very sensitive to the algorithm control parameters chosen. More importantly, ACO is better able to track a constant input power than either DE or PSO. This can be seen from the enlarged part of the constant power region in Fig. 4.19 and Fig. 4.20, where after the system reaches the steady state, ACO has less oscillation than the other two methods. The slight difference in the power obtained by each algorithm under the different shading patterns is due to the stochastic searching scheme of these algorithms. All MATLAB simulation files including the implementation of ACO, DE and PSO MPPT are provided in the Appendix.

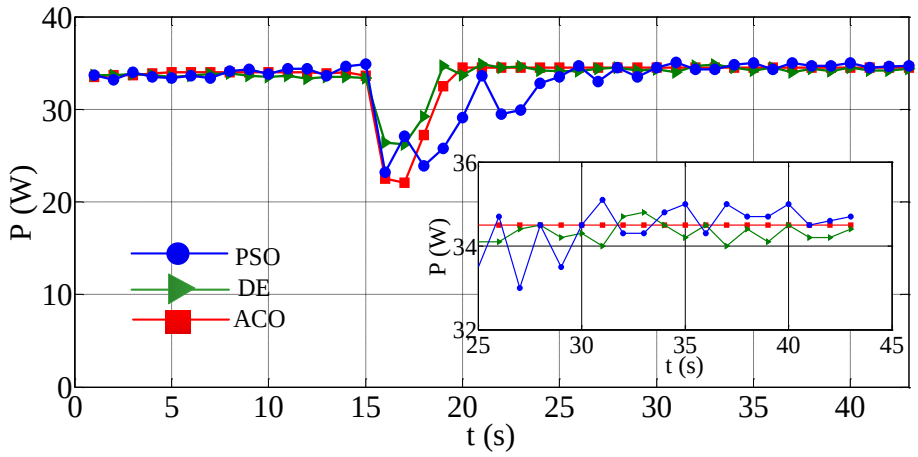

Fig. 4.19 The comparison of the experimental power output by PSO, DE and ACO based MPPTs when the shading pattern changes from SP1 to SP2.

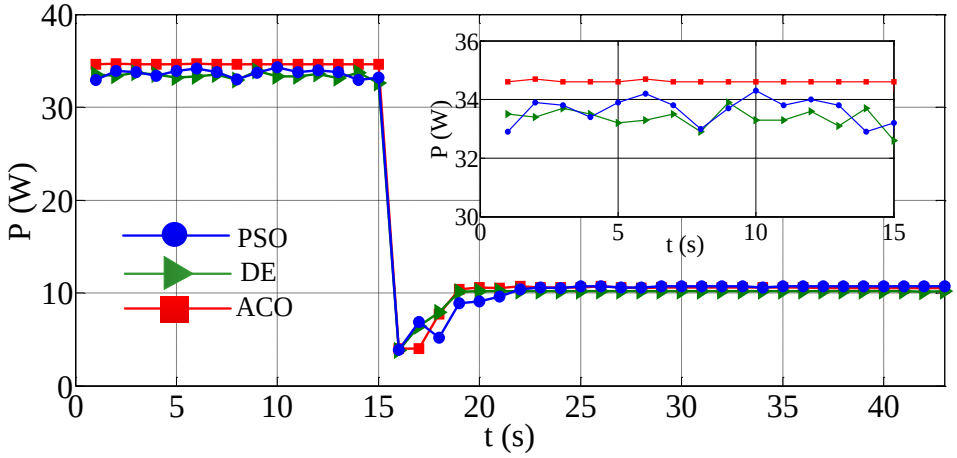

Fig. 4.20 The comparison of the experimental power output by PSO, DE and ACO based MPPTs when the shading pattern changes from SP1 to SP3.

4.6.3 Discussion

PV systems can be broadly categorized as: centralized, string-based and distributed architectures. Centralized architectures are typically characterized as being large systems with multiple PV strings and a single centralized inverter with MPPT, as shown in Fig. 4.21 (a). String-based systems are typically smaller mid-sized systems with one PV string (or a small number of PV strings) and a centralized inverter, as shown in Fig. 4.21 (b). Distributed architectures are characterized by module-level MPPT (possibly a small number of modules may share an MPPT) and can be configured as cascaded converter-MPPT architectures (as in Fig. 4.21 (c)) and module-MPPT architectures (as in Fig. 4.21 (d)). Fig. 4.21 shows a grid-tied system using DC-AC inverters connecting directly to the AC grid. In this situation, the MPPT, voltage amplification, and grid current control are all handled by this DC-AC inverter. Other inverter/converter structures are possible, including a dual-stage inverter [61, 62]. In the dual-stage inverter, the DC-DC converter is connected between the PV array and the DC-AC inverter. In this dual-stage structure, the MPPT and voltage amplification is handled by the DC-DC converter. The DC-AC inverter is responsible for the grid current control. When using a dual-stage structure, the DC-AC inverter in Fig. 4.21 is replaced by a DC-DC converter. The AC bus would then be replaced by a common DC bus between the DC-DC converters and the DC-AC inverter. Whatever the load side configuration, as the MPPT is on the PV module DC side of the inverter/converter, it is insignificant to this study.

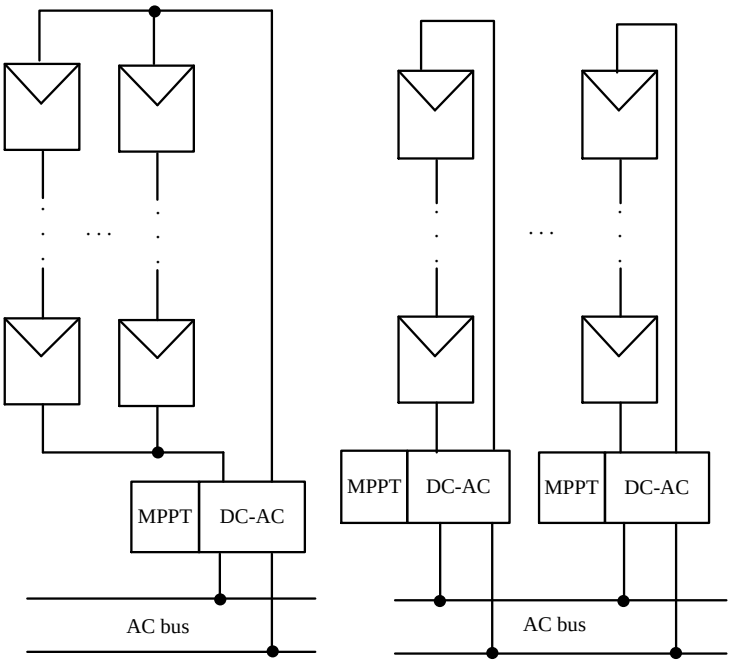

(a) (b)

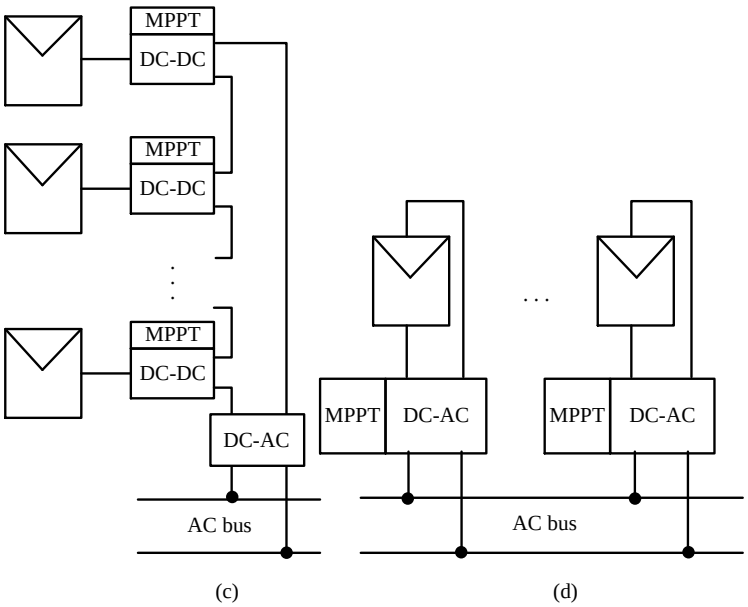

Fig. 4.21 Different PV system structures: (a) centralized-MPPT, (b) string-based-MPPT, (c) cascaded converter-MPPT and (d) module-MPPT.

4.6.3.1 Uniform implementation scheme with different PV array structures

Since MPPT can be considered as an optimization problem with multiple dimensions, many related evolutionary optimization algorithms can also be applied to solve this problem. Therefore, rather than just presenting our proposed ACO-based MPPT, a uniform scheme for the application of related evolutionary optimization algorithms to MPPT is presented. Thus, the MPPT problem is considered as a multi-dimensional optimization problem and uses an evolutionary algorithm to solve it. This requires a change of the PV architecture, so that multiple MPPTs are replaced by a single central MPPT which then provides individual control signals to each power converter, as shown in Fig. 4.22. That is, in all the MPPT structures, only one MPPT is used to control the entire PV array. For the centralized-MPPT, the control variable is scalar. For the string-based-MPPT, cascaded converter-MPPT and module-MPPT, the control variable (u) is multi-dimensional ($u = [u_1, u_2, \dots, u_n]$). The control variable could be the current/voltage of the PV array/module or the duty ratio of the power converter. In our work, the control variable for the PV string is the duty ratio (D) of the PWM signal sent to the DC-DC converter. Since a single PV string is tested, the control variable is a scalar. This will be seen in the following sections. There are two fundamental advantages to this approach. Firstly, the global power point for each power converter is able to be determined using just a single controller, and secondly, the number of voltage and current sensors can be significantly reduced, from a voltage and current sensor for each power converter (each MPPT in Fig. 4.21) to just a single voltage and current sensor at the AC (or DC microgrid) power bus.

One limitation of the proposed technique is that the dimension of the control variable should not be too large. Here, the dimension of the control variable refers to the number of PV strings because the control variable is a vector which consists of the voltage/current/duty ratio of the DC-DC converter for each PV string. This is because each particle in the optimization process is applied in a successive manner and using a high dimensional problem will result in a long search time and possibly in the algorithm failing to converge. However, if a large dimension problem is needed, it can be solved by separating the single distributed MPPT system into several smaller distributed MPPT systems where each sub-system has its own evolutionary algorithm MPPT.

A uniform implementation procedure for evolutionary optimization is proposed in Fig. 4.23. This process starts with the initialization of the algorithm parameters and the initial position of each particle (also called the possible solutions in the population). Then each particle is applied successively to the PV system. When the implementation of the last particle is complete, a new particle population is generated for the next generation. Updating particles in the new generation continues until the termination condition or the maximum number of iterations is reached. By using this scheme, a range of evolutionary optimization algorithms can be applied to MPPT, such as DE, PSO, and ACO, etc.

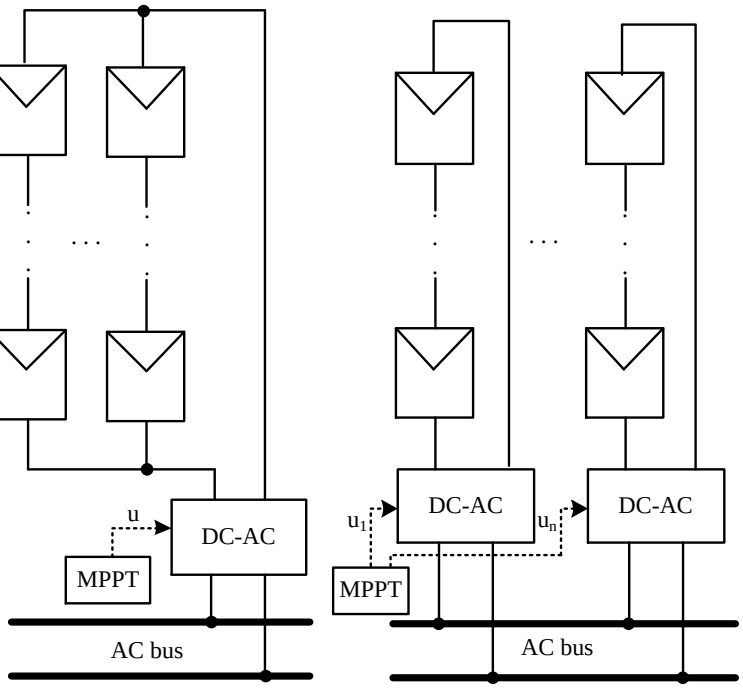

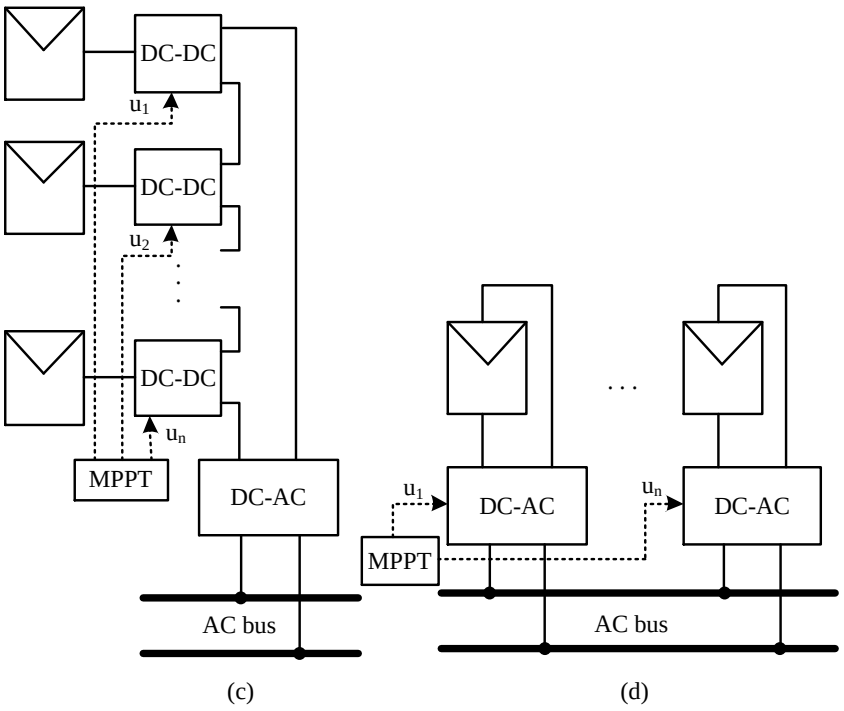

Fig. 4.22 The implementation of evolutionary optimization based MPPT into PV systems with (a) centralized-MPPT, (b) string-based-MPPT, (c) module-MPPT and (d) cascaded converter-MPPT architectures.

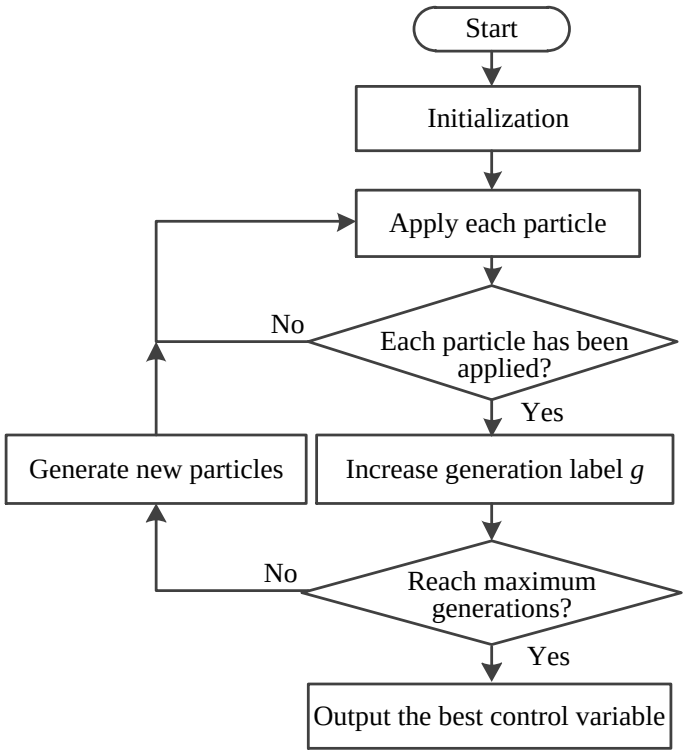

Fig. 4.23 Uniform procedure of applying particle based optimization for MPPT in PV systems.

4.6.3.2 Acceleration of the convergence speed

One of the major concerns of using evolutionary optimization for MPPT is the algorithm speed. In fact, the speed of the MPPT algorithms can be accelerated using a two stage search process by narrowing down the search range. Before executing the particle based algorithms, the variable step P&O, or IncCond, algorithm can be used to search for the first and last local MPP, as shown in Fig. 4.24. These two local peaks exist in the voltage range close to the I_{sc} and nV_{oc}, respectively, where I_{sc}, V_{oc} and n are the short circuit current, the open circuit voltage of the PV module and the number of modules connected in series respectively. Subsequently, the power values of these two local peaks are compared. If the local MPP on the I_{sc} side has a larger power value than the other local MPP, the local MPP at the I_{sc} side is then kept as the lower boundary of the search range (L). The local MPP at the nV_{oc} side is then used to calculate the upper bound. For instance, as shown in Fig. 4.24, if the power value of the first possible local MPP (A) is larger than the other local MPP (B), the lower boundary of the searching range will be the voltage of point A (V_A). Since the minimum voltage difference between two local MPP is V_{oc}, and when considering a safety margin, the upper boundary of the search range is defined as:

$$V_H = V_B - 0.8V_{oc} \tag{4.11}$$

where V_B is the voltage value of point B. If $P_A < P_B$, then the lower boundary of the search range is defined as:

$$V_L = V_A + 0.8V_{oc} \tag{4.12}$$

where V_A is the voltage value of point A. For I-V curves with more local peaks, it may not exhibit much acceleration due to the fact that the first and the last local peaks will be located very near to the I_{sc} and V_{oc}, respectively, which means the searching range is not reduced to a large extent, while for the I-V curves with fewer local peaks, it provides a significant advantage over the original algorithms.

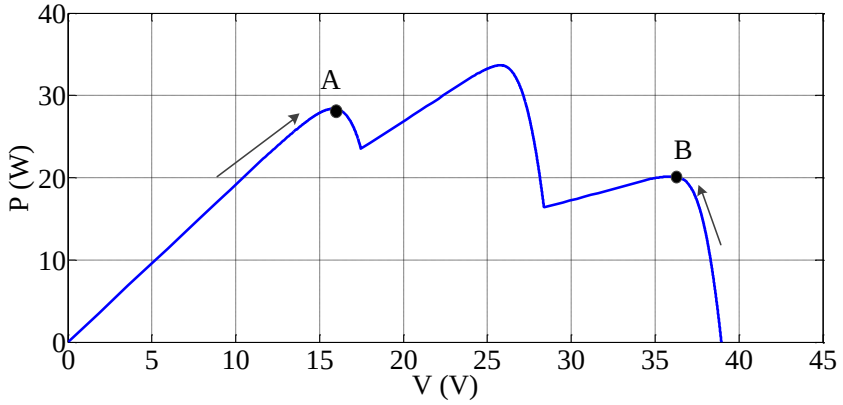

Fig. 4.24 The process of narrowing down the searching range for the MPPT using particle based optimization algorithms.

4.7 Summary

In this chapter, an ACO-based MPPT is proposed for PV systems under partially shaded conditions. The main contributions of this chapter are as follows.

(1) The feasibility of the proposed MPPT for PV arrays under steady and transient irradiance conditions are verified by simulation with various shading patterns. The results show that the proposed ACO-based MPPT is able to track the global maximum in all tested cases.

(2) Since many other evolutionary optimization algorithms (e.g. PSO, DE, and cuckoo search etc.) can be used in the same way, a uniform implementation schemes for evolutionary optimization based MPPTs with various structures are presented. It provides a general way of implementing various evolutionary optimization algorithms to MPPT techniques. For the centralized MPPT, the current/voltage output of the PV array or duty ratio applied to the converter is considered as a control scalar (or a particle). By applying these control scalars to the PV system in a successive manner, the global MPP can be obtained under the iteration of evolutionary algorithms. For the distributed MPPT, these algorithms can be applied by combining each control variable for the individual PV module as a control vector (or particle).

(3) Along with the introduction to the algorithms, a mechanism for accelerating the search speed using a two-stage scheme is addressed.

(4) The experimental results of PSO, along with two other widely used evolutionary algorithms, namely DE and PSO, are conducted and compared under uniform and nonuniform irradiance conditions. The results show that PSO has a distinct advantage over the techniques. For instance, ACO and DE based MPPTs show faster tracking speed than that of PSO which takes more steps to reach the global MPP. At the steady state of the system, the ACO based MPPT provides less oscillations than the other two methods. Since only a pair of current and voltage sensors are used, the proposed PV array structure contributes to a reduction in the system cost.

Chapter 5 Hybrid MPPT under partially shaded condition

5.1 Introduction

In Chapter 4, an ant colony optimization (ACO) based MPPT is proposed to track the global MPP for PV system when multiple peaks appear on the power versus voltage (P-V) curve. The most important advantages of the proposed method is that this global maximum power point tracking (MPPT) algorithm is an online tracking method and it does not need expensive irradiance or temperature sensors. Compared to other similar computational optimization MPPTs, it takes fewer iteration steps to reach the global MPP, which means that it has relatively faster tracking speed than the other two widely used algorithms, namely differential evolution (DE) and particle swarm optimization (PSO). However, the disadvantage of this method is that when there are rapid irradiance changes (e.g. in tropical areas), it may exhibit a tracking speed which is still too slow for the environmental conditions. It should be noted that currently there is no single MPPT method which can be applied to all scenarios. Therefore, for different conditions and applications, an appropriate MPPT method needs to be chosen based on the particular characteristics of the location.

From the review in Chapter 2, we know that the artificial neural network (ANN) is good at predicting the optimal operating point of photovoltaic (PV) systems. It is a global tracking method, and has a fast tracking speed due to its direct prediction within one iteration. In the conventional ANN based MPPTs, the ANN directly predicts the optimal voltage or current value at the MPP for a given irradiance and temperature condition [106]. The irradiance and temperature values on each solar module are usually used as the input to the ANN, while the output is the optimal voltage (and power) of a PV string (or the entire PV array) at the MPP. This type of MPPTs possesses a simple control structure and good irradiance tracking accuracy. However, it requires a large number of practical data points to train the network. Obtaining these training data values requires additional equipment and electrical components, which not only increases the system cost but is also time-consuming. In addition, due to system aging, the characteristic of the PV array may change after long-term operation, and thus, the neural network may need to be re-trained after some period.

In this chapter, we propose an efficient and fast hybrid MPPT. Compared to the ACO based MPPT proposed in Chapter 4, this hybrid MPPT provides faster tracking speed under transient irradiance changes for PV systems operating under partial shading

conditions. A fast response is important because in the tropics irradiance is highly influenced by local weather patterns. For example, in Singapore, which is just 1.5 ° north of the equator, there is little variation in temperature year round (usually the diurnal variation is between 22°C and 35°C), with a high relative humidity (the mean annual relative humidity is 84.2%). Unlike tropical regions further from the equator which have well defined wet and dry seasons, Singapore has no distinct wet or dry season, with significant rainfall throughout the year. Thus, there is significant moving cloud cover which results in rapid temporal and spatial irradiance change [191]. This rapid irradiance change requires that the MPPT has both a fast tracking speed and the ability to track the global MPP.

The proposed hybrid method combines an ANN-based technique with the conventional algorithm to track the MPP (such as, perturb and observe (P&O), incremental conductance (IncCond) or extremum seeking control (ESC)). This hybrid method features not only a simple control structure but also the ability to track the global MPP under various shading patterns with a fast tracking speed. The effectiveness of the proposed method is verified using both simulation and experimental results under various shading patterns. A method to predict the global MPP when irradiance sensors are not available is also proposed. This method samples the operating point on the stairs of I-V curve (see Fig. 5.5), which occur with partial shading, and uses the measured current value at each stair to predict the global MPP region. After the MMP region is determined, the P&O algorithm, or other efficient optimization algorithm for unimodal functions such as ESC or IncCond, is applied to the local area so that the system quickly reaches the global MPP. In our work, we choose P&O algorithm for comparison purposes due to its widespread use and the simplicity of the implementation. The tracking speed in the MPP region can be further accelerated using variable step P&O [68] or IncCond [70].

5.2 Artificial neural network

An ANN is a mathematical model inspired from biological neural networks. It is usually used to model complex relationships between inputs and outputs or to classify data patterns and has been used in various applications. A general introduction to the ANN was provided in literature review. Here we give the mathematical expressions of the calculations among each layer. A standard single hidden layer feedforward ANN consists of input, hidden and output layers [197], as shown in Fig. 5.1. Once an input vector, $X = [x_1, x_2, \ldots, x_n]$, is presented to the neural network, the sum of the weighted inputs are limited by a activation function, $f(.)$ which can be defined as a threshold function, piecewise-linear function or sigmoid function. A single layer ANN is used as a classifier in this work. Before using the ANN, the weight values between the input and hidden layers must be obtained by training

the neural network with pre-obtained inputs, $X = [x_1, x_2, \ldots, x_n]$, and target outputs ($Y_T$=[$y_{t1}$, y_{t2}, …, y_{tl}]). These target outputs can be measured from the real system. Mathematically, for a (n-h_1-l) dimensional single layer ANN as shown in Fig. 5.1, where n, h_1 and l are the number of input, the number of neurons in the single hidden layer, and the output dimension respectively. The outputs of the j^{th} neuron from the hidden layer is calculated as:

$$\phi_j(x) = f_j(\sum_{i=1}^{n} w_{ji} x_i) \tag{5.1}$$

where $f_j(.)$ is the activation function for the j^{th} node in the hidden layer, w_{ji} is the weight connecting the j^{th} hidden node with the i^{th} input x_i. In the output layer, the l^{th} network output is calculated as:

$$y_k = f_k(\sum_{j=1}^{h} w_{kj} \phi_j(x)) \tag{5.2}$$

where f_k is the activation function for the k^{th} node in the output layer, w_{kj} is the weight connecting the k^{th} output node with the j^{th} node in hidden layer. Training an ANN involves tuning the weight values between inputs (outputs) and the hidden layers of the ANN, by minimizing a performance criterion which is a function of the difference between the target output and the ANN predicted output. In this work we use the Levenberg - Marquardt algorithm to tune the weights and biases of the ANN. The hyperbolic tangent function is considered as the activation function. The cost function for the k^{th} sample data is given by:

$$E_k = 0.5(Y_{T_k} - Y_k)^2 \tag{5.3}$$

where Y_{Tk} is the target output and Y_k is the network output. The input dataset contains different shading patterns or current values on each I-V stair which will be explained in the following sections. The target output in this work is the region of the optimal voltage corresponding to the inputs, that is, the region of the MPP. The target output is coded in binary, where each region is represented as a binary-code using one-hot encoding. For example, ‘001’, ‘010’, and ‘100’ are used to represent three different regions. After training the ANN, it can be used as a classifier to recognize the region number for any given shading pattern.

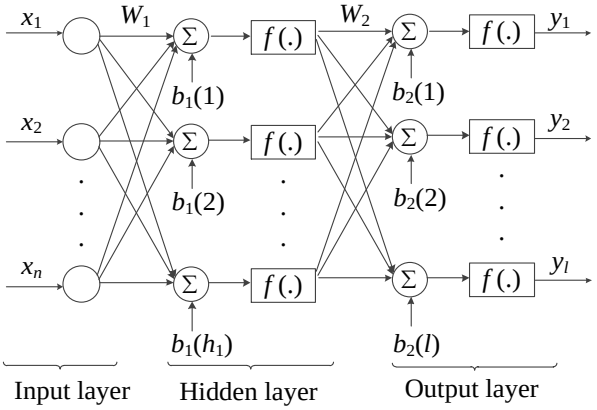

Fig. 5.1 ANN with a single hidden layer.

5.3 Proposed hybrid MPPT method

In this section, the proposed hybrid MPPT method is explained for two cases: (a) with and (b) without irradiance sensors. In order to demonstrate our proposed method, we take a small PV system as an example. This small PV system is shown in Fig. 4.16. It consists of four identical PV modules connected in series. Each PV module has a bypass diode connected in parallel to reduce the hotspot problem. However, these bypass diodes can generate multiple peaks on the P-V curve of the PV array if the irradiance is not uniform. The number of bypass diodes is equal to the maximum number of peaks on the P-V curve. The parameters of a PV module are listed in Table 5.1. For simplicity, we assume a constant module temperature of $40^{o}C$. For PV systems where there is a significant temperature variation, temperature compensation can be used for the corresponding MPP due to the linear relationship between the temperature and the MPP distance on the voltage axis, which will be discussed in the following section. By changing the irradiance on each module in $100W/m^2$ steps (from $100W/m^2$ to $1200W/m^2$), the MPP under various shading patterns can be generated, as shown in Fig. 5.2. From Fig. 5.2, we see that for a PV string, as in Fig. 4.16, the MPPs are located in particular regions, and thus the optimal working voltage can be classified into the four regions (*N* regions for an *N* module string). This is because when we set the temperature to a constant value and change the irradiance on each PV module, there will be four regions on the P-V curve for these four series connected PV modules. Therefore, based on the above observations, the idea of our proposed MPPT method is to identify the region of the optimal working voltage first and then based on this classified region, use a conventional optimization algorithm for unimodal functions such as P&O, IncCond and ESC algorithms to track the MPP within the local area. For the classification function, many methods can be used such as: ANN, Naive Bayes (NB) [198, 199], support vector machine (SVM) [200], k-nearest neighbors (k-NN) [198, 201], etc. Due to the simplicity of the implementation and the high accuracy of an ANN, we use an ANN as a classifier in our work. The irradiance values on the PV modules will be considered as the inputs for the ANN classifier when irradiance sensors are available and the current values measured on each stair of the I-V curve (as in Fig. 5.5) when irradiance sensors are not available.

Since the ANN is only used for classifying the approximate region of the MPP, a slight variation in the characteristic of the PV array will not influence the prediction results. Whereas, the conventional way of applying ANN is to directly predict the optimal voltage/current at the MPP, which puts a higher requirement on the accuracy of the training dataset under various environmental conditions, and even a slight change in the characteristic of the PV array due to system aging may have a large influence on the tracking performance of the MPPT. Thus, in the proposed method, the training dataset can

be easily generated by simulation, which significantly simplifies the complex process of obtaining practical data from a real PV array.

Table 5.1 Parameters of the tested PV module.

Maximum power (P_{max})	15W	Short circuit current (I_{sc})	1.90A
Optimum voltage (V_{mp})	8.55V	Number of cells in each module	18
Optimum current (I_{mp})	1.75A	Temp. coefficient of I_{sc} A /^oC	1.50×10^{-3}
Open circuit voltage (V_{oc})	10.55V	Temp. coefficient of V_{oc} V /^oC	-0.04

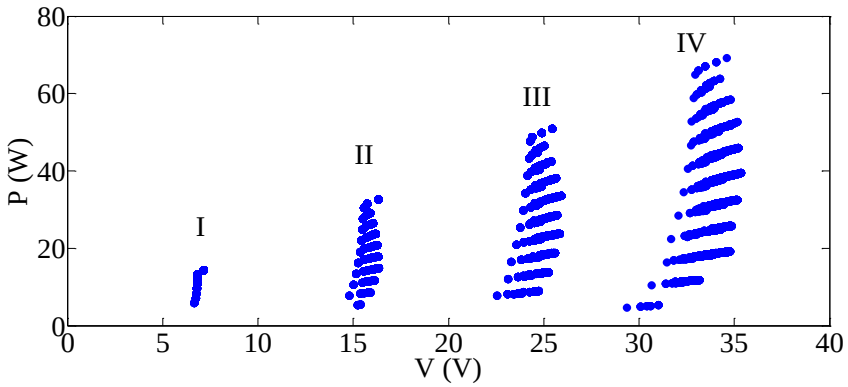

Fig. 5.2 Distribution of MPPs under various irradiance conditions. The MPP falls into one of the four regions (I, II, III, and IV).

5.3.1 Global MPPT with irradiance sensors

Due to the ability to model the solar cell/module with good accuracy and because of its simple implementation procedure, the analytical method is used to generate the training data. Compared to the single-diode model [19, 20, 128], the two diode model [20] provides better accuracy. Therefore, the two diode model, as described in Section 2.1.1.3, is used to generate the training dataset. The procedure for generating the simulated data includes the following steps: Firstly, based on the parameters provided by the datasheet, use the two-diode model to generate the I-V and P-V curves of the PV modules under various irradiance conditions, then find the location of MPP on each curve. Finally classify all the MPPs according to the location of the MPP for each shading pattern.

Fig. 5.3 shows the block diagram of a PV system using the proposed hybrid MPPT method. The system consists of a PV array simulator, MPPT, a buck converter operating in continuous conduction mode and a load. A buck converter is used in the experiment because of its simplicity and efficiency, it should be noted that in a practical system where the irradiance varies rapidly over a large range, such as the case in tropical climates, a buck-boost converter would be necessary. The experimental setup is the same as that used in Chapter 4. The only difference is the MPPT technique.

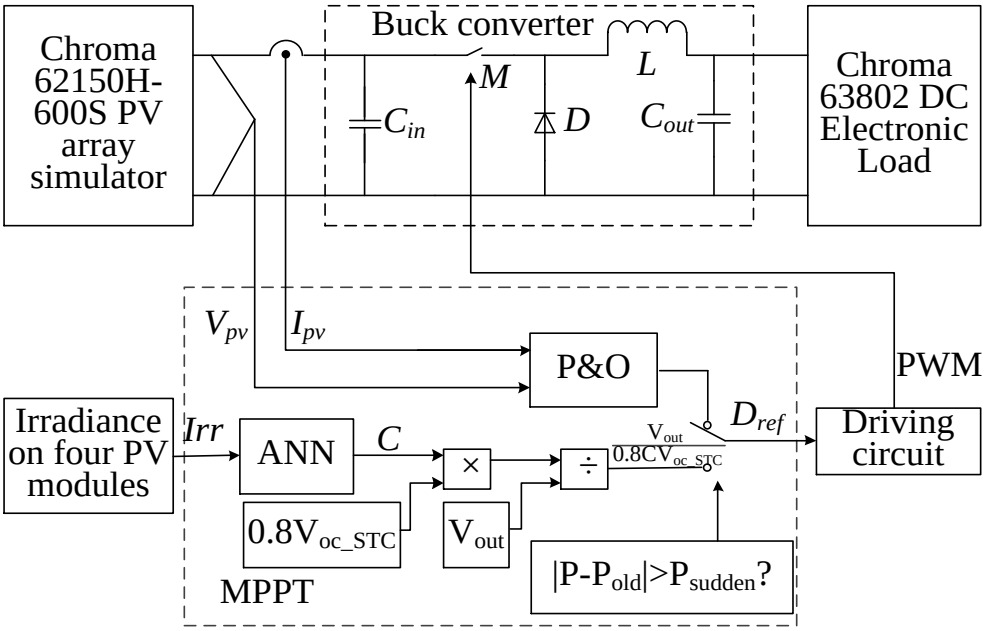

Fig. 5.3 Schematic diagram of the DSP-based MPPT for the PV system using a hybrid MPPT method.

The MPPT (indicated within the bottom dashed box in Fig. 5.3) is implemented on a Texas Instruments TMS-F28335 DSP. The parameters for the buck converter are the same as in Table 4.6. In the proposed hybrid MPPT algorithm, the ANN is used to classify the output reference voltage. In this section we assume that the irradiance sensors are available. Therefore, the input signals to the ANN are the spot irradiance values at the four PV modules, and the output signal is the region of the global MPP. During the process of searching around the MPP, the P&O algorithm uses the direct duty ratio perturbation method, whereby changing the duty ratio controls the voltage at the PV simulator output, thus driving the operation towards the MPP. When there is a sudden irradiance change, the ANN is triggered to predict the new region of the global MPP for the new irradiance condition. Based on the classified region, the voltage value of the initial tracking point for the P&O algorithm under the new irradiance condition is calculated by:

$$V_{ref} = 0.8 \times C \times V_{oc\_STC} \tag{5.4}$$

where V_{ref} is the optimal voltage of the PV array, V_{oc_STC} is the open circuit voltage at *STC* and C is the region number of the corresponding irradiance condition identified by the ANN. Since under uniform irradiance conditions, the MPP is usually located at around 80% of the open circuit voltage, we use this as the start value (the initial tracking point) for the P&O algorithm to track the MPP in the local area under the new irradiance condition. Then, for a load with constant voltage (V_{out}), the duty ratio (D_{ref}) of the PWM signal applied to drive the MOSFET power switch of the buck converter is given by:

$$D_{ref} = \frac{V_{out}}{V_{ref}}. \tag{5.5}$$

Fig. 5.4 shows the flowchart of the proposed hybrid MPPT method. When the absolute value of the power change in two subsequent perturbations (ΔP) is greater than a specified critical power variation (P_{sudden}), a new initial operating point for the P&O algorithm is set by the ANN based predictor and Eqs. (5.4) and (5.5). This is used to adjust the operating point of the P&O algorithm to the new MPP region. The value of the critical power variation, P_{sudden}, can be adjusted according to the PV system and its environment. Until another sudden change in irradiance occurs, the system remains at the current MPP by continuously implementing the P&O algorithm. The basic steps of the proposed MPPT method are described as follows.

(1) *ANN generation*: Simulate and generate the I-V curve for the PV system under various irradiance conditions offline. Train the ANN with the generated input and target output dataset.

(2) *Initialization*: Set the initial value of the duty ratio (D_{ref}), the previous value of the power output in the first step (P_{old}), and the power change caused by a sudden irradiance change (P_{sudden}).

(3) *Input data measurement*: Read the irradiance on each PV module: Irr_i, (i = 1, 2, 3, 4), the voltage ($V(k)$) and the current ($I(k)$) output from the PV string. Calculate the power value.

(4) *Region prediction*: Compare the error between the present and the previous power values with the critical power (P_{sudden}). If the absolute value of the error is larger than P_{sudden}, $|P - P_{old}| > P_{sudden}$, meaning there is a sudden change in the irradiance on the PV modules, then use the ANN to predict the region of the new MPP and determine the initial tracking voltage and duty ratio based on Eqs. (5.4) and (5.5). Set the duration of $D_{ref,}$ generated by Eq. (5.5) after this sudden irradiance change to T_d (T_d = 0.2s) to ensure the system has stabilized at the new location.

(5) Otherwise, continue to track the MPP using P&O, and limit the duty ratio within a predefined boundary ($0.05 < D_{ref} < 0.95$) to ensure the buck converter is operating in the appropriate region of the power curve.

(6) Update the previous power value with the present power value, $P_{old} = P$. Output the duty ratio produced by the MPPT algorithm. Go to step (3).

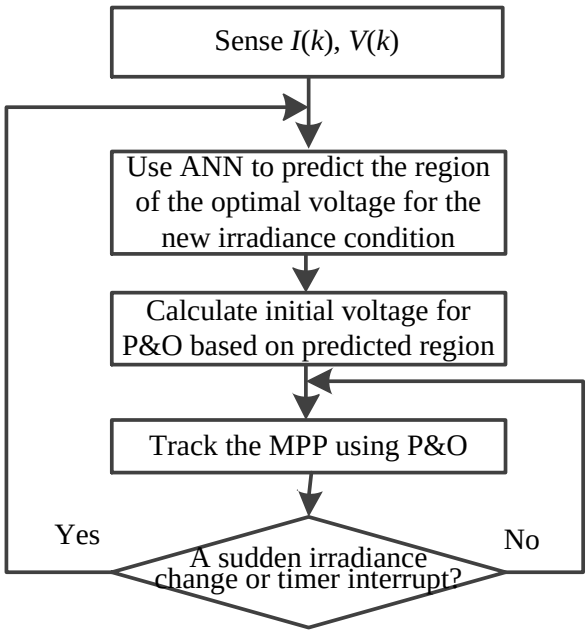

Fig. 5.4 The general process of the proposed hybrid MPPT.

Table 5.2 shows the pseudo code of the proposed hybrid MPPT within which the function, *ANN_classification* (.), is used to classify the inputs (the irradiance on the four PV modules).

Table 5.2 The pseudo code of the proposed hybrid MPPT.

Initialize the parameters for the algorithm, e.g P_{old}, $V_{ocn,}$ P_{sudden} and D_{ref}.
Read the irradiance on each PV module (Irr_i, (i = 1,2,3,4)), voltage (V (k)) and current (I (k))
$P = I \times V$;
If abs (P-P_{old}) > P_{sudden}
    C = *ANN_classification* (*Irr*);
    $V_{ref} = 0.8 \times C \times V_{oc\_STC}$;
    $D_{ref} = V_{out} / V_{ref}$;
Else
    $\Delta D = 0.02$;
    If ($P < P_{old}$)
        slope = - *slope*;
    End if
$D_{ref} = D_{ref} +$ *slope* $\times \Delta D$;
End if
if ($D_{ref} > D_U$)
    $D_{ref} = D_U$;
End if
If ($D_{ref} < D_L$)
    $D_{ref} = D_L$;
End if
$P_{old} = P$;

5.3.2 Global MPPT without irradiance sensors

The requirement for irradiance sensors in the hybrid MPPT adds to the cost of the system due to their relatively high price. While it would be possible to implement a cheaper solution which uses a small part of the module as the sensor, this may still be considered to be too expensive. In order to avoid the need for irradiance sensors, a scheme to predict the region of the MPP is proposed which directly uses the measured current value at a point on each stair of the I-V curve. The I-V curve exhibits a staircase effect when partial shading is present due to the nonlinear characteristic of PV cells and the function of the bypass diodes, as shown in Fig. 5.5. Thus, no irradiance sensors are required and the algorithm is able to track the global MPP for PV systems under non-uniform irradiance conditions. For example, when a sudden irradiance change occurs, the combination of the measured current at each of the stair points (such as points A, B, C and D) can be considered as the inputs for the ANN to predict the MPP region. The voltage values of these sampling points (V_{samp}) are set as:

$$V_{samp} = [V_A, V_B, ..., V_j, ..., V_{N_m}] = [0.5V_{ocn}, 1.5V_{ocn}, ..., (0.5 + j)V_{ocn}, ..., V_{N_m}], (j = 0,\ 1,\ 2,\ ,...,\ N_m) \tag{5.6}$$

where V_j are the voltage values of the stair points on the I-V curve, V_{ocn} is the open circuit voltage of one PV module under STC and N_m is the number of PV modules connected in series in the same PV string (also the number of maximum possible MPPs). These current values are measured continuously from the PV array when a partial shading event is sensed.

Temperature also affects the MPP region and should be considered as another input to the ANN. However, the temperature influence on the I-V curve makes the process of training the ANN more complex. Additionally, if the voltage values of the sampling points from the I-V curve are constant, it may lead the system to a negative current value, especially for the sampling point located in the MPP region close to the open circuit voltage, for instance, V_D. Therefore, we train the ANN with datasets generated with varying irradiance but only constant temperature, and then compensate for the influence of temperature on the I-V curve. When the temperature on the solar cell surface decreases/increases, the MPP locus will shift right/left along the voltage axis. As described in [202], the additional temperature compensation voltage is proportional to the panel temperature. Therefore, in order to make sure that there is a sampling point on each stair of I-V curve as well as to reduce the influence of the temperature, the voltage values are compensated based on the linear equation given by:

$$V_{samp} = V_{samp0} + V_{comp} \tag{5.7}$$

where V_{samp0} is the voltage value under STC and V_{comp} is the compensation voltage value based on the measured temperature. By observing the optimal point change on the I-V curves when temperature varies from 20°C to 60°C as shown in Fig. 5.6, it can be found that the proportion is different for each region of the MPP. Therefore, the relationship between the compensation voltage and the temperature can be determined as [202]:

$$V_{comp} = A(i) \cdot (25 - Temp(k)), \qquad (i = 1,2,..., N_m) \tag{5.8}$$

where $A(i)$ is the proportion for different MPP regions and $Temp(k)$ is the temperature value measured at the back of one of the panels at k^{th} time interval. Because the temperature difference between PV modules is relatively small, due to the same material and weather conditions, only one temperature sensor is needed for the PV system. The compensation proportion for each region can be determined from the voltage difference between the minimum and maximum temperature values for each sampling point. In the presented work, the temperature on the solar panels is assumed to vary within the range of 20°C to 60°C in the experiment. Thus, the proportion for each region is computed to be A = [1.42, 3.28, 5.14, 6.72]. After predicting the MPP region, the duty ratio value for the P&O algorithm to continue to search within the local area is calculated by:

$$D_{ref} = \frac{V_{out}}{(0.8 \cdot C \cdot V_{ocn} + V_{comp} + V_{out})}. \tag{5.9}$$

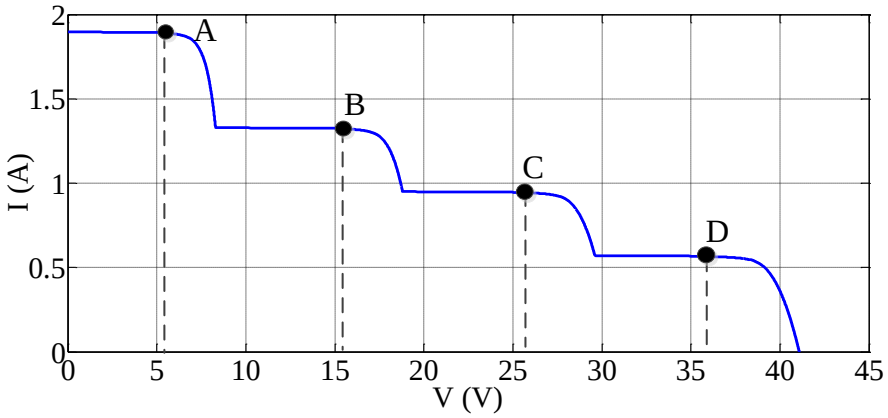

Fig. 5.5 Multiple steps on the I-V curve.

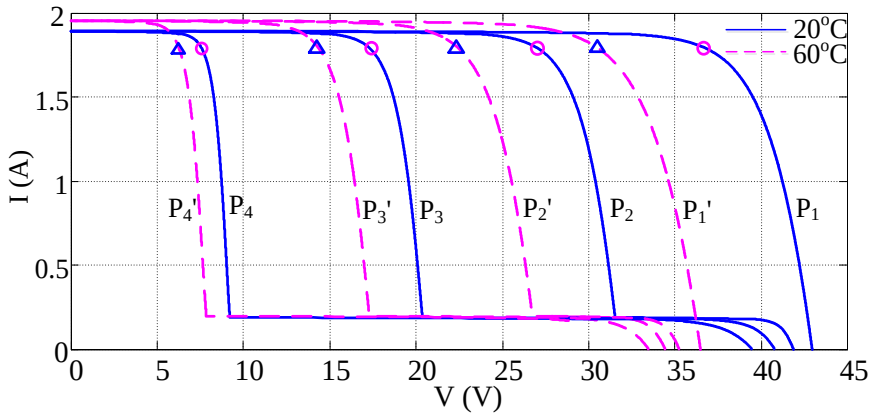

Fig. 5.6 The change in operating point (circle and triangle points) when the temperature varies from 20°C to 60°C. The I-V curves (P_1, P_2, P_3, P_4) and (P_1', P_2', P_3', P_4') are for 20°C and 60°C, respectively.

The detailed flowchart for the hybrid MPPT method without irradiance sensors is given in Fig. 5.7. Because four sampling points are sampled continuously for the experimental PV system (Fig. 5.3), a flag signal (j, (j = 1, 2, …, N_m)) is used to label the sequence of the sampling points. An additional completion signal (*flag*) is applied to ensure that the power difference between each sampling point (j) is not misinterpreted as a sudden irradiance change.

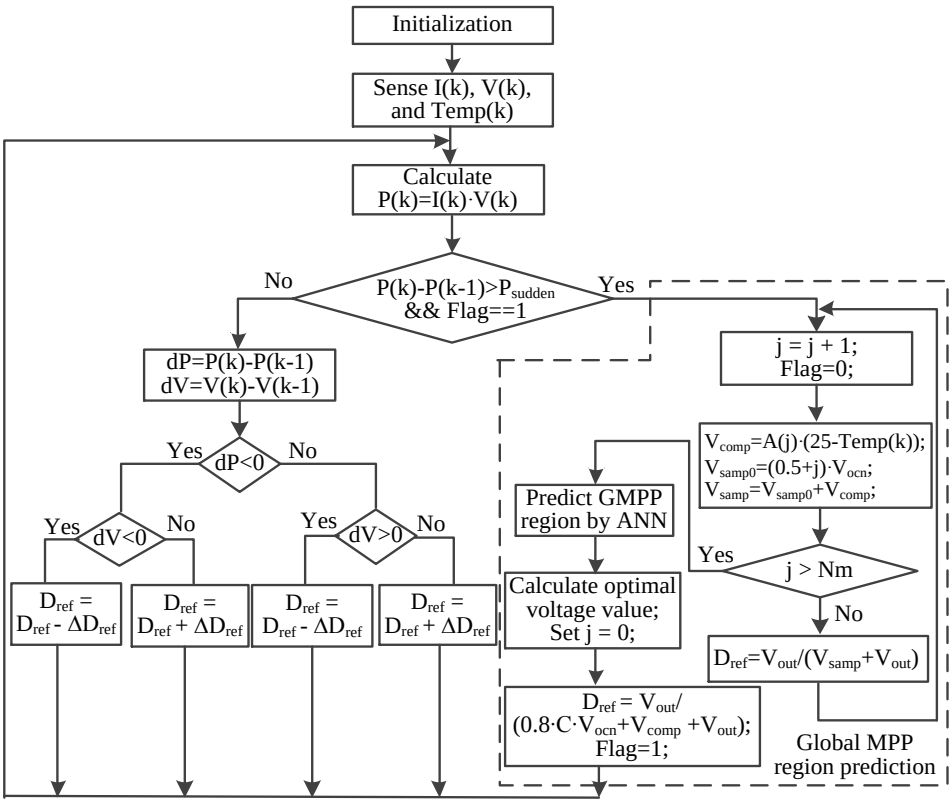

Fig. 5.7 Detailed flowchart for tracking the global MPP using the proposed hybrid MPPT without irradiance sensors.

The basic steps can be described as follows.

(1) *ANN predictor generation*: Simulate and generate the I-V curves based on the single/two diode model for the PV system under varying irradiance and constant temperature ($T = 25^{o}C$) conditions offline. Get the current values for the predefined sampling points. Prepare the training data for the ANN predictor. Train the ANN with the generated datasets.

(2) *Initialization*: Set the initial value of $N_m = 4$, $D_{ref} = 0.3$, $\Delta D = 0.002$, $P_{old} = 0$, $P_{sudden} =$ 5W, $V_{samp0} = [0.5, 1.5, 2.5, 3.5] \cdot V_{ocn}$, $j = 0$, $Flag = 1$.

(3) *Input data measurement*: Read the voltage ($V(k)$) and the current ($I(k)$) from the PV string and the solar cell temperature ($Temp(k)$). Calculate the power value ($P(k)$).

(4) *Region prediction*: Compare the error between the present and the previous power values with the critical power (P_{sudden}). If the absolute value of the error is larger than P_{sudden}, $|P - P_{old}| > P_{sudden}$, and the completion signal $Flag = 1$, which indicates the algorithm is ready for the next sudden irradiance change after the last global MPP has been reached, it means there is a sudden change in the irradiance on the PV modules. Then the algorithm starts to perform a global MPP region prediction. Firstly, the completion signal 'Flag' is set to 0. Then, for each sampling point (j), calculate the compensation voltage based on the measured temperature and then output the duty ratio and measure the current, until the last point is completed ($j > N_m$ is satisfied). Use the ANN to predict the region of the new global MPP and determine the initial tracking duty ratio value for the P&O algorithm to track the (global) MPP within the local area. Reinitialize j and $Flag$ to 0 and 1, respectively.

(5) Otherwise, continue to track the MPP using P&O, while limiting the duty ratio within a predefined boundary ($0.05 < D_{ref} < 0.95$) to ensure the buck converter is operating in the appropriate region of the power curve.

(6) Update the previous power value with the present power value, $P_{old} = P$. Output the duty ratio produced by the MPPT algorithm. Go to step 3.

5.4 Results and discussion

5.4.1 Simulation results

In order to verify the effectiveness, in particular the response to rapid irradiance changes, of the proposed hybrid MPPT, the tracking ability of the proposed hybrid MPPT algorithm, under various shading patterns, is examined by performing a number of simulations using Simulink/MATLAB. The structure of the tested PV system with buck converter is shown in Fig. 5.3. The parameters of the PV modules, configured as in Fig. 4.16, are the same

as in previous section in Table 4.5. The MPPT algorithm is updated every 0.12s (referred to as the update period of MPPT, $1/f_{mppt}$). The previous power value in the first step (P_{old}) is set to 0. The duty ratio changes with a step size of 0.02 (ΔD) in each MPPT update. It should be noted that too large a step size accelerates the tracking speed but leads to large oscillations around the MPP, while too small a step size reduces the oscillation around the MPP but slows down the tracking speed. The trade-off between the tracking speed and the oscillation around the MPP should be made when deciding the step size. The time that D_{ref} is applied to the inverter, before the P&O algorithm begins tracking the MPP after a sudden irradiance change (T_d) is set to 0.2s. The critical power variation for indicating a sudden irradiance change (P_{sudden}) is set to 5 W. Since it is difficult to test all possible shading patterns, we selected 24 typical shading patterns, as listed in Table 5.3. These shading patterns include both uniform (SP1) and non-uniform (SP2 through to SP24) irradiance conditions. For SP1, there is only one unique peak (the MPP) on the P-V curve, which is obviously the global MPP. For other shading patterns, there are multiple peaks in the power curve.

To examine the impact of transient shading patterns on the proposed hybrid MPPT algorithm, we examine three specific cases: SP1 to SP2 (SP1-SP2); SP1 to SP3 (SP1-SP3); and SP1 to SP4 (SP1-SP4). For each transient case, the final global MPP after transition is located in a different region: the global MPP for SP2, SP3, and SP4 are located within regions VI, III, and II, respectively, as shown in Fig. 5.2.

Table 5.3 The shading patterns for testing.

SP	SPs [M1, M2, M3, M4]	SP	SPs [M1, M2, M3, M4]
SP1	[600.0, 600.0, 600.0, 600.0]	SP13	[758.1, 764.0, 931.7, 613.3]
SP2	[600.0, 600.0, 300.0, 300.0]	SP14	[324.2, 943.4, 808.3, 229.1]
SP3	[900.0, 400.0, 800.0, 800.0]	SP15	[824.0, 743.8, 641.3, 852.3]
SP4	[400.0, 400.0, 100.0, 100.0]	SP16	[324.1, 943.4, 808.3, 229.1]
SP5	[209.3, 573.3, 852.3, 910.9]	SP17	[600.6, 677.0, 758.1, 943.4]
SP6	[532.2, 477.9, 871.1, 966.6]	SP18	[958.0, 931.7, 296.2, 743.8]
SP7	[764.0, 241.0, 811.8, 256.5]	SP19	[764.0, 240.9, 811.8, 256.5]
SP8	[616.5, 252.6, 677.0, 623.8]	SP20	[502.9, 808.3, 857.0, 532.2]
SP9	[462.8, 743.8, 870.3, 533.9]	SP21	[240.6, 857.0, 615.7, 824.0]
SP10	[631.0, 685.5, 296.2, 870.3]	SP22	[502.9, 808.3, 857.0, 532.2]
SP11	[870.3, 477.9, 451.0, 803.0]	SP23	[808.3, 641.3, 255.3, 213.0]
SP12	[808.3, 641.3, 255.3, 213.0]	SP24	[533.9, 455.8, 857.0, 852.3]

5.4.1.1 Simulation results with irradiance sensors

The change of operating point on the I-V and P-V curves using the proposed hybrid MPPT method with measured irradiance values for these three cases is shown in Fig. 5.8, Fig. 5.9,

and Fig. 5.10, respectively. The arrows in each figure illustrate the changing direction of the operating point. In Fig. 5.8, initially, with pattern SP1, the operating point starts from point O, and then the conventional P&O based MPPT moves the operating point to point A (A' on the I-V curve). While the irradiance remains constant, or varies only slightly, the operating point oscillates around point A. When the shading pattern suddenly changes from SP1 to SP2, the working point shifts from point A to point B (B' on the I-V curve). As a result, the simulation step sees a power change larger than P_{sudden} (5W). This triggers the ANN to estimate the region for the current irradiance condition. Based on the predicted region, the reference duty ratio is calculated using Eqs. (5.4) and (5.5) and as a result, the operating point is moved from point B to point C. Finally, the conventional P&O MPPT moves the operating point to point D, where it remains (oscillating slightly around point D). For this particular case (SP1-SP2), point C and D are coincidently identical. Similarly, for the other two cases (SP1-SP3 and SP1-SP4), the operating point moves to point A and then moves to point B and C, and finally fluctuates around the global MPP (point D). Thus we see that the proposed hybrid method can always track the global MPP, while the conventional P&O algorithm may be trapped in a local MPP.

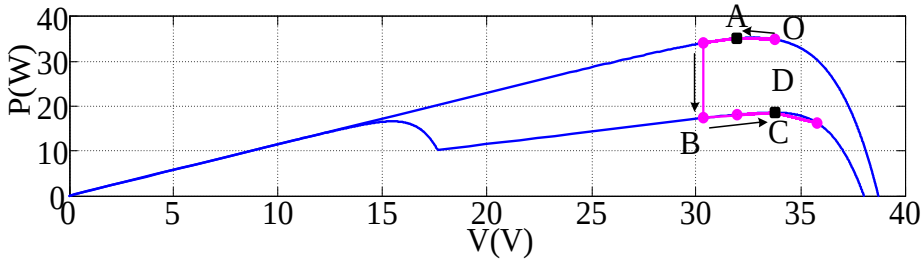

Fig. 5.8 The performance of proposed hybrid MPPT when the shading pattern changes from SP1 to SP2.

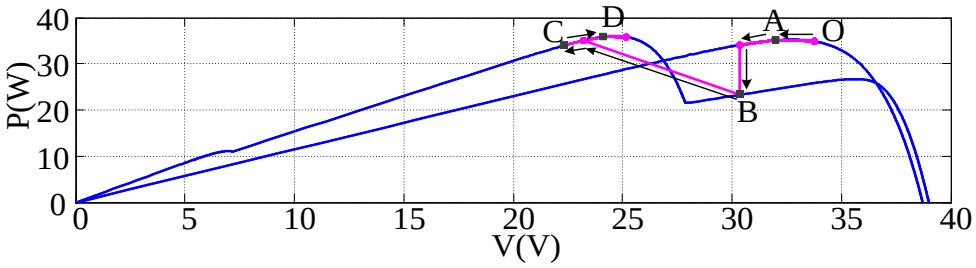

Fig. 5.9 The performance of proposed hybrid MPPT when the shading pattern changes from SP1 to SP3.

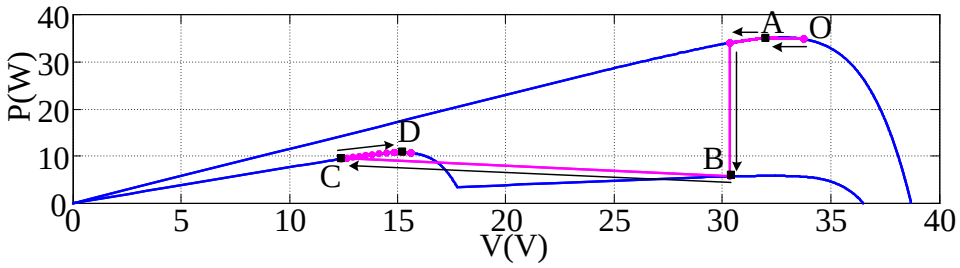

Fig. 5.10 The performance of proposed hybrid MPPT when the shading pattern changes from SP1 to SP4.

5.4.1.2 Simulation results without irradiance sensors

Fig. 5.11 shows the tracking locus on the P-V curve for the proposed method without irradiance sensors when the shading pattern changes from SP1 to SP2. When a sudden partial shading event is sensed, the process of sampling the four successive points within the four possible MPP regions is conducted. Thus, the corresponding working point moves from the original stable point O_1 to A, B, C, and finally D. It should be noted that in this simulation, a buck-boost converter is used so that the voltage below the output voltage value can also be reached, such as for point A. When the sampling process is completed, the ANN predictor is then activated to predict the global MPP region for the P&O algorithm to continue to track until the global MPP is reached. For this case, the final global MPP is located in region IV. Therefore, the final stable point is moved to O_2. Fig. 5.12, Fig. 5.13 and Fig. 5.14 show the power and the voltage values for shading pattern changes from SP1 to SP2, SP1 to SP3, and SP1 to SP4, respectively, during the sampling process using the proposed MPPT method. We can see from Fig. 5.12 that the power value changes from 35.2W to 18.5W which is the maximum power for shading pattern SP2. V_A, V_B, V_C, and V_D in Fig. 5.13 are the voltages of the corresponding sampling point. Other shading pattern combinations are handled in a similar way.

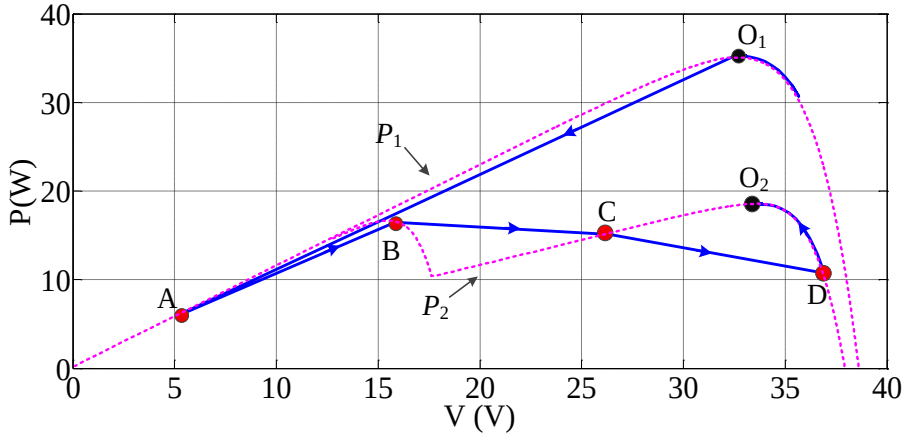

Fig. 5.11 The tracking locus on the P-V curve by the proposed method without irradiance sensors when the shading pattern changes from SP1 to SP2.

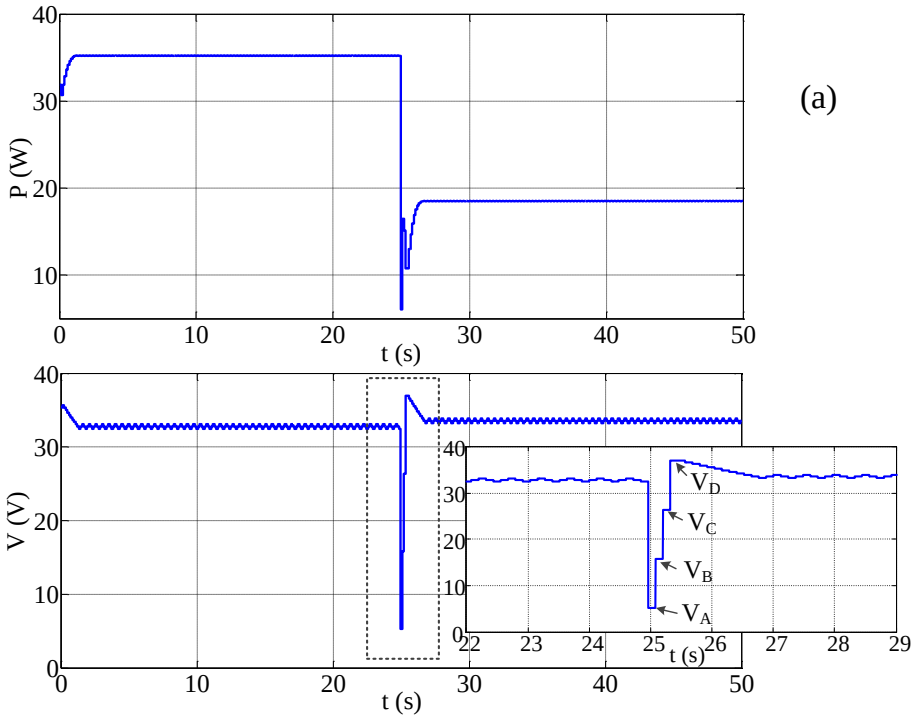

Fig. 5.12 The power and voltage values by the proposed MPPT without irradiance sensors when the shading pattern changes from SP1 to SP2.

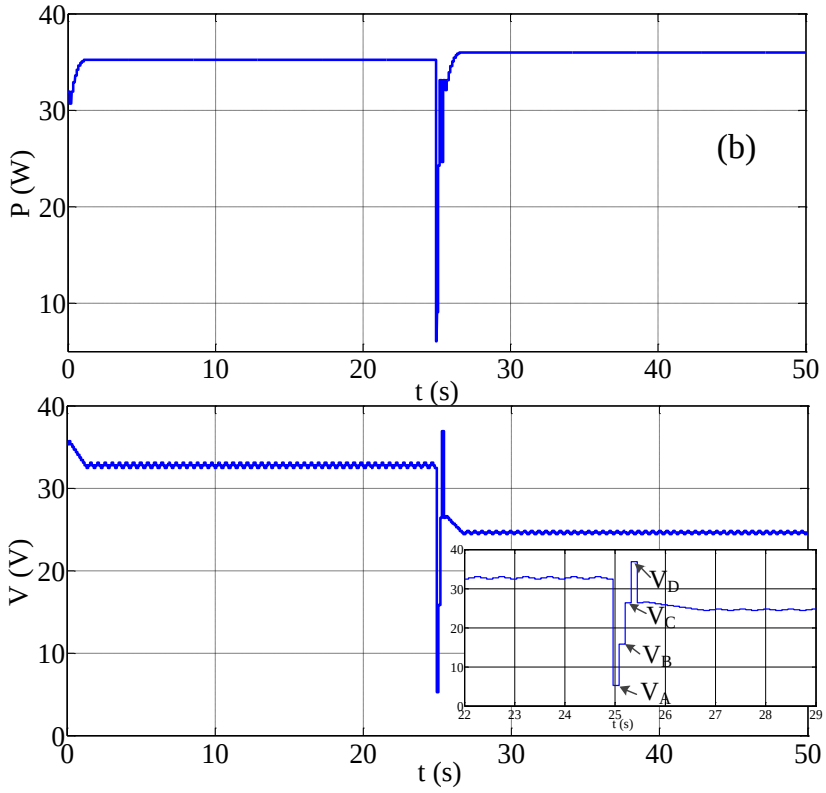

Fig. 5.13 The power and voltage values by the proposed MPPT without irradiance sensors when the shading pattern changes from SP1 to SP3.

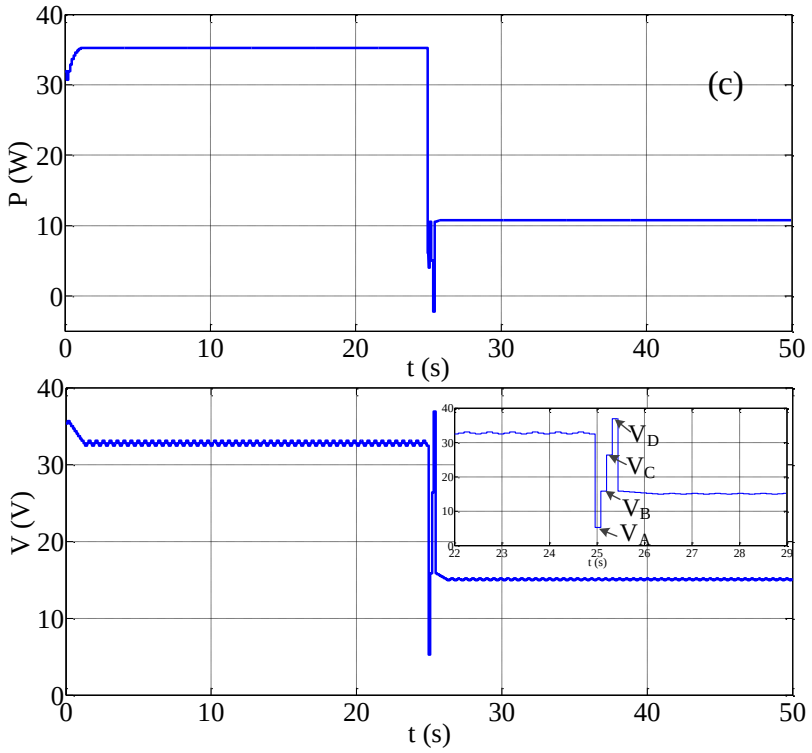

Fig. 5.14 The power and voltage values by the proposed MPPT without irradiance sensors when the shading pattern changes from SP1 to SP4.

5.4.2 Experimental results

The effectiveness of the proposed hybrid MPPT is verified using an experimental setup. Eight transient cases are first examined and then the transient response of the proposed MPPT using 25 shading patterns with a shading pattern shift every 10 seconds is tested.

5.4.2.1 Single transient response

After training the ANN-based predictor using simulated data, different shading patterns are applied (via the solar simulator) to the buck converter controlled by the hybrid MPPT. The initial parameters of the system are set to the same values as in the simulation section. In order to evaluate the efficiency of the hybrid MPPT, we define the energy capture (E) as:

$$E = \sum_{i=1}^{N_t} P(i) \tag{5.10}$$

where $P(i)$ is the power obtained by applying the MPPT algorithm at the i^{th} second and N_t is the total time in seconds. Additionally, we define the energy difference (δ_p) between the hybrid MPPT and the P&O MPPT as:

$$\delta_p = \frac{\sum_{i=1}^{N_t} | P_{Hybrid}(i) - P_{P\&O}(i) |}{\sum_{i=1}^{N_t} P_{P\&O}(i)} \times 100\% \tag{5.11}$$

where $P_{Hybrid}(i)$ and $P_{P\&O}(i)$ are the powers extracted by the hybrid and P&O MPPT at the i^{th} second, respectively.

To test the transient response of the hybrid MPPT, we examined eight separate test cases with a single shading pattern change. For all test cases, except the shading pattern change from SP1 to SP2, the global MPP region after the shading pattern change is different from the initial region. The PV array generates a different power value for each shading pattern. In this experiment, each shading pattern is applied for 25s. The energy captured from the PV modules by the proposed hybrid MPPT along with the energies from four existing methods, namely P&O [50, 52], Fibonacci search method [83], PSO [54], and DE [96, 203], are shown in Table 5.4. For the case SP1 to SP2, all the MPPT methods produce almost the same energy. This is as expected due to the similar location of the global MPP for these two shading patterns. The slight energy difference is due to a combination of the power capture mechanism of each method and system noise, resulting in the operating point fluctuating around the power maxima. The percentage in brackets indicates the energy increase of the corresponding MPPT technique compared to the standard P&O method. The energy increase is calculated based on Eq. (5.11). A negative value means that the MPPT technique produces less power than the standard P&O and thus results in a power loss. A value highlighted in grey indicates that the MPPT has not found the global maxima (the MPP) and is instead trapped at a local maxima.

As expected, P&O remains trapped at the local maxima when a shading pattern change causes a change in the region of the MPP. Thus, P&O is trapped at a local maxima for all cases except the shading pattern change from SP1 to SP2, where the global MPP for the two shading patterns is in the same region. For the Fibonacci search method, it has a fast convergence speed but is unable to guarantee convergence to the global MPP for all shading patterns. This can be seen from Table 5.4, where four shading pattern changes result in the Fibonacci search based MPPT converging to a local maxima, as indicated by the grey highlighting.

Similarly, for the PSO method, there is one case where the MPPT converges to a local maxima. It should be noted that for the DE and PSO based MPPTs, the choice of parameters significantly influences the tracking performance, and a poor choice can result in the operating point remaining trapped at a local maxima. Since the DE and PSO optimization algorithms always record the optimal point with the maximum power value during the iteration process, a sudden power change caused by an irradiance transient, system noise or from a change in the load may result in the algorithm tracking an incorrect operating point. This is further complicated by the relatively long convergence time in reaching the MPP, due to the stochastic mechanism of the DE and PSO algorithms.

Table 5.4. The energy capture by P&O, Fibonacci search, PSO, DE and the proposed hybrid MPPT, and the percentage change from P&O, for the shading pattern changes indicated.

Shading pattern	Energy Capture (J)				
	P&O	Fibonacci	PSO	DE	Hybrid
SP1-SP2	1367.8	1188.5 (-13.1%)	1263.6 (-7.6%)	1252.5 (-8.4%)	1346.3 (-1.6%)
SP2-SP3	1061.6	1108.1 (+4.4%)	1234.1 (+16.2%)	1254.9 (+18.2%)	1292.9 (+21.8%)
SP2-SP4	612.7	606.8 (-9.6%)	552.2 (-9.9%)	664.4 (+8.4%)	733.1 (+19.7%)
SP2-SP5	778.7	1116.1 (+43.3%)	1052.0 (+35.1%)	1076.9 (+38.3%)	1096.6 (+40.8%)
SP2-SP7	813.5	835.8 (+2.7%)	934.5 (+14.9%)	937.0 (+15.2%)	978.6 (+20.3%)
SP2-SP8	855.8	1084.7 (+26.7%)	1069.1 (+24.9%)	1068.3 (+24.8%)	1105.4 (+29.2%)
SP2-SP10	919.1	1095.2 (+19.2%)	1086.8 (+18.2%)	1093.6 (+19.0%)	1085.8 (+18.1%)
SP2-SP12	777.3	911.0 (+17.2%)	859.4 (+10.6%)	863.6 (+11.1%)	911.4 (+17.3%)

Compared to these four MPPTs, the proposed hybrid MPPT is always able to track the global MPP and generate a significantly increased energy output. In the proposed hybrid MPPT, the region of the global MPP is predicted in one step and then the global MPP is reached by applying a conventional P&O algorithm over the local area. Because of this, the tracking time is significantly reduced. In addition, the energy produced by the proposed hybrid MPPT is up to 40.8% higher than that of the P&O algorithm.

As an example, we examine the detailed transient response of one particular case (SP2-SP4). For this case, we would expect to move from location B to location D on the P-V curves given in Fig. 5.15. Fig. 5.16 shows the location of the experimentally measured operating point when the shading pattern changes from SP2 to SP4. From Fig. 5.16, we can see that the hybrid MPPT can transfer the operating point to the new global MPP (region B), which increases the power output. Fig. 5.17 shows the power output from the proposed hybrid MPPT, P&O, DE, PSO, and Fibonacci based MPPT. It clearly shows that the implementation of the P&O, Fibonacci, and PSO MPPTs are trapped at a local maxima when the shading pattern changes from SP2 to SP4. Whereas, the DE based MPPT and the proposed hybrid method are able to find and track the global MPP for the new shading pattern condition. The transient response time for the proposed method to track the new global MPP from SP2 to SP4 is around 1.5s.

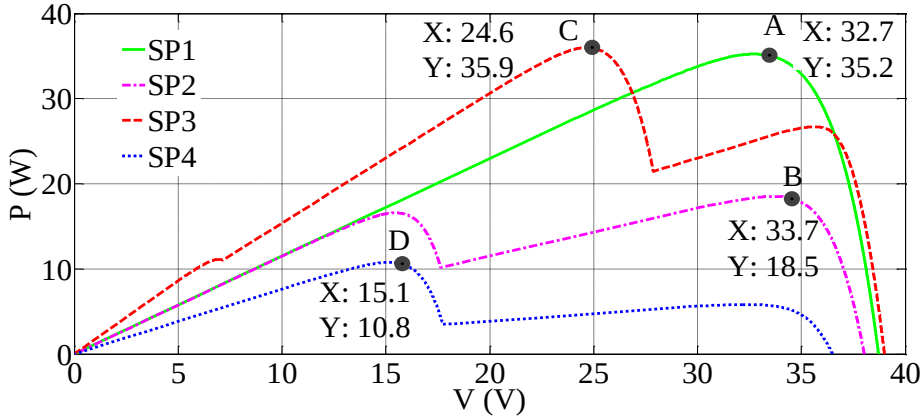

Fig. 5.15. P-V curves for SP1, SP2, SP3 and SP4.

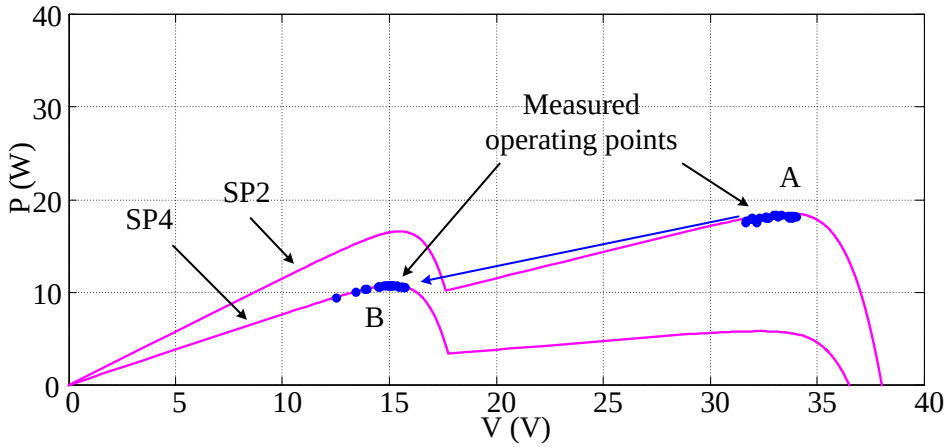

Fig. 5.16. Experimental operating point on P-V curves using the proposed hybrid MPPT when the shading pattern changes from SP2 to SP4.

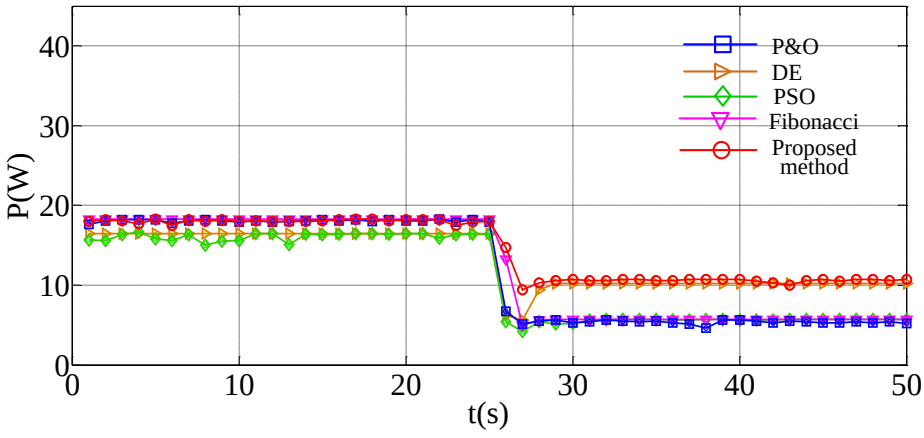

Fig. 5.17. The experimental power output (W) versus time (s) for the proposed hybrid MPPT and four existing MPPT methods (P&O, DE, PSO, and Fibonacci) for a shading pattern change from SP2 to SP4.

5.4.2.2 Transient response of multiple shading pattern shifts

In order to verify the energy capture increase of the proposed hybrid MPPT under various transient irradiance conditions, a transient test using 25 separate I-V curves, applied at 10s intervals, is examined. The MPPT parameters, including the MPPT update period ($1/f_{mppt}$), the sampling period of the ADC (T_s), the duty ratio step size (ΔD) and the time delay (T_d), are the same as for the previous section. The 25 shading patterns are the 24 shading patterns in Table 5.3, starting and finishing with SP1. The order of the shading patterns is as shown in Table 5.3, that is: SP1, SP2, …, SP24, SP1. These 25 I-V curves, with 128 data points for each curve, are imported into the memory of the PV simulator.

Table 5.5 shows the energy capture by the proposed hybrid MPPT and the four existing MPPT techniques under transient shading patterns. From Table 5.5, we can see that proposed method produce more energy than the other four MPPT techniques. For the PSO based MPPT, there are two critical aspects to take into consideration. One is the settings of the control parameters such as w, c_1 and c_2. Inappropriate values for these parameters can easily lead to a large error in the MPPT performance, resulting in a performance which is sometimes even worse than that of the conventional P&O algorithm. This can be seen from Table 5.5, where the PSO algorithm, with parameters c1 = 1.5, c2 = 1.6, w = 0.4, produces less power than the P&O algorithm. This is because inappropriate parameter settings cause a slow tracking speed which results in the algorithm not converging before the next perturbation occurs. While this method is very efficient for relatively stable and long non-transient partial shadings on the PV modules, it is not suitable when the PV system is located where many fast irradiance transitions occur, such as in the tropics [191]. This is because the global tracking PSO algorithm requires a relatively long time to track the global MPP.

Moreover, from the experiment we found that the performance of the PSO based MPPT is very sensitive to the parameter settings, whereas, DE based MPPT is less sensitive to the parameters than PSO for various shading pattern changes. As shown in Table 5.5, DE still can output more power than the conventional P&O algorithm and shows little difference in the power capture for different parameter settings. As expected, the Fibonacci search MPPT has a fast tracking speed but it is not a global tracking method and thus produces less power than that of the proposed method. Compared to these four MPPTs, the proposed hybrid MPPT can track the global MPP for all shading patterns with a relatively fast tracking speed and outputs the maximum energy. The corresponding power curve for each MPPT is shown in Fig. 5.18.

Table 5.5. The energy capture (in kJ) by the proposed hybrid MPPT and four existing MPPT techniques under transient shading patterns.

P&O (kJ) (ΔD=0.02)	PSO (kJ) (c_1=1; c_2=1.5; w=0.27)	PSO (kJ) (c_1=1.5; c_2=1.6; w=0.4)	DE (kJ) (F=1; CR=0.9)	DE (kJ) (F=0.8; CR=0.7)	Fibonacci (kJ) (N=13)	Hybrid MPPT (kJ)
5.81	5.98 (+2.9%)	5.68 (-2.2%)	6.06 (+4.3%)	5.97 (+2.8%)	6.02 (+3.6%)	6.70 (+15.3%)

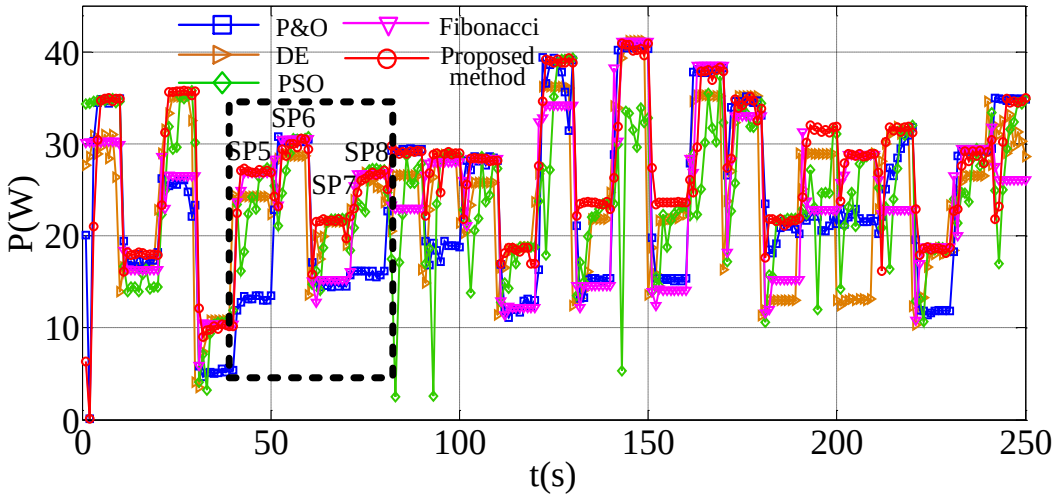

Fig. 5.18. A comparison of the experimental power output by proposed hybrid method, P&O, DE, PSO, and Fibonacci search method for varying shading patterns.

To illustrate the tracking performance of the proposed hybrid MPPT in detail, we examine the tracking mechanism for the 40s to 80s period (inside the dashed box) in Fig. 5.18. Four shading patterns (SP5, SP6, SP7 and SP8) are applied during this period. Fig. 5.19 shows the P-V curves (with the ordinate values of global MPPs) for these four shading patterns. From Fig. 5.18, we can see that the hybrid MPPT can successfully find the global MPP for all these four shading patterns, while P&O fails to track the global MPP for SP5, SP7 and SP8. DE tracks to the global MPP for SP6, SP7 and SP8 but converges to the local maxima for SP5 at point F as shown in Fig. 5.19. PSO takes a long time to converge to the global point A (SP5). The Fibonacci search method can track the global MPP for all shading patterns except SP7. All methods can adequately track to the global MPP for SP6. During the transition from SP5 to SP6, the operating point for the P&O algorithm is expected to move from point A to the local maxima (point E in Fig. 5.19). However, as this local maxima has a relatively small amplitude, system noise allows it to move to the global MPP (point B). It should be noted that when the operating current is low (under low irradiance), the power curve becomes very flat, such as the area from 20V to V_{oc_STC} for SP7 in Fig. 5.19. This may lead to the operating point shifting in a large range of voltage due to measurement noise in the voltage and current signals and may even cause the

operating point to move between adjacent local maxima. If the adjacent region contains the global MPP, it can improve the power capture, but if there is a local maxima which has lower power value, then it will decrease the performance of the system.

Fig. 5.20(a) shows the voltage and current readings from the PV array output for the complete experiment (250s) using the proposed hybrid MPPT, while Fig. 5.20(b) shows the zoomed region for SP5, SP6, SP7 and SP8. The voltage reading is measured from the output of the amplifier in the voltage sensor. The voltage and current gain are 33.7 and 1.3 respectively. From Fig. 5.20(b), we can see that the average transient time for tracking the global MPP for a new shading pattern is about 1.5 to 2 seconds. The transient time can be further improved by changing the values of MPPT frequency and the duty ratio.

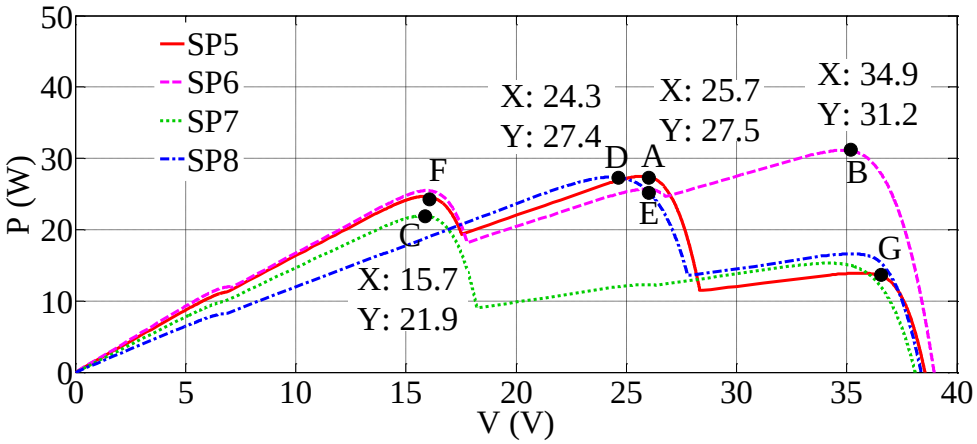

Fig. 5.19. P-V curves for SP5, SP6, SP7 and SP8.

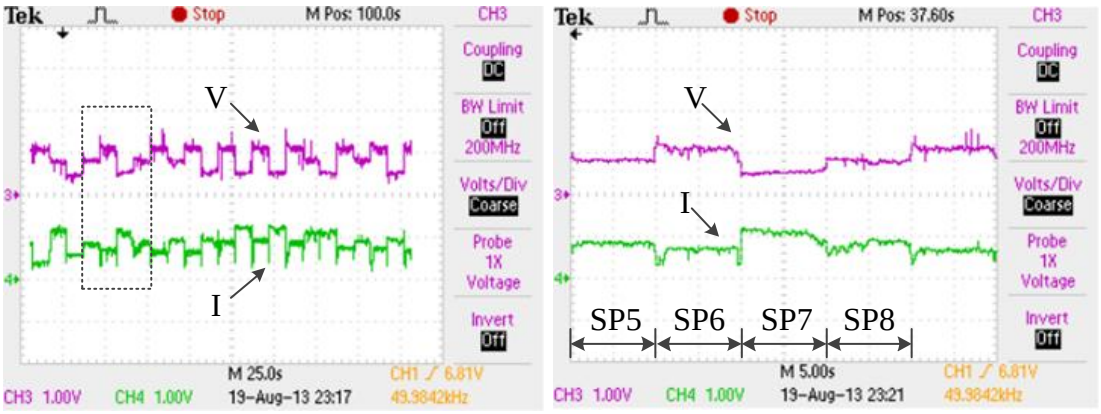

(a) (b)

Fig. 5.20. (a) The voltage and current readings at the output of the PV simulator using the proposed hybrid MPPT for 25 shading patterns, and (b) the zoomed region within the dashed box. The voltage and current gains are 33.7 and 1.3, respectively.

While the experimental results presented above are limited to an array string of only four modules, the proposed hybrid MPPT can be easily scaled to larger PV arrays with more series connected modules. The success of applying this technique depends on the classification ability of the neural network. For small or medium sized PV arrays, neural networks with a simple structure, such as widely used back propagation and feedforward neural networks, can be used as a classifier. For large scale PV arrays with a large number of PV modules connected in series, a neural network with a more complex structure, providing better classification ability, would optimally be required. However, for a large PV array operating in a tropical environment subjected to partial shading due to rapid irradiance transitions, it may be better to separate the array into several medium sized PV arrays (or use distributed MPPT) as a very large array with a central MPPT would be susceptible to a significant power loss.

Even though the proposed method is tested using a PV array simulator which outputs exactly the same I-V characteristics as the real PV modules, this proposed method can be applied to various PV systems which consists of large number of PV arrays with two different widely used solar cell techniques such as silicon multi-crystalline and silicon mono-crystalline solar cells wherever there are multiple peaks on its output P-V characteristic. For thin film solar modules, the partial shading problem is different because of its monolithic structure. Possible MPPT techniques for thin film solar modules are left for our future research.

5.5 Summary

In this chapter, an efficient hybrid MPPT algorithm for PV systems operating under partial shading conditions is proposed. It combines an ANN with the conventional P&O MPPT algorithm. The ANN is used as a classifier to predict the region of the new shading pattern on the P-V curve when a sudden irradiance change is detected. Two possible implementations are examined. The first uses relatively expensive irradiance sensors to provide the inputs to the ANN classifier, while the second is lower cost solution (actually, zero additional cost compared to the conventional P&O algorithm) which uses only one pair of current and voltage sensors because our proposed method uses the current values successively measured at discrete voltage points (corresponding to the I-V steps caused by shading) as inputs to the ANN classifier. In both implementations the ANN output is the region of the optimal MPP. The influence of temperature on the location of MPP is compensated for according to the linear relationship between the temperature value and the voltage value of the optimal MPP. Based on the predicted region, the initial operating point for the new shading pattern is generated, and then a conventional MPPT algorithm

(such as P&O or any other efficient local MPP search method) is used to search the local area for the global MPP.

The effectiveness of our proposed hybrid MPPT is verified using both simulation and experimental analysis. The step response and transient performance of the proposed method under various shading patterns is compared with the conventional P&O algorithm and three widely used computational MPPTs, namely the Fibonacci search method, PSO and DE. The results show that the proposed hybrid MPPT can efficiently track the global MPP under various shading patterns with much better tracking accuracy than the other compared methods. The system response time for transitioning between shading patterns is less than 2 seconds and this transient time can be improved by adjusting the step size and the frequency of the MPPT or by using a faster local MPP search technique (such as ESC). The proposed algorithm can also be applied to relatively large scale PV systems with large module strings. It could even be applied at the module level in distributed MPPT PV systems with an MPPT on each PV module, to eliminate modular level shading effects.

Chapter 6 Conclusions and future work

6.1 Conclusions

This thesis focuses on maximum power point tracking (MPPT) techniques for PV systems under partial shading and rapidly changing irradiance conditions. In achieving this aim, it became obvious that better parameter extraction and modeling of the photovoltaic (PV) cell/module/array were needed as these techniques are fundamental to our analysis and simulation of MPPT systems. Limitations to existing parameter extraction and modeling techniques for PV systems resulted in an extension of the scope of this thesis to also cover these topics. Modeling and parameter extraction of the PV module is examined in Chapter 3, while MPPT for PV systems under partially shaded conditions is examined in Chapter 4 and Chapter 5.

A review of the literature related to modeling methods for PV and of MPPT for PV systems is presented in Chapter 2. Each modeling method is described and compared with each other in terms of tracking accuracy, computational complexity, and other factors that influence the performance of MPPT. The MPPT techniques are evaluated using several characteristics, namely the global tracking ability, system dependency, tracking accuracy, implementation complexity, number of sensors required, type of implementation, and online or offline operation. The factors affecting the performance of each method are also given.

Based on the disadvantages of the existing modeling methods in the review, a Chebyshev functional link neural network (CFLNN) based model for the PV cell/module/array is introduced in Chapter 3. The advantages of this method include lower implementation complexity than the conventional multilayer perceptron (MLP) neural network due to the absence of hidden layers in the network and better accuracy than the conventional two diode model.

When the analytical method is used for PV array modeling, accurate parameter extraction of the PV cells is of major importance. Because of the limitations and the inaccuracies in existing parameter extraction techniques, an improved adaptive differential evolution (IADE) algorithm based optimization technique is proposed to extract the parameter values for the analytical models of the PV array. In this method, the scaling factor and crossover rate values in the standard differential evolution (DE) algorithm are updated according to the feedback of fitness value in each iteration step. This eliminates the need

for users to tune the control parameters for different environmental conditions. The simulation and experimental results show better accuracy than that provided by many other widely used optimization methods such as genetic algorithm (GA), conventional DE, simulated annealing (SA), particle swarm optimization (PSO), and an analytical method based on polynomial fitting and the Lambert W function.

Partial shading, particularly that associated with very rapid irradiance change, as experienced in the tropics, results in many existing MPPT algorithms extracting less than the optimum power. For the MPPT problem under partial shading conditions, a novel ant colony optimization (ACO) based MPPT is proposed in Chapter 4. This is the first time that ACO has been directly applied to the MPPT problem. The effectiveness of the proposed method is verified using both simulation and an experiment setup under various shading patterns. This method is able to track the global MPP without needing irradiance or temperature sensors, has a good tracking accuracy and compared to the PSO algorithm, has a faster tracking speed. As many other related evolutionary algorithms can also be applied to MPPT, we proposed a uniform application scheme for applying this type of algorithm into PV systems with various structures. Furthermore, a scheme for accelerating the tracking speed is also discussed.

Since the artificial neural network (ANN) has the ability to predict the result in one step, unlike the evolutionary algorithms which find the global MPP by successively perturbing the working point, a hybrid MPPT is proposed in Chapter 5. It combines an ANN and a conventional perturb and observe (P&O) MPPT. Unlike the conventional ANN, instead of predicting the optimal voltage/current at the MPP directly, the ANN is utilized to predict the region of the MPP. Then the conventional P&O algorithm is applied to track the global MPP within the local area. The temperature influence on the location of the MPP is compensated for according to the linear relationship between the voltage of PV array and the temperature. A new method to predict the global MPP region for the case when the irradiance sensors are not available is also investigated. In this method, the current values measured successively from the fixed points on the staircase of the I-V curve, which occurs during partial shading, are used as the inputs to the ANN. This hybrid MPPT has a fast response due to its direct prediction of the global MPP region within one step and is able to track the global MPP even without the irradiance sensors, making it relatively low cost. The effectiveness of the proposed hybrid MPPT is verified with both simulation and experimental setup under various shading patterns.

6.2 Future work

The single and two-diode models are two common analytical modeling methods for the conventional crystalline silicon PV cell/module/array. However there is less literature on

modeling for CIGS thin film PV cells. Thin film technology has been improved steadily over recent years and has become very competitive due to its better flexibility, lower price and simpler manufacturing process than the conventional crystalline silicon PV technology. Although there is some work on the electrical modeling for Copper-Indium-Gallium-Selenide (CIGS) thin-film solar cells in [204-212], the way of calculating parameters for the models needs to be improved by considering other factors, which can influence the results of the model, such as the irradiance and temperature.

Partial shading is also an important issue for other PV cell technologies, especially for monolithic thin film PV cells. For crystalline silicon PV cells, bypass diodes can be used to mitigate the shading effects, while for the monolithic thin film PV cell, there is little in the literature on this topic. Since in the fabrication process the thin film PV modules are produced monolithically, the characteristics of the cutting method for the PV cells, such as cutting shapes, orientations and sizes, can also influence the performance of the PV cell, thus the geometrical design of the PV cells may influence the performance under partial shading.

Based on the proposed a uniform implementation scheme in Chapter 4, more work can be done to improve the performance of MPPTs based on the evolutionary optimization algorithms. For example, the tracking ability of the standard ACO based MPPT can be enhanced by utilizing a variant of ACO [213, 214] or combining the advantages of different types of the evolutionary optimization algorithms. In addition, there are no clear criteria for the parameter settings of these algorithms in MPPT from the current literature, opening up a possible topic to study.

Apart from above topics, the detection of the partial shading condition is another important area to examine because the method to detect the occurrence of the partial shading can help to determine the characteristics of the PV array under the shading conditions. In tropical areas there are a large numbers of transient irradiance events due to rapidly moving clouds. Conventional MPPTs, as described in the review part in Chapter 2, are generally not able to track the global MPP under environmental conditions with large continuous transients. Therefore, more work needs to be done to develop MPPTs which are able to operate under rapid changing conditions. Moreover, for the large scale PV systems, distributed MPPT where each PV module is equipped with an MPPT is a potential strategy to relieve the partial shading issue. Applying evolutionary optimization algorithms or extremum seeking control methods into distributed MPPT and its performance comparison with different structures would be worthy research topics.

Bibliography

[1] S. A. Al Jaber, A. Z. Amin, C. Clini, and R. Dixon, *REN21 Renewables global status report*, 2012.

[2] M. J. de Wild-Scholten, "Energy payback time and carbon footprint of commercial photovoltaic systems," *Solar Energy Materials and Solar Cells,* vol. 119, pp. 296-305, 2013.

[3] Website. "http://www.epia.org/," Jul. 2014.

[4] "Market Report 2013," *European Photovoltaic Industry Association, http://www.epia.org/, Accessed Jul. ,* 2014.

[5] Website. "http://www.solar-thermal.com/solar_vs_pv.html," Jul. 2014.

[6] Website. "http://www.volker-quaschning.de/articles/fundamentals2/index.php," Jul. 2014.

[7] V. Devabhaktuni, M. Alam, S. Shekara Sreenadh Reddy Depuru, R. C. Green Ii, D. Nims, and C. Near, "Solar energy: Trends and enabling technologies," *Renewable and Sustainable Energy Reviews,* vol. 19, pp. 555-564, 2013.

[8] J. Bauer, J. M. Wagner, A. Lotnyk, H. Blumtritt, B. Lim, J. Schmidt, and O. Breitenstein, "Hot spots in multicrystalline silicon solar cells: avalanche breakdown due to etch pits," *Physica Status Solidi (RRL) - Rapid Research Letters,* vol. 3, no. 2, pp. 40-42, 2008.

[9] A. Woyte, J. Nijs, and R. Belmans, "Partial shadowing of photovoltaic arrays with different system configurations: literature review and field test results," *Solar Energy,* vol. 74, no. 3, pp. 217-233, 2003.

[10] T. Esram, and P. L. Chapman, "Comparison of photovoltaic array maximum power point tracking techniques," *IEEE Transactions on Energy Conversion,* vol. 22, no. 2, pp. 439-449, 2007.

[11] K. H. Hussein, I. Muta, T. Hoshino, and M. Osakada, "Maximum photovoltaic power tracking: an algorithm for rapidly changing atmospheric conditions," *IEE Proceedings of Generation, Transmission and Distribution,* vol. 142, pp. 1350-2360, 1995.

[12] Y. H. Ji, D. Y. Jung, J. G. Kim, J. H. Kim, T. W. Lee, and C. Y. Won, "A real maximum power point tracking method for mismatching compensation in PV array under partially shaded conditions," *IEEE Transactions on Power Electronics,* vol. 26, no. 4, pp. 1001-1009, 2010.

[13] B. Bletterie, R. Bruendlinger, and S. Spielauer, "Quantifying dynamic MPPT performance under realistic conditions first test results the way forward," in The 21st European Photovoltaic Solar Energy Conference and Exhibition, Dresden, Germany, 2006, pp. 2347-2351.

[14] D. Sera, "Real-time modelling, diagnostics and optimised MPPT for residental PV systems," Faculty of Engineering, Science & Medicine, Aalborg University, 2009.

[15] Y. J. Wang, and P. C. Hsu, "Analytical modelling of partial shading and different orientation of photovoltaic modules," *Renewable Power Generation, IET*, vol. 4, no. 3, pp. 272 - 282, 2010.

[16] W. Shockley, "The theory of p-n junctions in semiconductors and p-n junction transistors," *Bell System Technical Journal*, vol. 28, no. 3, pp. 435-489, 1949.

[17] T. Ikegamia, T. Maezonoa, F. Nakanishia, Y. Yamagatab, and K. Ebiharab, "Estimation of equivalent circuit parameters of PV modules and its application to optimal operation of PV system," *Solar Energy Materials and Solar Cells*, vol. 67, no. 1-4, pp. 389-395, 2001.

[18] F. Nakanishi, T. Ikegami, K. Ebihara, S. Kuriyama, and Y. Shiota, "Modelling and operation of a 10 kW photovoltaic power generator using equivalent electric circuit method," in IEEE Photovoltaic Specialists Conference, Anchorage, USA, 2000, pp. 1703-1706

[19] M. G. Villalva, J. R. Gazoli, and E. R. Filho, "Comprehensive approach to modeling and simulation of photovoltaic arrays," *IEEE Transactions on Power Electronics*, vol. 24, no. 5, pp. 1198-1208, 2009.

[20] K. Ishaque, Z. Salam, and Syafaruddin, "A comprehensive MATLAB Simulink PV system simulator with partial shading capability based on two-diode model," *Solar Energy*, vol. 85, no. 9, pp. 2217-2227, 2011.

[21] K. Ishaque, Z. Salam, and H. Taheri, "Accurate MATLAB simulink PV system simulator based on a Two-Diode model," *Journal of Power Electronics (JPE)*, vol. 11, no. 2, pp. 179-187, 2010.

[22] K. Nishioka, N. Sakitani, Y. Uraoka, and T. Fuyuki, "Analysis of multicrystalline silicon solar cells by modified 3-diode equivalent circuit model taking leakage current through periphery into consideration," *Solar Energy Materials and Solar Cells*, vol. 91, no. 13, pp. 1222-1227, 2007.

[23] A. N. Celik, and N. Acikgoz, "Modelling and experimental verification of the operating current of mono-crystalline photovoltaic modules using four- and five-parameter models," *Applied Energy*, vol. 84, no. 1, pp. 1-15, 2007.

[24] K. Ishaque, Z. Salam, and H. Taheri, "Simple, fast and accurate two-diode model for photovoltaic modules," *Solar Energy Materials and Solar Cells*, vol. 95, no. 2, pp. 586-594, 2011.

[25] E. Karatepe, M. Boztepe, and M. Colak, "Neural network based solar cell model," *Energy Conversion and Management*, vol. 47, no. 9-10, pp. 1159-1178, 2006.

[26] F. Almonacid, C. Rus, P. Perez-Higueras, and L. Hontoria, "Calculation of the energy provided by a PV generator. comparative study: conventional methods vs. artificial neural networks," *Energy*, vol. 36, no. 1, pp. 375-384, 2010.

[27] J. A.Gow, and C. D. Manning, “Development of a model for photovoltaic arrays suitable for use in simulation studies of solar energy conversion systems,” in The 6th International Conference on Power Electronics and Variable Speed Drives, 1996, pp. 69-74.

[28] L. Castaner, and S. Silvestre, *Modelling photovoltaic systems using Pspice*, New York: Wiley, 2003.

[29] M. Veerachary, “PSIM circuit-oriented simulator model for the nonlinear photovoltaic sources,” *IEEE Transactions on Aerospace and Electronic Systems,* vol. 42, no. 2, pp. 735-740, 2006.

[30] Website. "http://www.synopsys.com/Systems/Saber/Pages/default.aspx," Jul. 2014.

[31] A. Mellit, M. Benghanem, and S. A. Kalogirou, “Modeling and simulation of a stand-alone photovoltaic system using an adaptive artificial neural network: Proposition for a new sizing procedure,” *Renewable Energy,* vol. 32, no. 2, pp. 285-313, 2007.

[32] F. Almonacid, C. Rus, L. Hontoria, M. Fuentes, and G. Nofuentes, “Characterisation of Si-crystalline PV modules by artificial neural networks,” *Renewable Energy*, vol. 34, no. 4, pp. 941-949, 2009.

[33] B. Irie, and S. Miyake, “Capabilities of three-layer perceptrons,” in IEEE International Conference on Neural Networks, San Diego, CA, USA, 1988, pp. 641-648.

[34] K. Hornik, “Approximation capabilities of multilayer feedforward networks,” *Neural Networks,* vol. 4, no. 2, pp. 251-257, 1991.

[35] D. Svozil, V. Kvasnicka, and J. í. Pospichal, “Introduction to multi-layer feed-forward neural networks,” *Chemometrics and Intelligent Laboratory Systems,* vol. 39, no. 1, pp. 43-62, 1997.

[36] S. Haykin, *Neural Networks: A Comprehensive Foundation*: Prentice Hall PTR, 1998.

[37] Website. "http://scholarpedia.org/article/Kohonen_network," Nov. 2014.

[38] R. Hecht-Nielsen, “Theory of the backpropagation neural network,” in International Joint Conference on Neural Networks (IJCNN), Washington, DC, USA, 1989, pp. 593-605.

[39] M. J. L. Orr, *Introduction to Radial Basis Function Networks*, University of Edinburgh, Scotland, 1996.

[40] F. Girosi, and T. Poggio, “Networks and the best approximation property,” *Biological Cybernetics*, vol. 63, no. 3, pp. 169-176, 1990.

[41] G. Cybenko, “Approximation by superpositions of a sigmoidal function,” *Mathematics of Control, Signals and Systems,* vol. 2, no. 4, pp. 303-314, 1989.

[42] A. Mellit, and S. A. Kalogirou, “Artificial intelligence techniques for photovoltaic applications: A review,” *Progress in Energy and Combustion Science,* vol. 34, no. 5, pp. 574-632, 2008.

[43] A. N. Celik, “Artificial neural network modeling and experimental verification of the operating current of mono-crystalline photovoltaic modules,” *Solar Energy,* vol. 85, no. 10, pp. 2507-2517, 2011.

[44] S. A. Kalogirou, “Artificial neural networks in renewable energy systems applications: a review,” *Renewable and Sustainable Energy Reviews,* vol. 5, no. 4, pp. 373-401, 2001.

[45] K. Karabacak, and N. Cetin, “Artificial neural networks for controlling wind–PV power systems: A review,” *Renewable and Sustainable Energy Reviews,* vol. 29, no. 0, pp. 804-827, 2014.

[46] Z. Salam, J. Ahmed, and B. S. Merugu, “The application of soft computing methods for MPPT of PV system: A technological and status review,” *Applied Energy,* vol. 107, pp. 135-148, 2013.

[47] A. Mellit, S. A. Kalogirou, L. Hontoria, and S. Shaari, “Artificial intelligence techniques for sizing photovoltaic systems: A review,” *Renewable and Sustainable Energy Reviews,* vol. 13, no. 2, pp. 406-419, 2009.

[48] A. Reza Reisi, M. Hassan Moradi, and S. Jamasb, “Classification and comparison of maximum power point tracking techniques for photovoltaic system: A review,” *Renewable and Sustainable Energy Reviews,* vol. 19, pp. 433-443, 2013.

[49] M. A. Eltawil, and Z. Zhao, “MPPT techniques for photovoltaic applications,” *Renewable and Sustainable Energy Reviews,* vol. 25, pp. 793-813, 2013.

[50] K. Ishaque, and Z. Salam, “A review of maximum power point tracking techniques of PV system for uniform insolation and partial shading condition,” *Renewable and Sustainable Energy Reviews,* vol. 19, pp. 475-488, 2013.

[51] A. P. Bhatnagar, and B. R. K. Nema, “Conventional and global maximum power point tracking techniques in photovoltaic applications: A review,” *Journal of Renewable and Sustainable Energy,* vol. 5, no. 3, 2013.

[52] P. Bhatnagar, and R. K. Nema, “Maximum power point tracking control techniques: State-of-the-art in photovoltaic applications,” *Renewable and Sustainable Energy Reviews,* vol. 23, pp. 224-241, 2013.

[53] Syafaruddin, E. Karatepe, and T. Hiyama, “Artificial neural network-polar coordinated fuzzy controller based maximum power point tracking control under partially shaded conditions ” *Renewable Power Generation, IET,* vol. 3, no. 2, pp. 239-253, 2009.

[54] M. Miyatake, M. Veerachary, F. Toriumi, N. Fujii, and H. Ko, “Maximum power point tracking of multiple photovoltaic arrays: A PSO approach,” *IEEE Transactions on Aerospace and Electronic Systems,* vol. 47, no. 1, pp. 367-380, 2011.

[55] A. Khare, and S. Rangnekar, “A review of particle swarm optimization and its applications in solar Photovoltaic system,” *Applied Soft Computing,* vol. 13, no. 5, pp. 2997-3006, 2013.

[56] S. Hadji, F. Krim, and J. P. Gaubert, “Development of an algorithm of maximum power point tracking for photovoltaic systems using genetic algorithms ” in The 7th International Workshop on Systems, Signal Processing and their Applications (WOSSPA), Tipaza, Algeria, 2011, pp. 43-46.

[57] N. A. Kamarzaman, and C. W. Tan, "A comprehensive review of maximum power point tracking algorithms for photovoltaic systems," *Renewable and Sustainable Energy Reviews,* vol. 37, pp. 585-598, 2014.

[58] N. Khaehintung, K. Pramotung, B. Tuvirat, and P. Sirisuk, "RISC-microcontroller built-in fuzzy logic controller of maximum power point tracking for solar-powered light-flasher applications," in IEEE Annual Conference on Industrial Electronics Society, 2004, pp. 2673-2678.

[59] C. C. Liao, "Genetic k-means algorithm based RBF network for photovoltaic MPP prediction " *Energy,* vol. 35, no. 2, pp. 529-536, 2010.

[60] A. Messai, A. Mellit, A. Guessoum, and S. A. Kalogirou, "Maximum power point tracking using a GA optimized fuzzy logic controller and its FPGA implementation," *Solar Energy,* vol. 85, no. 2, pp. 265-277, 2011.

[61] D. C. Martins, "Analysis of a three-phase grid-connected PV power system using a modified dual-stage inverter," *ISRN Renewable Energy,* vol. 2013, pp. 18, 2013.

[62] M. Barghi Latran, and A. Teke, "Investigation of multilevel multifunctional grid connected inverter topologies and control strategies used in photovoltaic systems," *Renewable and Sustainable Energy Reviews,* vol. 42, pp. 361-376, 2015.

[63] C. Hua, and C. Shen, "Comparative study of peak power tracking techniques for solar storage systems," in IEEE International Conference and Exposition on Annual Applied Power Electronics, Anaheim, CA, 1998, pp. 697-685.

[64] I. Houssamo, F. Locment, and M. Sechilariu, "Maximum power tracking for photovoltaic power system: Development and experimental comparison of two algorithms," *Renewable Energy* vol. 35, no. 10, pp. 2381-2387, 2010.

[65] D. P. Hohm, and M. E. Ropp, "Comparative study of maximum power point tracking algorithms," *Progress in Photovoltaics: Research and Applications,* vol. 11, pp. 47-62, 2003.

[66] J. Hossain, and A. Mahmud, *Renewable energy integration: challenges and solutions*: Springer, 2014.

[67] P. Wang, H. Zhu, W. Shen, F. H. Choo, P. C. Loh, and K. K. Tan, "A novel approach of maximizing energy harvesting in photovoltaic systems based on bisection search theorem," in IEEE Applied Power Electronics Conference and Exposition, Palm Springs, CA, 2010, pp. 2143-2148.

[68] A. Al-Diab, and C. Sourkounis, "Variable step size P&O MPPT algorithm for PV systems," in The 12th International Conference on Optimization of Electrical and Electronic Equipment, Basov, New York, USA, 2010, pp. 1097-1102.

[69] N. Khaehintung, T. Wiangtong, and P. Sirisuk, "FPGA implementation of MPPT using variable step-size P&O algorithm for PV applications," in International Symposium on Communications and Information Technologies, Bangkok, Thailand, 2006, pp. 212-215.

[70] F. Liu, S. Duan, F. Liu, B. Liu, and Y. Kang, “A variable step size INC MPPT method for PV systems ” *IEEE Transactions on Industrial Electronics,* vol. 55, no. 7, pp. 2622-2628, 2008.

[71] A. M. Bazzi, and P. T. Krein, “Ripple correlation control: an extremum seeking control perspective for real-time optimization,” *IEEE Transactions on Power Electronics,* vol. 29, no. 2, pp. 988-995, 2014.

[72] G. Spiazzi, S. Buso, and P. Mattavelli, “Analysis of MPPT algorithms for photovoltaic panels based on ripple correlation techniques in presence of parasitic components,” in Brazilian Power Electronics Conference, Bonito-Mato Grosso do Sul, Brazil, 2009, pp. 88-95.

[73] A. Ghaffari, M. Krstic, and S. Seshagiri, “Power optimization for photovoltaic micro-converters using multivariable Newton-based extremum-seeking,” in IEEE Annual Conference on Decision and Control, Montreal, QC, Canada, 2012, pp. 2421-2426.

[74] T. Kitano, M. Matsui, and X. De-hong, “Power sensor-less MPPT control scheme utilizing power balance at DC link-system design to ensure stability and response,” in The 27th Annual Conference of IEEE Industrial Electronics Society, Denver, CO, USA, 2001, pp. 1309-1314.

[75] R. F. Coelho, F. M. Concer, and D. C. Martins, “A MPPT approach based on temperature measurements applied in PV systems,” in The 9th IEEE International Conference on Industry Applications, Sao Paulo, Brazil, 2010, pp. 1-6.

[76] P. Minwon, and Y. In-Keun, “A study on the optimal voltage for MPPT obtained by surface temperature of solar cell,” in The 30th Annual Conference of IEEE Industrial Electronics Society, 2004, pp. 2040-2045.

[77] L. L. Zhang, W. G. Hurley, and W. Wolfle, “A new approach to achieve maximum power point tracking for PV system with a variable inductor,” in The 2nd IEEE International Symposium on Power Electronics for Distributed Generation Systems, Hefei, China, 2010, pp. 948-952.

[78] A. Brambilla, M. Gambarara, A. Garutti, and F. Ronchi, “New approach to photovoltaic arrays maximum power point tracking,” in 30th IEEE Annual Power Electronics Specialists Conference, Charleston, South Carolina, USA, 1999, pp. 632-637.

[79] K. Kobayashi, I. Takano, and Y. Sawada, “A study of a two stage maximum power point tracking control of a photovoltaic system under partially shaded insolation conditions,” *Solar Energy Materials and Solar Cells,* vol. 90, no. 18-19, pp. 2975-2988, 2006.

[80] D. R. Jones, C. D. Perttunen, and B. E. Stuckman, “Lipschitzian optimization without the Lipschitz constant,” *Journal of Optimization Theory and Applications,* vol. 79, no. 1, pp. 157-181, 1993.

[81] T. L. Nguyen, and K. S. Low, "A global maximum power point tracking scheme employing DIRECT search algorithm for photovoltaic systems," *IEEE Transactions on Industrial Electronics,* vol. 57, no. 10, pp. 3456-3467, 2010.

[82] O. Yayenie, "A note on generalized Fibonacci sequences," *Applied Mathematics and Computation,* vol. 217, no. 12, pp. 5603-5611, 2011.

[83] N. Ahmed, and M. Miyatake, "A novel maximum power point tracking for photovoltaic applications under partially shaded insolation conditions," *Electric Power Systems Research,* vol. 78, no. 5, pp. 777-784, 2008.

[84] E. V. Solodovnik, S. Liu, and R. A. Dougal, "Power controller design for maximum power tracking in solar installations," *IEEE Transactions on Power Electronics,* vol. 19, no. 5, pp. 1295-1304, 2004.

[85] M. Boztepe, F. Guinjoan, G. Velasco-Quesada, S. Silvestre, A. Chouder, and E. Karatepe, "Global MPPT scheme for photovoltaic string inverters based on restricted voltage window search algorithm," *IEEE Transactions on Industrial Electronics,* vol. 61, no. 7, pp. 3302-3312, 2014.

[86] J. Kennedy, and R. Eberhart, "Particle swarm optimization," in IEEE International Conference on Neural Networks, Perth, Australia, 1995, pp. 1942-1948.

[87] I. C. Trelea, "The particle swarm optimization algorithm: convergence analysis and parameter selection," *Information Processing Letters,* vol. 85, no. 6, pp. 317-325, 2003.

[88] M. Jiang, Y. P. Luo, and S. Y. Yang, "Stochastic convergence analysis and parameter selection of the standard particle swarm optimization algorithm," *Information Processing Letters,* vol. 102, no. 1, pp. 8-16, 2007.

[89] M. Clerc, and J. Kennedy, "The particle swarm - explosion, stability, and convergence in a multidimensional complex space," *IEEE Transactions on Evolutionary Computation,* vol. 6, no. 1, pp. 58-73, 2002.

[90] J. Kennedy, R.C. Eberhart, and Y. Shi., *Swarm intelligence*, San Francisco: Morgan Kaufmann Publishers, 2001.

[91] B. Frans Van Den, "An analysis of particle swarm optimizers," University of Pretoria, South Africa, 2002.

[92] Y. Shi, and R. C. Eberhart, "Parameter selection in particle swarm optimization," in Proceedings of the 7th International Conference on Evolutionary Programming VII, 1998, pp. 591-600.

[93] S. Ghosh, S. Das, A. V. Vasilakos, and K. Suresh, "On convergence of differential evolution over a class of continuous functions with unique global optimum," *IEEE Transactions on Systems, Man, and Cybernetics, Part B: Cybernetics,* vol. 42, no. 1, pp. 107-124, 2012.

[94] M. G. Epitropakis, D. K. Tasoulis, N. G. Pavlidis, V. P. Plagianakos, and M. N. Vrahatis, "Enhancing differential evolution utilizing proximity-based mutation operators," *IEEE Transactions on Evolutionary Computation,* vol. 15, no. 1, pp. 99-119, 2011.

[95] M. F. N. Tajuddin, S. M. Ayob, Z. Salam, and M. S. Saad, "Evolutionary based maximum power point tracking technique using differential evolution algorithm," *Energy and Buildings,* vol. 67, pp. 245-252, 2013.

[96] H. Taheri, Z. Salam, K. Ishaque, and Syafaruddin, "A novel maximum power point tracking control of photovoltaic system under partial and rapidly fluctuating shadow conditions using differential evolution " in IEEE Symposium on Industrial Electronics & Applications, Penang, Malaysia, 2010, pp. 82-87.

[97] S. Hadji, J. P. Gaubert, and F. Krim, "Genetic algorithms for maximum power point tracking in photovoltaic systems," in Proceedings of European Conference on Power Electronics and Applications, Birmingham, UK, 2011, pp. 1-9.

[98] R. Ramaprabha, V. Gothandaraman, K. Kanimozhi, R. Divya, and B. L. Mathur, "Maximum power point tracking using GA-optimized artificial neural network for solar PV system," in 1st International Conference onElectrical Energy Systems, Newport Beach, CA, USA, 2011, pp. 264-268.

[99] K. M. Passino, and S. Yurkovich, *Fuzzy Control*, Department of Electrical Engineering, Ohio State University: An Imprint of Addison-Wesley Longman, Inc., 1998.

[100] T. Senjyu, and K. Uezato, "Maximum power point tracker using fuzzy control for photovoltaic arrays " in IEEE International Conference on Industrial Technology, Guangzhou, China, 1994, pp. 143-147.

[101] N. Patcharaprakiti, and S. Premrudeepreechacharn, "Maximum power point tracking using adaptive fuzzy logic control for grid-connected photovoltaic system," in IEEE Power Engineering Society Winter Meeting, 2002, pp. 372-377.

[102] M. Veerachary, T. Senjyu, and K. Uezato, "Neural-network-based maximum-power-point tracking of coupled-inductor interleaved-boost-converter-supplied PV system using fuzzy controller " *IEEE Transactions on Industrial Electronics,* vol. 50, no. 4, pp. 749-758, 2003.

[103] H. T. Duru, "A maximum power tracking algorithm based on Impp=f(Pmax) function for matching passive and active loads to a photovoltaic generator," *Solar Energy,* vol. 80, no. 7, pp. 812-822, 2006.

[104] A. W. Leedy, and K. E. Garcia, "Approximation of P-V characteristic curves for use in maximum power point tracking algorithms," in The 45th Southeastern Symposium on System Theory, , Baylor University, Waco, TX, USA, 2013, pp. 88-93.

[105] Nobuyoshi Takehara, and S. Kurokami, *Power control apparatus and method and power generating system using them*, USA,to Canon Kabushiki Kaisha, 1997.

[106] A. B. G. Bahgat, N. H. Helwa, G. E. Ahmad, and E. T. Shenawy, "Maximum power point tracking controller for PV systems using neural networks," *Renewable Energy*, vol. 30, no. 8, pp. 1257-1268, 2005.

[107] H. M. Mashaly, A. M. Sharaf, M. Mansour, and A. A. El-Sattar, "A photovoltaic maximum power tracking using neural networks " in The IEEE Conference on Control Applications Glasgow , UK, 1994, pp. 167-172.

[108] A. M. Torres, F. L. M. Antunes, and F. S. Reis, "An artificial neural network-based real time maximum power tracking controller for connecting a PV system to the grid," in IEEE Annual Conference on Industrial Electronics Society, Aachen, Germany, 1998, pp. 554-558.

[109] F. Giraud, and Z. M. Salameh, "Analysis of the effects of a passing cloud on a grid-interactive photovoltaic system with battery storage using neural networks," *IEEE Transactions on Energy Conversion*, vol. 14, no. 4, pp. 1572-1577, 1999.

[110] E. Koutroulis, and F. Blaabjerg, "A new technique for tracking the global maximum power point of PV arrays operating under partial-shading conditions," *IEEE Journal of Photovoltaics*, vol. 2, no. 2, pp. 184-190, 2012.

[111] H. Patel, and V. Agarwal, "Maximum power point tracking scheme for PV systems operating under partially shaded conditions," *IEEE Transactions on Industrial Electronics*, vol. 55, no. 4, pp. 1689-1698, 2008.

[112] M. Bodur, and M. Ermis, "Maximum power point tracking for low power photovoltaic solar panels," in The 7th Mediterranean Electrotechnical Conference, Antalya, Turkey, 1994, pp. 758-761.

[113] K. Il-Song, K. Myung-Bok, and Y. Myung-Joong, "New maximum power point tracker using sliding-mode observer for estimation of solar array current in the grid-connected photovoltaic system," *IEEE Transactions on Industrial Electronics*, vol. 53, no. 4, pp. 1027-1035, 2006.

[114] Z. Miao, W. Jie, and Z. Hui, "The application of slide technology in PV maximum power point tracking system," in The Fifth World Congress on Intelligent Control and Automation, 2004, pp. 5591-5594.

[115] Y. J. Zhan, C. C. Chan, and K. T. Chau, "A novel sliding-mode observer for indirect position sensing of switched reluctance motor drives," *IEEE Transactions on Industrial Electronics*, vol. 46, no. 2, pp. 390-397, 1999.

[116] L. V. Hartmann, M. A. Vitorino, M. B. R. Correa, and A. M. N. Lima, "Combining model-based and heuristic techniques for fast tracking the maximum-power point of photovoltaic systems," *IEEE Transactions on Power Electronics*, vol. 28, no. 6, pp. 2875-2885, 2013.

[117] R. Khanna, Z. Qinhao, W. E. Stanchina, G. F. Reed, and M. Zhi-Hong, "Maximum power point tracking using model reference adaptive control," *IEEE Transactions on Power Electronics*, vol. 29, no. 3, pp. 1490-1499, 2014.

[118] C. Larbes, S. M. Aït Cheikh, T. Obeidi, and A. Zerguerras, "Genetic algorithms optimized fuzzy logic control for the maximum power point tracking in photovoltaic system," *Renewable Energy*, vol. 34, no. 10, pp. 2093-2100, 2009.

[119] A. Messai, A. Mellit, A. Guessoum, and S. A. Kalogirou, "Maximum power point tracking using a GA optimized fuzzy logic controller and its FPGA implementation," *Solar Energy*, vol. 85, no. 2, pp. 265-277, 2011.

[120] T. Mishima, and T. Ohnishi, "A power compensation strategy based on electric double layer capacitors for a partially shaded PV array," in The 5th International Conference on Power Electronics and Drive Systems, 2003, pp. 858-863.

[121] T. Mishima, and T. Ohnishi, "Experimental evaluation of the EDLC-based power compensator for a partially shaded PV array," in IEEE Annual Conference on Industrial Electronics Society, 2003, pp. 1308-1313.

[122] E. Karatepe, T. Hiyama, M. Boztepe, and M. Colak, "Voltage based power compensation system for photovoltaic generation system under partially shaded insolation conditions," *Energy Conversion and Management*, vol. 49, no. 8, pp. 2307-2316, 2008.

[123] R. C. N. Pilawa-Podgurski, and D. J. Perreault, "Submodule integrated distributed maximum power point tracking for solar photovoltaic applications," *IEEE Transactions on Power Electronics*, vol. 28, no. 6, pp. 2957-2967, 2013.

[124] N. Femia, G. Lisi, G. Petrone, G. Spagnuolo, and M. Vitelli, "Distributed maximum power point tracking of photovoltaic arrays: novel approach and system analysis," *IEEE Transactions on Industrial Electronics*, vol. 55, no. 7, pp. 2610-2621, 2008.

[125] G. Petrone, G. Spagnuolo, and M. Vitelli, "An analog technique for distributed MPPT PV applications," *IEEE Transactions on Industrial Electronics*, vol. 59, no. 12, pp. 4713-4722, 2012.

[126] A. Elasser, M. Agamy, J. Sabate, R. Steigerwald, R. Fisher, and M. Harfman-Todorovic, "A comparative study of central and distributed MPPT architectures for megawatt utility and large scale commercial photovoltaic plants," in The 36th Annual Conference on IEEE Industrial Electronics Society, Glendale, AZ, 2010, pp. 2753-2758.

[127] L. L. Jiang, D. L. Maskell, and J. C. Patra, "Chebyshev functional link neural network-based modeling and experimental verification for photovoltaic arrays," in IEEE International Joint Conference on Neural Network (IJCNN), Australia, 2012, pp. 1-8.

[128] L. L. Jiang, D. L. Maskell, and J. C. Patra, "Parameter estimation of solar cells and modules using an improved adaptive differential evolution algorithm," *Applied Energy*, vol. 112, pp. 185-193, 2013.

[129] J. C. Patra, R. N. Pal, B. N. Chatterji, and G. Panda, "Identification of nonlinear dynamic systems using functional link artificial neural networks," *IEEE Transactions on Systems, Man, and Cybernetics, Part B: Cybernetics*, vol. 29, no. 2, pp. 254-262, 1999.

[130] J. C. Patra, and A. C. Kot, “Nonlinear dynamic system identification using Chebyshev functional link artificial neural networks,” *IEEE Transactions on Systems, Man, and Cybernetics, Part B: Cybernetics,* vol. 32, no. 4, pp. 505-511, 2002.

[131] J. C. Patra, and D. L. Maskell, “Estimation of dual-junction solar cell characteristics using neural networks,” in IEEE Photovoltaic Specialists Conference, Honolulu, HI, 2010, pp. 2709-2713.

[132] M. Klassen, P. Yoh-Han, and V. Chen, “Characteristics of the functional link net: a higher order delta rule net,” in IEEE International Conference on Neural Networks, 1988, pp. 507-513.

[133] "Artificial Neural Network User's Guide," Mathworks Inc, 2011.

[134] G. M. Foody, M. B. McCulloch, and W. B. Yates, “The effect of training set size and composition on artificial neural-network classification,” *International Journal of Remote Sensing,* vol. 16, no. 9, pp. 1707-1723, Jun, 1995.

[135] T. Rajkumar, and B. Jorge, “Training data requirement for a neural network to predict aerodynamic coefficients,” in SPIE Proceedings of Independent Component Analyses, Wavelets, and Neural Networks, Orlando, USA, 2003.

[136] G. Lera, and M. Pinzolas, “Neighborhood based Levenberg-Marquardt algorithm for neural network training,” *IEEE Transactions on Neural Networks,* vol. 13, no. 5, pp. 1200-1203, 2002.

[137] Y.-H. Pao, *Adaptive pattern recognition and neural networks*: Addison-Wesley Longman Publishing Co., Inc., 1989.

[138] S. Dehuri, and S.-B. Cho, “A comprehensive survey on functional link neural networks and an adaptive PSO–BP learning for CFLNN,” *Neural Computing and Applications,* vol. 19, no. 2, pp. 187-205, 2010.

[139] M. Wright, and A. Uddin, “Organic - inorganic hybrid solar cells: A comparative review,” *Solar Energy Materials and Solar Cells,* vol. 107, pp. 87-111, 2012.

[140] N. Asim, K. Sopian, S. Ahmadi, K. Saeedfar, M. A. Alghoul, O. Saadatian, and S. H. Zaidi, “A review on the role of materials science in solar cells,” *Renewable and Sustainable Energy Reviews,* vol. 16, no. 8, pp. 5834-5847, 2012.

[141] L. L. Jiang, D. L. Maskell, and J. C. Patra, “A novel ant colony optimization-based maximum power point tracking for photovoltaic systems under partially shaded conditions,” *Energy and Buildings,* vol. 58, pp. 227-236, 2013.

[142] D. P. Hohm, and M. E. Ropp, “Comparative study of maximum power point tracking algorithms using an experimental, programmable, maximum power point tracking test bed ” in IEEE Photovoltaic Specialists Conference, Anchorage, AK, 2000, pp. 1699-1702.

[143] F. Blaabjerg, C. Zhe, and S. B. Kjaer, “Power electronics as efficient interface in dispersed power generation systems,” *IEEE Transactions on Power Electronics,* vol. 19, no. 5, pp. 1184-1194, 2004.

[144] M. Chegaar, Z. Ouennoughi, and A. Hoffmann, "A new method for evaluating illuminated solar cell parameters," *Solid-State Electronics,* vol. 45, no. 2, pp. 293-296, 2001.

[145] K. Bouzidi, M. Chegaar, and M. Aillerie, "Solar cells parameters evaluation from dark I-V characteristics," *Energy Procedia,* vol. 18, pp. 1601-1610, 2012.

[146] D. S. H. Chan, and J. C. H. Phang, "Analytical methods for the extraction of solar-cell single- and double-diode model parameters from I-V characteristics," *IEEE Transactions onElectron Devices,* vol. 34, no. 2, pp. 286-293, 1987.

[147] T. Easwarakhanthan, J. Bottin, I. Bouhouch, and C. Boutrit, "Nonlinear minimization algorithm for determining the solar cell parameters with microcomputers," *International Journal of Solar Energy,* vol. 4, pp. 1-12, 1986.

[148] M. Zagrouba, A. Sellami, M. Bouaïcha, and M. Ksouri, "Identification of PV solar cells and modules parameters using the genetic algorithms: Application to maximum power extraction," *Solar Energy,* vol. 84, no. 5, pp. 860-866, 2010.

[149] M. Ye, X. Wang, and Y. Xu, "Parameter extraction of solar cells using particle swarm optimization," *Journal of Applied Physics,* vol. 105, no. 9, pp. 094502-094508, 2009.

[150] K. M. El-Naggar, M. R. AlRashidi, M. F. AlHajri, and A. K. Al-Othman, "Simulated annealing algorithm for photovoltaic parameters identification," *Solar Energy,* vol. 86, no. 1, pp. 266-274, 2012.

[151] A. Askarzadeh, and A. Rezazadeh, "Parameter identification for solar cell models using harmony search-based algorithms," *Solar Energy,* vol. 86, no. 11, pp. 3241-3249, 2012.

[152] M. F. AlHajri, K. M. El-Naggar, M. R. AlRashidi, and A. K. Al-Othman, "Optimal extraction of solar cell parameters using pattern search," *Renewable Energy,* vol. 44, pp. 238-245, 2012.

[153] K. Ishaque, Z. Salam, S. Mekhilef, and A. Shamsudin, "Parameter extraction of solar photovoltaic modules using penalty-based differential evolution," *Applied Energy,* vol. 99, pp. 297-308, 2012.

[154] J. C. Patra, "Chebyshev neural network-based model for dual junction solar cells," *IEEE Transactions on Energy Conversion,* vol. 26, no. 1, pp. 132-139, 2011.

[155] J. C. Patra, and D. L. Maskell, "Modeling of multi-junction solar cells for estimation of EQE under influence of charged particles using artificial neural networks," *Renewable Energy,* vol. 44, pp. 7-16, 2012.

[156] L. Sandrolini, M. Artioli, and U. Reggiani, "Numerical method for the extraction of photovoltaic module double-diode model parameters through cluster analysis," *Applied Energy,* vol. 87, no. 2, pp. 442-451, 2010.

[157] J. C. Patra, "Neural network-based model for dual-junction solar cells," *Progress in Photovoltaics: Research and Applications,* vol. 19, no. 1, pp. 33-44, 2011.

[158] A. Ortiz-Conde, F. J. García Sánchez, and J. Muci, "New method to extract the model parameters of solar cells from the explicit analytic solutions of their illuminated I–V characteristics," *Solar Energy Materials and Solar Cells,* vol. 90, no. 3, pp. 352-361, 2006.

[159] M. Chegaar, G. Azzouzi, and P. Mialhe, "Simple parameter extraction method for illuminated solar cells," *Solid-State Electronics,* vol. 50, no. 7–8, pp. 1234-1237, 2006.

[160] M. Haouari-Merbah, M. Belhamel, I. Tobías, and J. M. Ruiz, "Extraction and analysis of solar cell parameters from the illuminated current–voltage curve," *Solar Energy Materials and Solar Cells,* vol. 87, no. 1–4, pp. 225-233, 2005.

[161] R. Storn, and K. Price, "Differential evolution - A simple and efficient heuristic for global optimization over continuous spaces," *Journal of Global Optimization,* vol. 11, no. 4, pp. 341-359, 1997.

[162] A. Ghosh, A. Datta, and S. Ghosh, "Self-adaptive differential evolution for feature selection in hyperspectral image data," *Applied Soft Computing,* vol. 13, no. 4, pp. 1969-1977, 2012.

[163] F. S. Al-Anzi, and A. Allahverdi, "A self-adaptive differential evolution heuristic for two-stage assembly scheduling problem to minimize maximum lateness with setup times," *European Journal of Operational Research,* vol. 182, no. 1, pp. 80-94, 2007.

[164] A. K. Qin, and P. N. Suganthan, "Self-adaptive differential evolution algorithm for numerical optimization," in IEEE Congress on Evolutionary Computation, Nanyang Technological University, Singapore, 2005, pp. 1785 - 1791.

[165] J. Liu, and J. Lampinen, "A fuzzy adaptive differential evolution algorithm," *Soft Computing,* vol. 9, no. 6, pp. 448-462, 2005.

[166] J. Brest, S. Greiner, B. Boskovic, M. Mernik, and V. Zumer, "Self-adapting control parameters in differential evolution: A comparative study on numerical benchmark problems," *IEEE Transactions on Evolutionary Computation,* vol. 10, no. 6, pp. 646-657, 2006.

[167] J. Zhang, and A. C. Sanderson, "JADE: Adaptive differential evolution with optional external archive," *IEEE Transactions on Evolutionary Computation,* vol. 13, no. 5, pp. 945-958, 2009.

[168] R. Mallipeddi, P. N. Suganthan, Q. K. Pan, and M. F. Tasgetiren, "Differential evolution algorithm with ensemble of parameters and mutation strategies," *Applied Soft Computing,* vol. 11, no. 2, pp. 1679-1696, 2011.

[169] Y. Wang, Z. Cai, and Q. Zhang, "Differential evolution with composite trial vector generation strategies and control parameters," *IEEE Transactions on Evolutionary Computation,* vol. 15, no. 1, pp. 55-66, 2011.

[170] R. Gamperle, S. D. Muller, and P. Koumoutsakos, "A parameter study for differential evolution," in WSEAS International Conference on Advances in Intelligent Systems, Fuzzy Systems, Evolutionary Computation, 2002, pp. 293-298.

[171] Y. Chen, X. Wang, D. Li, R. Hong, and H. Shen, “Parameters extraction from commercial solar cells I-V characteristics and shunt analysis,” *Applied Energy*, vol. 88, pp. 2239-2244, 2011.

[172] F. Ghani, M. Duke, and J. Carson, “Numerical calculation of series and shunt resistances and diode quality factor of a photovoltaic cell using the Lambert W-function,” *Solar Energy*, vol. 91, pp. 422-431, 2013.

[173] S. Subiyanto, M. Azah, and M. A. Hannan, “Intelligent maximum power point tracking for PV system using Hopfield neural network optimized fuzzy logic controller,” *Energy and Buildings*, vol. 51, pp. 29-38, 2012.

[174] L.L. Jiang, D.L. Maskell, and J. C. Patra, “A FLANN - based controller for maximum power point tracking in PV systems under rapidly changing conditions,” in IEEE International Conference on Acoustics, Speech, and Signal Processing (ICASSP), Kyoto, Japan, 2012, pp. 2141-2144.

[175] D. Martens, M. De Backer, R. Haesen, J. Vanthienen, M. Snoeck, and B. Baesens, “Classification with ant colony optimization,” *IEEE Transactions on Evolutionary Computation*, vol. 11, no. 5, pp. 651-665, 2007.

[176] D. Picard, M. Cord, and A. Revel, “Image retrieval over networks : active learning using ant algorithm,” *IEEE Transactions on Multimedia*, vol. 10, no. 7, pp. 1356-1365, 2008.

[177] J. Zhang, H. Chung, W. L. Lo, and T. Huang, “Extended ant colony optimization algorithm for power electronic circuit design,” *IEEE Transaction on Power Electronics*, vol. 24, no. 1, pp. 147-162, 2009.

[178] E. Diaz-Dorado, A. Suarez-Garcia, C. Carrillo, and J. Cidras, “Influence of the shadows in photovoltaic systems with different configurations of bypass diodes,” in International Symposium on Power Electronics Electrical Drives Automation and Motion, Pisa, Italy, 2010, pp. 134 - 139.

[179] H. Patel, and V. Agarwal, “MATLAB-based modeling to study the effects of partial shading on PV array characteristics,” *IEEE Transactions on Energy Conversion*, vol. 23, no. 1, pp. 302-310, 2008.

[180] B. N. F. M. T. Alajmi, K. Ahmed, S. Finney, B. Williams, B. N. F. M. T. Alajmi, K. Ahmed, S. Finney, and B. Williams, “A maximum power point tracking technique for partially shaded photovoltaic systems in microgrids,” *IEEE Transactions on Industrial Electronics*, vol. 60, no. 4, pp. 1596-1606, 4, 2013.

[181] R. Alonso, E. Roman, A. Sanz, V. E. M. Santos, and P. Ibanez, “Analysis of Inverter-Voltage Influence on Distributed MPPT Architecture Performance,” *Industrial Electronics, IEEE Transactions on*, vol. 59, no. 10, pp. 3900-3907, 2012.

[182] A. Barchowsky, J. P. Parvin, G. F. Reed, M. J. Korytowski, and B. M. Grainger, “A comparative study of MPPT methods for distributed photovoltaic generation,” in IEEE conference on Innovative Smart Grid Technologies (ISGT), 2012, pp. 1-7.

[183] M. Balato, and M. Vitelli, “A new control strategy for the optimization of distributed MPPT in PV applications,” *International Journal of Electrical Power & Energy Systems*, vol. 62, pp. 763-773, 2014.

[184] C. Liang-Rui, T. Chih-Hui, L. Yuan-Li, and L. Yen-Shin, “A biological swarm chasing algorithm for tracking the PV maximum power point,” *IEEE Transactions on Energy Conversion*, vol. 25, no. 2, pp. 484-493, 2010.

[185] M. Dorigo, “Optimization, learning and natural algorithms,” PhD thesis, Politecnico di Milano, Italy., 1992.

[186] M. Dorigo, and T. Stützle, *Ant colony optimization*: MIT, 2004.

[187] K. Socha, and M. Dorigo, “Ant colony optimization for continuous domains,” *European Journal of Operational Research*, vol. 185, no. 3, pp. 1155-1173, 2008.

[188] T. Liao, M. A. M. d. Oca, D. Aydin, T. St, #252, tzle, and M. Dorigo, “An incremental ant colony algorithm with local search for continuous optimization,” in Proceedings of the 13th annual conference on Genetic and evolutionary computation, Dublin, Ireland, 2011, pp. 125-132.

[189] L. Chen, J. Shen, and H. Chen, “An improved ant colony algorithm in continuous optimization,” *Journal of Systems Science and Systems Engineering*, vol. 12, no. 2, pp. 224-235, 2003.

[190] T. Liao, T. Stützle, M. A. Montes de Oca, and M. Dorigo, “A unified ant colony optimization algorithm for continuous optimization,” *European Journal of Operational Research*, vol. 234, no. 3, pp. 597-609, 2014.

[191] R. Jayaraman, and D. L. Maskell, “Temporal and spatial variations of the solar radiation observed in Singapore,” *Energy Procedia*, vol. 25, pp. 108-117, 2012.

[192] W. Herrmann, W. Wiesner, and W. Vaassen, “Hot spot investigations on PV modules-new concepts for a test standard and consequences for module design with respect to bypass diodes,” in 26th IEEE Photovoltaic Specialists Conference, Anaheim, California, USA, 1997, pp. 1129-1132.

[193] Y. Shi, and R. Eberhart, "Parameter selection in particle swarm optimization," *Evolutionary Programming VII*, Lecture Notes in Computer Science V. W. Porto, N. Saravanan, D. Waagen and A. E. Eiben, eds., pp. 591-600: Springer Berlin Heidelberg, 1998.

[194] T. Stützle, M. López-Ibáñez, P. Pellegrini, M. Maur, M. Montes de Oca, M. Birattari, and M. Dorigo, "Parameter adaptation in ant colony optimization," *Autonomous Search*, Y. Hamadi, E. Monfroy and F. Saubion, eds., pp. 191-215: Springer Berlin Heidelberg, 2012.

[195] F. Moussouni, S. Brisset, and P. Brochet, "Comparison of two multi-agent algorithms: ACO and PSO for the optimization of a brushless DC wheel motor intelligent computer techniques in applied electromagnetics," *Intelligent Computer Techniques in Applied*

Electromagnetics, Studies in Computational Intelligence 119, S. Wiak, A. Krawczyk and I. Dolezel, eds., pp. 3-10: Springer Berlin Heidelberg, 2008.

[196] S. Paterlini, and T. Krink, "Differential evolution and particle swarm optimisation in partitional clustering," *Computational Statistics & Data Analysis,* vol. 50, no. 5, pp. 1220-1247, 2006.

[197] C. M. Bishop, *Neural Networks for Pattern Recognition*: Oxford University Press, 1995.

[198] S. B. Kotsiantis, "Supervised machine learning: A review of classification techniques," in Proceedings of the 2007 conference on Emerging Artificial Intelligence Applications in Computer Engineering: Real Word AI Systems with Applications in eHealth, HCI, Information Retrieval and Pervasive Technologies, 2007, pp. 3-24.

[199] I. Rish, "An empirical study of the naive bayes classifier," *IJCAI 2001 workshop on empirical methods in artificial intelligence,* vol. 3, no. 22, pp. 41-46, 2001.

[200] G. Steve R, *Support vector machines for classification and regression*, Image Speech and Intelligent Systems Group, Department of Electronics and Computer Science, University of Southampton, UK, 1998.

[201] Sandrine Dudoit, Jane Fridlyand, and T. P. Speed, "Comparison of discrimination methods for the classification of tumors using gene expression data," *Journal of the American Statistical Association,* vol. 97, no. 457, pp. 77-87, 2002.

[202] Y.-H. Liu, and J.-W. Huang, "A fast and low cost analog maximum power point tracking method for low power photovoltaic systems," *Solar Energy,* vol. 85, no. 11, pp. 2771-2780, 2011.

[203] K. Ishaque, Z. Salam, A. Shamsudin, and M. Amjad, "A direct control based maximum power point tracking method for photovoltaic system under partial shading conditions using particle swarm optimization algorithm," *Applied Energy,* vol. 99, pp. 414-422, 2012.

[204] B. Werner, W. KoŁodenny, M. Prorok, A. Dziedzic, and T. Żdanowicz, "Electrical modeling of CIGS thin-film solar cells working in natural conditions," *Solar Energy Materials and Solar Cells,* vol. 95, no. 9, pp. 2583-2587, 2011.

[205] S. Dongaonkar, and M. A. Alam, "A shade tolerant panel design for thin film photovoltaics," in IEEE Photovoltaic Specialists Conference (PVSC), Austin, TX, 2012, pp. 002416-002420.

[206] S. Dongaonkar, C. Deline, and M. A. Alam, "Performance and reliability implications of two-dimensional shading in monolithic thin-film photovoltaic modules," *IEEE Journal of Photovoltaics,* vol. 3, no. 4, pp. 1367-1375, 2013.

[207] I. Bouchama, K. Djessas, F. Djahli, and A. Bouloufa, "Simulation approach for studying the performances of original superstrate CIGS thin films solar cells," *Thin Solid Films,* vol. 519, no. 21, pp. 7280-7283, 2011.

[208] A. Benmir, and M. S. Aida, "Analytical modeling and simulation of CIGS solar cells," *Energy Procedia,* vol. 36, pp. 618-627, 2013.

[209] T. O. Saetre, O.-M. Midtgård, and G. H. Yordanov, “A new analytical solar cell I–V curve model,” *Renewable Energy*, vol. 36, no. 8, pp. 2171-2176, 2011.

[210] J. Song, S. S. Li, C. H. Huang, O. D. Crisalle, and T. J. Anderson, “Device modeling and simulation of the performance of Cu(In1−x,Gax)Se2 solar cells,” *Solid-State Electronics*, vol. 48, no. 1, pp. 73-79, 2004.

[211] H. Movla, E. Abdi, and D. Salami, “Simulation analysis of the CIGS based thin film solar cells,” *Optik - International Journal for Light and Electron Optics*, vol. 124, no. 22, pp. 5871-5873, 2013.

[212] M. A. Mannan, M. S. Anjan, and M. Z. Kabir, “Modeling of current–voltage characteristics of thin film solar cells,” *Solid-State Electronics*, vol. 63, no. 1, pp. 49-54, 2011.

[213] M. Dorigo, and C. Blum, “Ant colony optimization theory: A survey,” *Theoretical Computer Science*, vol. 344, no. 2-3, pp. 243-278, 2005.

[214] M. Dorigo, M. Birattari, and T. Stutzle, “Ant colony optimization,” *Computational Intelligence Magazine, IEEE*, vol. 1, no. 4, pp. 28-39, 2006.

LIST OF FIGURES

LIST OF TABLES

LIST OF ABBREVIATIONS

ACO	Ant Colony Optimization
ANN	Artificial Neural Network
BOS	Balance of System
BL	Bridge-Link
BST	Bisection Search Theorem
BP	Back Propagation
CFLNN	Chebyshev Functional Link Neural Network
CST	Concentrating Solar Thermal
COS	Center of Singleton
COG	Center of Gravity
DE	Differential Evolution
DIRECT	Dividing Rectangles
DMPPT	Distributed MPPT
ESC	Extremum Seeking Control
EPBT	Energy Payback Time
FLANN	Functional Link Artificial Neural Network
FL	Fuzzy Logic
FEB	Functional Expansion Block
FADE	Fuzzy Adaptive DE
GA	Genetic Algorithm
HS	Harmony Search
IADE	Improved Adaptive Differential Evolution
IncCond	Incremental Conductance
INR	Incremental Resistance
LM	Levenberg - Marquardt
MPP	Maximum Power Point
MPPT	Maximum Power Point Tracking
MLP	Multilayer Perceptron
MSE	Mean Squared Error
MAPE	Mean Absolute Percentage Error
P&O	Perturb and Observe
PSO	Particle Swarm Optimization
PV	Photovoltaic
POT	Power Operating Triangle

PS	Pattern Search
RCC	Ripple Correlation Control
RMSE	Root Mean Square Error
SA	Simulated Annealing
SAG	Sloped Air-Gap
SP	Series-Parallel
STC	Standard Test Conditions
TCT	Total Cross Tied
VWS	Voltage Window Search